THE UNIVERSITY OF HULL

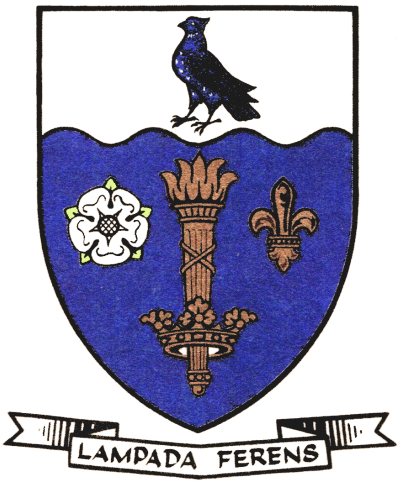

A Multi-Disciplinary Study of Insect Adhesion: Functional Biomechanics and Applications

being a Thesis submitted for the Degree of Doctor of Philosophy
in the University of Hull

by

Matthew James Anyon BSc (Hons)

February 2013

Declaration of Authorship

I, MATTHEW JAMES ANYON, declare that this thesis titled, 'A Multi-Disciplinary Study of Insect Adhesion: Functional Biomechanics and Applications' and the works presented in it are my own.
I confirm that:

- This work was completed wholly or mainly while in candidature for a research degree at this University.
- Where any part of this thesis has previously been submitted for a degree or any other qualification at this University or any other institution, this has been clearly stated.
- Where I have consulted the published work of others, this is always clearly attributed.
- Where I have quoted from the work of others, the source is always given. With the exception of such quotations, this thesis is entirely my own work.
- I have acknowledged all main sources of help.
- Where the thesis is based on work done by myself jointly with others, I have made clear exactly what was done by others and what I have contributed myself.

MJA, 2012

Abstract

The ability of insects to successfully attach to a wide variety of surfaces with seemingly little to no effort has fascinated naturalists and researchers for hundreds of years. The observation of a fly climbing up a window, or spider walking upside down on our ceilings is a commonly overlooked and under-appreciated sight. The advanced ability of insects to attach themselves successfully to different surfaces for the purpose of locomotion, under different orientations and in a fast, reliable and efficient manner is not only an impressive natural capability but also crucial to the survival and ecology of the insect, and by extension to the success of the species as a whole. To achieve this adhesive ability insects utilise a 'wet' adhesive system, making use of specialised functional adhesive pad structures which deploy a liquid secretion to the contact zone which aids adhesion through capillary and viscous forces. These attachment pads can be loosely classified as either 'smooth' or 'hairy' and are found in most insect species studied to date. Predictions from a small number of simple theoretical models of insect attachment have been experimentally verified for a number of insects species, however, due to the vastness of the insect world, the exact physical mechanisms underlying insect adhesion for the majority of insects is still unclear.

Through the use of qualitative and quantitative experiments of several species of ant (Hymenoptera; Formicidae) and ladybird (Coleoptera; Coccinellidae) we characterise the functional morphology of the attachment devices and properties of the adhesive secretion of smooth and fibrillar attachment devices found in these insects. In an effort to gain a greater understanding of the physical mechanism of wet insect adhesion to smooth surfaces, we compare *in vivo* force measurement results from several custom-built force measurement techniques with predictions from a number of theoretical contact-mechanic models under conditions of adhesion normal to, and friction forces tangential to the substrate. By varying the physico-chemical properties of the substrates within these experiments, and the orientation of the insects under investigation, the magnitudes of these contributions under different experimental conditions is determined, and the results are discussed in the context of the magnitudes of different surface forces that may be acting during adhesive and frictional detachment processes, as well as the influence of the substrate surface energy.

By applying this understanding towards the investigation and development of novel anti-adhesive surfaces for use in domestic and industrial settings, several methods of reducing or preventing insect attachment forces are investigated and discussed in the context of creating environmentally and ecologically friendly strategies of pest control.

In summary this thesis provides evidence for links between the physico-chemical properties of a substrate and adhesive forces generated by insects during locomotion, and how an insects' adhesive ability on a particular substrate may influence their behaviour. Results from this study will be helpful in designing the next generation of smart adhesives, but could also lead to novel anti-adhesive barriers for environmentally friendly strategies of pest-control.

Publications & Presentations

Publications

- **M.J. Anyon, M.J. Orchard, D.M.A. Buzza, S. Humphries, M.M. Kohonen**,
  The effect of particulate contamination on adhesive ability and repellance in two species of ant (Hymenoptera; Formicidae)
  Journal of Experimental Biology 215:605–616,**2012** (doi:10.1242/jeb.063578)

Oral Presentations

- Speaker at 2011 Physical Sciences Ph.D. Research Colloquia, University of Hull, UK;
  M.J. Anyon; *Biomechanics of 'wet' insect adhesion*
  * This talk won the 2011 Physical Sciences Ph.D. Research Colloquia Prize

- Speaker at 2011 Society of Experimental Biology Annual Main Meeting, SECC Glasgow, UK;
  M.J. Anyon; *Biomechanics of 'wet' insect adhesion*
  (`http://www.sebiology.org/meetings/Past_Meetings/Glasgow_2011/docs/Abstracts.pdf`)

- Speaker at Department of Physics 2011 Seminar Series, Physics Department, University of Hull, UK;
  M.J. Anyon; *Biomechanics of wet insect adhesion*

- Speaker at 2010 Institute of Physics (IOP) Physics Meets Biology Conference, St. Catherines College, Oxford University, UK;
  M.J. Anyon; *Towards a Simple Model of Insect Adhesion*

- Joint speaker at Surfactant & Colloid Group 2010 Seminar Series, Department of Chemistry, University of Hull, UK;
  M.J. Anyon, M.J. Orchard; *Investigation of biological adhesion and locomotion via powder barrier experiments on ants*

Poster Presentations

- Presenter at Institute Of Physics (IOP) Biological & Soft Matter Conference, Warwick University, UK;

- Presenter at UK Polymer Colloids Forum, University of Hull, UK.

Acknowledgements

To my primary supervisor, Dr Martin Buzza, for his continuous guidance and help throughout my entire postgraduate experience; as both a scientific mentor and a perpetual force continuously pushing me towards the finish line, I owe a great debt. Thanks to Dr Mika Kohonen for his assistance with the experimental portions of this thesis and Dr Tommy Horozov. Thanks must go to Prof. Bernie Binks and members of the Surfactant & Colloid Group, University of Hull, for support throughout this project, as well as for tolerating a physicist studying biology in their pristine chemistry laboratories, and to the University of Hull for awarding me an 80th Anniversary Scholarship, and providing me with the opportunity to undertake such fascinating research at this institution.

My thanks go to the undergraduate project students with whom I worked, and who made a significant contribution in time and effort towards gathering some of the data used during this project, and for being test subjects for preliminary designs of experiments eventually used within this thesis, namely Matthew Lambert, Michael Pardoe, Joe Mazzon, Ben Scragg and Vicky Knight.

I thank members of the Physics Department with whom I have shared my postgraduate experience, and for some more unfortunate than others, shared an office, notably; Igor Sapina, Anthony Edwards, Aaron Whitham, Stephen Myers, Abigail Merchant, David Staveneau, Stephanie Cockcroft, Dr Angela Dyson, Prof. Mary O'Neill, and Mrs Chris Kirman.

Thanks to Dr Adam Law, now at the Max Planck Institut für Intelligente Systeme in Stuttgart, Germany, for welcoming me into the Theoretical Physics office, and for being a true friend at work for over 2 years - able to make the most stressful moments disappear with nothing but a raising of an eye-brow. Similarly, thanks go to Daniel R. Naylor for his tolerance, his friendship, his seemingly un-ending 'tech-support', his occasional practical jokes, his help with an innumerable amount of questions, his witty conversations and his fervent challenges to my beliefs and opinions - every bit of it was enjoyed and deeply appreciated.

My most sincere and deepest thanks go to Michael Orchard (Department of Biological Sciences), with whom I have shared this interdisciplinary project; for his immeasurable support throughout the last 3 years, and for sharing with me a truly peaceful place to live. He has been a constant help, and a pillar of knowledge to call upon for anything and everything I needed help with regarding the biological sciences. For his help, support, tolerance, understanding and friendship I extend my true gratitude.

Finally thank you to my family, especially my parents Stephen and Alison Anyon, for pushing me towards taking on this Ph.D. to begin with, for assuaging my fears and doubts and for simply being there. This thesis is in no short order a direct result of your actions and guidance - thank you.

MJA

'To a first approximation, all multicellular species on earth are insects'

N. E. Stork
Nature, 2007

felix qui potuit rerum cognoscere causas

Virgil
Georgics, 42 BC

Table of Contents

Dedicated to my Dad; to keep my promise...

Chapter 1

Introduction

'It can run up and down a tree in any way, even with the head downwards'

Aristotle

1.1 Biological Attachment

The sight of a fly climbing up a window, or spider walking upside down on our ceilings has fascinated scientists for millennia [1, 2] and is a commonly overlooked and under-appreciated sight. For insects the capability of adhesion is not only an impressive natural capability but also crucial to the survival and ecology of the individual insect, and by extension to the success of the species as a whole, for example during prey capture [3–5], mating and oviposition [6–10], or the selection and construction of nesting sites [11, 12].

Although adhesion to different substrates is widespread amongst insects, having been perfected over the course of evolution for millions of years, the capabilities of individual species can vary, and even closely related species can have dramatically different adhesive abilities [13]. A combination of nano- and microstructured dynamic attachment structures, interactions of viscoelastic materials and adhesive secretions, the use of different gaits and posture, and the insects' behaviour are all responsible for the resulting adhesion. Therefore using an integrative and multidisciplinary approach to study this ability is crucial, taking into consideration the multiple factors at play.

Adhesion in biological organisms can be classified as being either permanent and rigid, or temporary and releasable (transitory). Mechanisms for permanent adhesion are used

by non-mobile organisms to attach themselves to one place for a long period of time, and can be achieved by a number of different techniques described in the literature (eg., see Nachtigall [14]). Transitory adhesion is used by organisms which need to maintain a strong attachment to a surface, resisting external detachment forces whilst also enabling the organism to move across the surface efficiently, often carrying several times their own body weight, Figure 1.1.1. Invertebrates run and climb over almost every terrain on earth and usually must do so rapidly. In some cases the substrate possesses enough texture to allow claws to grip, and these structures are found in the vast majority of insects. However, when the surface is smooth and relatively stiff (for example a sheer rock face, or the smooth outer cuticle of a plant), claws will no longer support the animal [15] so another mechanism of attachment, making use of a combination of adhesion and friction forces, is needed. A wide variety of natural adhesive organs have therefore evolved to cope with these problems which are found in numerous places on the insect body, display a great many functional forms [14, 16–19] and can be classified as either 'smooth' or 'hairy'

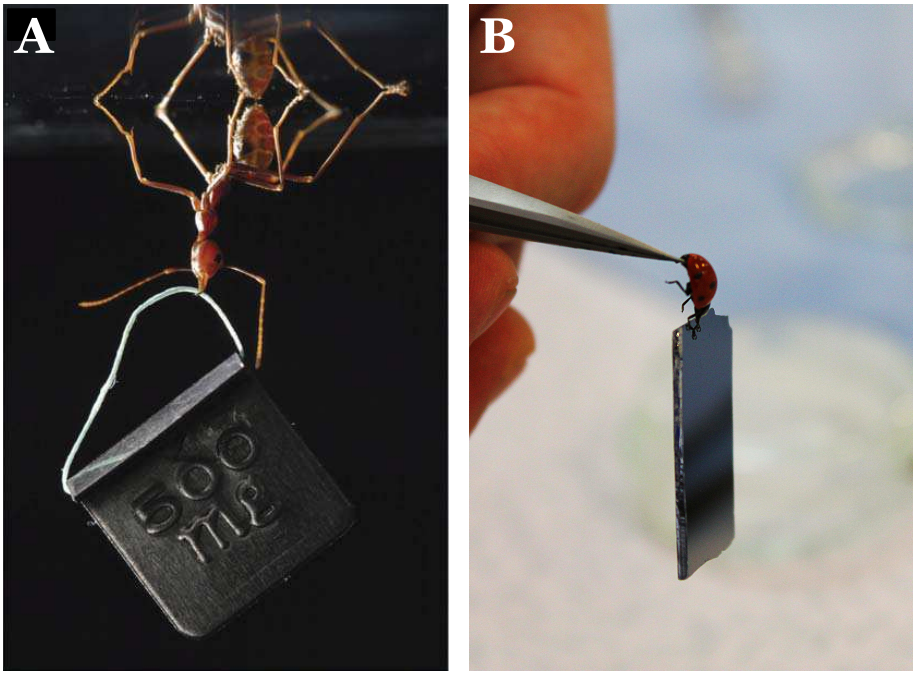

Figure 1.1.1: Insects carrying heavy loads on smooth surfaces. A) The weaver ant *Oecophylla smaragdina* carrying approximately 100 times its body weight upside down on smooth glass. B) A 7-spot ladybird *Coccinella septempunctata* holding a silicon-wafer weighing approximately 50 times its body-weight using only two of its legs. A) Photograph taken by T. Endlein, University of Glasgow, B) Photograph taken by J. Moore, University of Hull.

[17]. Smooth systems make use of extended, compliant materials to form pads on the tarsi, and are found in several orders of insect including Hymenoptera and Orthoptera such as bees [20], ants [12], wasps, locusts [21], stick insects [22] and grasshoppers [23], but are not limited to these types of insect [7]. Fibrillar or 'hairy' systems employ arrays of densely packed thin, flexible hairs found on the tarsus. They can be found in many insect orders including Diptera, (eg. flies) [24], Coleoptera [6, 25], and can also be found in arachnids, [26] and a number of lizards [27]. Both systems give rise to adhesion through a combination of intermolecular, capillary and viscous forces in varying degrees of magnitude. A recent review by Peattie [28] outlined three broad criteria required for dynamic biological adhesion as: *i*) *reusability* - the attachment device must be able to attach and detach to the substrate rapidly and repeatedly without wear, be self-cleaning, and able to replenish itself naturally, *ii*) *reversibility* - attachment must be able to support the organisms' body weight plus strong accelerations during locomotion, the organism must be able to rapidly reverse attachment at will with a low detachment force, *iii*) *substrate tolerance* - natural surfaces can be smooth or rough, dry or wet, hard or soft, hydrophobic or hydrophilic, clean or contaminated, or a combination of these, so attachment devices should be able to cope with as broad a range of substrates as possible. Because natural surfaces have unpredictable surface profiles, and have roughness on different length scales, insects require a highly adaptive attachment system capable of fulfilling the above criteria for successful adhesion and locomotion.

As such, the field of insect adhesion has recently seen a surge in increased attention from the disciplines of biology, physics, materials science and engineering, and has become a field of true interdisciplinary research. Due to recent rapid technological advances, the capability to study small insects and the processes behind their ability to successfully traverse many different surfaces, under vastly different situations in order to become so ecologically successful across the natural world, has become relatively easier. Understanding the biomechanics and physical processes behind insect adhesion will further advance

our knowledge of adhesion phenomena, which can be applied towards the synthetic reproduction of these abilities in a new generation of bio-inspired adhesives, or conversely to develop more efficient ecologically friendly methods of insect pest control in agricultural and domestic environments.

1.2 Aim of Thesis

The aim of this thesis is to study the underlying physical mechanisms of 'wet' adhesion and friction generated by both smooth and hairy attachment pads of insects, which is currently less well understood than dry adhesion, such as that used by the Gecko lizard. Using Ladybirds (Coleoptera; Coccinellidae) and Ants (Hymenoptera; Formicidae) as representative insects possessing these different attachment pads, we perform detailed morphological and structural characterisations of the wet adhesive systems found in these insects, make use of *in vivo* measurement of attachment forces, and theoretical modelling to understand the functional morphology of these systems when in contact with smooth surfaces. In the latter part of this thesis, this understanding is further applied towards investigation and development of novel anti-adhesive surfaces for use in domestic and industrial settings.

As such, Chapter 2 gives a literature review of current knowledge of wet insect adhesion, including morphological details of the different attachment pads found in insects, properties of the adhesive secretions used by these insects to generate wet-adhesion, the magnitude of forces generated by insects under different experimental conditions and a description of some of the experimental methods used to measure insect attachment forces. The different surface forces which act during insect attachment will also be outlined, and in Chapter 3 we give a review of current knowledge on natural and synthetic barriers to insect adhesion, including examples of barriers to insect attachment found in the natural world. Details of the known physical and morphological characteristics of different epicuticular waxes used by many plants to achieve this end are also discussed, along with a review of

current anti-stick technologies which have been developed through taking influence from super-hydrophobic, 'self-cleaning', surfaces found in nature, such as the Lotus plant.

In order to model the adhesive systems used by insects to generate strong, reversible adhesion it is required to create simple theoretical models and characterise the attachment systems of insects representative of the two attachment pad forms. As such, Chapter 4 describes different theoretical contact mechanics models for smooth and hairy pads and gives detailed morphological data of the attachment pads and adhesive secretion of the Asian Weaver ant *Polyrhachis dives* and the Harlequin ladybird *Harmonia axyridis*. Chapter 5 details centrifuge force-experiments used to measure adhesion and friction force in the ant *Polyrhachis dives* and ladybird *Harmonia axyridis* on smooth glass surfaces of different hydrophobicities. Using the morphological characteristics of the adhesive systems of these insects detailed in Chapter 4 within the theoretical models, forces from each model are calculated for both insects and compared with attachment forces measured *in vivo*. Results of the models are discussed in terms of the physical forces which act during both adhesion normal to the substrate, and friction tangential to the substrate.

Chapter 6 describes the use of custom built force measurement techniques constructed to compare detachment forces during dynamic and quasi-static perturbations. Using a 'Direct Force Measurement' technique, adhesion and friction forces generated by tethered insects are measured, and a novel 'Impact-rig' experiment is used to measure forces of insects subjected to short, unexpected, impulsive detachment forces. To our knowledge, no such force measurement technique has previously been used in the study of insect attachment, and the results are compared to other force measurement techniques, including the results from Chapter 5.

Chapters 7 and 8 describe results of experiments designed to investigate different routes for reducing and preventing insect attachment. Specifically, in Chapter 7 we describe powder barrier experiments conducted to study the effect of particulate contamination on adhesive ability in two species of ant: *Polyrhachis dives* and *Myrmica scabrinodis*. The

effects of the powder particles on attachment ability were investigated systematically to elucidate the factors affecting insect adhesion after contamination with synthetic particles. By investigating observed repellence behaviour by both ant species, we develop and test hypotheses to explain erroneous results from these experiments, and discovered possibly advantageous limitations to the sensing abilities of these ants' antennae. In contrast, Chapter 8 details investigations of surface coatings constructed from colloidal solutions of glass nano-particles which form rigid barriers. These barriers' capability for reducing insect attachment forces in comparison to commercially available barriers already available which claim to achieve this goal is discussed.

It should be noted that, within this thesis, the term *adhesion* shall be defined to specifically refer to attachment forces generated by insects in the direction normal to the substrate, and *friction* to be defined as the attachment forces generated tangential to the substrate. *Attachment*, or *attachment ability* will be terms used to describe the general phenomena of insects traversing vertical or inverted surfaces against the force of gravity, being either friction or adhesion.

The results of this research project are inherently linked to, and complemented by, those of the related research of M.J. Orchard, which concentrates on the behavioural and ecological implications of insect adhesion. In order to give a comprehensive understanding of the findings, the results of both projects should to be viewed in conjunction, and this thesis therefore includes some results which were the result of a collaborative effort between the author and M.J. Orchard. The results of these collaborative efforts are indicated and referenced where appropriate. Nevertheless, the interested reader shall be referred to the thesis of M.J. Orchard for further reading and details.

Chapter 2

Literature Review
Mechanisms of Insect Adhesion

'by this the Flies are inabled to walk against the sides of Glass, perpendicularly upwards, and to contain themselves in that posture as long as they please; ...their suspension therefore is wholly to be ascrib'd to some Mechanical contrivance in their feet.'

Robert Hooke (1665)

Human fascination with the natural world has been present since the earliest days of natural science, and has led to numerous attempts to understand and replicate natural processes. An excellent example of this is the interest focused on the impressive abundance of biological attachment structures [1, 2, 14, 16]. Structures used for dynamic attachment can be found on the feet of lizards, amphibians, mammals, arachnids, and the vast majority of insects. Following recent advances in the field of material science numerous attempts have been made to replicate the advanced adhesive ability of the gecko lizard and several insects, and the ability to study small insects and the processes behind their ability to successfully traverse many different surfaces has become easier. However, many questions remain as to the actual physical mechanisms underlying this ability in insects.

The aim of this chapter is to outline the current literature regarding wet insect adhesion, including morphological details of the different attachment pads found in insects, properties of the adhesive secretions deployed by these pads to generate adhesion, and the experimental methods used to measure insect attachment forces. The different surface forces which act during insect attachment will also be outlined.

2.1 Conventional Adhesives & Dahlquist Criterion

For two dry surfaces to experience a strong adhesion they must be brought within molecular-order distances of each other, since the adhesive forces of molecular adhesion act over only very short distances. However, in reality, on a micro- or macroscopic scale this is extremely difficult to achieve, and there are many barriers to overcome in achieving such intimate contact. Direct contact will occur only where the tips of surface asperities meet, and since intermolecular interactions between neutral solids are very short-ranged, and due to the ubiquitous presence of surface roughness on most surfaces, the adhesion of two bodies is dominated by the real area of contact between them. Most 'real' surfaces are far from perfectly smooth, possessing varying degrees of surface roughness, particularly so for natural surfaces such as the cuticle of plants. Natural surfaces are also usually covered by some form of surface contamination, further reducing area of contact and adhesion between surfaces, Figure 2.1.1. A strong interaction is therefore usually facilitated by at least one of the surfaces being elastically soft, allowing it to deform to contours of the interface in order to generate a large area of contact. Conventional macroscopic adhesives, such as tapes and other pressure-sensitive adhesives (PSAs) function by this principle by having a low elastic modulus, which makes the material able to generate a relatively large contact

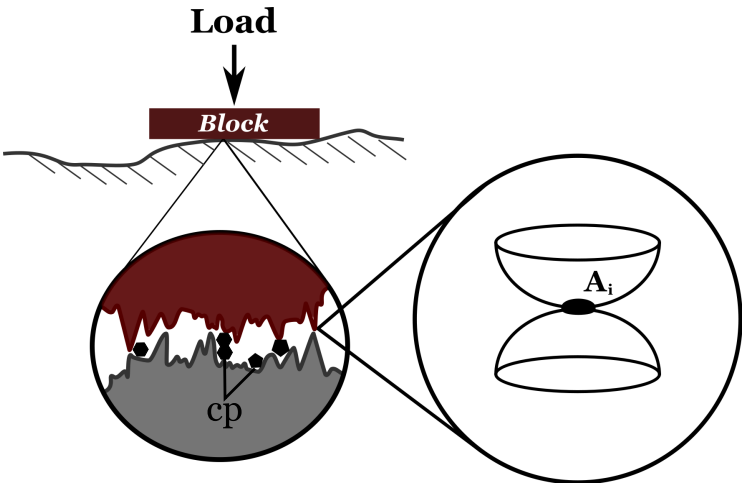

Figure 2.1.1: Contact of a flat solid under a load on a 'real' surface. Intimate contact is only achieved at the peaks of surface asperities, each with contact area A_i. Surface contamination also acts to reduce real contact area between surfaces. *cp* contaminating particles.

area, even on rough surfaces, when a loading force is applied. The required compliance was quantified by the *Dahlquist criterion* which states that a pressure-sensitive adhesive material may exhibit 'tackiness' if its effective elastic modulus is of the order 100 kPa or less [29]. The effective elastic modulus of a fibrillar array, for example, can defined as:

$$E_{eff} = \frac{stress}{strain} = \frac{F/A}{\delta/h} \tag{2.1.1}$$

where A is the total projected area of the pad, F the perpendicular loading force acting on the array, δ is the vertical displacement and h the height of the array ($h = l \sin\theta$), see Figure 2.1.2. However, conventional PSAs' ability to deform in this way is also the source of their greatest weakness. With repeated use they easily pick up contaminating particles which are difficult to remove and cause the adhesive to fail after only a few cycles, and because they are made from relatively weak materials they are susceptible to wear, breaking down quickly. This is in stark contrast to biological adhesive systems made from materials derived from the insect cuticle, which are significantly sturdier, having elastic moduli many orders of magnitude greater than PSAs. Specialised attachment devices derived from this cuticle material have evolved to provide ingenious and tailored solutions to the challenge of adhesion within the insect world, and will be described in the following section.

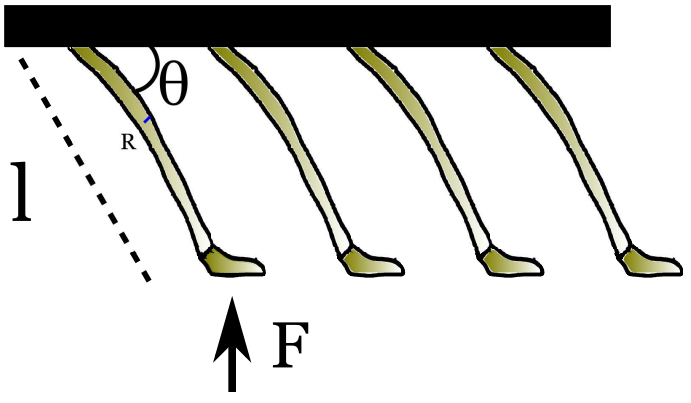

Figure 2.1.2: Schematic of fibrillar array showing dimensions and angles of rigid setae of radius R, length l, angle from horizontal plane θ and elastic modulus E, under an applied load of F. Given that elastic modulus is defined as the ratio of stress to strain, Equation 2.1.1, the effective elastic modulus of a fibrillar array can be determined if the characteristic properties of the array are known.

2.2 Morphology of Insect Adhesive Pads

As briefly mentioned in Chapter 1 insects have developed specialised attachment pads on their tarsi, structured to allow for strong and reversible attachment to a variety of surface profiles [30–32]. Studies of the morphological and ultrastructural characteristic properties of attachment systems in insects have been performed across a number of different orders including Blattodea (eg: cockroaches) [33], Coleoptera (eg: ladybirds) [34–36], Diptera (eg: flies) [37, 38], Orthoptera (eg: grasshoppers, locusts) [23, 39], Hymenoptera (eg: wasps, bees, ants) [12, 20, 40–42], and a number of other insect orders [7, 43]. The specialised attachment structures are not restricted to one particular part of the insect leg, and can be found on different parts of the tibia, tarsus, or pre-tarsus, and occur in different numbers dependent on species, Figure 2.2.1. For example, cockroaches and grasshoppers possess several smooth pads known as euplantulae along the length of each of their tarsi, Figure 2.2.1F, whereas ants or wasps possess a single pad situated on the most distal part of each leg, Figure 2.2.1A. Although the particular structure of an insects' attachment

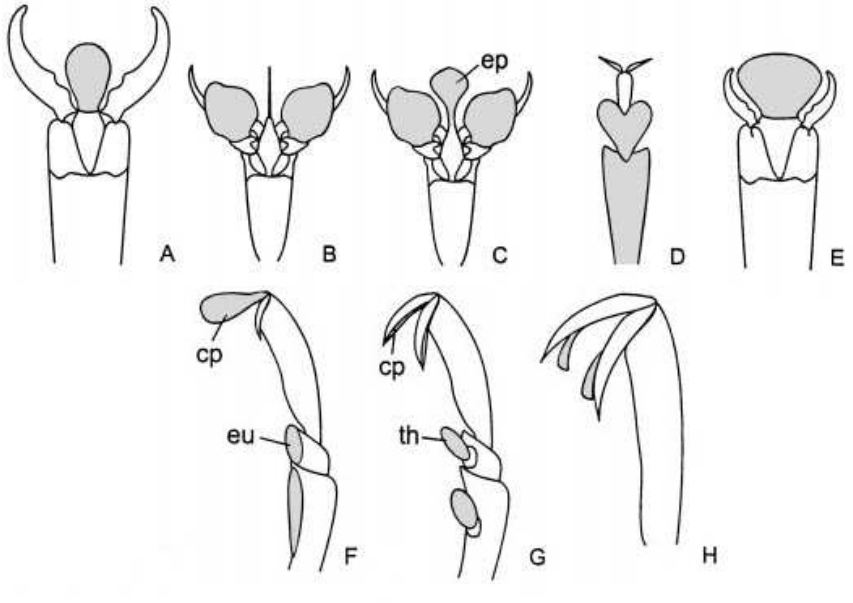

Figure 2.2.1: Diversity of attachment pad morphology in insects (grey areas). A) arolium, B) pulvilli, C) empodial pulvillus (ep), D) hairy adhesive pads of tarsomeres, E) pretarsal bladder, F) euplantulae (eu) and claw pads (cp), G) tarsl thorns developed into adhesive structures (th). Adapted from Beutel & Gorb [32].

pad system is often tailored to that species, during the course of evolution the diversity of attachment pad structural morphology has converged upon two functional forms for the purpose of locomotory adhesion, namely *hairy* or *setose* structures, and *smooth* flexible pads [44], Figure 2.2.2. Hairy pads are arrays of fine hairs known as *setae* or *acanthae*, made of stiff cuticle material but, due to their high aspect-ratio, have an overall flexibility and can achieve intimate contact with the substrate *via* the many individual small contacts to achieve a large total contact area. Smooth pads are large, soft and deformable organs known as *arolia* or *euplantulae* that maximise their contact area with the substrate due to their specialised material structure and structural properties.

Both type of functional structures have surface and material properties which function to maximise the real area of contact with diverse substrate profiles and materials, and both types of adhesive pad deploy an adhesive liquid secretion to the contact zone during locomotion. The addition of a layer of viscous adhesive liquid can aid contact formation by filling in surface roughness and increase detachment forces by generating both capillary adhesion and viscous friction forces during detachment [46]. The influence of this secretion on adhesion & friction will be discussed in greater detail in Sections 2.3 and 2.4. The two structural designs of insect attachment pads will be described in detail separately in the following sections.

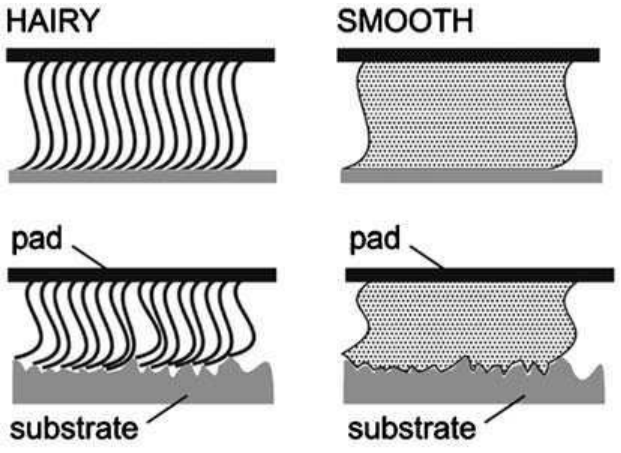

Figure 2.2.2: Hairy and smooth pad systems found in insects. Both systems are able to conform to the surface profile. Adapted from Gorb [45]

2.2.1 Smooth Pads

Smooth adhesive pads, known as *arolia* or *euplantulae*, are soft deformable organs which have a specialised internal structure which makes them capable of replicating the unevenness of various substrate profiles [23], Figure 2.2.3. Appearing smooth under optical microscopy, under greater magnification they can be seen to possess patterned microstructures on their surface, for example; the hexagonal structuring found on the cricket *Tettigonia viridissma* [48, 49], Figure 2.2.3E, or the patterns of parallel ridges running perpendicular to the length axis of the tarsus [49, 50] seen in the scorpionfly *Panorpa communis* [32]. Derived from the cuticle [17, 49] smooth pads consist of an internal structure of long, thin, rod-like filaments oriented at an angle to the cuticle surface, which in turn are composed of many single fibres [51], Figure 2.2.4. Filaments branch into finer

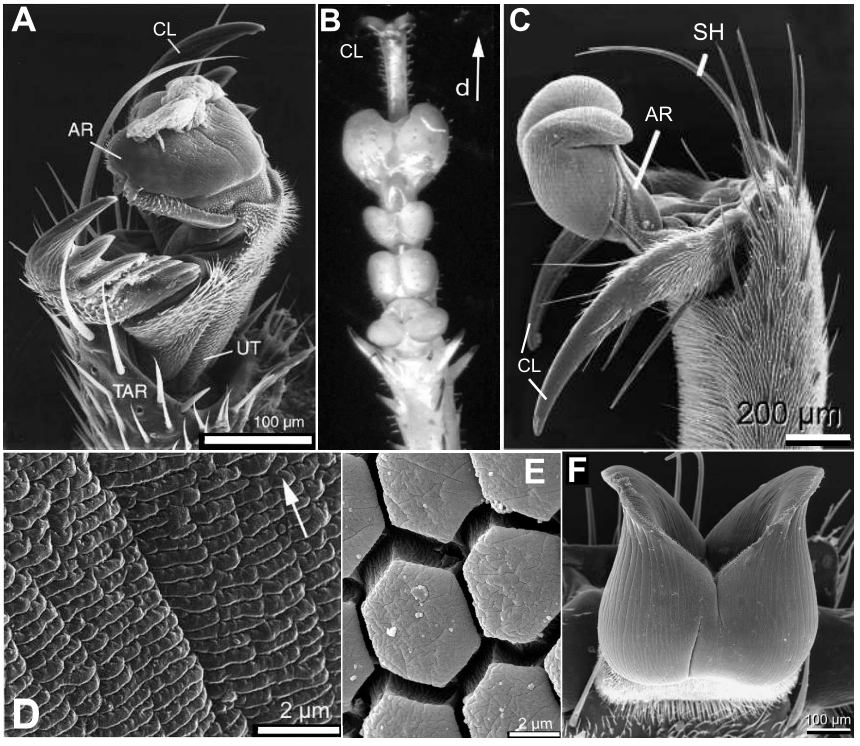

Figure 2.2.3: Diversity of smooth attachment pad external morphologyand surface structuring. A) The common scorpionfly *Panorpa communis* arolium situated between the claws, B) Tarsus of the Green Bush-Cricket *Tettigonia viridissima* with four euplantulae and claws, C) pre-tarsus of the hornet *Vespa crabro* showing claws and partially expanded arolium. D) arolium surface of *Panorpa communis*, E) Hexagonal structures of *Tettigonia viridissima* euplantulae, F) ventral view of a *Vespa crabro* partially expanded arolium showing the indented striations running along the length axis. *AR* arolium, *CL* claws, *TAR* tarsomere segment, *SH* sensing hairs, *d* distal direction. A) & D) Adapted from Beutel & Gorb [32], B) & E) Adapted from Gorb *et al.* [44], C) & F) Adapted from Frantsevich & Gorb [47].

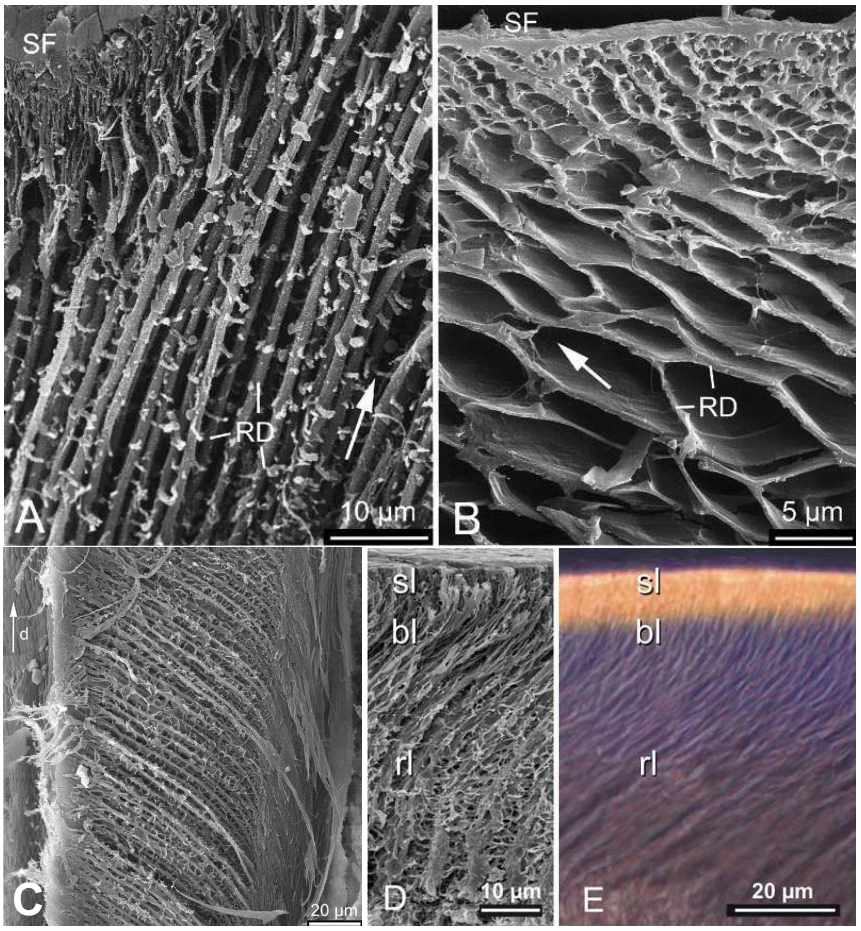

Figure 2.2.4: Internal material structure of smooth pads. A) Inner structure of the smooth pad of *Tettigonia viridissima* euplantulae, and B) *Cercopis vulnerata*, C) inner rods of euplantulae of *T. viridissima* angled at $\sim 45^\circ$ to the surface. D) SEM image of internal structure of the locust *Locusta migratoria* showing crosslinking of the rods, E) Fluorescence microscopy image of *L. migratoria* pad under the UV, green & red band (superimposed) showing increased density of crosslinking towards the surface layer. *SF* surface, *RD* chitinous threads, *Sl* surface layer, *bl* branching rod layer, *rl* primary rod layer. A) & B) Adapted from Beutel & Gorb [32], C) Adapted from Gorb *et al.* [44], D) & E) Adapted from Perez Goodwyn *et al.* [23].

fibres toward the outer epicuticle [22, 32, 49, 52]. The internal filaments can change their shape and angle of orientation under loading forces, leading to a flexibility of the pad as a whole [53], and regular cross-linking along their lengths has been hypothesised to prevent buckling during contact [23]. The internal architecture, and degree of branching near the cuticle surface is believed to correlate with the flexibility of the adhesive pads, for example; Perez Goodwyn *et al.* [23] studied the material stiffness of smooth adhesive pads of the locust *Locusta migratoria* and found the higher density of filaments and cross-linking in this species' euplantulae gave this pad a higher elastic modulus than that of the cricket *Tettigonia viridissima*.

2.2.2 Hairy Pads

The hairy pad system consists of arrays of highly ordered filament structures in the form of long thin hairs known as *setae* or *acanthae* which make contact with the substrate, Figure 2.2.5. Despite the diversity of hairy pads in arthropods, all setae are elongate structures with high aspect ratios ranging from 10 to 80 [31, 54, 55], are between several micrometers to several millimetres in length and regularly bear specialised terminal elements, or tips. These tips can have very different shapes, ranging from longitudinal, tapered tips to broadened triangular or circular end-plates, often featuring a concave surface or a bulged rim [24, 31], Figure 2.2.6. In Coleoptera, of which ladybirds and beetles are members, tips are separated into three distinct morphologies: *i*) pointed tips, *ii*) spatulate tips, and *iii*) discoidal tips, Figure 2.2.6. The large number of possible contact sites and small dimensions of the tips leads to a large area of close contact between the organism and the substrate, generating strong adhesion forces. The setal hairs of the adhesive pads, in their bulk form, are fairly rigid with an elastic modulus in the MPa - GPa range

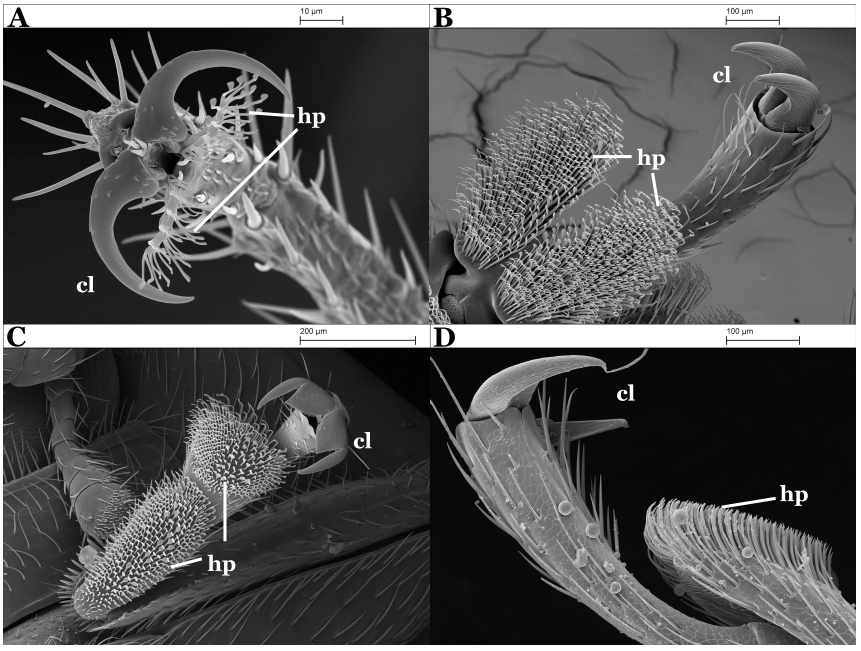

Figure 2.2.5: Diversity of hairy adhesive pads. A) The fly *Drosophilia melanogaster*, B) the Cardinal beetle *Pyrochroa coccinea*, C) the 2-spot ladybird *Adalia bipunctata*, and D) the Harlequin ladybird *Harmonia axyridis*. Scale bars A) 10 μm B,D) 100 μm and C) 200 μm. Images taken by T. Sinclair of University of Hull. *cl*: claws, *hp*: hairy pad.

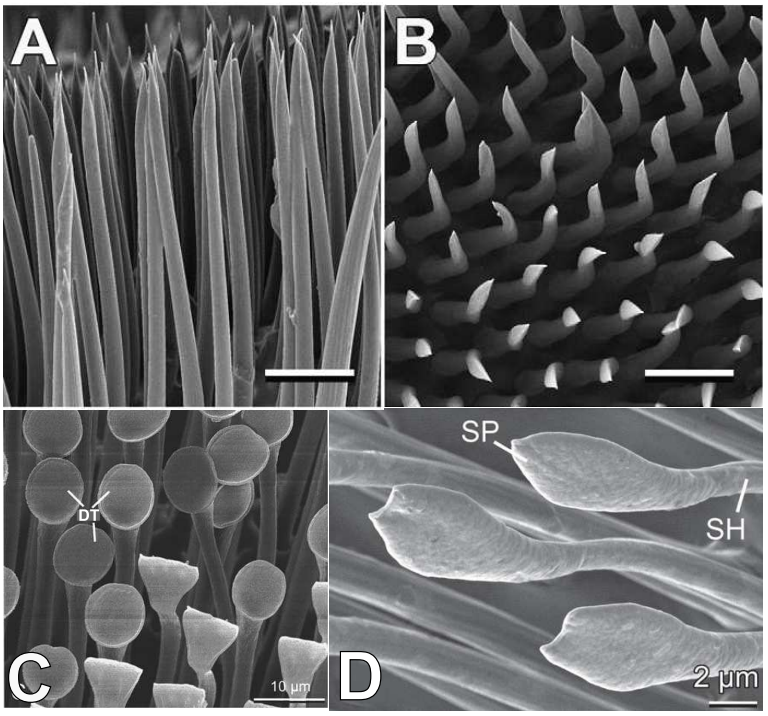

Figure 2.2.6: Different seta tip geometries in insects. A) & B) Pointed tips of the beetle *Leptinotarsa viridula* (from Voigt *et al.* [6]), C) Discoidal tips from the beetle *Chrysolina fastuosa* (from Gorb & Gorb [55]), and D) Spatulate tips from the dock beetle *Gastrophysa viridula* (from Hosoda & Gorb [56]). Scale bars A),B) 20 μm, C) 10 μm, D) 2 μm. sp, spatulae, sh, shaft, dt, discoidal tip.

[57, 58]. In a number of insects it has been demonstrated that the proportions of different tip geometries within their pads can generate varying forces on either smooth or rough substrates [6, 27, 59], a subject which will be returned to in Section 2.4. Due to the large numbers, ordered distribution and high aspect ratio of setae, the hairy pad as a whole has a relatively low *effective* elastic modulus, Equation 2.1.1. The 'dry' hairy pad system of the gecko lizard is perhaps the most highly structured, and the most extensively studied hairy pad to date. In this case forces of adhesion primarily derive from van der Waals forces, and it is often stated as fact that the Gecko does not use an adhesive secretion, however some debate over this has emerged in recent literature [60–62]. Contribution of van der Waals forces to insect adhesion has been considered in a small number of studies, and will also be discussed at greater length in section 2.4.

2.3 Adhesive Secretion in Insects

The presence of a liquid secretion delivered from insect adhesive pads during locomotion was proposed by Blackwall in 1830 [2] and has been observed experimentally for some time since then [14, 34, 37, 63–65]. Its presence is ubiquitous across both functional forms of attachment pads in insects and has been studied across numerous insect species and taxa, including Coccinellid beetles [35, 66], flies [37], cockroaches [33], ants [12], reduviid bugs [67], grasshoppers [39], locusts [21] and aphids [65, 66], amongst others. Although both adhesive pad morphologies facilitate high levels of deformability, maximising contact area with diverse substrates, there is still a limit to how much a pad can deform to follow very rough substrates. The addition of a liquid film to the contact zone would increase contact area, Figure 2.3.1 [46, 68]. In addition, the adhesive secretion contributes to adhesion and friction through the actions of capillary and viscous forces, although the underlying physical mechanism for this adhesive process is still not fully understood. An early study by Edwards & Tarkanian [67] found adhesion forces of the insect *Rhodnius prolixus* treated with solvents were much poorer than untreated pads, and Dixon [66] found adhesion forces on smooth substrates in aphids decrease dramatically after they were made to walk over silica gel. Both studies concluded that the liquid secretion is indeed crucial for adhesion, and Stork [34] established that the liquid adhesive played a fundamental role during adhesion to smooth surfaces in the beetle *Chrysolina polita* due to surface

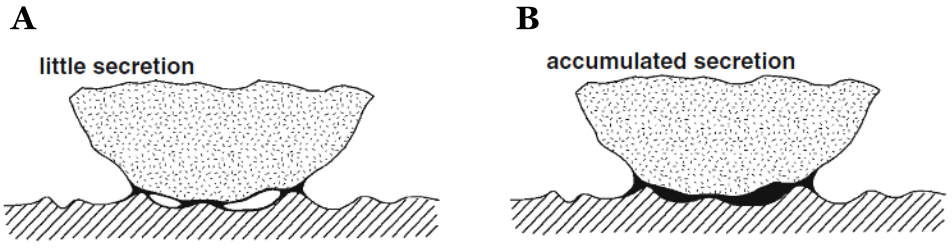

Figure 2.3.1: Schematic diagram illustrating the adhesion-enhancing role of insect pad secretion on a rough substrate. Due to the surface roughness, the pad cannot completely fill the substrate cavities. A) When there is only little secretion only small menisci form at the tips of surface asperities and the real area of contact is small. B) If there is more liquid present in the contact zone, 'accumulated secretion', the small menisci merge and create a larger contact area, giving rise to greater adhesion. Adapted from Drechsler & Federle [68].

tension forces and capillary action, which has been further confirmed by more recent studies through various experimental procedures [69, 70]. The influence of the tarsal secretion on attachment performance in the stick insect *Carausius morosus* was investigated by Drechsler & Federle [68] who found that when secretion was depleted by continuous pull-off actions on rough substrates adhesive forces decreased, demonstrating that one of the primary functions of the adhesive secretion is to provide sufficient attachment to rough surfaces by increasing the contact area between pad and substrate. Similarly it was found in toe pads of tree frogs that attachment to very rough surfaces was improved by wetting the surface with a stream of water [71].

2.3.1 Chemical Composition

The composition of any given secretion is a highly complex mixture of many types of molecules [19], and as such the exact composition is likely to have an influence on the adhesive forces generated. Early observations of footprint deposits on smooth substrates indicated a stable, hydrophobic liquid and early studies hypothesised that this liquid would have an oily composition [65]. Several studies have attempted to characterise the composition of these tarsal adhesive secretions using techniques including thin-layer chromatography (TLC) [35], gas-chromatography mass-spectrometry (GC-MS) [72, 72, 73], and infra-red spectroscopy [36], yet the modes of action of the compounds detected in these secretions during the adhesive process are still relatively poorly understood.

Nonetheless, it is known that arthropod adhesives used for locomotion have constituents generally belonging to: aliphatic lipid compounds, carbohydrates, amino acids and proteins, amongst others, consistent with the hypothesis that it is a hydrophobic liquid. The first studies to report chemical analyses of these secretions by use of TLC of the ladybird *Epilachna vigintioctomaculata* reported mainly hydrocarbons, triglycerides, fatty acids and alcohols [35]. Vötsch *et al.* [21] studied the composition of footprints of the locust

Locusta migratoria using GC-MS, finding shorter-chain fatty acids (C_{16}-C_{20}) and significant amounts of polar components, whereas more recent studies in beetles and ants found mainly hydrocarbons and waxes, together with mixtures of saturated and unsaturated linear hydrocarbons of chain length C_{20}-C_{28} which corresponded well to the composition of the cuticular lipid layer [36, 74–77]. The epicuticular lipid layer which naturally covers the body of insects has long been known to protect the insect from dessication due to evaporative water loss (see [63, 73, 78–80]), as well as contain a multitude of chemical communication cues [81, 82], particularly in the social insects (*eg.*, termites and ants) [83]. Several studies making comparison between the composition of cuticular lipids and that of the adhesive secretions [36, 72, 74, 77, 84] have found a strong chemical congruence between the two, suggesting that adhesive secretions may be a derivative of the cuticular lipid layer.

Some microscopy evidence exists to support the hypothesis that these secretions may have an emulsion composition including stable hydrophobic and volatile hydrophilic components for the purpose of acting as a coupling agent between otherwise incompatible materials [21], which shall loosely be referred to as the *emulsion hypothesis*, and will be discussed in more detail in the following section. However, as pointed out by Geiselhardt *et al.* [77], even after several studies of the composition of insect adhesive secretions, in several species, in no case has a volatile hydrophilic liquid been successfully characterised directly. Thus a general lack of consensus regarding the chemical nature of these secretions in insects prevails.

2.3.2 Physical Properties of Insect Secretion

Secretion deposits consisting of microscopic droplets can be easily observed with light-microscopy after insects have walked across a smooth substrate, particularly under phase-contrast microscopy. The pattern of deposited droplets usually conforms to the geometry of the insect adhesive pad which deposited them. For example, insects with hairy pads

such as ladybirds deposit prints with a regular pattern corresponding to the distribution of the setal hairs, Figure 2.3.2, whereas smooth pads leave randomly distributed deposits [39]. Adhesive secretion deposits generally have low contact angles with hydrophilic surfaces [12, 85], are able to wet substrates with a range of surface energies, and can be found several hours after deposition suggesting at a non-volatile, hydrophobic composition. Hasenfuss [85] observed that droplets left behind by several insect species remained liquid for several weeks when left in air, solidifying thereafter by oxidation, and the droplets' liquidity could be maintained by keeping the droplets in an oxygen-free environment. These fluid droplets can also be well visualised and characterised using interference reflection

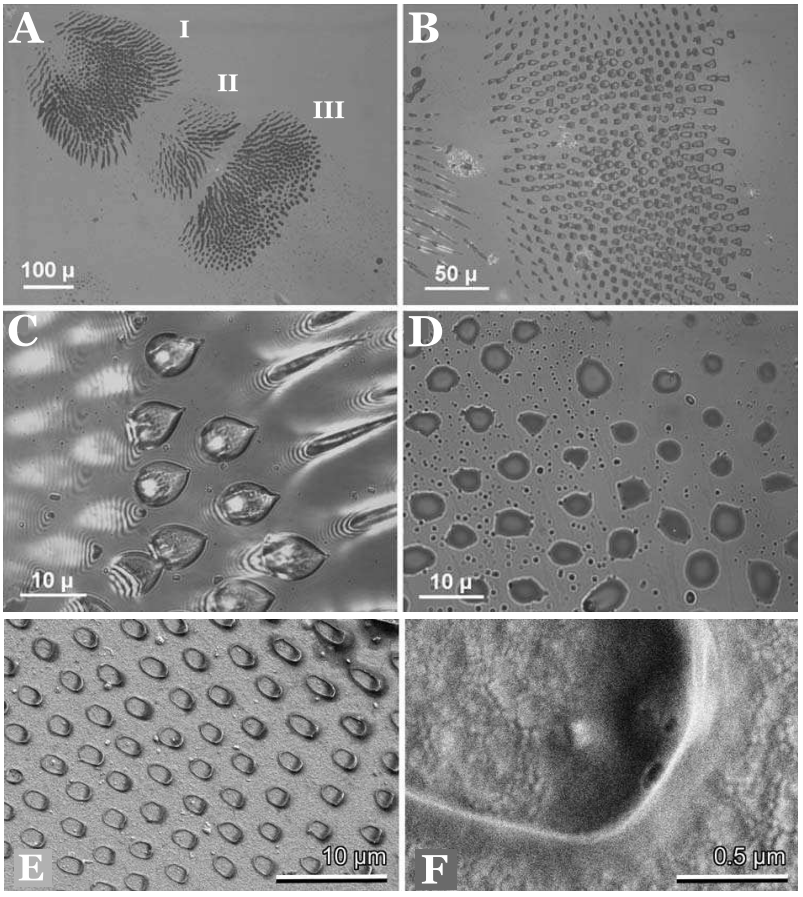

Figure 2.3.2: A-C) Interference microscopy images of *G. viridula* tarsal adhesive setae in contact with a glass plate, and D) of droplets of adhesive liquid deposited by individual setae at detachment. E–F) Cryo-SEM image of uncoated footprints of the fly *Calliphora vicina*, frozen while the adhesive hairs were in contact with the substrate. Fluid menisci between each hair tip and the substrate can be seen. A) *Top left to bottom right* tarsal segments I-III, B) tarsal segment III with simple pointed setae (*left*), discoidal (*centre*) and spatula-shaped setae (*right*), C) two types of adhesive hairs in contact with glass: discoidal setae on the left and pointed on the right; interference rings indicate zones of incomplete contact. E) An array of prints, corresponding to the pattern of setal hairs of the adhesive organ. F) Meniscus of the print of a single hair tip. A-D) Adapted from Geiselhardt *et al.* [84], E-F) Adapted from Gorb *et al.* [86].

microscopy (IRM), which can be used to gather information about droplet volume and contact angles [87]. Bauchenß [88] measured the contact angles of the secretion of the blue blowfly *Calliphora erythrocephala* on a variety of solid surfaces, including glass, plant leaves, and polyethylene; the observed contact-angles were between 16 and 28°, and an angle of 50° was measured on polytetrafluoroethylene (PTFE). However, characterisation of small-volume droplet parameters becomes significantly more difficult as the size of the individual droplets decreases. Conventional scanning electron microscopy (SEM) techniques fail due to the vacuum required for imaging, and the instability of the liquid droplets under the electron beam [86]. This issue has been partly resolved with the use of environmental-SEM (ESEM) - but this system is restricted in its resolution. Recently Gorb *et al.* [86] developed a cryo-SEM method to visualise fluid droplets in contact with biological and artificial interfaces. The freezing of liquid droplets also allowed for the use of transmission electron microscopy (TEM) to view secretion droplets of the locust *Locusta migratoria* [21]. Droplets were found to be circular and flat, and to contain smaller droplets on their surface which were interpreted as evidence for a dispersed phase within the bulk liquid.

Atomic force microscopy (AFM) can also be used to detail characteristic properties of liquid droplets, however to date, this approach has only been used in a single study to investigate the adhesive secretion of insects. Peisker & Gorb [89] followed the evaporation dynamics of tarsal footprints in the fly species *Calliphora vicina* and the 7-spot ladybird *Coccinella septempunctata*. Although this approach is capable of achieving relatively high resolution, the scanning procedure can take a long time and the volume of any volatile liquids cannot be measured due to fast-acting evaporative effects, limiting its usefulness for answering questions regarding the emulsion hypothesis.

Federle *et al.* [12] performed *in vivo* observations of ant secretion in the contact zone *via* IRM and reported that the liquid consists of an oily bulk phase containing dispersed hydrophilic droplets [90]. Some authors have proposed that an emulsion composition would act to promote and strengthen adhesion between incompatible substrates [21, 49]. However, whilst a valid point, this hypothesis may be unnecessary since liquids with low

polarity can wet substrates with high surface polarity if the substrate also shows a high free-surface energy, and surfaces with low surface polarities, such as waxy plant surfaces, can still be wetted by nonpolar compounds if the surface polarities of the two surfaces are not too dissimilar [19, 91], see Chapter 5. Thus, the benefits to insect attachment of an emulsion composition to the secretion and how it may aid adhesion is still a topic of debate and active investigation. Insect liquid adhesives are a currently under-explored source of adhesives and may have large biomimetic application potential. For example, clinical and medical fields have a need for strong, bio-compatible adhesives able to work in humid or wet environments, and potential applications may include wound healing, surgical repair and dentistry.

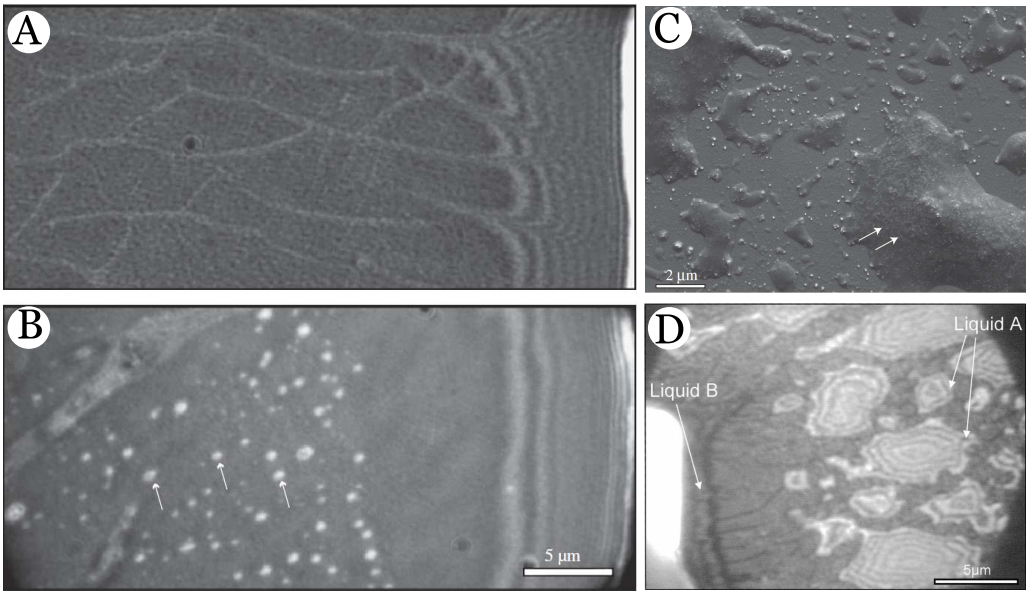

Figure 2.3.3: Evidence for emulsion composition of adhesive secretion, visualised with IRM. A-B) Secretion liquid of stick insects *C. morosus* on A) thick (2-4 μm) absorbent polyimide-coated surface which removes any water components from the droplets, and B) thin (0.6-0.9 μm) polyimide substrate. The presumed hydrophilic component of the emulsion (droplets, arrows) was only visible for pads in contact with the thin polyimide, indicating that the absorption is smaller owing to the insufficient volume of the polymer layer. C) Cryo-SEM image of a footprint of *C. morosus* on glass. The fluid droplets contain nano-structures (arrows). D) Two-phase adhesive secretion in the pad contact zone of the ant *O. smaragdina* on glass. Liquid A is immersed in the bulk Liquid B. A-C) Adapted from Dirks *et al.* [90], D) Adapted from Federle *et al.* [12].

2.3.3 Delivery of Secretion to Contact Zone

The exact origins of the tarsal secretion is still unclear, however it is known that insects possess many different glandular cells in their cuticle for the production of the vast array of pheromones and chemicals used for different signalling functions, generally known as *exocrine glands*. For insects possessing the hairy pad system, evidence for channels within the setal hairs exists which could function to deliver the adhesive secretion to the contact zone *via* routes within the cuticle [92], but this is still to be confirmed. Geiselhardt *et al.* [72] found that addition of synthetic hydrocarbons to the cuticular hydrocarbons of the beetle *Leptinotarsa decemlineata* led to these compounds being detected within the tarsal secretion after several hours, confirming in beetles atleast, that transport of lipids from the cuticle to the tarsal adhesive secretion can occur. The changes incurred within the tarsal secretion also influenced attachment forces of these insects.

Dirks & Federle [92] investigated the rate of adhesive secretion production from the smooth pads of the stick insect *Carausius morosus* and the cockroach *Nauphoeta cinerea* and found that the 'sponge-like' internal structural morphology of smooth adhesive pads, Figure 2.2.4, provides for a storage volume of secretion which is constantly replenished within the cuticle [92], but can be depleted over the course of consecutive steps. It was proposed that the adhesive pads mechanically control the release of fluid upon contact through deformation of the soft cuticle, and that the adhesive fluid is either mechanically driven into the contact zone *via* compression of the pad, or by capillary action, and it was suggested that the volume of secretion deposited during contact may be controlled *via* passive mechanisms, such as capillarity, ensuring the right amount of fluid reaches the contact zone [40]. Several authors have also hinted at the possibility of direct neuronal control of the secretion volume delivered to the contact zone [92], for example; free running *Phytolacca americana* cockroaches were observed to deposit no visible footprints, but pads manually placed on a substrate left 'greasy' imprints [33], and so neuronal control over secretion deposition cannot be wholly ruled out.

2.4 Adhesion Forces

Different surface forces will act in varying degrees of magnitude and direction dependent upon the particular attachment scenario the insect is engaged in, such as; climbing, remaining stationary, running, landing or reattachment to a surface after falling. Detachment forces an insect may encounter can differ strongly in their direction and magnitude, and must be withstood under both dynamic and static scenarios. Forces can act in the direction perpendicular (normal) to the substrate, or in the direction parallel (tangential) to the surface, Figure 2.4.1. In the early period of investigations into insect adhesion, several possible attachment mechanisms were proposed. These included attachment *via* suction, interlocking with surface asperities, electrostatics, or adhesion through surface tension. It has since been confirmed that the principle mechanisms by which insects adhere to surfaces

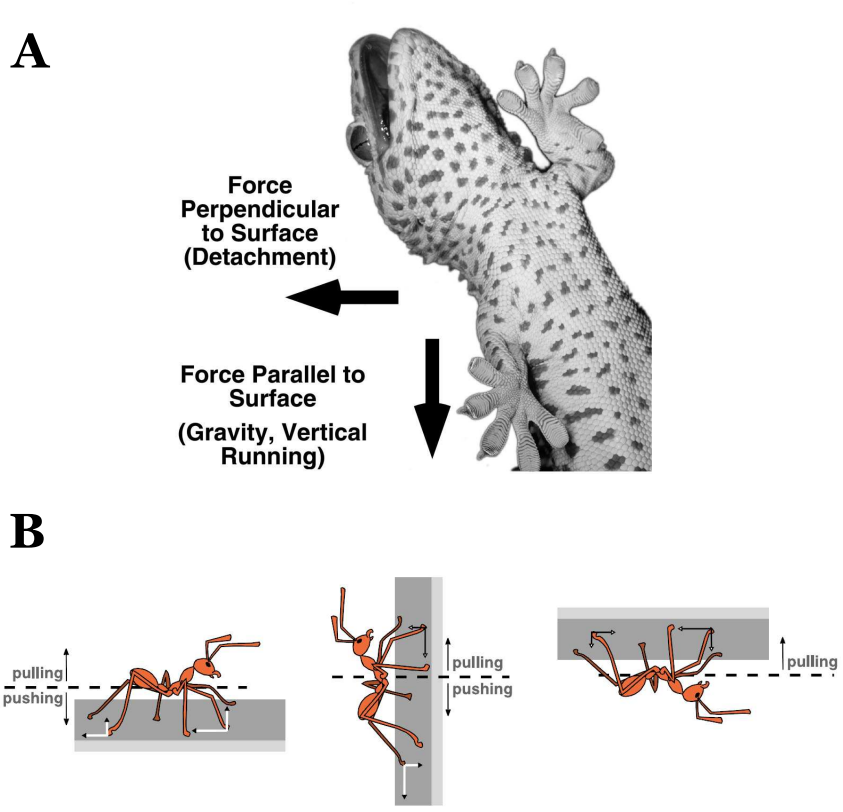

Figure 2.4.1: A) Ventral view of a tokay gecko (*Gekko gecko*) climbing a vertical glass surface. Arrows represent the forces acting on the gecko's feet as it climbs. Adapted from Autumn & Peattie [93]. B) An insect walking under different orientations. When climbing vertically the legs above the center of mass pull inward while the legs below the center of mass tend to push the animal upward. Inverted, the animal must pull inward across all legs to remain attached, adapted from Peattie [28].

are capillary adhesion, viscous forces due to the secretion, and possible contributions from intermolecular, van der Waals forces, derived from direct contact between the adhesive pad and the substrate. In the remainder of this section we will describe contact mechanics models such as the JKR (Johnson-Kedall-Roberts) model, DMT (Derjaguin-Muller-Toporov) model, and Griffith fracture theory, and discuss the types of adhesion forces to be found in insect adhesion systems. In section 2.5 frictional forces will be discussed.

2.4.1 Forces in Dry Environments

2.4.1.1 Interfacial Energy & Work of Adhesion

Before discussing how different surfaces interact with each other during adhesion it is convenient to first introduce the concepts of interfacial energy and the work of adhesion.

When two materials A & B contact each other, the interface between them has an energy γ_{AB} associated with it [94]. The *work of adhesion* is the free energy change, or reversible work done, per unit area to separate the two media A and B from contact to infinity, and is denoted by W_{AB} [94, 95]. The energy associated with creating a unit of surface area of a material exposed to vacuum is equivalent to separating two half-units from contact defined as γ_A and γ_B, Figure 2.4.2. When two interfaces are created the change in total free energy going from contact to separation is given by:

$$W_{AB} = \gamma_A + \gamma_B - \gamma_{AB} \tag{2.4.1}$$

where γ_{AB} is the interfacial energy of the A/B interface. The first two terms are the final free energy, and the third term is the initial free energy [95]. Rearranging Equation 2.4.1 gives us the *Dupré equation*:

$$\gamma_{AB} = \gamma_A + \gamma_B - W_{AB} \tag{2.4.2}$$

For solids (S) adhering in a liquid medium (L), Good and Girifalco [96, 97] developed an approach of estimating the solid work of adhesion W_{SL} as the geometric mean of γ_S and

γ_L using:

$$W_{SL} = 2\Phi\sqrt{\gamma_S \gamma_L} \tag{2.4.3}$$

where Φ is a correction factor dependent upon the correlation between intermolecular interactions between the two media. If they are similar then Φ is close to unity. If the interactions are dissimilar, Φ is less than unity, usually taking a value around 0.5 [94].

In reality, when the creation of new interfaces occurs within a third medium, such as a vapour phase, adsorption of vapour molecules such as water, or hydrocarbons, will take place. This has the effect of reducing the surface energy of materials from their theoretical values in a vacuum.

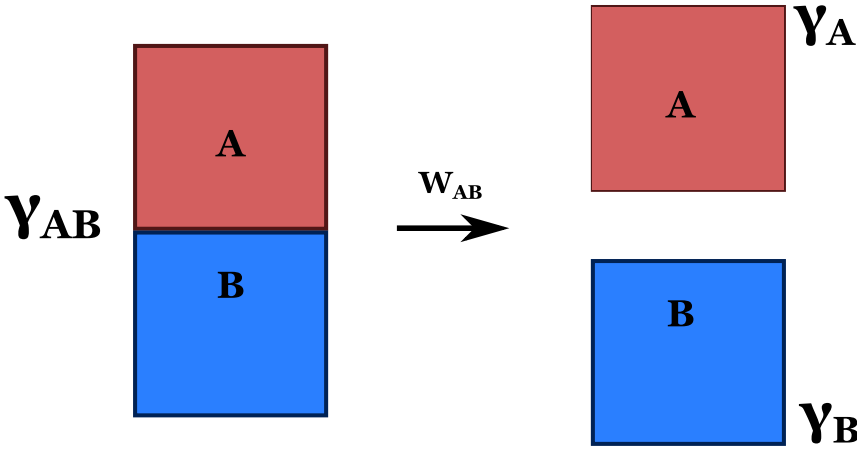

Figure 2.4.2: Schematic depicting the change in free surface energy - or work of adhesion - when moving two planar surfaces from contact to separation.

2.4.1.2 Physical Origin of Dry Contact Forces

The intermolecular forces that determine a materials' surface energy are the same as those that determine properties such as latent heat and boiling point [95], and substances with high boiling points, such as metals, usually also have high surface energies. At very close separation distances there exists interactions between individual atoms and molecules, other than those due to covalent bonds or the electrostatic interaction of ions, but due to the interaction of those molecules' electric dipoles known as van der Waals (VDW), intermolecular forces.

Three types of VDW interactions occur, shown in Figure 2.4.3, namely the permanent dipole-permanent dipole (Keesom), permanent dipole-induced dipole (Debye), and induced dipole-induced dipole (London or Dispersion) interactions [95].

Because these forces are always present between atoms, being relatively long ranged and attractive or repulsive [95], they play an important role in a number of phenomena such as adhesion, surface tension and wetting [95], the properties of thin films [98] and the behaviour of colloidal solutions and powders [99].

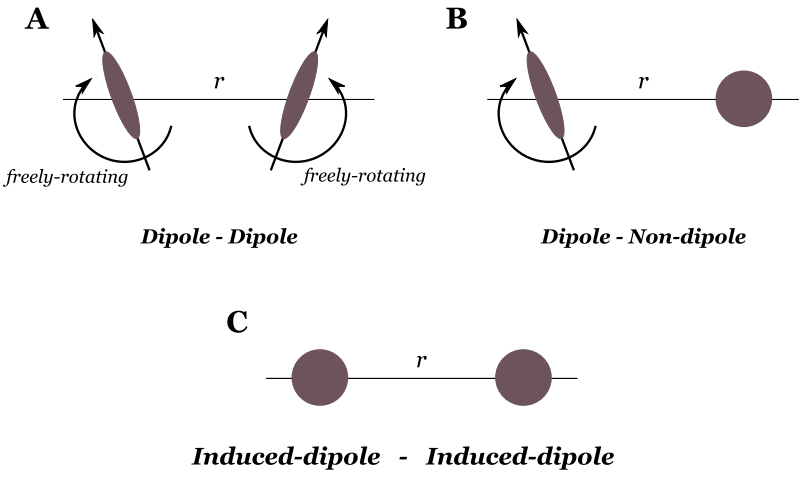

Figure 2.4.3: Schematic of the three types of van der Waals interactions between molecules. A) *Orientation interaction* between two freely rotating polar molecules, B) *Induction interaction* between a polar molecule and a non-polar molecule, C) *Dispersion interaction* between two non-polar molecules.

2.4.1.3 Van der Waals Interactions Between Parallel Plates

The van der Waals energy per unit area between two parallel plates is given by [95]:

$$\omega(D)_{flat-flat} = -\frac{A}{12\pi D^2} \tag{2.4.4}$$

where A is the so-called *Hamaker* constant [94]. The above expression is valid for the interaction between two planar surfaces provided the separation distance between the surfaces D is much less than the length scale of the surface, but limited by the lower value that D can take.

The limiting value of D is usually taken to be approximate to an atomic distance, and Israelachvili [95] takes the absolute 'cut-off' distance to be D=0.165 nm. From the interaction energy, the VDW force per unit area acting between two surfaces is determined as:

$$F(D)_{flat-flat} = \frac{\partial \omega(D)_{flat-flat}}{\partial D} = -\frac{A}{6\pi D^3} \tag{2.4.5}$$

2.4.1.4 Griffith criteria - Cohesive Failure *vs.* Crack Propagation

In truth, Equation 2.4.5 described above represents the theoretical maximum stress required to separate two flat interfaces from each other, if detachment occurs through cohesive failure.

Griffith [100] showed in 1921 that if the dimensions of an interface exceeds a critical length, failure will occur *via* crack propagation - or peeling - from the edge of the contact zone. A key concept in the theory of crack propagation and flaw tolerance is that cracks confined to a small interface do not propagate until the stress of the material around the crack uniformly reaches the theoretical strength of the material σ_{th} [101, 102]. In this case the strength of the material can be calculated as [103]:

$$\sigma = \sqrt{\frac{4\gamma E^*}{h_c}} \tag{2.4.6}$$

where γ is the surface energy, h_c is a characteristic length scale of the interface, and $E^* = E/(1-\nu^2)$ with Poisson ratio ν. The strength of the material approaches its maximum theoretical value as the length scale of the interface is reduced. Rearranging Equation 2.4.6 it is found that a crack will propagate if its length exceeds a critical value given by the *Griffith criterion*:

$$h_c \geq \frac{\alpha \gamma E^*}{\sigma_{th}^2} \tag{2.4.7}$$

where α is a parameter determined by the geometry of the crack [102] (and usually takes values < 5). Using Equation 2.4.7, with typical values for the parameters of van der Waals interactions and the Young's modulus of keratin spatulae in geckos, as quoted by Gao *et al.* [27] of $\sigma_{th} = 20\ MPa$, $\gamma = 0.01\ Jm^{-2}$ and $E^* = 2\ GPa$, an estimate of the critical length scale for the gecko lizard yields a value $h_c \cong 225\ nm$ which matches well with the radii of gecko spatula, typically around 100–250 nm [27]. Using typical values for the setae of beetles [104] of $E^* \sim 1\ GPa$ and $\gamma = 50\ mJm^{-2}$ gives a value of approximately 500 nm.

Typical dimensions for setae in insects are greater than h_c (eg., radius $> 1\ \mu m$, see Chapter 4), so in constructing adhesion models for insects, a more realistic model for adhesion failure in hairy pads would be that of a rigid sphere-on-flat geometry, which will be explained in the following sections. For soft adhesive pads, detachment generally also occurs *via* peeling as described by the JKR model for a soft sphere-on-flat. Departures from JKR theory can occur for situations involving large detachment velocities due to the viscoelastic material properties, which are discussed in Chapter 6.

2.4.1.5 Dry Contact Force Between Sphere & Plate

Since many flat interfaces detach *via* crack propagation it is useful to calculate detachment forces between curved surfaces which more accurately predict the adhesive strength of the interface. Additionally, in reality, surfaces are rarely perfectly flat and on the microscopic scale, (eg., comparable to the range of the VdW forces) the surface roughness of a substrate

or of an insect attachment pad, may have a significant influence on the adhesive forces. Although Equation 2.4.5 depicts the interaction between two planar surfaces it is often applied to the interaction between non-parallel solids, as first proposed by Derjaguin. The *Derjaguin approximation* states that the interaction energy between two small solid surfaces, which may be curved or slightly inclined to each other, is the same as the energy per unit area between two parallel planes if the separation distance D of the two surfaces is significantly less than their radii of curvature [94]. For two spheres with radii R_1 and R_2 for any force law that is a function of separation distance:

$$F(D)_{sphere-sphere} = 2\pi \left(\frac{R_1 R_2}{R_1 + R_2} \right) W(D) \tag{2.4.8}$$

making it possible to estimate the force between two spheres of radii R_1 and R_2 separated by a distance D from the interaction energy per unit area W of two planar surfaces separated by the same distance [94, 95].

Rigid Sphere-on-Plate

For a given geometry, the form of the dry contact force also depends on the rigidity of the contacting materials [94]. For a rigid sphere on a rigid flat surface, Figure 2.4.4, with $\gamma_A = \gamma_B = \gamma$ so that $W_{AB} = 2\gamma$, and assuming the surface roughness to be negligible, ($D \rightarrow$ atomic distance), $W(D)$ becomes the work of adhesion W_{AB} and the dry contact force is described by the Derjaguin-Muller-Toporov (DMT) model [94, 105]

$$\begin{aligned} F^N_{DMT} &= 2\pi R W_{AB} \\ &= 4\pi R \gamma \end{aligned} \tag{2.4.9}$$

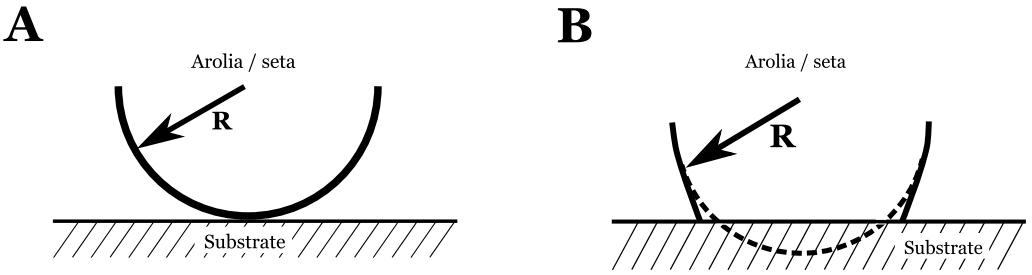

Figure 2.4.4: Schematics for different contact-geometries of insect attachment devices. A) Rigid sphere on a flat, B) soft sphere on a flat.

Soft Sphere-on-Plate

However, the DMT model is limited in its applicability, to rigid particles. For soft adhesive contacts, the dry contact force is described by the Johnson-Kendall-Roberts (JKR) model [106]. Consider two spheres of radii R_1 and R_2, and surface energy W_{12} per unit area, which flatten when pressed together under an external load F such that the contact area has a contact radius given by:

$$a^3 = \frac{R}{K}\left[F + 3\pi R^* W_{12} + \sqrt{6\pi R^* W_{12} F + (3\pi R^* W_{12})^2}\right] \tag{2.4.10}$$

where R^* is the reduced radius of curvature, defined as:

$$R^* = \frac{R_1 R_2}{R_1 + R_2} \tag{2.4.11}$$

with bulk elastic modulus K, given by:

$$\frac{1}{K} = \frac{3}{4}\left(\frac{1-\nu_1^2}{E_1} + \frac{1-\nu_2^2}{E_2}\right) \tag{2.4.12}$$

where $\nu_{1,2}$ is the Poisson ratio of each surface. Thus, for a sphere of radius R on a flat surface $R_2 = \infty$, $R_1 = R$ and if both surfaces have the same surface energy γ, under zero load ($F = 0$) the contact radius has a finite value and under small negative loads ($F < 0$) the solids remain in contact until some critical negative force is reached where the surfaces suddenly jump apart. For a sphere-on-flat geometry the adhesion or 'pull-off' force is given

by:

$$F_{JKR}^{N} = \frac{3}{2}\pi R W_{AB}. \tag{2.4.13}$$

The above equation has been verified experimentally in studies showing that contacting surfaces separate spontaneously when the contact radius drops to approximately 60% of the equilibrium radius a_0. As a result, the DMT model predicts detachment to occur *via* cohesive failure of the contact while in the JKR model, detachment occurs *via* peeling from the edge of the contact zone.

Transition from DMT to JKR

In the limit of small deformations the adhesion force changes from the 'JKR limit', Equation 2.4.13, to the 'DMT limit', Equation 2.4.9, since each model represents a limiting case where one extreme is strong adhesion with highly compliant materials and the other extreme is low adhesion with rigid materials. Maugis [107] showed that the transition from the JKR to DMT limit depends on a single dimensionless parameter:

$$\lambda_M \approx \left(\frac{R\sigma_0}{Y\delta_c}\right)^{1/3} \tag{2.4.14}$$

where σ_0 is the critical stress for detachment of the dry contact, Y is the Young's modulus of the adhesive pad and δ_c is the range of the van der Waals force. Large values of λ_M correspond to the JKR limit while small values of λ_M correspond to the DMT limit. In the context of insect attachment devices, for smooth adhesive pads, the arolium is soft (Y small) [23] and R is large, and it is assumed the JKR limit is valid. Conversely, for hairy pads of ladybirds, individual setae are hard (Y large) and R is small, so it is assumed the DMT limit is valid, see Chapter 4.

2.4.2 Forces in Wet Environments

2.4.2.1 Capillary Force

The mechanical and adhesive properties of most surfaces are sensitive to the presence of even trace amounts of vapour in the atmosphere, and in nature the influence of water vapour due to the relative humidity of the surrounding air can be particularly influential.

Capillary Force Between Parallel Plates

The presence of liquid between contacting surfaces gives rise to capillary forces, Figure 2.4.5. If a liquid film with surface tension γ_L separates two surfaces by a distance h it forms a capillary bridge characterised by a radius r_1 and a surface area $A = \pi r_2^2$ [94], Figure 2.4.5. The pressure difference $\triangle P$ associated with a curved liquid surface is known as *Laplace pressure* and is described by the equation derived by Young and Laplace in 1805:

$$\triangle P = \gamma \left(\frac{1}{r_1} - \frac{1}{r_2} \right) \tag{2.4.15}$$

where r_1 and r_2 are the principle radii of curvature of the curved surface, the geometric signs of which depend on which way the surfaces are curved. If the surfaces are clean and hydrophilic, water makes a small contact angle θ ($< \pi/2$) so the meniscus takes a concave arrangement and the wetted surfaces can stick together with considerable strength. Contact angles greater than $\pi/2$ generate a positive pressure which works to separate the two surfaces. The adhesive force due to the meniscus is the sum of two components: a surface tension force F_{ten} and a capillary pressure force F_{cap} [94, 95].

However, when a meniscus is small the magnitude of the surface tension contribution is small compared to that from the Laplace pressure, F_{cap}, and the meniscus force can be approximated as being equal to the capillary force ($F_{men} \approx F_{cap}$) [16, 95]. The adhesive force due to the Laplace pressure, is simply the product of the Laplace pressure and the

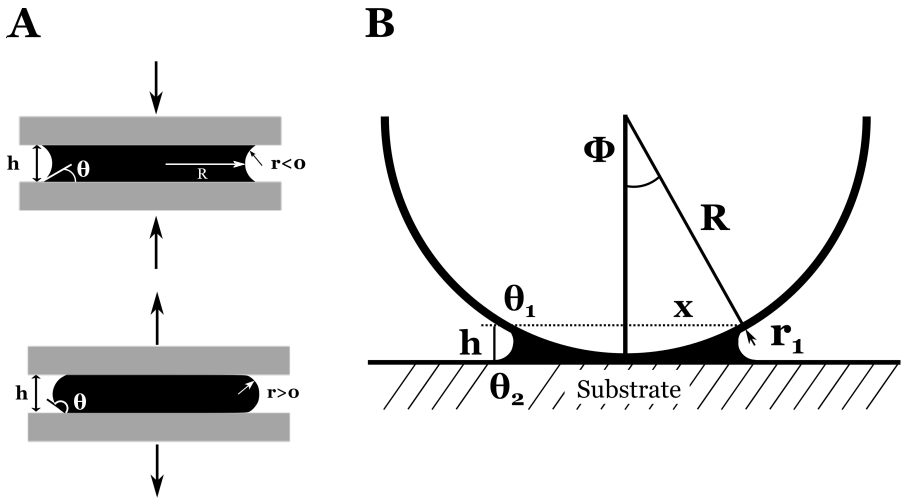

Figure 2.4.5: Capillary bridge geometries. A) Capillary bridge between two planar surfaces with a contact angle θ, separated by a distance h. When the contact angle is less than 90° the pressure difference across the air-liquid interface is negative, and positive if the contact angle is greater than 90°. B) Capillary bridge separating a spherical particle with radius R from a flat surface.

contact area πx^2, and is given by:

$$F^N = \gamma\pi R^2 \left(\frac{1}{r} - \frac{1}{R}\right) \approx \frac{\gamma A_c}{r} \tag{2.4.16}$$

where γ is the surface tension of the secretion, R is the radius of the contacting sphere, r is the radius of curvature of the liquid meniscus at the edge of the liquid film, and in the second equality, we assume that $R \gg r$, see Figure 2.4.5.

Capillary Force Between Rigid Sphere & Plate

For a rigid sphere on flat geometry, Figure 2.4.5B, the Laplace pressure given by Eqn 2.4.15 acts over an area of $\pi x^2 \approx 2\pi Rh$, where R is the radius of the particle. For small filling angle Φ, $h \approx 2r_1 cos\theta$, and the force pulling the surfaces together is:

$$F = \gamma \left(\frac{1}{r_2} - \frac{1}{r_1}\right) \approx 2\pi R\gamma_L(cos\theta_1 + cos\theta_2) \tag{2.4.17}$$

Capillary Force Between Soft Sphere & Plate

To estimate the adhesive force between a soft elastic material and a rigid flat surface we consider a soft material with Youngs modulus E and Poisson ratio ν that is covered by a uniform thin film of adhesive secretion of thickness h and surface tension γ. Assuming that the attractive force arises from capillary forces due to the adhesive secretion and that the secretion perfectly wets both surfaces, the attractive force between them is given by

$$F = 4\pi\gamma R + \left(\frac{\pi\gamma}{2r}\right)^3 \frac{2R^2}{3E^{*2}} \tag{2.4.18}$$

where R is the radius of the particle, r is the radius of curvature of the meniscus formed by the thin film of adhesive secretion wicking up around the particle, and $E^* = E/1 - \nu^2$ is the effective elastic modulus.

The first term on the right-hand side of Equation 2.4.18 represents the capillary force between a rigid particle and a rigid flat substrate [94] whereas the second term is the additional contribution to the capillary force arising from the deformation of the soft elastic pad [108]. For soft substrates with small menisci of radii r, the second term can be significant. However, its exact magnitude is difficult to estimate because it contains a number of parameters such as E, ν and r that are difficult to measure and are therefore not accurately known for the system at hand. Fortunately it is sufficient to approximate this force using only the first term if it is noted that this will therefore represent a *lower bound* estimate, due to the extra contribution of the second term (see discussion in Chapter 7 and Appendix A).

2.4.2.2 Normal Viscous Force - Stefan Force

Because the viscosity of a liquid corresponds to its resistance to shear movements, the presence of a liquid between contacting surfaces can also give rise to an adhesive force, known as 'Stefan adhesion'. Modelled from fluid mechanics, the form of the equation and strength of the force is determined by the geometry of the contacting surfaces, Figure 2.4.6.

Stefan Force Between Parallel Plates

Under this geometry, assuming two plates of radius R separated by a distance h filled by a liquid of viscosity η, as the plates move perpendicularly away from each other at a rate dh/dt, the viscosity of the fluid flowing into the contact zone resists the separation [109], and gives rise to the Stefan adhesive force [110]:

$$F_{\perp} = \frac{3\pi\eta R^4}{2h^3}\frac{dh}{dt} \tag{2.4.19}$$

If the liquid between the surfaces is highly viscous, separation may take an appreciable force over a considerable length of time, or if moved apart from each other in a short time, will require a considerable amount of force to complete the action [16].

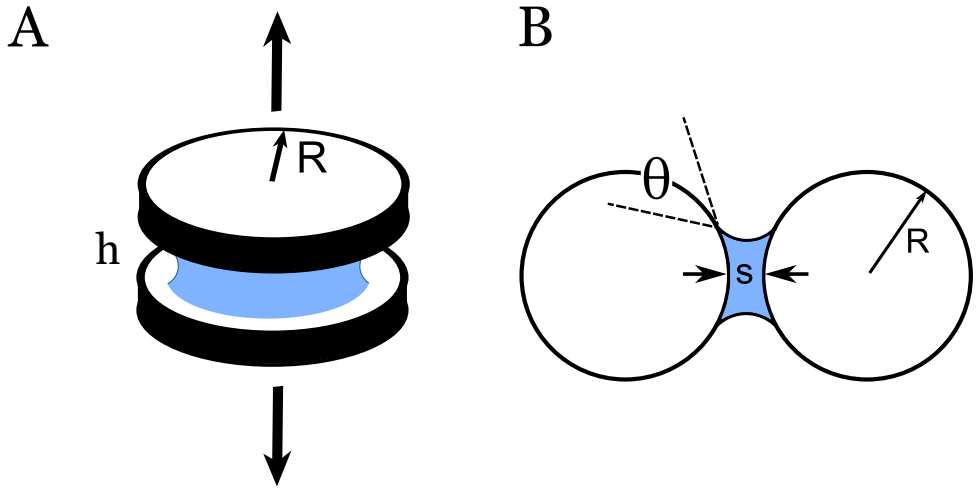

Figure 2.4.6: Stefan adhesion forces between A) two flat-discs geometry, and B) sphere-on-sphere geometry. B) A liquid capillary bridge is formed between the two surfaces of radius R. The capillary bridge spans a distance h between the two spheres, until it 'pinches' off at a critical distance s.

Stefan Force Between Two Spheres

The Stefan force between two spheres is given by [111, 112]:

$$F_{\perp} = \frac{3\pi}{2} R^2 \frac{\eta}{h} \frac{dh}{dt} \tag{2.4.20}$$

where, in this case, h corresponds to the closest separation distance of the two spheres, Figure 2.4.6. This equation also applies equally well to forces between a sphere and a flat surface, it simply needs to be remembered that, for formulas developed for two spheres, the radius of the sphere must be multiplied by two, which corresponds to the well known *Derjaguin approximation* [112]. During detachment normal to the substrate, Stefan adhesion forces are generally considered to be negligible for insect adhesion, but the viscous contribution to friction forces in plane with the substrate is considered to be substantial, and will be discussed in Section 2.5.

2.4.2.3 Equal Load Sharing *vs.* Stress Concentration in Hairy Pads

The fibrillar nature of hairy pads require consideration of how the adhesion forces are distributed across the large number of individual contacts. In many adhesive models for hairy pads, it is assumed that the adhesive load is equally shared between all setae in the pad. However it is possible that the loading force is distributed asymmetrically by the attachment devices, and during detachment concentration of stress at the peeling edge may occur [59]. Equal load sharing holds if the pad is small, setae are compliant and the structures from which they emerge are stiff [59, 113]. However if these conditions are not met, Hui *et al.* [113] showed that the stress may be concentrated along the peeling edge in the hairy pad; in the extreme case along one row of setae along the peeling edge of the pad. Both equal load sharing and stress concentration scenarios are considered when we construct theoretical models for hairy attachment pads in Chapter 4.

2.5 Friction Forces

2.5.1 Dry Friction

Friction between two contacting dry surfaces is a common phenomenon that is encountered daily in micro- and macro-scopic situations. On a macroscopic level, friction is the resistance to the movement of one surface over another and is separated into two components: *i*) static friction, and *ii*) dynamic friction. Static friction is the resistance needed to be overcome for one surface to begin moving across another, the dynamic friction is the force required to continue the movement of that same surface after it has begun, and static friction is nearly always greater than dynamic friction. Amontons' laws of friction state that during sliding:

• Friction force is proportional to the normal load, L, which can be expressed by the well known equation:

$$F = \mu L \tag{2.5.1}$$

where μ is the coefficient of friction.

• Friction force is independent of the *apparent* area of contact.

The third 'law' of friction was provided by Coulomb eighty years later:

• Dynamic friction is independent of sliding velocity.

Typical values of μ for friction between rigid solids are in the range $\mu \sim 0.1 - 0.4$ [114], but values of μ greater than unity are possible for dry friction involving soft, viscoelastic materials such as rubber where friction is dominated by adhesion [115–117]. In this case it is often more useful to consider the normal force acting towards the substrate to be the sum of the external load L and the force of adhesion F^N, modifying Equation 2.5.1 to:

$$F = \mu(L + F^N) \tag{2.5.2}$$

Insect attachment pads use a proximal pull of the pad to generate as large a contact area as possible by initiating and maintaining a shear force by the pads with the substrate. Due to the flexibility in the tarsi, and the elasticity of the attachment pads, the maintaining of strong shear forces can contribute significantly to attachment forces in insects, often generating a coefficient of friction $\mu > 1$ [12], suggesting that friction is not generated by simple Amonton friction.

2.5.2 Wet Viscous Friction

Under wet conditions, an additional friction force is generated by the presence of a liquid within the contact zone of two surfaces due to the viscosity of the liquid, η. The parallel frictional force generated by the shearing of a Newtonian liquid of viscosity η between two surfaces of contact area A, and height h is a function of the sliding v_s given by:

$$F = \frac{Av_s\eta}{h} \tag{2.5.3}$$

Velocity dependent rheology of the secretion may aid insects during adhesion from preventing sudden detachment due to perturbations such as sudden wind gusts, or during landing scenarios for flying insects. Insects such as the weaver ant *O. smaragdina* must generate significant shear forces during their complex nest construction behaviours [4], and are therefore likely to take advantage of viscous forces provided by their adhesive secretions.

2.6 Force Measurement Techniques

The first quantitative measurements of insect attachment forces to smooth surfaces were conducted by Stork [34] on the beetle *Chrysolina polita*. By attaching a thread between a force transducer and the beetle, and allowing the tethered insect to pull on the thread for several minutes, measurements of the 'pulling force' were conducted on several different surfaces. A similar technique was used by Dixon [66] to study the mechanism of adhesion in aphids, and more recently in studies on spiders [118], and cockroaches [52, 119]. Several early studies of attachment forces also used a simple method of attaching weights to the thread, increasing the load on an inverted insect until detachment occurred [35, 65].

Force-strain transducers have been used to measure adhesion and friction forces in immobilised insects on the level of single attachment pads. Drechsler & Federle [68] used foil strain gauges attached to a substrate held in a micromanipulator to measure adhesion and friction forces to smooth substrates in the stick insect *Carausius morosus*, Figure. 2.6.1. This technique was also used to measure attachment of single pads of *Carausius morosus* and the beetle *Gastrophysa viridula* by Bullock *et al.* [120], and provides for control of the normal load on the pads and substrate velocity during the experiment, making it possible

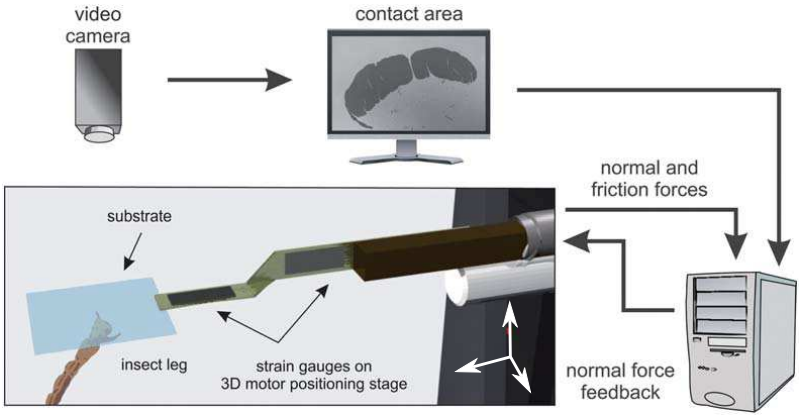

Figure 2.6.1: Schematic illustration of the experimental set-up to measure adhesion and shear stress of adhesive pads *in vivo*. Using a computer-controlled translation stage, a force transducer with attached surfaces can be moved in three dimensions. The normal force can be controlled during friction measurements using a feedback system. The contact areas of the adhesive pads are imaged from above under reflected light using synchronised digital cameras. Adapted from Dirks *et al.* [90].

to investigate the subtle influences of pad-load and sliding velocity on adhesion and friction forces [52]. Measurement of adhesive forces generated by individual setae of several different insects and arachnids have been performed using the atomic force microscope (AFM) which allows for measurement of forces down to nano-Newton resolution. Langer [24] studied the forces of single seta of the fly *Calliphora vicina*, Kesel *et al.* [26, 121] measured the adhesive force of single cuticular contact elements, or *setules*, in the spider *Evarcha arcuata*, and recently Huber *et al.* [60] measured forces generated by individual contacts of the gecko lizard.

Centrifuge devices have been used extensively to measure insect adhesion on the level of the whole insect. This simple system can be used to calculate the detachment force of an insect from its mass, angular velocity and its radial distance at the point of detachment, and has been proven to be a highly reliable force measurement technique. The attachment force of the insect resists the centrifugal force during rotation, and the magnitude of this force at any given time is given by:

$$F_{cent} = m\omega^2 r \tag{2.6.1}$$

where ω is the angular velocity, r is the radial distance of the object from the centre of rotation and m is the mass of the insect. Dixon *et al.* [66] used a hand-driven centrifuge to measure the shear force required to detach the aphid *A. fabae* from glass surfaces, and Brainerd [122] performed different types of force measurement with ants on smooth surfaces - which including a motorised centrifuge. More recently the centrifuge technique was further developed and extensively used to measure attachment forces in unrestrained insects by W. Federle and coworkers at Cambridge [13]. Based on simple physical principles this technique is extremely effective at measuring attachment forces in a wide range of insects, and has several advantages over the 'restrained' techniques: *i*) no prior manipulation of the insects is needed, allowing for measurement of whole-insect forces in a more natural manner, *ii*) adhesion and friction forces can be measured by simply changing the

geometry of the experiment, *iii*) different types of surfaces can be easily tested, and this technique has become a standard and well-used experiment for measuring adhesive forces on the scale of whole insects.

Federle *et al.* [13] compared the adhesion forces of the ant *O. smaragdina* as measured with a direct-force technique and a centrifuge device. Measured forces were found to be of the same order of magnitude, but significantly greater with the centrifuge experiment. This was interpreted as being due to the prior manipulation of the insect needed for the direct force transducer, such as the need to anaesthetise the insect and tie threads to their bodies. Restraining insects during measurement of forces could have unintended influences on an insects' behaviour which may influence the measurements, and may not be a true description of what the insect is capable of achieving when unrestrained making it important to compare results from both restrained and unrestrained insects. Force-experiments described within this thesis, in Chapters 5 & 6, were performed with both untethered and tethered insects, and a comparison is drawn between the results from each.

To date, no measurements of impulsive perturbations have been performed. Insects are subjected to sudden perturbations in nature which will act to detach the insects from the surface they are traversing if adhesion cannot be enabled to a sufficient magnitude within a fast enough time. Forces due to sudden gusts of wind, falling raindrops, preying insects and other animals, or other unpredictable influences could work to detach an insect from a surface at any time. To address this, we measure impulsive detachment forces in the weaver ant *Polyrhachis dives* and the Harlequin ladybird *Harmonia axyridis*, results of which are detailed in Chapter 6. Moreover, direct comparison of insect attachment forces as measured with more than one technique within a single study are rare in the literature. To address this issue, in Chapter 6 adhesion and friction forces of the ladybird *Coccinella septempunctata* and the ant *Polyrhachis dives* were measured using several force measurement techniques.

Chapter 3

Literature Review
Barriers to Insect Adhesion

'if some simple barrier could be found which would prevent the ant from penetrating where he is not wanted, there is no doubt that the waste of vast amounts of food could be prevented; and a great deal of human discomfort and annoyance avoided'

Thomas Merton (1955)

Within the natural world it has been observed that many plants possessing fragile wax layers and crystals are able to provide effective barriers against climbing insects. Mimicking the effect of natural barriers has the potential to aid the production and development of more efficient synthetic means of controlling pest species in agriculture, as well as domestic situations. Such barriers could potentially be used as an ecologically friendly method for the control of insect pest species, however, until recently there have been few systematic studies of how the anti-adhesive properties of natural or synthetic barriers depend on the physico-chemical properties of the materials.

In this chapter we will outline the different types of surface properties which have been found to reduce attachment forces in insects, together with how these properties are deployed by both natural and man-made surfaces and materials to reduce the forces of adhesion in insects possessing both types of adhesive pad. The discussion will be separated in two parts to differentiate between *i*) surfaces which act as barriers to insects - preventing further ingress *via* locomotion once these surfaces have been encountered - and *ii*) anti-adhesive, or non-stick, surfaces which, due to their intrinsic material and surface

properties, significantly reduce adhesion and friction forces not only between insects and these surfaces, but also other organisms, and materials.

Insect adhesive forces can be reduced by a number of substrate characteristics, including reduced surface energy and wettability, surface roughness, the presence of surface contamination, or a combination of these factors, and these factors have been studied in detail in recent years with regards to insect attachment.

For example, Al Bitar *et al.* [8] measured attachment ability of the codling moth *Cydia pomonella* on surfaces of varying surface roughness. It was found that surface topography significantly influences friction forces, with a maximum of force measured on smooth substrates, whereas a minimum of force was found on micro-rough substrates with asperities of diameter 0.3–1.0 μm. Forces were reduced to approximately 50% of the maximal force in this range. On surfaces of greater roughness friction forces were significantly higher but remained lower than those on the smooth substrate, consistent with data of previous authors, for example, Voigt *et al.* [6] who found that on similarly rough substrates friction forces of the beetle *Leptinotarsa decemlineata* were drastically reduced, and the beetle *Gastrophysa viridula* showed a similar effect in the study of Gorb *et al.* [54]. This effect was termed 'critical-roughness' and is used to describe the surface roughness capable of minimising attachment forces in insects, Figure 3.0.1, and lies approximately in the region of asperity diameters of 0.1–3.0 μm. This size range also corresponds well to the size of epicuticular wax (EW) crystals found on many plants [123, 124], Figure 3.0.2, a subject which will be returned to in section 3.1.

A small number of studies have investigated how attachment forces for a given insect differ between surfaces of varying surface energy, *i.e.* between hydrophilic *vs.* hydrophobic surface chemistries. For example, Gorb & Gorb [125] measured the effect of surface topography and chemistry on the attachment ability of the beetle *Gastrophysa viridula* (Coleoptera; Chrysomelidae), possessing the hairy pad. Forces were found to be greater on hydrophilic compared with both natural and synthetic hydrophobic surfaces, consistent

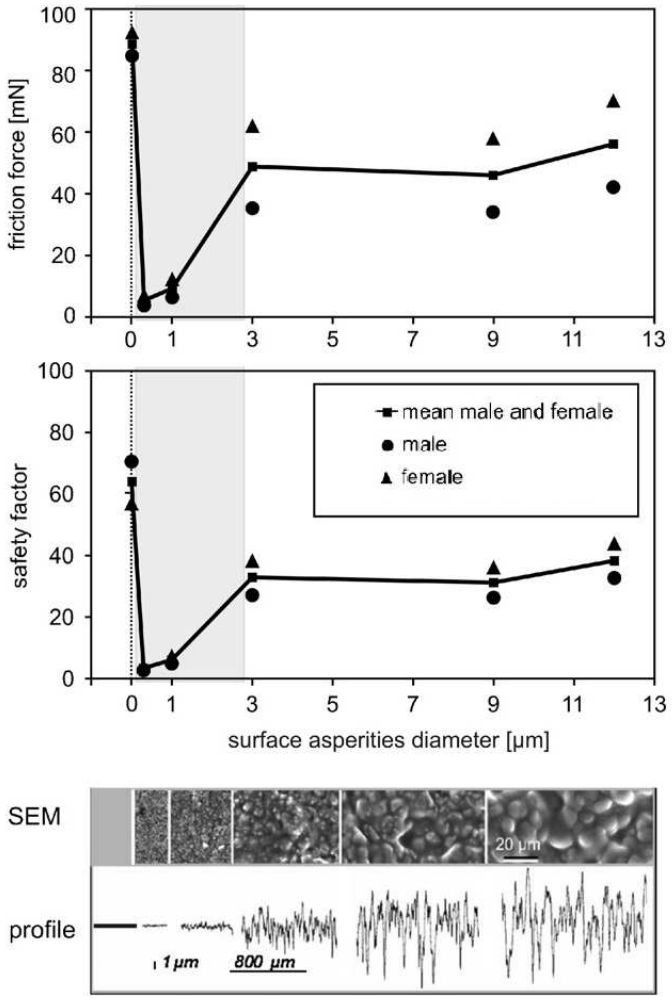

Figure 3.0.1: Dependence of friction forces and safety factors of *Leptinotarsa decemlineata* obtained with a centrifuge device for substrates with different surface roughness. Grey boxes within graphs indicate the minimum of friction forces and safety factors. The figure at the bottom shows SEM micrographs and surface profile graphs of the different surface asperities used. Adapted from Voigt *et al.* [6].

with the theory that forces are derived from capillarity. An increased hydrophobicity was reported to explain a decrease in attachment force on hydrophobic glass, corresponding to roughly a 50% drop in force.

Although investigation of the effect of surface energy on the adhesion force of insects has only been conducted on a small number of insects, the data available seems to suggest that the surface energy of a substrate has a greater effect on insects possessing the hairy fibrillar pads, such as beetles, compared to insects with smooth attachment devices, such as ants. For example, in contrast to the results for *G. viridula* described above, Al Bitar *et al.* [7] measured the attachment ability of the codling moth *Cydia pomonella*, possessing a smooth

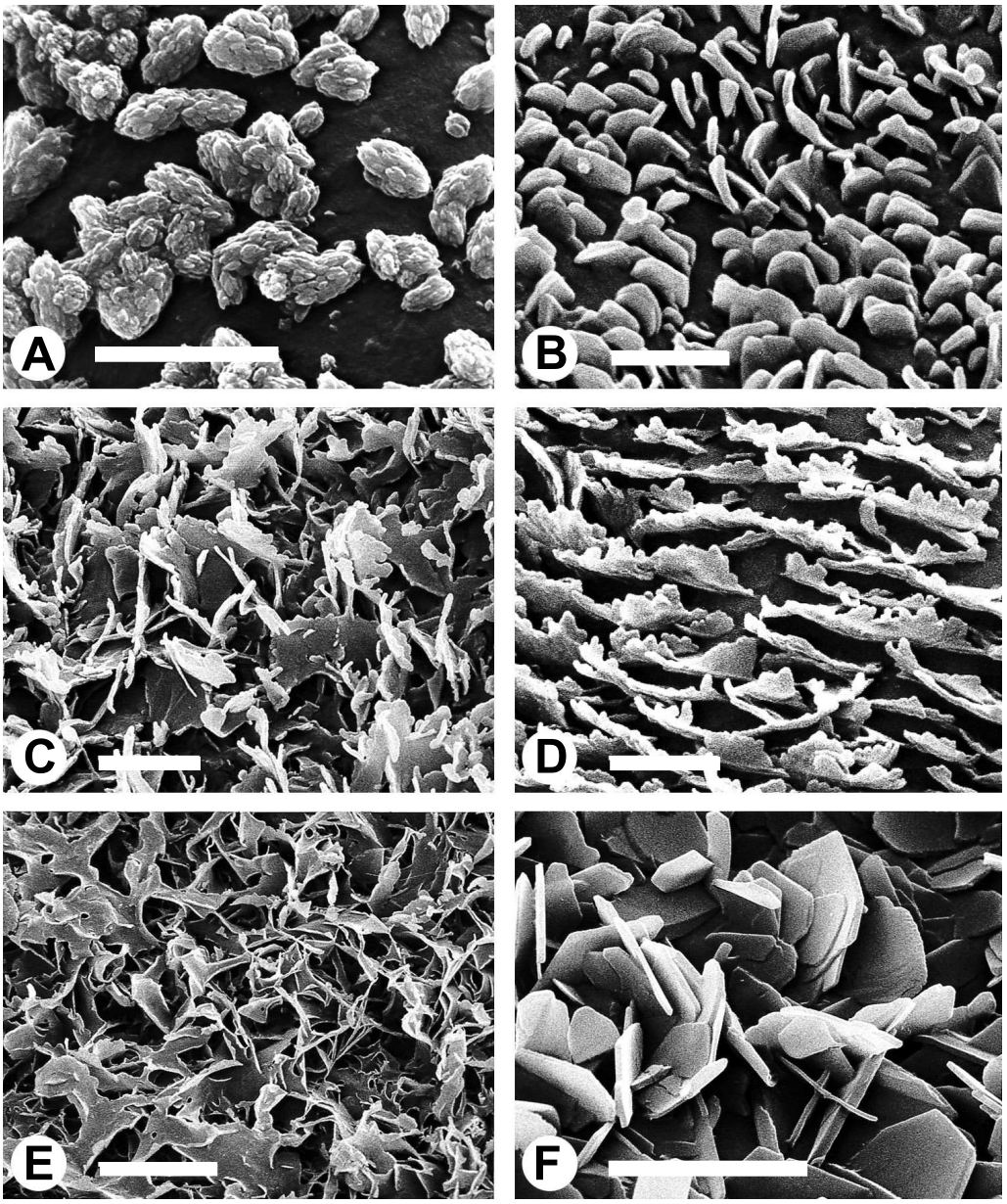

Figure 3.0.2: Wax crystal morphology. A) Granules of *Aegiceras corniculatum* Scale bar = 5 μm B) Platelets of *Habropetalum dawei* Scale bar = 1 μm C) Platelets of *Odosicyos* spec. Scale bar = 2 μm D) Platelets of *Grevillea bipinnatifada* Scale bar = 1 μm E) Membranous platelets of *Tilia miqueliana* Scale bar = 10 μm F) Plates of *Lecythis chartacea* Scale bar = 5 μm. Image adapted from Barthlott *et al.* [126].

arolium, on smooth hydrophilic and hydrophobic glass using a centrifuge device, and found both males and females of this species generate similar forces across the two substrates. It was concluded that because codling moth adhesion does not vary significantly from physico-chemical properties of the substrate, this facilitates the species with the ability to disperse and infest a diversity of host plants, with different surface polarity and wettability, found in their natural habitat.

However, whilst the properties of surface energy and roughness can reduce attachment ability, they alone cannot fully prevent an insect from traversing a particular substrate during inverted or horizontal locomotion, albeit at reduced speed and efficiency. But a combination of these factors can successfully prevent an insect from generating sufficient attachment force to a substrate to allow it to walk across it. Natural surfaces usually make use of the combination of low free surface energy (FSE) and micro-scale surface roughness, generated by the presence of epicuticular wax coverings on their surfaces, to achieve this effect. For example, in their study of beetle attachment forces Gorb & Gorb [125] also found that when a low FSE is combined with surface roughness such as that found on hydrophobic leaf surfaces, the decrease in insect attachment force is amplified. For the beetle *G. viridula*, it was found that attachment force was significantly affected by a combination of the physico-chemical properties *and* surface roughness [55, 125].

Comparing males to females, Voigt *et al.* [6] studied the influence of surface roughness on the friction force of the beetle *Leptinotarsa decemlineata*. A significant sexual dimorphism of attachment force was found on rough substrates, with female attachment being significantly stronger than males, attributed to the presence of discoidal shaped tips (described in Section 2.2.2) found in the pads of males only. Theoretical investigations of the influence of tip shape on the pull-off force for single contacts have been conducted [127], together with experimental measurements of man-made analogues of fibrillar adhesives [128, 129], which found that wide, flat tips similar to the discoidal shaped tips in male beetles showed the highest pull-off forces giving credence to this hypothesis. Bullock & Federle [130] came to a similar conclusion for the tarsal adhesive pads of male and female Dock beetles, *G. viridula*.

In the following section, the different ways that natural surfaces, such as leaves and plant cuticle, use the factors of FSE, surface roughness, and microscopic particulates to reduce or prevent insect attachment ability will be described.

3.1 Natural Barriers

Insects walking on plant surfaces interact directly with the epicuticular wax layer, making it important to gather knowledge about the chemical, mechanical and morphological properties of these wax layers in order to understand their functionality. Many climbing insects (e.g., ants and beetles) spend much time walking on plant surfaces and require strong adhesion when walking vertically or upside down, sometimes carrying the equivalent of several times their own body weight [4]. As such it is necessary to continually maintain effective functioning of adhesive devices to ensure that the insect does not inadvertently fall from the plant. Crawling insects such as ants would likely not survive falling from plants or trees which they inhabit because they could find themselves in territories of hostile ants, or in a location where no odour trails guide them back to their nest [12]. Because living plant surfaces are permeated and covered by layers of lipophilic materials known as surface waxes, Figure 3.0.2, and since plant surfaces can range from smooth to very rough, and be covered in wax crystals or sticky hairs and glands known as *trichomes*, insect-plant interactions will depend on the insect attachment ability to the particular plant surface.

Epicuticular waxes are primarily responsible for protecting the plant cuticle from loss of water through evaporation, and for protecting the cuticle from pathogens. They are composed of micrometre-scale crystals ranging in size, shape and aspect ratio, and can be loosely classified as filaments, rods, tubules, platelets, granules and crystals [126, 131]. Waxes cause a micro-roughness of plant surfaces which leads to a strongly decreased wettability, but their complex composition and structural morphology are also important for the mechanical interactions between the plant and insects [132, 133], and many plants possessing fragile wax crystal layers are able to generate effective barriers against climbing insects [11, 13, 25, 134–136]. These surface waxes have complex compositions, but are primarily composed of hydrophobic hydrocarbons [131, 137], making the plant surfaces slippery as well as rough.

Gorb and Gorb [55] studied the effects of different plant surfaces on the attachment ability of the beetle *Chrysolina fastuosa*, which possesses the hairy pad system, and found that attachment ability was diminished on waxy surfaces. Adhesive ability and attachment forces of insects are almost always reduced by the presence of the EW blooms, with plants benefiting from the reduction of herbivorous predation. Figure 3.1.1 depicts the four proposed hypotheses used to explain the reduction of insect attachment by natural waxes:
(*1*) Roughness hypothesis, Figure 3.1.1A; due to the small size of the wax crystals ($\sim$ 0.3-1.0 μm), the real contact area of the setal pads is reduced. Since attachment force is highly dependent on contact area the insect may not be able to produce sufficient adhesive forces to stay attached.
(*2*) Wax-dissolving hypothesis, Figure 3.1.1B; previous investigations into the adhesive secretion of beetles [35, 138] has yielded evidence it is composed of hydrocarbons, fatty acids and alcohols. The secretion could possibly dissolve the wax crystals of the plant surface, leaving a slippery layer of fluid which would decrease adhesion.
(*3*) Contamination hypothesis, Figure 3.1.1C; because wax crystals are easily eroded from the surface, they may detach and contaminate the adhesive pads, preventing attachment on subsequent steps.
(*4*) Fluid-absorption hypothesis, Figure 3.1.1D; it is proposed [139] that the hydrophobic waxes of plant surfaces are wetted by the oily secretion of insects. This waxy coverage may absorb the fluid from the setae of the insects pad, reducing overall adhesion.

We now consider in turn each of the above mentioned hypotheses in detail. The influence of surface roughness on insect adhesion has been studied experimentally in a number of studies, as discussed in the previous section [6, 8, 54, 125], and as such will not be discussed in detail again. The findings for roughness dependent attachment apply equally well to natural surface as they do synthetic, with attachment forces invariably greater on very smooth surfaces, decreasing with increasing surface roughness.

To date, no evidence has arisen supporting the wax-dissolving hypothesis and it has not

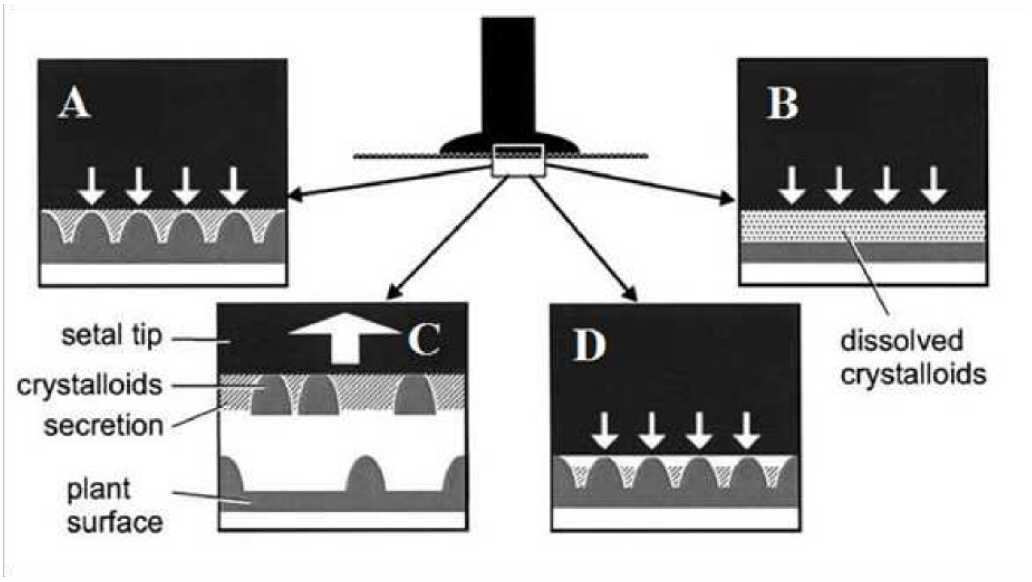

Figure 3.1.1: Hypothesised anti-attachment mechanisms for hairy pads on a pruinose waxy surface. A) Roughness-hypothesis B) Wax dissolving-hypothesis C) Contamination-hypothesis D) Fluid-absorption-hypothesis. Adapted from Gorb & Gorb [55].

been directly tested experimentally, and the fluid absorption hypothesis has been investigated in only a single study which used porous sapphire (Al_2O_3) discs with fixed pore sizes, but different degrees of porosity [140]. Attachment forces were found to be reduced on porous substrates but it was not possible to definitively differentiate between the influences of fluid absorption and the effects of surface roughness.

In contrast to these, the contamination hypothesis has been more extensively studied. Contamination of attachment pads can drastically reduce the contact area between pad and substrate reducing overall adhesive forces, and levels of contamination depend on the micro-morphology of the wax crystals, such as largest length dimension and aspect ratio [139]. Contamination is an important factor affecting the adhesion of insects to surfaces with natural contaminants [135, 141], and similar anti-adhesive effects have also been found for a small number of synthetic powders which can form effective barriers against crawling insects [142]. Synthetic particulate barriers, and other forms of man-made insect barriers will be discussed in more detail in Section 3.2. Thus a combination of factors can be employed by plant EW for superior anti-adhesive properties for insects; micrometre sized particles, a fragile coating of particles capable of detaching from the plant, a low

FSE, and surface porosity can generate efficient insect barriers.

A notable example of natural insect barriers is found with the plant species *Macaranga* [11, 137, 143]. The stems and leaves of these ant-plants are covered by EW crystals which render the surface slippery for insects, acting as selective barriers which exclude generalist ant species from walking on them, but allow for locomotion of specialist ant species of genera *Crematogaster* and *Camponotus*, Figure 3.1.2. Federle *et al.* [11] found that the repellence and exclusion produced by these wax barriers was not chemical in nature but was determined by physical factors only, and the extent to which foreign ants were excluded was dependent upon the physical characteristics of the waxy stem sections. Although the wax-running ants were found to be capable of walking across these waxes with relative ease, it was found that their ability to walk on smooth surfaces was actually diminished, contradictory to the hypothesis that the ability to walk on the glaucous waxes of their host plants was due to general superior attachment ability. Knowledge of how these plant waxes function as barriers to insect adhesion will be important for the development of new generations of synthetic anti-adhesives and pest controls, as well as for understanding the complex ecological interactions between insects and plants.

Figure 3.1.2: The protective barrier effect of slippery epicuticular wax crystal layers in *Macaranga*. The ant on the upper section is able to walk across the wax layers, where-as the ants on the lower clean section are unable to do so, and are excluded. Adapted from Federle *et al.* [13].

3.2 Synthetic Barriers & Insect Repellence

The proficiency with which insects can navigate various surfaces is certainly impressive, but it can also be an annoyance for many. Insect pests can not only be annoying in domestic situations but they can also be a persistent threat to successful agriculture, and are responsible for significant degrees of food loss, and may contribute to the spread of disease. Hence, the search for an effective barrier against crawling insect pests has been the goal of many for decades [142, 144].

Often the use of pesticides is the easiest and most cost effective option, but growing concern for human and environmental health has led to an effort to reduce the amount of toxic pesticides used in agriculture [142, 144–147]. This approach has been termed *integrated pest management* and is aimed at reducing the toxicity and damaging effects of insect deterrents. Glenn *et al.* [142] studied the use of inert hydrophobic particle films on the suppression of arthropod pests on pear-tree surfaces. Plant surfaces coated with layers of particles of average diameter $\sim 2\ \mu m$ were found to be protected from insect pests. These methods may prove useful for repelling arthropod pests in some agricultural situations, offering an alternative pest control strategy with improved safety to humans and the environment, but have the drawback of requiring continuous applications of the particle films. Such barriers could potentially be used as ecologically friendly methods for the control of insect pest species [147, 148]. However there have been few systematic studies of how the anti-adhesive properties of synthetic particle barriers depend on the physico-chemical properties of the contaminating particles. In order to investigate this relationship, in Chapter 7 we focus attention on the smooth adhesive pads of ants and study systematically how particulate contamination by synthetic powders, and the subsequent loss of adhesion, depends on particle size, particle surface energy and humidity.

It has been shown that insects are able to reduce the detrimental effects of attachment pad contamination by using a number of different strategies which can be categorised under i) passive 'self-cleaning' mechanisms - which have been found in insects with both smooth

and hairy pad types (eg; Clemente *et al.* [149] and Orchard *et al.* [150]), as well as geckos [151, 152], and *ii*) active grooming behaviours (see Hosoda & Gorb [56]). In particular, it has been found that both smooth and hairy pads exhibit self-cleaning properties when contaminated with glass micro-spheres with a range of sizes (1–45μm) and that adhesion forces can return to normal after several steps [149]. Specifically for smooth adhesive pads, it was found that self-cleaning was aided by shear movement of the tarsal pads in the proximal direction, and that the reattainment of adhesion is strongly influenced by particle-material and size [149, 150]. For hairy pads Orchard *et al.* [150] found that self-cleaning is significantly influenced by particle size and hydrophobicity, and concluded that the hairy adhesive organs of ladybird beetles (Coleoptera) appear to possess superior self-cleaning abilities compared with those of ants (Hymenoptera).

Reduction of adhesive force has also been found to trigger grooming behaviour in beetles walking on manufactured nano-structured surfaces [56], demonstrating that the reduction of adhesion or friction force between tarsal attachment pads and the substrate provides the insect with information on the amount of contamination on its adhesive pad, influencing their behaviour. However, while grooming behaviours can remove particles from already contaminated attachment pads, to prevent contamination from initially occurring in the first place it is reasonable to assume that insects may possess a system of detection and avoidance *via* their antennae. Specifically it is possible that insects may also be able to use their antennae to 'detect' the material properties, such as surface morphology and roughness, of a substrate. Indeed it is documented that insects use their antennae to detect numerous aspects of their surroundings [153, 154], with recent work demonstrating that the information relayed from tactile influences [155, 156] can be used in decision making [157]. To further address this question in a systematic way for loose synthetic powder barriers, in Chapter 7 the extent to which two ant species were repelled by loose powder barriers *prior* to crossing these barriers, and how this behaviour may also be influenced by the physico-chemical nature of the powders, is investigated.

3.3 Anti-Adhesive Surfaces

By modification of a plants surface chemistry and structural morphology, as described in the preceding sections, many plant species have developed advanced anti-adhesive properties. Anti-adhesive surfaces found in nature are powerful examples of structured functional surfaces.

The 'Lotus Effect'

For several thousand years it has been observed that a number of plants invariably have clean leaf surfaces, despite living in relatively 'dirty' environments, the most notable example being the Lotus Flower *Nelumbo nucifera*, which typically grows in swamps and shallow waters of eastern Asia and North America. The leaves of this plant are constantly kept clean due to the particular ultrastructural properties of its surfaces, *via* a process known as 'self-cleaning' [158]. Although we now understand the processes behind this phenomenon, the Lotus flower had fascinated and influenced scholars, scientists and philosophers alike since ancient times; due to its cleanliness, and seemingly unexplainable self-cleaning ability this flowering-plant inspired Buddhist monks to declare it a symbol of purity, as well as being mentioned in the *Egyptian Book of the Dead* as a symbol of resurrection [160]. However the mechanisms behind this fascinating effect remained a mystery until the development of high-resolution electron microscopes in the 1960's [161] which revealed the true nature of the micro-scale surface structuring found on these plants' surfaces. Quantitative investigations of the 'Lotus effect', or self-cleaning of biological surfaces, which included a large number of different plant surfaces, was conducted by Barthlott & Neinhuis [162]. Together with morphological data from similar studies, results indicated a structural basis for the self-cleaning effect. A hydrophobic wax decreases wettability and in combination with two or more levels of sculptured roughness, Figure 3.3.1, leads to self-cleaning *via* superhydrophobicity [162, 163]. Other notable examples of self-cleaning in plants include;

water ferns (*Salvinia*) [164], Lady Mantle (*Alchemilla mollis*) and broccoli (*Brassica oleracea*) [165], see Figure 3.3.2, and the Indian cress *Tropaeolum majus* [162, 166].

Superhydrophobicity

In recent years, several reviews on superhydrophobic self-cleaning plant surfaces, and bio-inspired materials which aim to achieve the same effects synthetically, have been published (see reviews [166–169]), the main points being summarised as follows; The fundamental requirement for self-cleaning is water repellency, usually termed superhydrophobicity, which leads to an almost complete surface purification *via* the process of contaminating particles being picked up by water droplets which are then removed from the plant as the droplets roll off the leaves, Figure 3.3.2. Advanced water-repellency also includes characteristics

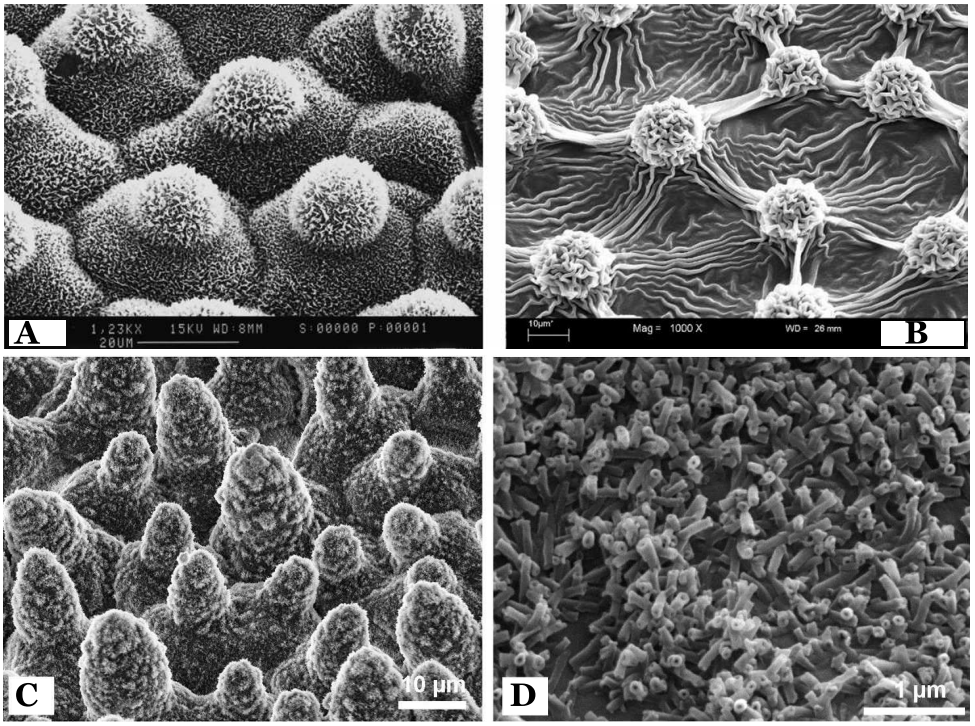

Figure 3.3.1: Examples of dual-scale roughness and surface structuring in nature. A -B) SEM micrographs of the Taro plant (*Colocasia esculenta*) and the Elephant Ear Taro (*Alocasia macrorrhiza*). A) The upper surface of *Colocasia* is characterized by convex hexagonal cells with centrally placed papillae and a dense cover of wax platelets. B) The lower surface of *Alocasia* shows papillose cells and prominent cuticular folds. C - D) SEM image of the upper leaf side of *(Nelumbo nucifera* showing the hierarchical surface structure consisting of papillae, wax clusters and tubules. D) Wax tubules on the upper leaf side. Scale bars A) 20 μm, B & C) 10 μm, D) 1 μm. A & B) Adapted from Solga *et al.* [159], C & D) adapted from Ensikat *et al.* [158].

such as low tilt angle (the angle to the normal plane the substrate takes at the point the droplets begin to freely roll), small contact-angle hysteresis, and low water-holding capacity [159]. The term superhydrophobicity is neither well defined nor consistently used in the literature, but generally means that water droplets exhibit contact angles $\geqslant 140°$. This loose definition, however, does not take into account effects due to contact angle hysteresis and so the term *ultrahydrophobic* was coined to define surfaces with a contact angle $\geqslant 150°$, with a low contact angle hysteresis (usually 5° or less) [170, 171].

For smooth substrates, the modification of surface chemistry alone cannot achieve contact angles greater than $\approx 120°$, and so a second factor is required for superhydrophobicity -

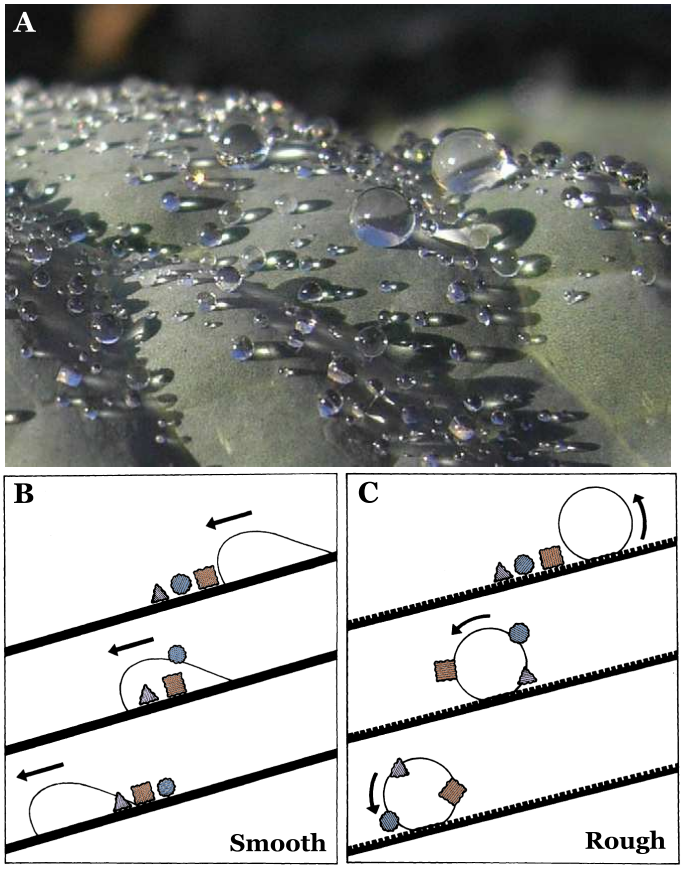

Figure 3.3.2: A) Water droplets after a rain shower on a leaf surface of cabbage (*Brassica oleracea*), as an example of the wetting behaviour of superhydrophobic surfaces by water droplets. The superhydrophobic surface is created by the epicuticular wax layer. B - C) Diagram of the mechanism of self-cleaning by water droplets. B) While on smooth surfaces particles are mainly redistributed by water droplets, but in C) they adhere to the droplets on rough surfaces and are removed from the leaves. Adapted from Barthlott and Neinhuis [162].

surface structuring. The increase of surface roughness of a solid surface leads to two different regimes of wetting, the Wenzel state, and the Cassie & Baxter state, Figure 3.3.3. With the increase of a solid's surface roughness, the actual area of the solid-liquid interface is increased, so for a droplet of a given volume, the total liquid-solid interaction is greater on a rough surface. This is the Wenzel state of wetting, shown in Figure 3.3.3B. If a smooth solid surface has a contact angle greater than 90°, the presence of surface roughness further increases this angle, and if θ is less than 90° the surface roughness decreases this angle [172]. The Wenzel equation expresses a general increase of the wettability induced by surface roughness, which amplifies the inherent contact angle of the surface, and applies where the contact angle of the droplet is in equilibrium. This equation thus does not take into consideration contact angle hysteresis induced by pinning effects or surface-chemistry heterogeneity.

For non-wetting liquids which cannot penetrate fully into the pores of a surface, air pockets remain and the Wenzel equation cannot be applied due to the lack of solid-liquid interface, Figure 3.3.3C. For heterogeneous surfaces, like that shown in Figure 3.3.3C, a more complex model is needed to measure how the apparent contact angle θ_c changes when a surface made of various materials is involved with different materials having area fractions f_i and corresponding contact angles θ_i. In 1944 Cassie & Baxter derived an equation which

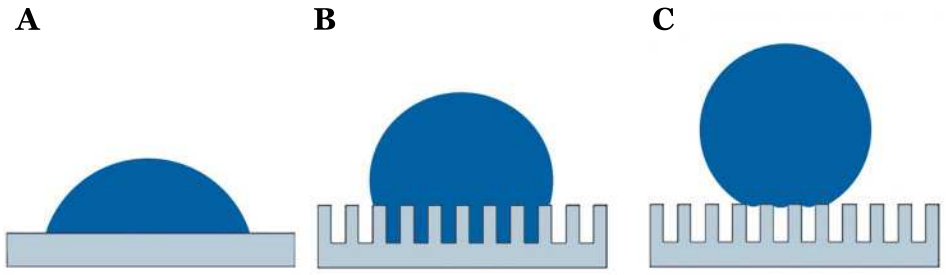

Figure 3.3.3: Effect of surface structuring on the wetting behaviour of solid substrates. A) A liquid droplet on a flat surface - *Young mode*, B) Wetted contact between the liquid and the rough substrate - *Wenzel mode*, C) Non-wetted contact between the liquid and the rough substrate - *Cassie mode*. Adapted from Feng and Jiang [167].

describes the apparent contact angle for a liquid on such a surface [172, 173]:

$$\cos\theta_c = \sum_i f_i \cos\theta_i \tag{3.3.1}$$

When one of the components in this equation is taken to be air with a contact angle = 180°, and when the fraction of solid surface tends to zero, the effective contact angle of droplets in the Cassie-Baxter state θ_c approaches 180° since it is energetically more favourable for the droplet to rest on the tops of the pillars droplets, taking an almost spherical shape through minimisation of surface area. For droplets in the Cassie-Baxter state, the presence of air-pockets in the substrate means that the attachment force between the droplet and the solid is significantly reduced [172], and droplets can be rolled off the surface with very little effort, leading to superhydrophobicity Figure 3.3.2.

New commercial products based on the 'Lotus effect', such as self-cleaning paints and windows, have recently been produced [174], the field of microfluidics has also benefited from further advancement of anti-stick surfaces, and research into mimicking this effect has increased significantly in the past decade [175]. Yet there have been few studies investigating the effects these man-made superhydrophobic structures have on insect-adhesion, if any. However, since the factors of low surface energy, and a high level of surface roughness have also been shown to be important for the reduction of insect-attachment on both natural and man-made substrates [55, 125, 176] it is plausible that such highly structured surfaces could be replicated and used as insect barriers, but function in a different manner to those which primarily contaminate insect adhesive pads.

Indeed, a notable example of plants which use a combination of low surface energy and microscale surface structuring to achieve the specific goal of reducing insect adhesion would be those of the Carnivorous plant genus *Nepenthes*, the pitcher plants. This plant genus has evolved specialised pitcher-shaped trapping organs adapted for attraction, capture, retention and digestion of arthropod prey, which provides the plants with essential nutrients, such as nitrogen and phosphorous, which would otherwise be lacking due to

nutrient-deficient soil [5, 177, 178]. These pitchers form a 'pitfall' trap originating from modified leaf surfaces, and in most *Nepenthes* species the specialised morphology of the plant renders its surface slippery for insects. Different functional zones are distinguished by their morphological and physicochemical surface characteristics, Figure 3.3.4, which all contribute to the anti-adhesive ability [123]. Details of the different functional zones are described in the literature (see Gorb & Gorb [177] and Scholz *et al.* [123]), and, although significant morphological diversity is present within this genus, a brief description of the general functional morphological traits are given in the following section.

The peristome rim, at the top of the pitcher Figure 3.3.4B, is characterised by a regular microstructure with ridges of smooth overlapping epidermal cells which form a sequence of

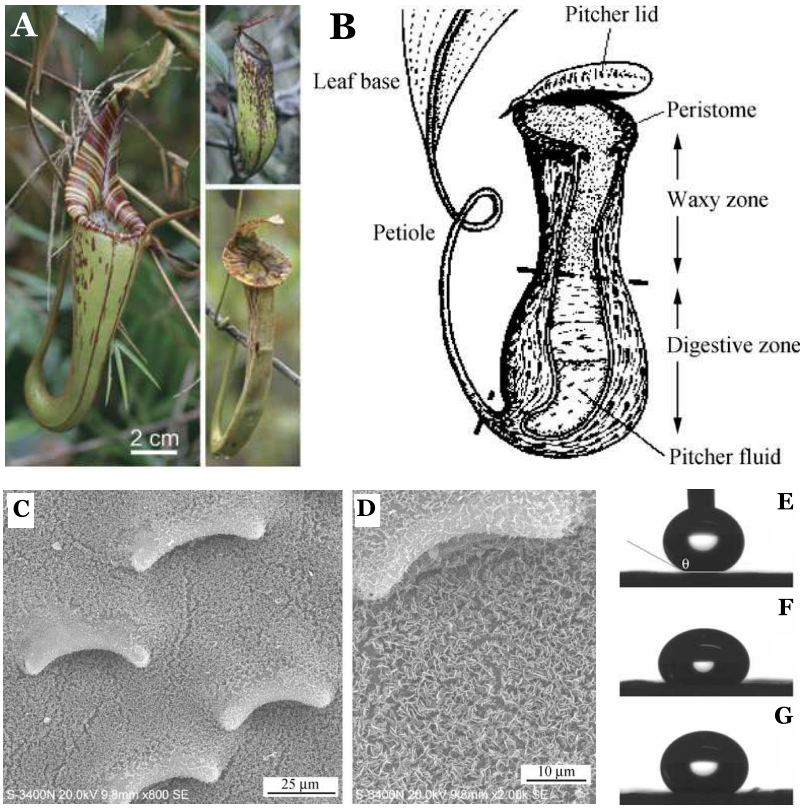

Figure 3.3.4: Pitcher plants and their morphology. A) Examples of *Nepenthes* pitcher plants showing three examples of the interspecific variation in the size and shape of their traps and of the upper pitcher rim (peristome), left: *N. hurreliana*, upper right: *N. muluensis*, lower right: *N. mirabalis* var. *echinostoma*. B) Schematic of a *Nepenthes* leaf showing the different zones of the pitcher. C - D) SEM micrographs of the waxy zone. C) The waxy zone with downward-directed lunate cells - enlarged overlapping guard cells; D) lunate cells covered with microscopic wax crystals. E - G) Contact angles of E) water, F) diiodomethane, and G) ethylene glycol on the waxy surface of the slippery zone. A) Adapted from Bauer *et al.* [179]. B - D) Adapted from Wang *et al.* [178]. E - G) Adapted from Gorb & Gorb [180].

steps towards the inner surface of the pitchers. The peristome surface is perfectly wettable by nectar secreted by the peristome (presumed to be present for attraction of arthropod prey) and by rain water, so that under humid or wet conditions the surface is covered with a homogeneous liquid film [181], which causes aquaplaning of the attachment devices of arthropods. The surface is wettable by water, and has a microroughness which increases wettability, consistent with the Wenzel state of wetting.

The conductive zone immediately beneath the peristome rim is an essential part of the trapping and retention mechanism due to its special downward directed cells, Figure 3.3.4C, and the thick covering of the surface of this zone with micro-metre scale wax crystals [123]. The wax crystal layers function *via* a combination of contamination of the adhesive pads by detachable crystals, reduced adhesion due to micro-metre scale roughness, and low surface energy. The digestive zone at the bottom of the pitcher does not play a specific role in the trapping of insect prey, but the digestive liquid in which insects find themselves is viscous enough to prevent insects from escaping.

Taking influence from natural surface such as these which do not primarily function *via* heavy contamination of insect attachment devices to prevent their locomotion, it becomes clear that chemical and structural modification of a substrate can have a detrimental effect on insect attachment forces. However, it remains unclear whether the decrease is a consequence of the substrates' surface energy, surface roughness, or an interaction between these factors. Chapter 8 describes experimental investigations into synthetically created superhydrophobic and superhydrophilic substrates constructed in an effort to further understand the biomechanics of insect adhesion, and how these structured surfaces may be used to prevent adhesion in insects for practical application. We also studied the durability of these surfaces in natural environments to determine possibilities for commercial use of such systems.

Chapter 4

Physical Mechanisms of Insect Adhesion - Theoretical Models and Characterisation of Adhesive Systems

4.1 Introduction

The aim of Chapters 4 & 5 is to characterise the functional morphology of the attachment pads and properties of the adhesive secretion of insects representative of the two distinct pad types, in an effort to further understand the physical mechanisms behind the wet adhesion of insects. In order to identify the key issues that will be addressed in these chapters, we now briefly review previous work in this area.

In terms of the adhesive force, a simple model that has been used for wet adhesion is to assume that the secretion forms a uniform thin film in the contact zone between the adhesive pad (i.e., arolia or individual setae) and the substrate, and adhesive forces arise from the capillary force between two rigid parallel plates [34, 66, 109], as described in Section 2.4.2. However, while this rigid parallel plate model correctly predicts that the adhesive force is proportional to the area of the adhesive pad and inversely proportional to the film thickness [68, 109], it over predicts the actual adhesive force by several orders of magnitude [109]. This large discrepancy is due to the model oversimplifying actual wet adhesive systems in several important respects. Firstly, the geometry of the adhesive pad and the small size of the arolia or setae means that the adhesive pads may not be flat on the roughness scale of the substrate [90], as discussed in Chapter 2. Secondly, there may be dry contact between the adhesive pad and the substrate so that, in addition to capillary forces, dry adhesive forces (e.g., van der Waals forces) will also need to be taken into account, see Section 2.4. Finally, both smooth and hairy pads in insects are not in fact rigid but soft [22, 48, 59], so detachment may not occur by cohesive failure of the contact zone but by *peeling* from the edge of the contact zone; this would lead to a significant

reduction of the detachment force. In order to account for some of the above effects, a more appropriate model for the adhesive force may therefore be to consider a sphere on flat model [12, 182].

In terms of the frictional force, the simple rigid-parallel-plate model correctly predicts that the frictional force should be inversely proportional to the liquid film thickness [12, 40], as described in Section 2.5. However, in some cases it *under* predicts the frictional forces by at least an order of magnitude, and more importantly it does not explain the ability of many insects to sustain significant *static* friction [12, 68, 183]. Two possible explanations exist to account for this discrepancy; i) frictional force in insects are primarily due to dry 'rubber' friction arising from direct contact between the soft, deformable adhesive pad and the substrate [12, 183], and, ii) adhesive secretions are non-Newtonian emulsions consisting of a hydrophilic and hydrophobic phase, see Chapter 2, and the static friction arises from the yield stress of the emulsion [12, 90].

To date there has not been a systematic comparison between these models to determine which can be considered the most reasonable quantitatively. In an effort to address this important gap in the literature and gain a greater understanding of the physical mechanism of wet insect adhesion, in this chapter and chapter 5 we perform an integrative study of adhesive and friction forces in the Asian weaver ant *Polyrhachis dives* and the Harlequin ladybird *Harmonia axyridis*. These insects possess smooth and hairy adhesive pads respectively and are therefore representative of the two main classes of adhesive pads found in insects. Specifically, in this chapter, we consider different candidate models for wet insect adhesion and characterise the adhesive pad system and liquid footprints for both insects. In Chapter 5 we then feed these characteristic parameters into the different candidate models and compare these predictions with adhesive and frictional forces measured using a centrifuge technique on smooth surfaces.

4.2 Materials & Methods

Study Insects

In order to use theoretical models to perform predictive calculations in Chapter 5, we must measure or estimate the input parameters for these models from living insects. The Harlequin ladybird and the Asian Weaver ant were selected as representative species possessing the hairy and smooth pad forms respectively.

The Harlequin ladybird *Harmonia axyridis* [Pallas, 1773] (Coleoptera; Coccinellidae), or multicoloured Asian lady beetle, Figure 4.2.1A, is a polymorphic beetle species originally native to Asia occurring in three main colour forms; red or orange with black spots (known as form (*succinea*); black with four red spots (form *spectabilis*); and black with two red spots (form *conspicua*). This Coccinelid has been used several times in the latter quarter of the 20th Century as a biological control agent in the Americas and Europe, and can now be found as far north in the UK as southern Scotland, and is presently considered by many to be an unwelcome invasive species. Adults are approximately 6–9 mm in length. The Asian weaver ant *Polyrhachis dives* [Smith, 1857] (Hymenoptera; Formicidae) are medium sized black ants, Figure 4.2.1B, the workers of which are approximately 5–10 mm long, native to the Australasia and Polynesian regions of the pacific. The colloquial name refers

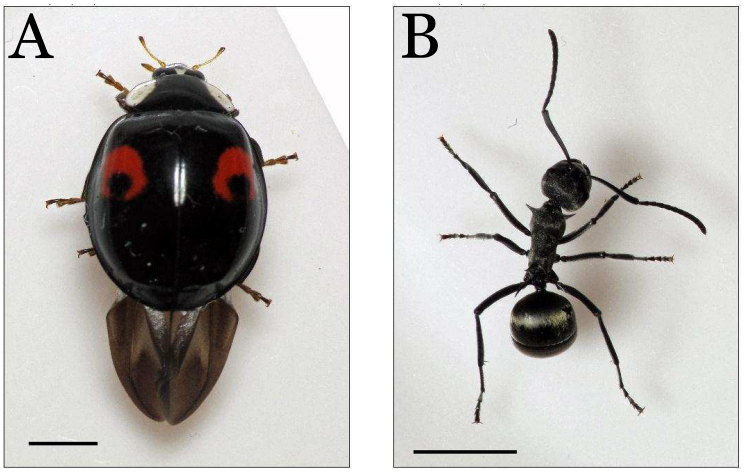

Figure 4.2.1: A) Top view of a Harlequin ladybird, *Harmonia axyridis conspicua*. B) Top view of an Asian weaver ant, *Polyrhachis dives*. Scalebars = 2 mm.

to their nest building abilities, which are similar, but not as complex, as the intricate nest building behaviours of the related genus *Oecophylla* [4].

Adult ladybirds were collected from the University of Hull campus, England, and surrounding areas (53°44'N, 00°20'W) between the months of April and September. Colonies of Weaver ants were purchased from a supplier (Antstore, Berlin, Germany). A significant difference between the attachment ability of males and females has been previously found in insects with hairy attachment pads, eg., Voigt *et al.* [6], however a study of any sexual dimorphism in *H. axyridis* is beyond the remit of the current project, so we report results for male ladybirds only in this chapter.

Insects were held in glass formicaria (dimensions: 300(L) x 200(H) x 200(W) mm, Antstore, Berlin, Germany) with a light:dark regime of 14:10 hrs, temperature range 22 – 27 °C and relative humidity (RH) 30 – 50 %, monitored using a thermo-hygrometer (RH83, Omega Engineering, Manchester, UK). Insects were fed a mixture of sugar solution and dried seeds purchased from Antstore (ants), or a prepared food mixture (ladybirds) as described by Majerus [184] *ad libitum*. Average body mass was 29.8±8 mg (N=20, mean±s.d.) for *H. axyridis* and 7.0±1 mg for *P. dives* (N=20, mean±s.d.) (t-test, t= 243.335, $P < 0.001$).

Microscopy

Morphological studies of insect attachment systems were performed using scanning electron microscopy (SEM) (Zeiss EVO60, Carl Zeiss AG, Germany). Samples were air dried, mounted on sample studs and sputter-coated with 2 nm of gold-palladium, then imaged in high-vacuum mode at 2 kV beam voltage.

Phase-contrast optical microscopy images of secretion deposits on glass substrates were captured using a digital camera (Canon Powershot S31S, Canon (UK) Ltd, Surrey, UK) connected to an optical microscope (Olympus-BX41, Olympus Microscopy, Southend-on-Sea, UK) *via* an adaptor mount (MM99 S/N-3506, Martin Microscope Co., Easley, SC, USA).

High-speed photography was used to make dynamic measurements of attachment devices and adhesive secretion in contact with glass substrates. Arolia of ants in contact with a substrate unfold with small pulls in the proximal direction [12, 40], we used this 'passive extension' to measure arolium contact area in the unfolded position in live ants; the arolia of workers held with entomological forceps (Paradox Co, Poland) in contact with glass microscope slides were observed under the objective of an optical microscope, and images were captured using a high-speed video camera (Pixci Silicon Video 642M, Epix Inc, IL, USA). Image analysis was conducted with ImageJ (ImageJ **v**.1.40, NIH, Bethesda, USA) [185]. Contact angles of secretion droplets deposited by insects were measured on hydrophilic and hydrophobic refelective silicon substrates (Siltronix Silicon Wafers, PI-KEM Ltd., Tamworth, UK) with interference reflection microscopy (IRM). Using a Zeiss IRM microscope equipped with an Epiplan-HD 40/0.85 objective, light was passed through a bandpass filter which isolated the green spectrum from a white light source, centred around $\lambda = 510\ nm$.

Substrates

Reflective silicon substrates used for IRM measurements were cut to size from large wafers (Siltronix Silicon Wafers, PI-KEM Ltd., Tamworth, UK), and were used in an untreated condition (hydrophilic) and after chemical silanisation (hydrophobic) with dichlorodimethylsilane ($(Si(CH_3)_2Cl_2)$; 99%, Sigma Aldrich, UK) using a method based on procedures found in the literature [186]. The wettability of the substrates was measured by measuring the contact angles of Millipore water (droplet volume 5 μL) using an optical drop shape analysis machine (Krüss DSA-10, Krüss GmbH, Hamburg, Germany).

All substrates were ultrasonically cleaned in hexane for 5 mins (>99.5%, Fisher Scientific, Loughborough, UK), iso-propanol for 5 mins (HPLC Grade, Fisher Scientific UK, Ltd, Loughborough, UK), rinsed in iso-propanol, and dried under a nitrogen stream before use.

Characterisation of Adhesive Pads & Secretion

Collection of Adhesive Secretion

To collect adhesive secretion footprints, insects were allowed to walk upon horizontal hydrophilic and hydrophobic silicon substrates for 1 hour by placing them within a small '*insect cell*', Figure 4.2.2, with an internal radius of 1 cm and height of 2 cm which was placed above the desired substrate. The insect could then freely move about over the substrate. Isolated footprints were carefully selected for analysis from their size, geometry and droplet distribution, ensuring that only droplets deposited by the adhesive pad were counted.

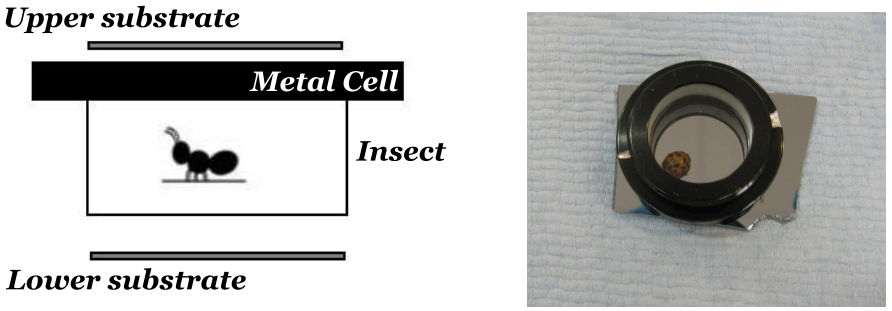

Figure 4.2.2: Insect-cell for collecting of secretion deposits. The metal cell holds the insect with an upper and lower glass substrate, and can be placed on to other substrates for collection of footprints from freely walking insects.

Contact Angle & Volume of Secretion Deposits

Contact angles were determined following a method similar to that described in the literature [87, 187], which is briefly outlined as follows. Due to the extremely small size of the droplets, it can be safely assumed that gravitational forces are negligible compared with surface tension and droplets take a spherical cap geometry so that under monochromatic light interference fringes are produced at positions of equal height. Using the *ImageJ* macro '*Dynamic Profiler*'[1] the light intensity and position of the Newton ring pattern was evaluated along a cross-section through the centre of the droplet, Figure 4.2.3. The

[1] http://rsbweb.nih.gov/ij/plugins/dynamic-profiler.html

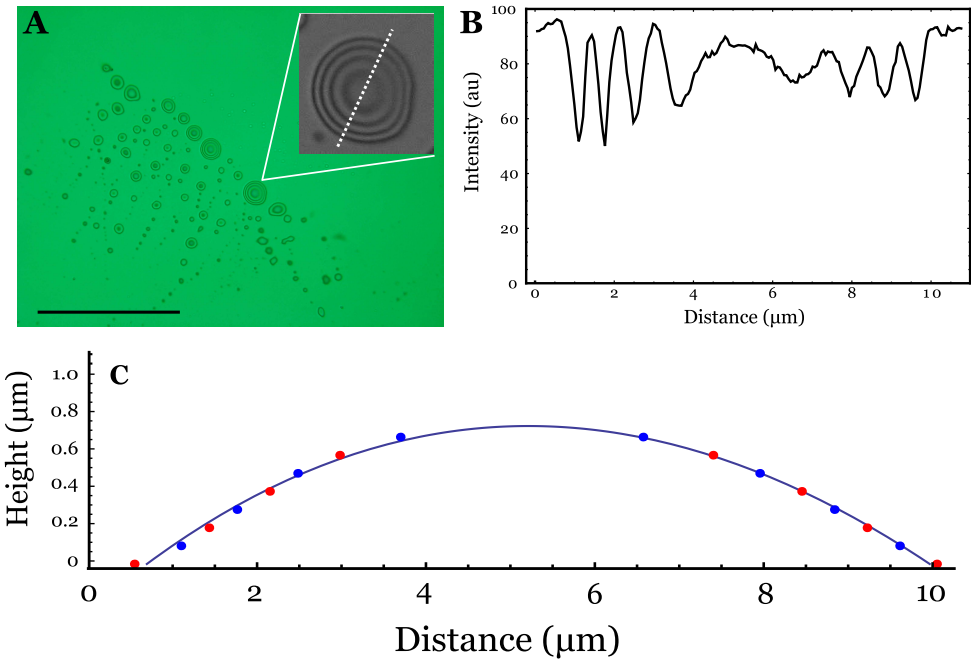

Figure 4.2.3: Interference method for measuring contact angles of microscopic droplets. A) Interference fringes in secretion droplets of *H. axyridis* on a hydrophilic reflective silicon substrate, scale bar = 50 μm (image size 155 × 116 μm^2). Inset shows a magnification of the droplet analysed along the dotted cross-section. B) Intensity profile along the dotted line in the inset of A). C) Drop profile fitted to the interference fringe height data from A) & B).

positions of intensity maxima and minima were determined manually, and the heights at these positions were calculated using:

$$h_{constructive} = \frac{N\lambda}{2n} \tag{4.2.1}$$

$$h_{destructive} = \frac{(N+0.5)\,\lambda}{2n} \tag{4.2.2}$$

where N is a positive integer (0,1,2...) and is the fringe order, λ is the wavelength of light in air and n is the refractive index of the liquid. In all calculations the refractive index of the secretion droplets was assumed to take the value of $n = 1.43$ in line with Federle *et al.* [12] who performed similar experiments with the ant species *Oecophylla smaragdina*, and consistent with findings that insects secretions are principally composed of liquid hydrocarbons [21, 77], see Section 2.3.1. From this information the drop profile can be determined by fitting an appropriate curve, Figure 4.2.3. The contact angle was

then obtained using [172, 188]:

$$\theta = 2arctan\left(\frac{h}{r_b}\right) \tag{4.2.3}$$

where r_b is the drop radius at the surface and h is the maximum height of the droplet determined from the droplet profile.

The secretion volume of an individual droplet is further determined by:

$$V = \pi r_b^3 \cdot \frac{2 - 3cos\theta + cos^3\theta}{3sin^3\theta} \tag{4.2.4}$$

where $2 - 3cos\theta + cos^3\theta/3sin^3\theta$ is a constant which depends on the contact angle θ. To estimate the volume of secretion deposited within each 'footprint', we used Equation 4.2.4 together with the mean contact angle θ for each insect and sum the total number of droplets within images of footprints.

Viscosity

When a liquid is sheared across a glass surface to a height below a critical thickness e_c, the resulting thin-film is meta-stable and undergoes spontaneous dewetting, breaking into small droplets [189, 190], eg., Figure 4.2.4. By observing the dynamics of dewetting of the secretion on smooth surfaces, an estimation of the liquid viscosity can be obtained by measuring the insect droplets' dewetting velocity on smooth hydrophilic glass substrates, using an approach similar to that reported by Federle *et al.* [12] for the ant *Oecophylla smaragdina*.

From dimensional analysis the dewetting velocity, v of a thin film can be described as the competition between surface tension and viscous forces:

$$v = q(\theta)\frac{\gamma}{\eta} \tag{4.2.5}$$

for the spontaneous dewetting of a uniform film below its critical thickness, where $q(\theta)$ is a dimensionless constant which is a function of the contact angle θ [189, 190]. By using the control liquid squalane ($C_{30}H_{62}$) (Fisher Scientific, Loughborough, UK) which has similar contact angle and surface tension as the secretion (eg., see Section 4.4.2.3), from Equation 4.2.5 it follows that:

$$\eta_{sec} \simeq \frac{\upsilon_{squalane}}{\upsilon_{secretion}} \cdot \eta_{squalane} \tag{4.2.6}$$

The secretion viscosity of *P. dives* and *H. axyridis* was estimated by measuring the dewetting velocity of droplets deposited on hydrophilic glass substrates using high-speed photography. Droplets deposited on substrates were manually sheared using a hydrophobic entomological needle under the objective of an optical microscope filmed using a high speed camera. Dewetting velocities were determined by tracking the movement of the three-phase contact line and plotting distance *vs.* time graphs and taking the mean value of several measurements.

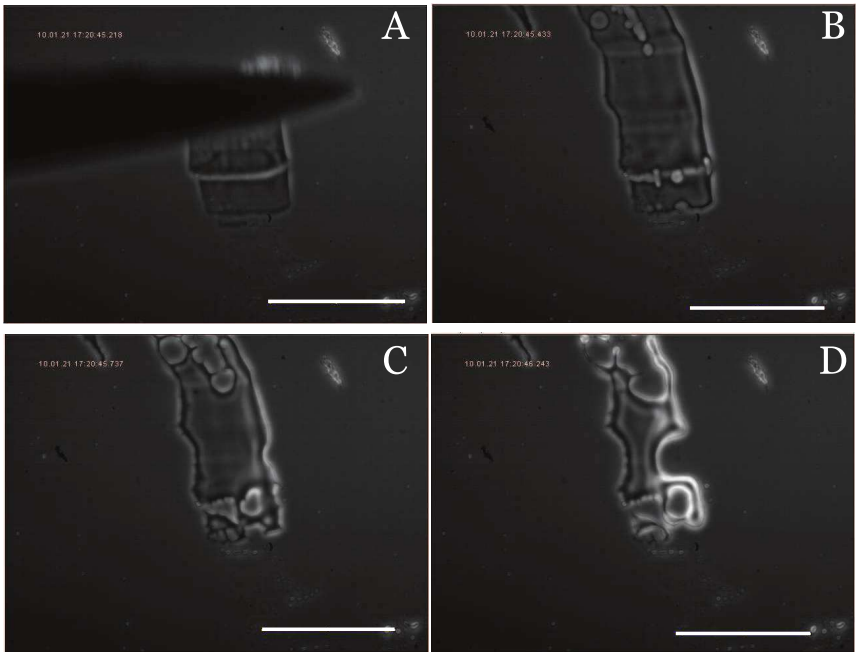

Figure 4.2.4: High-speed photography images of the shearing of a droplet of the control liquid (squalane) on a hydrophilic glass substrate. The resulting thin film is meta-stable and spontaneously de-wets into many small droplets. The three-phase contact line moves at a particular velocity determined by the competition between surface tension and viscosity forces. Scale bars = $200\mu m$.

Chemical Composition

In an effort to determine the chemical composition of the adhesive secretion of the Weaver ant *Polyrhachis dives*, footprint deposits from several ants were analysed using gas chromatography - mass spectrometry (GCMS). Four individual workers were placed within a glass Petri-dish ($r = 6.4$ cm) for 18 hours to collect multiple footprints. Dishes containing insect footprints were rinsed with 100 μL hexane, and reduced *via* evaporation under a pure nitrogen stream. A further 100 μL of hexane was added to the dish and transferred to GC extraction vials. Footprint washes were analysed on a gas chromatograph (GC) (Hewlett-Packard 6890) with a split/splitless injector (250 $^{\circ}C$ splitless injection) with a 10 μL 7673 injector (injection volume 1.0 μL) connected to a 5973 mass selective detector (Agilent Technologies). A capillary column (HP-5, 26.5 m x 250 μm nominal diameter, 0.25 μm film thickness) was used with a helium carrier gas flow of 1.5 $mLmin^{-1}$. A temperature programme of initial temperature 30 $^{\circ}C$, 30 s isoth., 5 $^{\circ}C/min$ to 150 $^{\circ}C$, then 10 $^{\circ}C/min$ to 280 $^{\circ}C$ was used. Chemical identifications were performed on a coupled GC-MS system (HP 6890 GC/HP 7673 MSD) with electron impact ionisation of 71 eV.

4.3 Theoretical Models for Adhesion & Friction

In order to understand the physical origin of insect adhesion and friction, it is necessary to compare experimental measurements of insect adhesion forces with predictions from theoretical models. As discussed in Section 2.2, the actual morphology of both smooth and hairy insect pads is complex and variable. Therefore, in order to proceed with constructing usable models we consider some simple idealised models for the adhesive pads. Although these models are relatively simplistic, we believe that these models cover a wide enough range of relevant contact geometries and contact mechanics as to allow us to draw some useful conclusions regarding the underlying mechanism of wet adhesion in real systems. In this section, we briefly discuss the specific models we consider in this study for the adhesive forces normal to the substrate and friction forces tangential to the substrate.

4.3.1 Models for Adhesion Force

Rigid-Parallel-Plate

Although it has been previously stated that the parallel-plate-model is an idealised model which does not account for many aspects of insect adhesion, we wish to quantify these discrepancies in order to determine to what extent other models are an improvement, or not, over this model, and as such it will be included in our analysis. Assuming that the secretion forms a uniform thin film in the contact zone between the adhesive pad (i.e., arolia or individual seta) and the substrate [34, 66, 109] which act as rigid plates, Figure 4.3.1A. Let θ_1, be the contact angles of the secretion with the substrate , and assuming the secretion wets the adhesive pad perfectly with contact angle $\theta_2 \to 0$, and denoting $\theta_1 = \theta$, from simple geometry it can be shown that the adhesive force per arolium or seta is given by

$$F^N_{smooth} = \frac{\gamma A_c}{h}(cos\theta + 1). \tag{4.3.1}$$

To obtain the total force for a hairy adhesive pad, it is assumed that the adhesive load is shared equally between all setae in the pad so that the total adhesive force per hairy pad is

$$F_{hairy}^{N} = n_{seta}\frac{\gamma A_t}{h}(cos\theta + 1) \tag{4.3.2}$$

where A_t is the average setal tip area and n_{seta} is the average number of setae per hairy pad. Finally, the film thickness h in the above equations is related to the volume of the secretion V (Equation 4.2.4) according to $h = V/A_c$.

Sphere on Flat Models

As discussed in Section 2.4, detachment of dry contact between insect adhesive pads and the substrate (even when the contact is flat) generally occurs *via* crack propagation rather than cohesive failure. The detachment force in the former case is more accurately modelled by the detachment force between a sphere and a flat rather than between two flat surfaces. In addition, the arolia or setae may not be flat on the roughness scale of the substrate, see Figure 4.4.3. A more realistic model for the contact mechanics and contact geometry

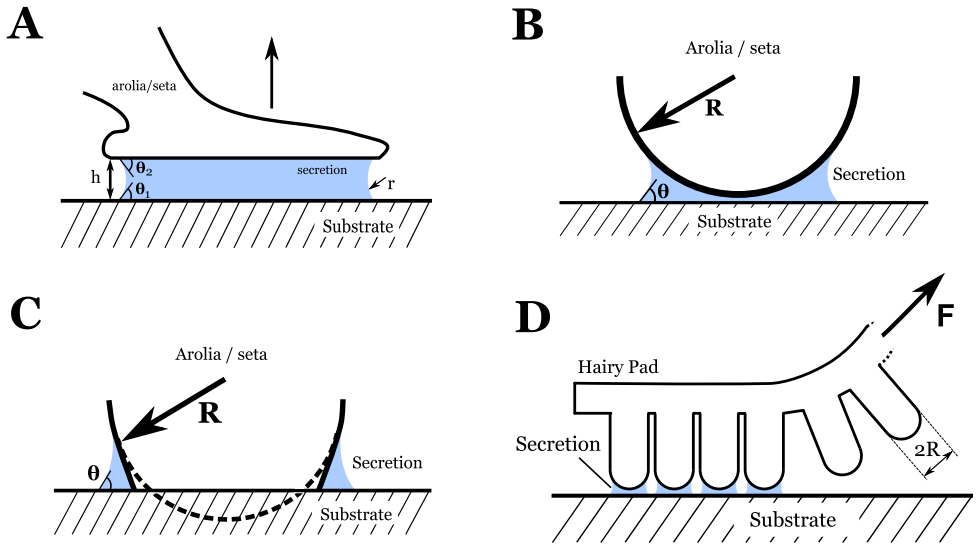

Figure 4.3.1: Schematic diagram of the contact zone geometry used for smooth and hairy pads for the different theoretical models. A) Rigid parallel-plate-model, B) sphere-on-flat for DMT theory, C) sphere-on-flat for JKR theory, D) Peeling model for fibrillar pads. θ contact angle, h, film thickness, r radius of curvature of liquid meniscus, F, direction of force.

of the contact zone is to assume that the secretion is sandwiched between a spherical pad of radius R and flat substrate [109], shown in Figure 4.3.1B,C, for rigid and soft adhesive pads respectively [108, 191]. These contact geometries modify the form of the capillary force (due to the non-uniform thickness of the secretion), and introduce dry contact forces to the total adhesive force (due to presence of direct dry contact between the adhesive pad and substrate). As discussed in Section 2.4.1.5 many flat interfaces detach *via* crack propagation or peeling, and it is useful to calculate detachment forces between curved surfaces which more accurately predict the adhesive strength of the interface. In particular for rigid and soft spheres, the dry contact forces are given by the Derjaguin-Muller-Toporov (DMT) model (Derjaguin *et al.* [105]) and the Johnson-Kendall-Roberts (JKR) model (Johnson *et al.* [106]) respectively, see Chapter 2.

Therefore the total adhesive force per smooth pad given is by:

$$F^N_{smooth} = \frac{3}{2}\pi R W_{AB} + 2\pi R\gamma(1 + cos\theta) \tag{4.3.3}$$

where W_{AB} is the work of adhesion for solid-solid contact between the adhesive pad (A) and the substrate (B) (i.e., the work done per unit area of a planar interface to separate the two contacting surfaces) in the presence of the secretion, see section 4.3.1. The first term on the right hand side is the JKR dry contact force and the second term is the capillary force between a sphere and a flat. For the capillary force term we neglect the additional contribution from the deformability of a soft-sphere, as discussed in Section 2.4.2. As such, Equation 4.3.3 represents a *lower bound* for the capillary force in this case. On the other hand, for hairy pads, again assuming the adhesive load is equally shared between the setae in the pad, the total adhesive force per hairy pad is given by:

$$F^N_{hairy} = n_{seta}\left[2\pi R W_{AB} + 2\pi R\gamma(1 + cos\theta)\right] \tag{4.3.4}$$

where the first term on the right hand side is the DMT dry contact force and the second term is the capillary force between a sphere and a flat. For hairy pads of insects, individual

setae are much more rigid than smooth attachment pads [192], so the capillary force term in Equation 4.3.4 should capture the actual capillary force well in this case. Note that in contrast to the rigid parallel plate model, the capillary force in the sphere on flat model is independent of the volume of the secretion and is proportional to the contact radius R rather than R^2.

Peeling Model for Hairy Pads

In the above two models for hairy pads, it has been assumed that the adhesive load is equally shared between all setae in the pad. Equal load sharing holds if the pad is small, setae are compliant and the structures from which they emerge are stiff [59, 113], Section 2.4.2.3. If this is not the case, Hui *et al.* [113] showed that stress may be concentrated along the peeling edge in the hairy pad; in the extreme case along one row of setae along the peeling edge of the pad, Figure 4.3.1D. In order to allow for this possibility, in addition to the equal load sharing models for hairy pads discussed above, a third model is considered where the adhesive force per hairy pad is given by:

$$F^N_{hairy} = n_{edge}\left[2\pi R\gamma(1 + cos\theta) + 2\pi R W_{AB}\right]. \tag{4.3.5}$$

where n_{edge} is the mean number of setae along the peeling edge of the hairy pad. The theoretical models used in Chapter 5 to model adhesive forces in both smooth and hairy pads are summarised in Table 4.3.1.

Dynamic Adhesive Forces

Dynamic attachment may be aided by the viscosity of the adhesive secretion deposited by most insects during locomotion, which can give rise to rate-dependent normal adhesion forces (Stefan adhesion, Section 2.4.2.2). Within the centrifuge experiment, normal detachment is a relatively slow, quasi-static process, and as such dynamic forces will not

be considered within this chapter, or Chapter 5. However Stefan adhesion will be relevant for fast detachments, and will therefore be considered within Chapter 6 for impulsive detachment experiments.

Calculation of Work of Adhesion W_{AB}

A key quantity required for calculating dry contact forces in the models above is the work of adhesion W_{AB} between the adhesive pad (A) and the substrate (B) in the presence of secretion (L). We calculate W_{AB} using the Good-Girifalco equation [94, 97]:

$$W_{AB} = 2\Phi\sqrt{\gamma_{AL}\gamma_{BL}} \tag{4.3.6}$$

where γ_{AL} is the adhesive pad/secretion interfacial energy, γ_{BL} is the substrate/secretion interfacial energy and Φ is a correction factor related to the mismatch in intermolecular interactions between A and B [95]. For example, if both A and B are non-polar solids Φ is close to unity, while if one solid is polar and the other non-polar, Φ is significantly less than unity, usually around 0.5. The interfacial energies γ_{AL}, γ_{BL} can in turn can be calculated by combining Equation 4.3.6 with the Duprè equation [94]:

$$\gamma_{AL} = \gamma_A + \gamma_L - W_{AL} = \gamma_A + \gamma_L - 2\Phi\sqrt{\gamma_A\gamma_L} \tag{4.3.7}$$

where γ_A, γ_L are the surface energies of the pad and the liquid secretion respectively in air. The interfacial energy γ_{BL} can be similarly calculated by replacing A with B.

Table 4.3.1: Summary of theoretical models used in Chapter 5 to calculate the adhesive force per adhesive pad for both ants (smooth pad) and ladybirds (hairy pads).

Model/Insect		Equation
Rigid Parallel Plate	Ants	$F^N_{smooth} = \frac{\gamma A_c}{h}(1 + cos\theta)$
	Ladybirds	$F^N_{hairy} = \frac{\gamma A_t}{h}(1 + cos\theta)n_{seta}$
Sphere-on-flat	Ants	$F^N_{smooth} = \frac{3}{2}\pi R W_{AB} + 2\pi R\gamma(1 + cos\theta)$
	Ladybirds	$F^N_{hairy} = [2\pi R W_{AB} + 2\pi R\gamma(1 + cos\theta)]\, n_{seta}$
Peeling Model	Ladybirds	$F^N_{hairy} = [2\pi R W_{AB} + 2\pi R\gamma(1 + cos\theta)]\, n_{edge}$

4.3.2 Models for Friction Force

Rigid Parallel-Plate-Model

Assuming the rigid parallel-plate geometry shown in Figure 4.3.2, and that the secretion is Newtonian, the tangential frictional force per arolium or seta due to viscous forces of the secretion is given by

$$F^T_{smooth} = \frac{\eta v A_c}{h} \tag{4.3.8}$$

where η is the viscosity of the liquid secretion, A_c is the area of the adhesive pad, v is the velocity of the pad relative to the substrate and h is the thickness of the liquid film given in Section 4.3.1. To obtain the total force per hairy pad, again it is assumed that all setae in the pad contribute equally to the frictional force so that the total friction force per hairy pad is

$$F^T_{hairy} = \frac{\eta v A_t}{h} n_{seta} \tag{4.3.9}$$

In principle there could also be a contribution to the tangential force from the meniscus due to contact angle hysteresis between the advancing and receding contact angles. However Federle *et al.* [183] showed that this contribution is negligible and it will not be considered

here. Note that in the above equations, friction forces are predicted to depend only on the properties of the secretion and, as such, should be independent of the substrate.

Dry Friction

If there is dry contact between the adhesive pad and the substrate, e.g., for contact geometries shown in Figures 4.3.1B,C, there will be a contribution to the tangential force from dry friction. The dry frictional force per adhesive pad according to Amonton's law of friction [94]

$$F^T = \mu(L + F^N) \tag{4.3.10}$$

where μ is the static friction coefficient, F^N is the normal adhesive force per pad and L is the additional load on the pad due the insect's weight (see Chapter 2). As there are no simple relationships relating μ to material properties of the substrate and pad, it is not possible to use Equation 4.3.10 within a predictive model for the frictional force. Instead, Equation 4.3.10 can be used to extract effective values of μ for adhesive pads from measured values of normal adhesive and tangential frictional forces. This allows us to make determinations about the nature of the adhesive pad. Note that the equations summarised in Table 4.3.1 and Equations 4.3.8 & 4.3.9 are the force per tarsus. In order to obtain the force acting on the whole insect, we must multiply these forces by the number of adhesive pads in contact with the substrate. In Chapter 5 the centrifuge force measurements are carried out above a threshold velocity where insects exhibit the so called 'freezing response' with all six legs in contact with the substrate.

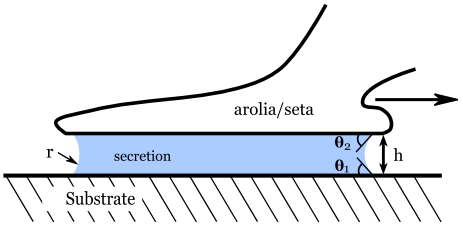

Figure 4.3.2: Parallel-plate-model schematic of the contact zone under shear during tangential movement. The liquid adhesive provides a viscous friction resistance to the movement provided the secretion thickness h is not too high.

4.4 Results & Discussion

In this section are results of the characterisation of the adhesive pad morphology and adhesive secretion of the Harlequin ladybird and the Asian weaver ant; namely the average radius of the arolia or setae R, secretion surface tension γ, contact angle θ, volume V, viscosity η, work of adhesion W_{AB} between adhesive pads and the substrate, and the tangential sliding velocity ν. This is performed in this section.

4.4.1 Adhesive Pads

4.4.1.1 Morphology - Smooth Pad

Consistent with other representatives of the order Hymenoptera the ant *Polyrhachis dives* has a tarsus terminated by the pre-tarsus (the most distal tarsal segment) which is separated into 5 tarsomeres, Figure 4.4.1A.

The pre-tarsus of the ant *P. dives* possesses an adhesive arolium situated within the most distal tarsomere, between the tarsal claws, on each leg, which can be expanded and inflated *via* movement of the claws, Figure 4.4.2. The claws are sickle shaped structures which extend distally and ventrally from the terminal end of the fifth tarsomere, these structures can interlock with substrate protrusions on rough surfaces [15]. The arolium appears smooth at low magnification (optical and SEM), though under closer magnification surface micro-structures and patterning is observed including ridged indentations running along the length axis of the tarsus and surface protrusions approximately 5–10 μm in length, and micro-fold, Figure 4.4.1C. These surface structures are possibly important for the delivery of the adhesive secretion to the contact zone, and for allowing rapid and easy retraction within the distal tarsomere between steps without the organ inadvertently sticking to itself [193].

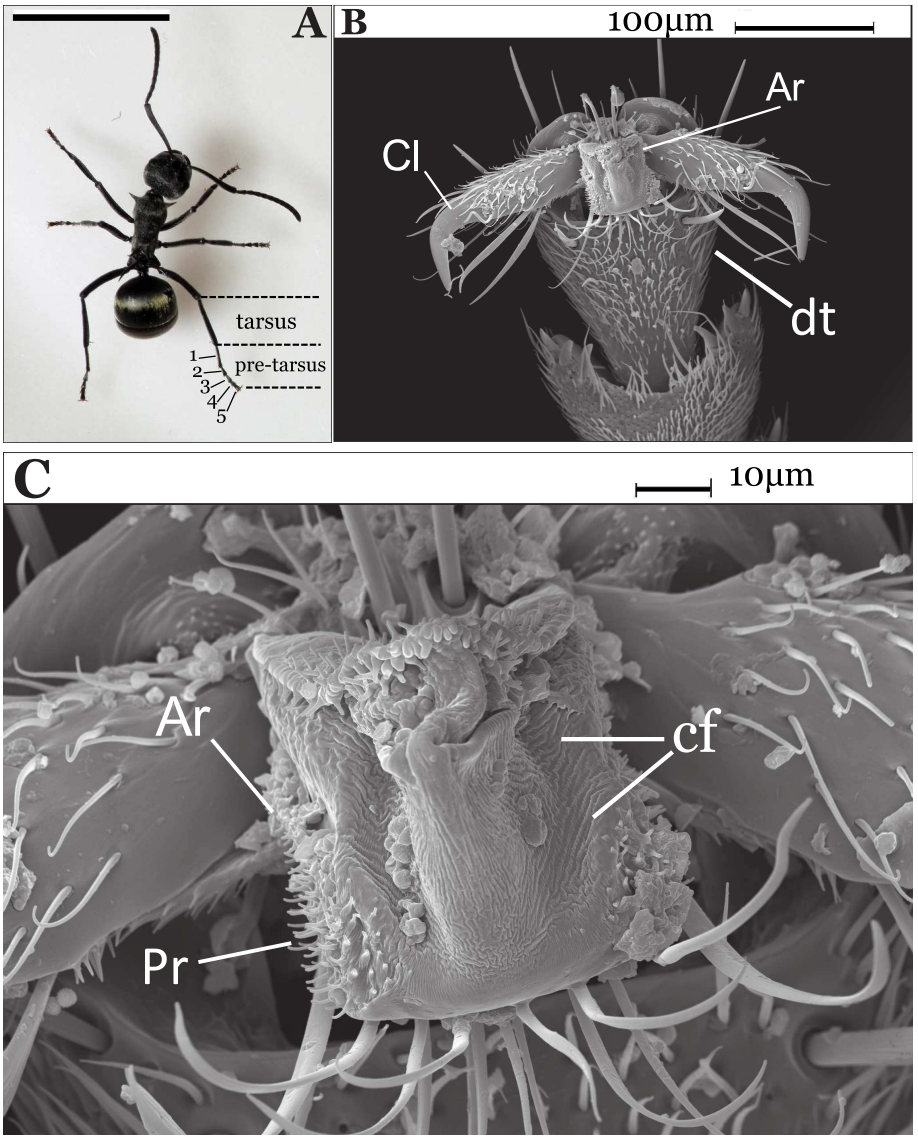

Figure 4.4.1: Scanning electron micrographs of the pre-tarsus and attachment devices of *Polyrhachis dives*. *A)* The Weaver ant *Polyrhachis dives*, *B*) *P. dives* pre-tarsus, ventral view, including tarsal claws and adhesive arolium in the retracted position. *C*) Higher magnification view of retracted arolium situated between the tarsal claws. Under greater magnification the 'smooth' arolium has visible surface structures and cuticular folds. *Ar*, arolium; *cl*, claws; *pr*, surface protrusions; *cf*, cuticle folds; *dt*, distal tarsomere; $1-5$, tarsomere sections of pretarsus. Scale bars (**A**) 2 mm, (**B**) 100 μm, (**C**) 10 μm

Consistent with previous morphological and kinematic studies of Hymenoptera tarsi [42, 49], we observe the claw movement was directly linked to arolium deployment on smooth surfaces, and the arolium deployment mechanism in this species is similar to that previously described for the ant *Oecophylla smaragdina* [12, 41], with inflation of the arolium coupled to retraction of the claws, Figure 4.4.2. The contact area with the substrate rapidly extends *via* proximal retraction of the claws [12] causing the ventral surface in contact with the

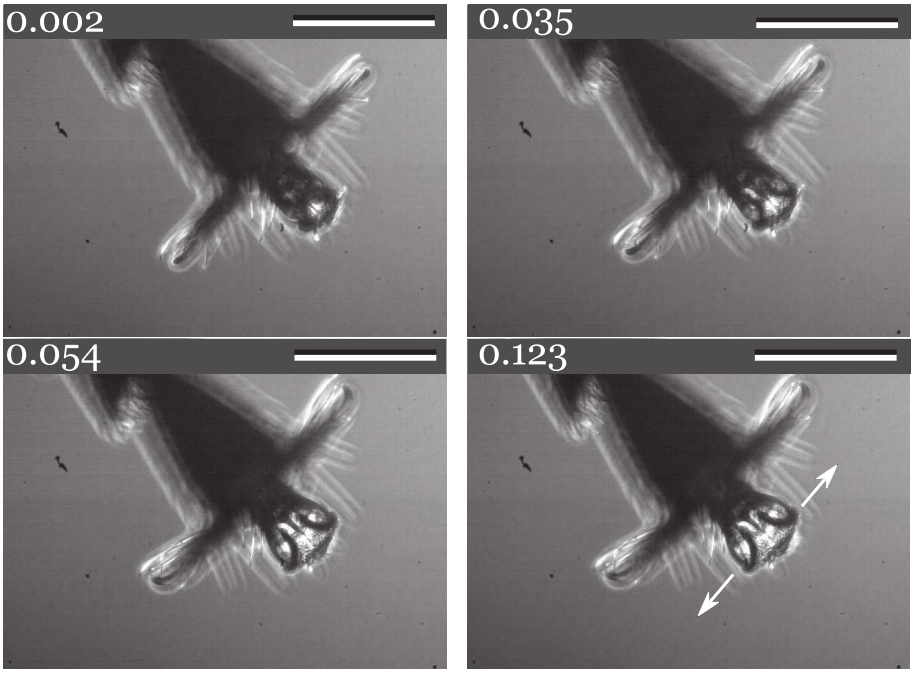

Figure 4.4.2: High speed video stills of the deployment of the arolium of *P. dives* in contact with a hydrophobic glass substrate. The arolium is a highly deformable organ which is capable of changing its contact area with the surface rapidly. Retraction of the claws in the proximal direction increases arolium inflation. Numbers in white correspond to cumulative time in seconds. Scale bars 100 μm.

substrate to expand in size both distally and laterally. The arolium can be deployed and the claws retracted through a large angle in approximately $\sim 100\ ms$, as measured with high-speed videography.

4.4.1.2 Morphology - Hairy Pad

The pre-tarsus of each leg of the ladybird *H. axyridis* is comprised of three tarsomere segments (T1–T3): the two proximal tarsal segments (T1 and T2) possess attachment pads on the ventral surface densely packed with setal hairs, while a pair of claws is situated on the most distal tarsomere (T3), Figure 4.4.3B. When the ladybird walks upon a smooth substrate the claws cannot grasp any surface asperities, and the adhesive pad found on T2 comes into almost complete contact with the substrate, and partial contact is made by the T1 pad. Due to the flexibility of the tarsal chain, the T1 pad is drawn into greater contact with the surface after a proximal pull of the tarsus. The hairy pads of *H. axyridis*, as found in other representative species of Coleoptera [6], consist of setae with

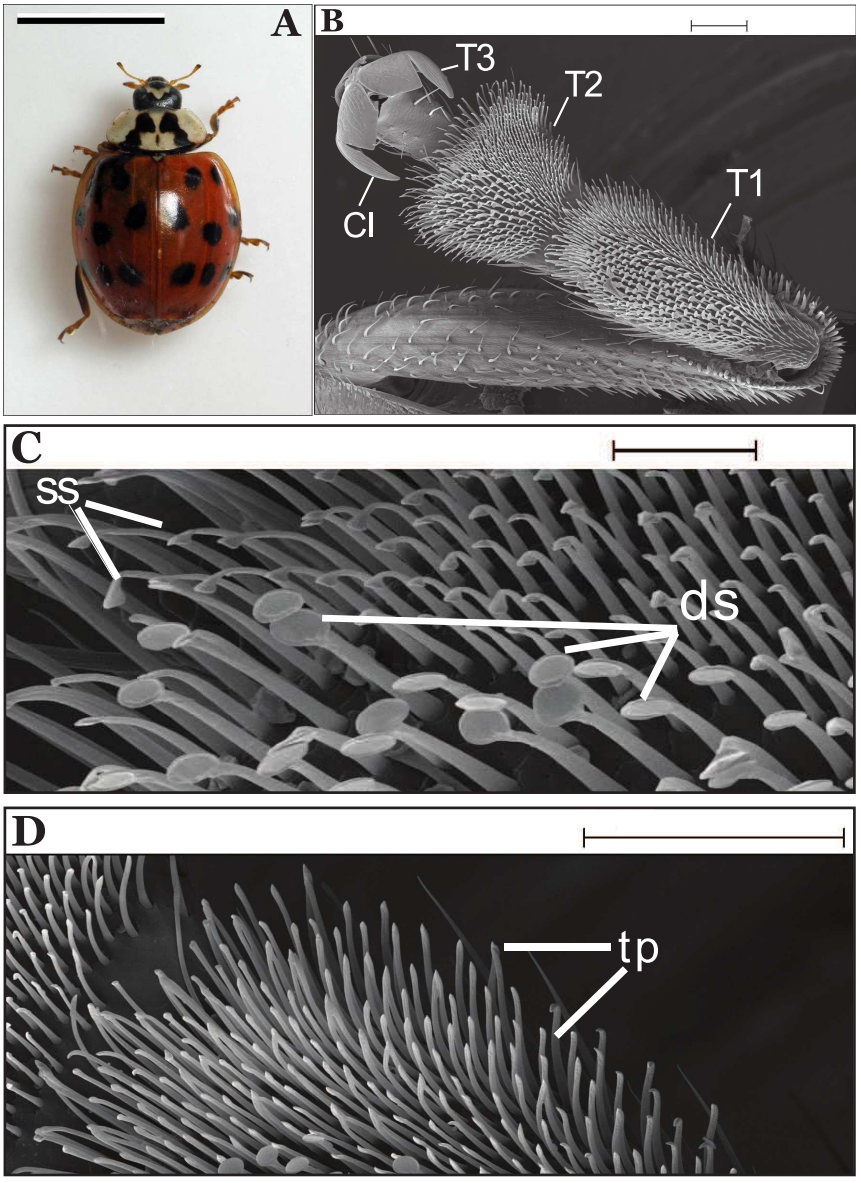

Figure 4.4.3: *A)* The Harlequin ladybird *Harmonia axyridis*. *B - D)* Scanning electron micrographs of the pre-tarsus and attachment devices of *Harmonia axyridis*. *B*) *H. axyridis* pre-tarsus, ventral view, including tarsal claws and setal attachment pads on the ventral surface. *C*) Higher magnification view of setal hairs possessing discoidal and spatulate tips, *D)* Higher magnification view of setal hairs possessing pointed, tapered tips. *T1–T3*, tarsomere segments; *cl*, claws; *ss*, spatulate tips; *ds*, discoidal tips; *tp*, pointed tips. Scale bars (**A** 2 mm, **B,D**) 100 μm, (**C**) 20 μm.

several morphologically distinct tip geometries, including tapered, spatulate and discoidal, Figure 4.4.3C,D & Figure 4.4.5.

The presence of different tip geometries found in the pad system of *H. axyridis* has been reported previously in Coleoptera [36] and Voigt *et al.* [6] reported a significant sexual dimorphism of setal tip geometries in the Colorado potato beetle *Leptinotarsa decemlineata*

with males having large numbers of discoidal tips, but females having none. The number of different setal tips in male ladybirds were denoted as n_t for tapered, n_s for spatulate, and n_d for discoidal, and Figure 4.4.5 depicts the distribution of the different setae tips in male Harlequin ladybirds. Different numbers of the three tip types were found on the different legs, Figure 4.4.4. Discoidal tips were most abundant on the front tarsi, fewer were found on the middle legs and no discoidal tips were found on the hind legs. Areas of discoidal tipped setae were found to be positioned off-centre towards the insects' body (proximally) within the hairy pads, and were surrounded by the other tip types. The presence of different tips in the beetle *L. decemlineata* corresponded to a significant difference between attachment ability of males and females on rough surfaces. Conversely, different tip geometries have also been found to be important for generation of strong attachment forces to smooth surfaces, and are found in abundance on the tarsi of the male dock beetle *G. viridula*, allowing for strong adhesion to the smooth elytra of the female during copulation [130], and Bullock & Federle [194] found that discoidal tips generated greater pull-off forces on smooth polystyrene than the other tips in this beetle. The asymmetrical distribution of setal tips may have advantages for adhesion during copulation, due to the curved shape and smooth surface of the female elytra. This could possibly be the reason for their presence in *H. axyridis*.

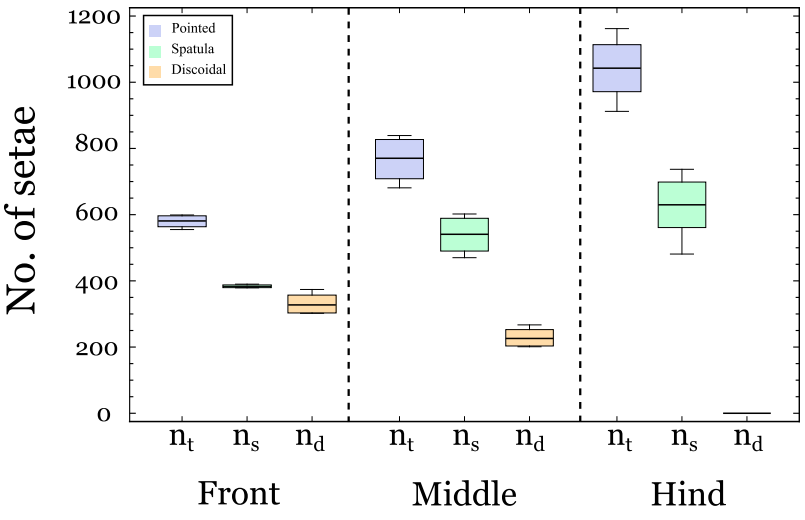

Figure 4.4.4: The proportion of the different setae *pointed, spatulate, discoidal* found in front, middle and hind legs of the male Harlequin ladybirds *H. axyridis*. Setal tips are proportioned differently between the different legs, and males have no discoidal shaped setal tips on their hind legs.

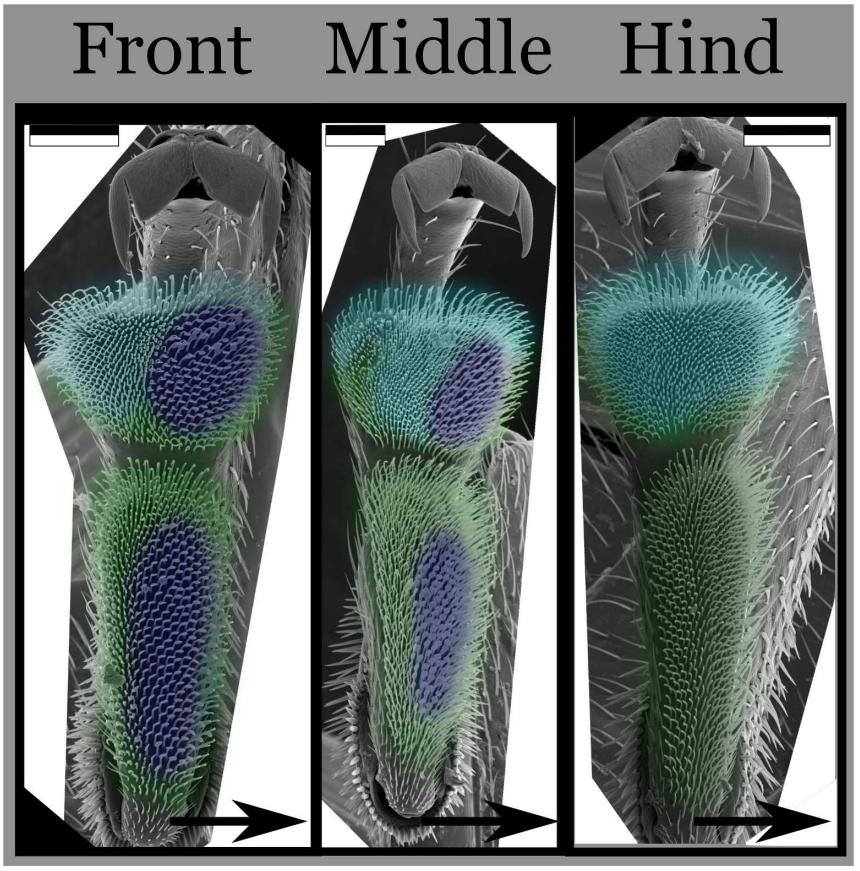

Figure 4.4.5: SEM images of the front, middle and hind tarsi in male Harlequin ladybirds showing the two tarsal pads and the claws situated on the most distal section. Colour coding indicates distribution of seta types on each of the legs. No discoidal tips are found on the hind legs of the male ladybirds. Arrows indicate the direction of the insects' body. Scale bars 100 μm.

4.4.1.3 Radius of Curvature & Contact Area

The radius of the contacting arolium and setae, together with the projected, or maximum available contact area of the adhesive pads of the ants and ladybirds was determined from optical and scanning electron microscopy images. For setae within the hairy pads, the radius of contact area is similar to the radius of curvature R of a curved surface. For the smooth pads of ants, the contacting arolium forms a flat contact when unfolded, eg., Figure 4.4.2. However, as discussed in Section 2.4.1.5, detachment of soft interfaces occur *via* peeling, and the detachment force is more accurately estimated from a sphere-on-flat model than that of two parallel plates, where the radius of the sphere R is comparable to the radius of the contact area. Therefore we will use the radius of the contact area as an estimate of R for the smooth arolia of the ants. The procedure for determining the radius

R and contact area A_c for each pad type is outlined in the following section.

Hairy Pads

Using SEM images, the number of different tips were counted manually for the attachment pads of front, middle, and hind legs. The total number of setae (T1 & T2) for the different legs were counted, Table 4.4.1, and the proportions of each tip type was determined, Figure 4.4.4. By measuring the radius of the different setal tip geometries the mean setal tip radius for each geometry was found as R_d=5±1 μm for discoidal (N=20), R_s=1.65±0.5 μm for spatulate (N=20) and R_t =1.25±0.25 μm for tapered tips (N=15). The mean radius of curvature R was then determined by:

$$R = \frac{n_t \cdot R_t + n_s \cdot R_s + n_d \cdot R_d}{n_t + n_s + n_d} \tag{4.4.1}$$

The total mean projected area for front, middle, and hind legs was calculated, Figure 4.4.7, and finally the number of setae along the peeling edge N_{edge} was determined by counting the number of setae which crossed a line drawn perpendicular to the length axis of the tarsus at 10 positions along each pad (T1 and T2 separately), and the mean value taken.

Table 4.4.1: Characteristic measurements of the hairy adhesive pads of male Harlequin ladybirds *H. axyridis*. Sample size N refers to the number of ladybird tarsi which were measured, n refers to number of individual insects.

Parameter	**Symbol**	**Value**	**N**	n
Mean No. of setae, front leg	N_{front}	1292 ± 18	6	3
Mean No. of setae, mid leg	N_{mid}	1537 ± 64	6	3
Mean No. of setae, hind leg	N_{hind}	1672 ± 84	8	4
Mean No. of setae per leg	n_{seta}	1500 ± 142	20	4
Mean No. of setae along peeling edge	N_{edge}	21 ± 8	8	4

Smooth Pads

The 'passive extension' of Hymenoptera arolia was used to measure contact area in the unfolded position in live ants [12, 40], for front, middle and hind legs during proximal sliding by manually drawing polygons around the edge of the contact zone, Figure 4.4.6 (N=50). The planar area A was then assumed to approximate to the shape of a circle and R calculated from $R = \sqrt{A/\pi}$.

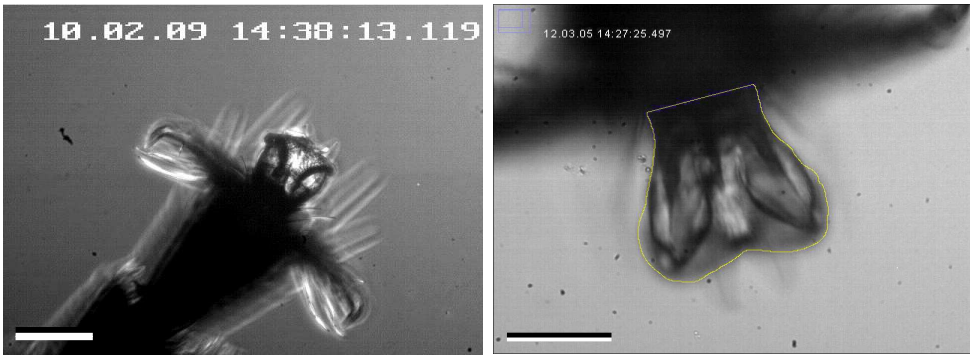

Figure 4.4.6: Top-down view of extended arolia of the weaver ant *P. dives* on a hydrophilic surface. Projected contact areas were determined by drawing polygons around the periphery of the contact zone.

Overall Contact Area

The mean value for the total contact area for hairy pads of male ladybirds was found to be 22,380±6400 μm^2 ($\sim$ 0.022 mm^2), and the front and middle legs were found to have significantly greater available contact areas than hind legs (t-test, P<0.001). Although the hind legs were found to have the largest mean number of hairs, the lack of any discoidal tips led to the hind legs having the least available contact area. The ant *P. dives* was found to have a total projected contact area that was significantly different between all legs (ANOVA: $F_{2,149}$=103.45, P<0.001), and, in contrast to the ladybird, contact area increased from the front to the hind legs, Figure 4.4.7A. The mean contact areas A_c for each insect are given in Table 4.4.5 and Table 4.4.4. The contact area of *H. axyridis* ($\sim$ 0.02 mm^2) is comparable to the *real* area of contact generated by the lighter beetle *G. viridula* in contact with glass cover-slips, as measured by Bullock *et al.* [120] with reflected light microscopy (body mass; *G. viridula* 10.4±0.4 mg, *H. axyridis* 29.8±8 mg). Similarly

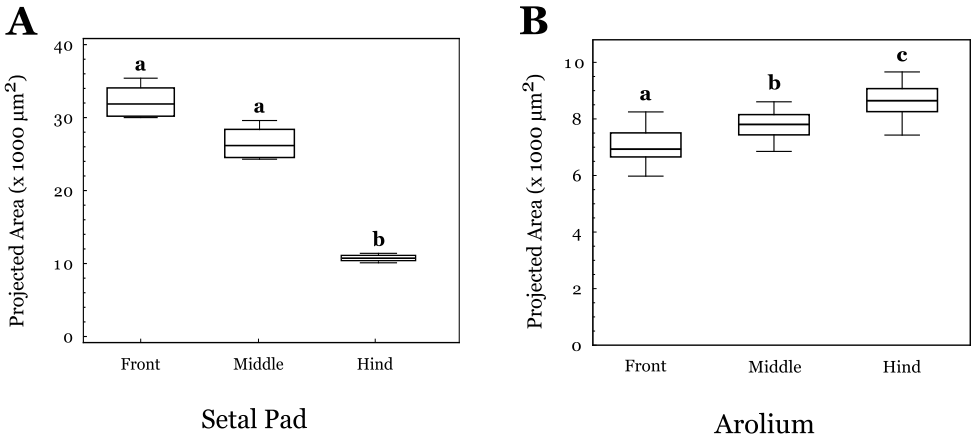

Figure 4.4.7: Projected contact area of A) *Harmonia axyridis* & B) *Polyrhachis dives* for front, middle and hind legs. Lower case letters denote statistical differences between legs. Ladybirds; N=4 insects, n=3 legs, t-test, P<0.001. Ants; N=5 insects, n=10 measurements each. ANOVA: P<0.001.

the contact area of the euplantulae of the cockroach *N. cinerea* (mean body mass; 372 mg) was found to be 46,351±6256 μm^2 [92].

4.4.2 Adhesive Secretion

4.4.2.1 General Appearance

Secretion footprint droplets from both insects are easily observed under low magnification with light microscopy, identified by the characteristic pattern conforming to the geometry of the adhesive pad morphology for each insect, Figure 4.4.8. Harlequin ladybirds were observed to deposit secretion droplets much more readily than the weaver ant on smooth surfaces which they had walked upon for the same amount of time on both hydrophilic and hydrophobic substrates. Footprints of *H. axyridis* were found in abundance, whereas deposits from *P. dives* were sparsely distributed over the solid surfaces investigated. Footprints of *H. axyridis* consist of droplets with diameter of approximately 1–6 μm depending on the hydrophobicity of the substrate, but droplets were greater in number, and generally smaller in base radius r_B on hydrophobic substrates, suggesting an increase in contact angle (eg., Equation 4.2.3). A crucial difference was observed between the print marks of ladybirds and ants; when dragging the adhesive pads of *P.dives* ants across hydrophilic

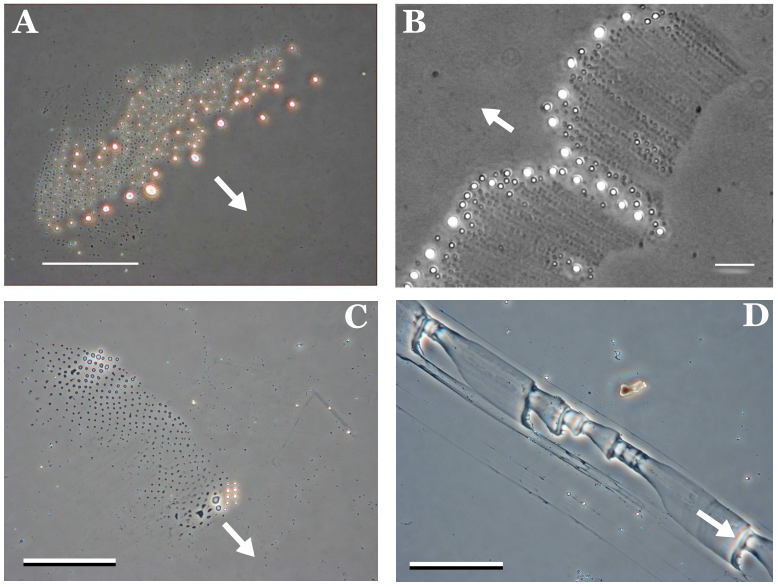

Figure 4.4.8: Phase-contrast optical microscopy image of the secretion footprints of A)& C) the Harlequin ladybird from T2 on hydrophobic and hydrophilic substrates respectively, and B)& D) the Asian weaver ant arolium, deposited on on hydrophobic and hydrophilic glass respectively. Arrows indicate distal direction. Scale bars; A),C),D) 100 μm, B) 10 μm

glass slides a smeared trail of secretion would be left behind. Shearing of the the attachment pad across the substrate produced ridged patterning within the secretion trails with a clear periodicity. Ridged positions were separated by approximately 5 – 10 μm, Figure 4.4.9, which we interpreted as possible evidence for an oscillatory 'stick-slip' motion during the sliding process, and may be a possible indication of dry contact during sliding scenarios, as will be discussed in Chapter 5.

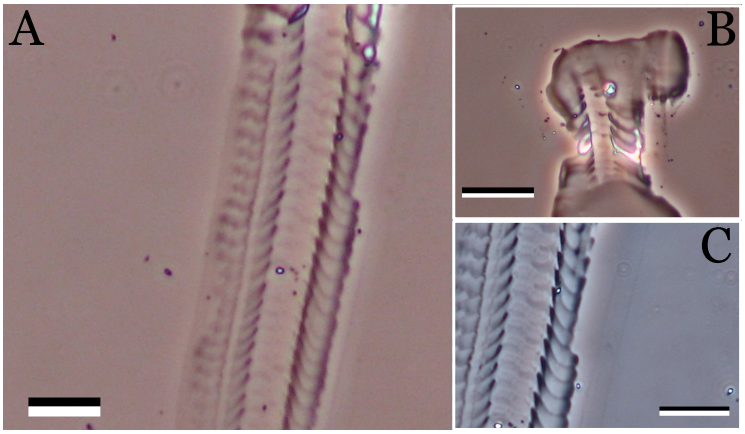

Figure 4.4.9: Possible stick-slip evidence within secretion deposits of *P. dives* on hydrophilic glass which would indicate dry contact between the pad and substrate. A & C) Shearing of the the attachment pad across the substrate produced ridged patterning with a clear periodicity. B) The beginning of the trail forms a shape similar to the shape of the deployed arolia. Scale Bars = 100 μm.

Solidification

In the course of following individual droplets during evaporation, it was sometimes observed that secretion droplets not only changed shape and size during the course of observation but also appeared to solidify, Figure 4.4.10. This was most noticeably observed to occur within the larger droplets; the droplets no longer exhibited interference fringes, and appearance changed from circular and completely transparent to consisting of translucent portions as well as darker, jagged opaque areas under the IRM microscope. Possible solid structures within the droplets have distinct edges and a jagged nature similar to crystal structures. This may be evidence of crystallisation of the secretion as the bulk of the liquid evaporates, and requires further investigation to clarify their nature. Sometimes these structures were observable within a liquid droplet during the evaporation process, but more often they were left behind after the evaporation of the liquid had completed.

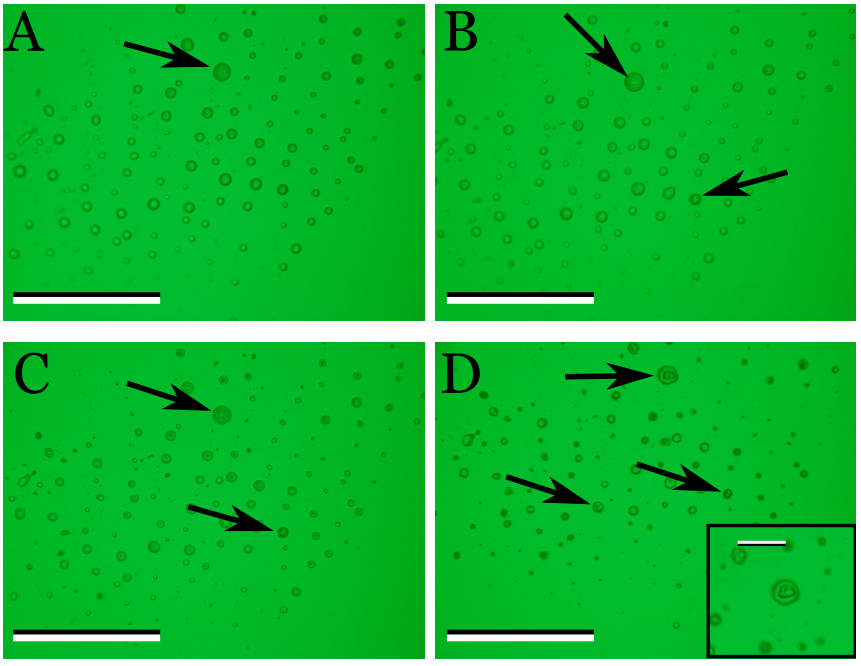

Figure 4.4.10: IRM images showing possible evidence of secretion crystallisation in *H. axyridis* droplets. After approximately 12–18 hours, a number of larger droplets begin to show opaque, jagged structures within the liquid. Arrows indicate the droplet which had these structures within them at different times after deposition to the substrate by the insect. A) Within 1 hour of collection, and after B) 2 hours, C) 3 hours, D) 18 hours, inset is after 24 hours. Scale bars = 100 μm, inset scale bar = 20 μm.

4.4.2.2 Chemical Composition

In an effort to determine the chemical composition of the adhesive secretion of the Weaver ant *Polyrhachis dives*, footprint deposits from several ants (N=10) were collected and analysed with GC-MS. Results indicated that the secretion droplets comprised of (in descending order of prevalence), n-alkanes, monomethylalkanes, dimethylalkanes, n-alkenes, phenols, fatty acids and esters. Compounds of a variety of chain-lengths were found, but those of C_{18}–C_{29} dominated. The most common molecules discovered, present in all samples analysed, are given in Table 4.4.2. Example chromatographs are shown in Figures 4.4.11 & 4.4.12.

The composition of *P. dives* adhesive secretion corresponds well to the composition of the cuticular hydrocarbon (CHC) profiles of other ants, and that of the adhesive secretions of insects found by previous authors, including other beetles [77], and ants [73]. Containing principally long chain hydrocarbons (alkanes), together with branched alkanes, fatty acids, and esters the secretion can be described as hydrophobic [21, 35, 74]. We did not detect any aqueous or volatile hydrophilic compounds [12], which could form the hydrophilic phase of an emulsion, however even if these compounds were present we would not expect to identify them given the nature of the secretion collection process. Any volatile compounds would have evaporated well before the extraction process began.

At ambient, or STP, conditions, n-alkanes larger than C_{18} are solid, Table 4.4.2, however the addition of a double bond or methyl group into the alkane reduces the melting temperature T_m by up to 25°C depending on the backbone structure and branch-position [73, 195], with internal branching having a greater effect than terminal branching [195, 196]. Also, although the melting temperature of a given alkane has a narrow T_m range, the presence of several different alkanes, and methylalkanes, within a fluid broadens the melting temperature so that melting occurs continuously over a broader temperature range [73]. Vötsch et al. [21] postulated that short-chained fatty acids and carbohydrates are responsible for the fluid properties necessary for its adhesive function in locusts. Thus, it is possible

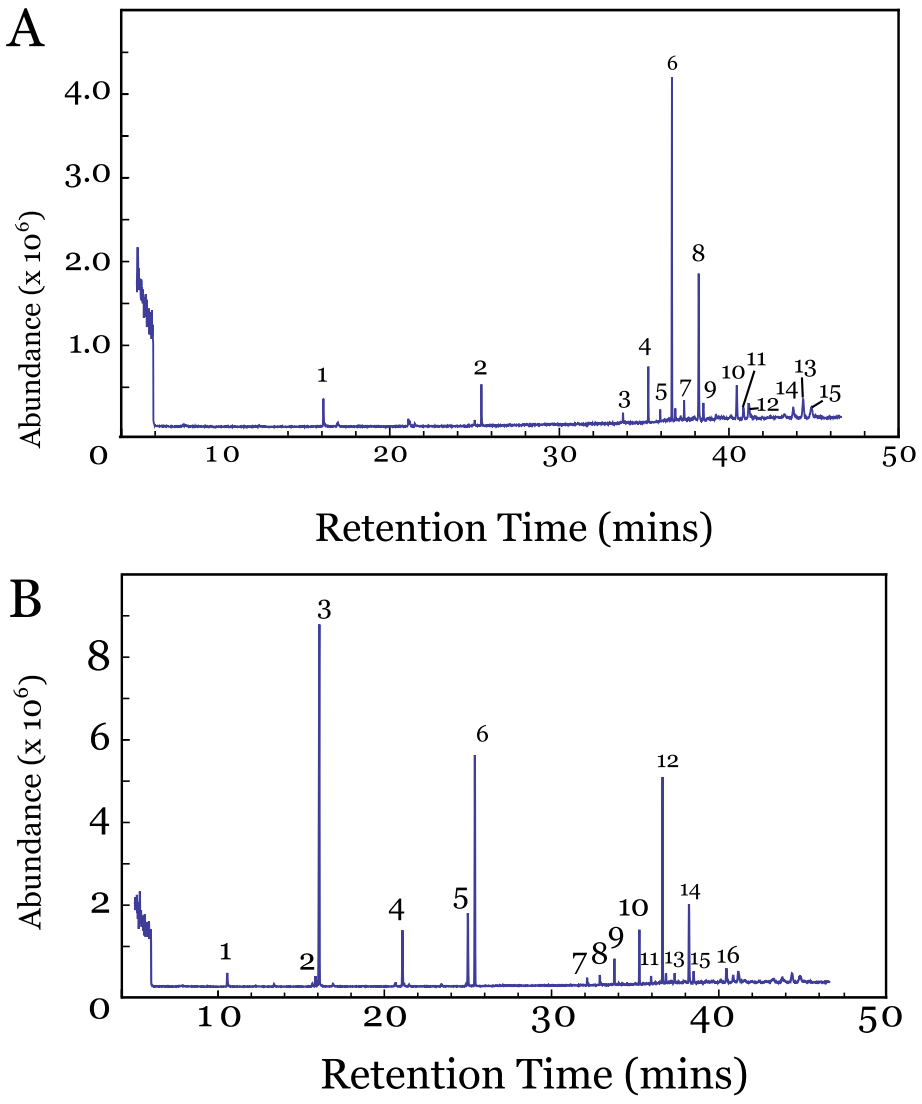

Figure 4.4.11: Two GC-MS chromatographs for *P. dives* secretion. **A**) Identified molecules: 1) tridecane, 2) heptadecane, 3) eicosane, 4) heptacosane, 5) pentacosane, 6) nonacosane, 7) unidentified fatty acid, 8) hexacosane, 9) nonacosane, 10) hexatriacontane, 11) nonacosane, 12) 3-methyl-heptadecane, 13) unidentified, 14) eicosane, 15) heneicosane. **B**) Identified molecules: 1) undecane, 2) 5-tridecene, 3) tridecane, 4) pentadecane, 5) 8-heptadecane, 6) heptadecane, 7) 11-decyl-heneicosane, 8) 3,7,11-trimethyl-2,6,10-dodecatrien-1-ol, 9) pentacosane, 10) heptacosane, 11) tetratriacontane, 12) nonacosane, 13) unidentified, 14) pentacosane, 15) hexacosane, 16) tetratriacontane. Peaks at higher retention times were not identified.

that these molecules, combined with the presence of mono- and dimethylalkanes, would facilitate maintaining the secretion fluidity over a larger temperature range for use as an adhesive liquid. GC-MS results seem to qualitatively support this hypothesis.

The chemical congruence between CHC and adhesive secretion in several insect species suggests that these lipids may be engaged in chemical exchange, and this has indeed been confirmed in beetles [77]. This similarity between CHC profiles of other insects and the

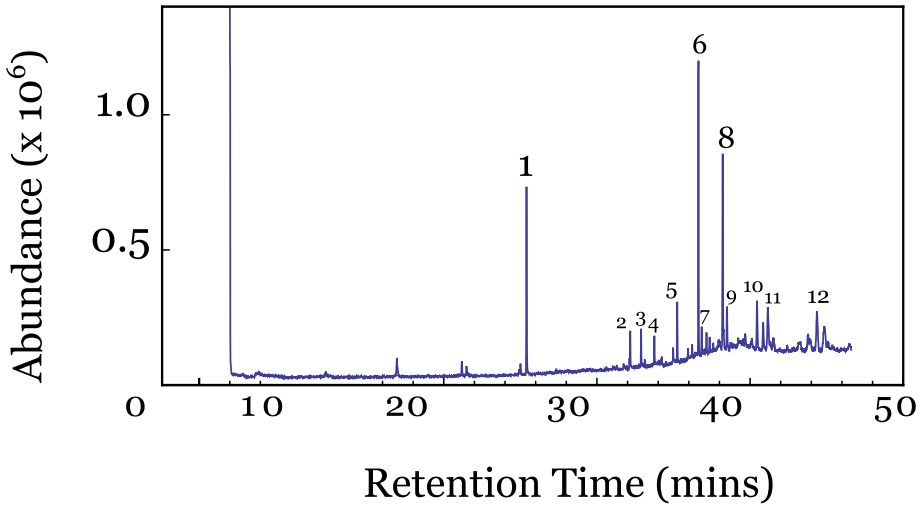

Figure 4.4.12: GC-MS profile of *P. dives* secretion. Identified molecules: 1) heptadecane, 2) N-2-trifluoromethylphenyl-piridine-3-carboxamide, 3) 2,6,10,14,18-pentamethyl-2,6,10,14,18-eicosapentaene, 4) octadecane, 5) heptacosane, 6) nonacosane, 7) unidentified phenol, 8) nonacosane, 9) 11-methyl-nonacosane, 10) hexatriacontane, 11) eicosane, 12) 1-bromoeicosane.

Table 4.4.2: The most common and abundant molecules detected within the footprint droplets of the adhesive secretion of the ant *P. dives*.

Molecule	**Formula**	Phase at STP
Tridecane	$C_{13}H_{28}$	Liquid
Heptadecane	$C_{17}H_{36}$	Liquid
2-methyl-hexadecane	$C_{17}H_{36}$	Liquid
Octadecane	$C_{18}H_{38}$	Solid
3-methyl-heptadecane	$C_{18}H_{38}$	Solid
Eicosane	$C_{20}H_{42}$	Solid
Heneicosane	$C_{21}H_{44}$	Solid
Pentacosane	$C_{25}H_{52}$	Solid
Hexacosane	$C_{26}H_{54}$	Solid
Heptacosane	$C_{27}H_{56}$	Solid
9-octyl- eicosane,	$C_{28}H_{58}$	Liquid
Nonacosane	$C_{29}H_{60}$	Solid
11-decyl-heneicosane	$C_{31}H_{64}$	Liquid-Solid
13-methyl-hentriacontane	$C_{32}H_{66}$	Liquid-Solid
Tetratriacontane	$C_{34}H_{70}$	Solid

composition of *P. dives* adhesive secretion may be indicative of a similar exchange mechanism at play for this species, however the gathered data does not allow for anything other than speculation in the present case. Martin & Drijfhout [73] note that odd-numbered C_{25}–C_{35} *n*-alkanes are typically found in ant CHC profiles, and C_{19}–C_{33} chain-lengths dominate. The most abundant molecule found in the adhesive secretion of *P. dives*, present in all samples and demonstrating the highest peaks, was nonacosane $C_{29}H_{60}$, Table 4.4.2.

It has been found that a number of mono-methylalkanes are used within the chemical communication systems of insects, for example, nonacosane and octadecane have been reported to play a role in the chemical communication of the mosquito *Anopheles stephensi* (Diptera: Culicidae) [197], *n*-pentacosane has been identified as a cuticular hydrocarbon of a number of insects (see Blomquist & Bagnères [196] and references within), and the dimethylalkane 13-methylhentriacontane is a known antennating stimulant in the parasitic wasp *Microplitis croceipes*, suggesting that the tarsal adhesive-secretion may have more than just an adhesive function.

Whilst the mixture of different alkanes can lead to a broadening of the T_m range, mixtures of waxes with alkanes and alkenes do not form mixed crystals, since alkenes and alkanes crystallise seperately [198], resulting in solid alkane crystals suspended within a liquid alkene 'matrix', as hypothesised by Betz [19, 91]. This may be a possible explanation for the presence of the observed crystal structures within secretion footprint droplets several hours after deposition, Figure 4.4.10. This hypothesis could be tested by further, more in-depth, comparative analysis of the adhesive secretion and CHC compositions of this species together with GC-MS analysis of any crystal structures found within secretion droplets. Unfortunately, this was not possible during the current research project, and could be the focus of further study.

4.4.2.3 Contact Angle & Volume

Contact angles (CA) of secretion droplets of both insects are shown in Figure 4.4.13 and Tables 4.4.4, 4.4.5. Most droplets remained present for at least 24 hours after deposition without any significant change in droplet base radius, indicating the liquid deposits consist of mainly stable, non-volatile, compounds [39], qualitatively consistent with the GC-MS analysis above, and in the literature [21, 35, 74]. However, given the nature of the footprint collection, it would be unlikely to observe any evaporation of hydrophilic components.

For both insects, the CA of the secretion was greater on hydrophobic compared with hydrophilic silicon substrates, but were not dramatically affected by the surface energy of the substrate. For *H. axyridis* CAs were 17.0±6° (N=15, mean±s.d.) on hydrophilic and 27.4±2° (N=15) on hydrophobic silicon, significantly different between substrates (Mann-Whitney U-test, Z=0, P<0.001). The CA values for *P. dives* were 21.9±3° (N=15, mean±s.d.) on hydrophilic and 28.3±2° (N=11) on hydrophobic silicon, and were also significantly different between substrates (t-test, t=28.1512, P<0.001). Although a significant difference was found for the CAs of insect secretion between hydrophilic and

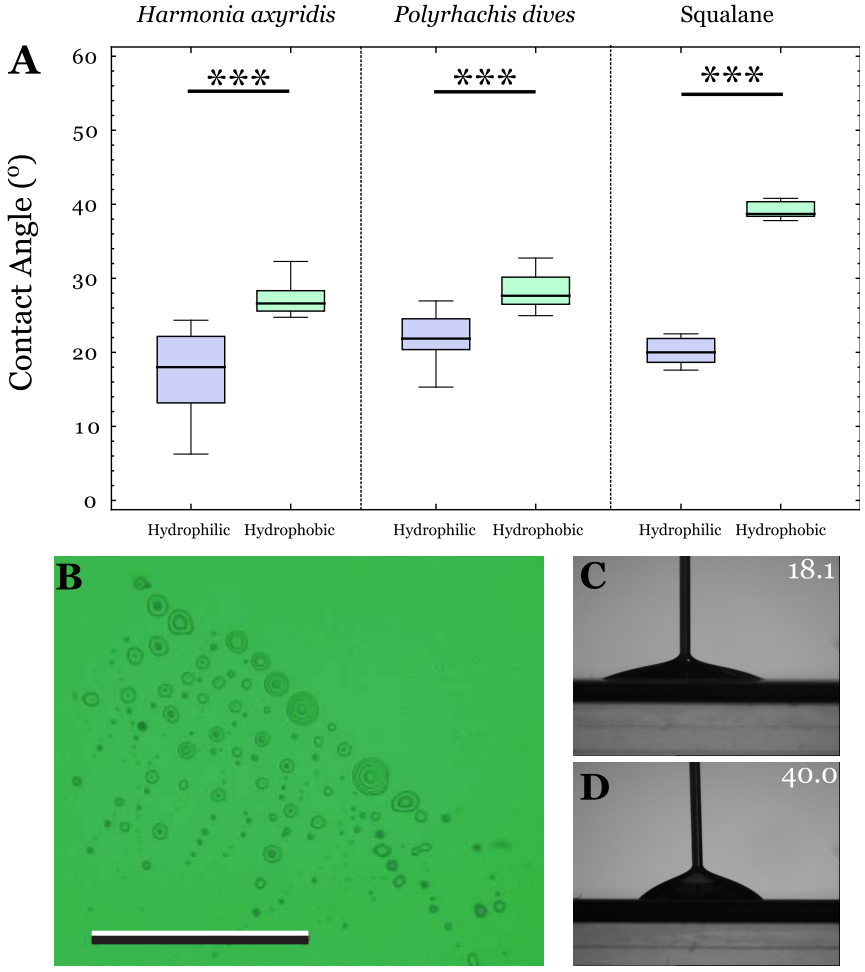

Figure 4.4.13: Contact angle values of adhesive secretion measured on hydrophilic and hydrophobic silicon substrates, and those of the hydrophobic liquid squalane. A) Measured contact angles of secretion of *H. axyridis* and *P. dives* as measured with IRM, and squalane measured with the DSA, on hydrophilic and hydrophobic silicon substrates. A significant difference between substrates was found for both insects. **B**) Interference reflection microscopy image of secretion droplets deposited by *H. axyridis* on a hydrophilic silicon substrate. C-D) Squalane droplets as measured with the DSA. White numbers denote CA values. Box-plots show upper and lower quartiles with a median line between them. Whiskers represent 10th and 90th percentiles, black dots represent outliers. Scale Bar = 50 μm. *** P < 0.001, ns = not significant.

hydrophobic substrates, this difference was only small and the secretion still generates a CA well below 90°.

It is noted that our result for *P. dives* on hydrophobic substrates is in contrast to measurements of the secretion of the Weaver ant *Oecophylla smaragdina* reported by [12], who found a large decrease in CA between hydrophilic glass (17.6±7°) and hydrophobic polyimide (1.3±0.4°). At present we have no explanation for the difference between our observations and those of Federle *et al.*. Interestingly however, we find that the CA of moderately long-chain hydrocarbons such as squalane ($C_{30}H_{62}$) are also relatively insensitive to the surface energy of the substrate, Figure 4.4.13 CA = 20.2±2 hydrophilic, and 39.2±1 hydrophobic (mean±s.d.).

It could be argued that finding the CAs of the adhesive secretion of both insects to be relatively insensitive to the surface energy of the substrate is entirely consistent with previous chemical analyses of the adhesive secretion which show that they consist of hydrophobic liquid hydrocarbons in the range C_{16}–C_{28}, eg., Figures 4.4.11–4.4.12 [21, 74].

The total volume of several footprint deposits by single adhesive pads on smooth hydrophilic and hydrophobic silicon was also measured using IRM, and the results are shown in Figure 4.4.14 and collected in Tables 4.4.4 & 4.4.5.

The volumes deposited by single pads of ants and ladybirds on hydrophilic and hydrophobic substrates is given in Figure 4.4.14, and summarised in Tables 4.4.5 & 4.4.4. The volumes reported here should be considered a *lower* bound of the true volume in the contact zone during locomotion since some secretion is likely to remain on the adhesive pad after detachment, and any evaporative effects are not taken into account [89]. However, we note that the volumes reported here are comparable to previous estimates for aphids, and other species of ant. For example, using a similar approach Lees & Hardie [65] determined the volume of secretion deposited by the aphid *Megoura viciae* to be between 7–144 μm^3, and calculated the thickness of the fluid layer in the contact zone to be 17.7 *nm*. Dixon [66] calculated an approximate secretion thickness of 500 *nm* for *Aphis fabae*, and Federle *et*

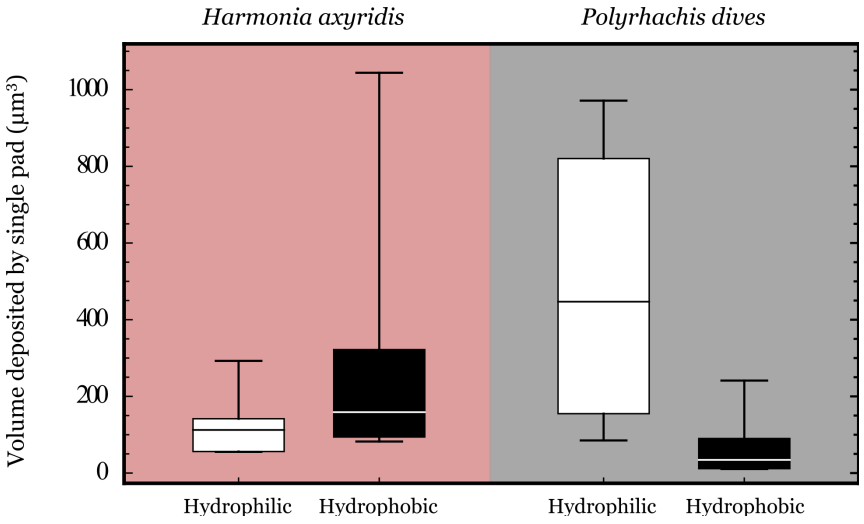

Figure 4.4.14: Volume of secretion deposited by single arolia of *P. dives* ants (hydrophilic, N=4; hydrophobic, N=5), and single T2 tarsomere pads of *H. axyridis* (hydrophilic, N=9: hydrophobic, N=9). Boxes represent upper and lower quartiles, whiskers represent 10 and 90th percentiles with a median line between them.

al. [12] estimated the thickness to be between 90 and 160 *nm* for ants (*O. smaragdina*) and stick insects (*C. morosus*) near the edge of the contact zone. However, as pointed out by Lees & Hardie [65]: *'since the oil deposits left on glass vary so substantially it is clear that their volume does not afford a reliable guide to the thickness of the adhesive layer between the pulvillus and the substratum'*.[2] This may be an explanation for the variability of volumes deposited, shown in Figure 4.4.14, and the fact that a significantly greater volume of secretion was found for *P. dives* on the hydrophilic substrate, but greater amounts of liquid were found on hydrophobic surfaces for the ladybirds, and could be evidence of direct, neuronal-control over the secretion process by the insect.

Peisker & Gorb [89] showed that the evaporation dynamics of adhesive secretions can be quite different between species, making it difficult to draw any quantitative conclusions about the thickness of the secretion layer by observing and measuring properties of secretion droplets several minutes, or hours, after they are deposited upon substrates. This may warrant the development of contact models which do not directly depend upon the volume of secretion within the contact zone (which is difficult to quantify reliably), see Chapter 5.

[2] pp.217 of Lees & Hardie [65]

Surface Tension & Viscosity

Based on previous literature values [12], we estimate the surface tension of the secretion to be $\gamma = 30\text{mNm}^{-1}$, consistent with the chemical composition of the secretion being hydrocarbons with chain-lengths in the range C_{16}–C_{28} [21, 73, 74], and in line with previous studies who make the same approximation [12]. To determine the viscosity with Equation 4.2.6, as a control we first measured the dewetting velocity of droplets of the long-chain hydrocarbon squalane ($C_{30}H_{62}$), see Figure 4.2.4, which has similar surface tension (approximately 30 mN/m, see above) and CA values to the insect secretion (CAs; Squalane: 20.2°, *H. axyridis*: 17.0°, *P. dives*: 22.0°), to be 370 ± 128 μms^{-1} (mean ± s.d).

We measure the dewetting velocity in the Harlequin ladybird *H. axyridis* to be 117±17 $mm \cdot s^{-1}$ (mean ± s.e.m), Figure 4.4.15A, and the dewetting velocity of the Weaver ant *P. dives* to be 470±110 $mm \cdot s^{-1}$, Figure 4.4.15B. Using Equation 4.2.6 and the viscosity of the adhesive secretion of *H. axyridis* and *P. dives* was determined to be between 80–134 mPas and 20–36 mPas. Values estimated for the secretion determined by dewetting experiments are comparable to estimates from similar experiments, e.g., Federle *et al.* [12] who estimate the secretion viscosity of *O. smaragdina* to be within the range 40–150 mPas. Also, despite the relatively crude method of determining the viscosity value we have found values which are in good agreement with those reported from nano-rheology techniques, for example the secretion viscosity of the Colorado Potato Beetle was found to be of the order of 100 $mPas$ [199]. However, we note that the shear rate of the perturbations was not controlled, and so no inference can be made about any non-Newtonian, or rate-dependency. Given the approximate nature of this approach, and the assumptions made in deriving Equation 4.2.6, this agreement with literature values for similar insects is somewhat encouraging.

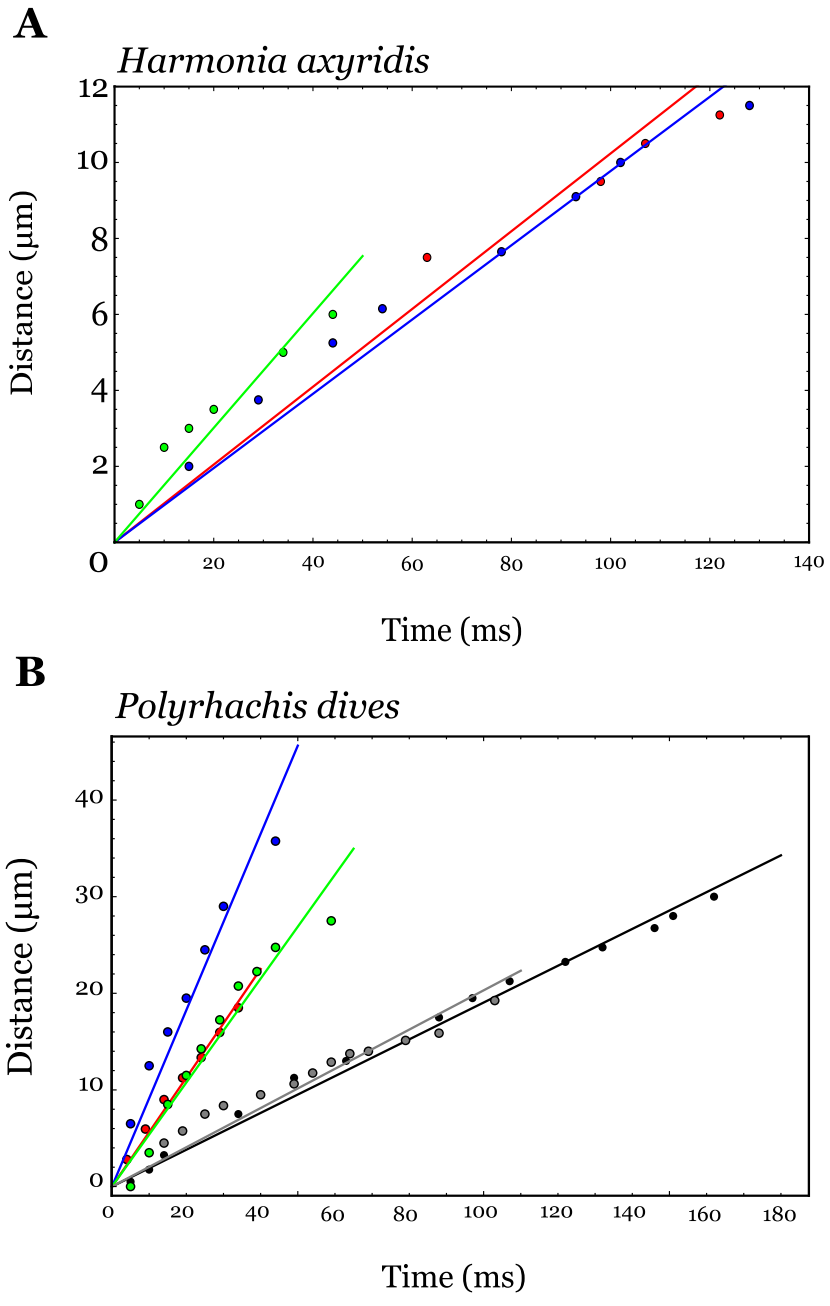

Figure 4.4.15: Dewetting velocity of the adhesive secretion of A) *Harmonia axyridis* and B) the Weaver ant *Polyrhachis dives*.

4.4.3 Work of Adhesion W_{AB}

Here the work of adhesion between adhesive pad and substrate is estimated for a smooth and hairy adhesive pad of ants and ladybirds respectively, using the Good-Girifalco equation [94, 97], with γ_{AL} as the adhesive pad/secretion interfacial energy, and γ_{BL} as the substrate/secretion interfacial energy. For both the arolia of ants and setae of ladybirds, it is assumed that $\gamma_A = 50$ mN·m^{-1}, consistent with literature values for similar bio-materials [200]. For bare glass, we take the value of $\gamma_B = 500$ mN·m^{-1} as quoted by Griffin [100], while for hydrophobic glass it is assumed $\gamma_B = 18$ mN·m^{-1}, *i.e.*, the surface energy of PTFE [94]. Finally it is assumed that $\gamma = 30$ mN·m^{-1} [12]. From the Duprè equation [94], Equation 4.3.7 it is found that $\gamma_{AL} = 2.54$ mN·m^{-1} ($\Phi = 1$), $\gamma_{BL} = 407$ mN·m^{-1} for bare glass ($\Phi = 0.5$) and $\gamma_{BL} = 24.8$ mN·m^{-1} for hydrophobised glass ($\Phi = 1$). Using these surface energy values in Equation 4.3.6, it is found for bare glass that $W_{AB} = 64.3$ mN·m^{-1} ($\Phi = 0.5$) and for hydrophobic glass $W_{AB} = 7.9$ mN·m^{-1} ($\Phi = 1$). These calculated values are summarised in Table 4.4.3.

Table 4.4.3: Summary of values used to calculate the work of adhesion W_{AB} between the adhesive pads (surface **A**) of insects in contact with hydrophilic and hydrophobic substrates (surface **B**), mediated by a liquid secretion with surface tension γ_L=30mNm^{-1}. Φ is the intermolecular correction factor dependent upon the correlation between the interactions between the two media.

γ_A (mNm^{-1})	γ_B (mNm^{-1})	Φ	γ_{AL} (mNm^{-1})	γ_{BL} (mNm^{-1})		W_{AB} (mNm^{-1})
50	500	0.5	2.54	407	Hydrophilic	64.3
50	18	1	2.54	24.8	Hydrophobic	7.9

4.4.4 Summary of Results

The characteristic properties of the adhesive secretion and attachment pads of the ladybird *Harmonia axyridis* and Weaver ant *P. dives* are summarised in Table 4.4.4 and Table 4.4.5 respectively. Within these tables the tangential sliding velocities ν are also reported, which are described and measured in Chapter 5, and used within the calculations of the sliding friction forces in the centrifuge device.

Table 4.4.4: Mean measured parameters of attachment system in *H. axyridis* on both hydrophilic and hydrophobic glass substrates showing characteristic properties of attachment pads and secretion; average projected contact-area per leg, A_c, viscosity, η, calculated radius of contact zone (individual setal tip) R, mean number of setae per leg n_{seta}, mean number of setae along the peeling edge n_{edge}, together with substrate dependent properties; contact angle of secretion θ, volume deposited by a single attachment pad V, and tangential sliding velocity of the whole insect v.

A_c (μm^2)	η ($mPas$)	R (μm)	n_{seta}	n_{edge}		θ (°)	V (μm^3)	ν (mms^{-1})
22,380 ± 6400	107 ± 27	2.22 ± 0.4	1500 ± 142	21 ± 8	Hydrophilic Hydrophobic	17±6 27±2	121±25 291±112	2.4±1 3.8±2

Table 4.4.5: Mean measured parameters of the attachment system in *P. dives* on both hydrophilic and hydrophobic glass substrates showing characteristic properties of attachment pads and secretion; average projected contact-area per leg A_c, viscosity, η, calculated radius of contact zone (arolium) R, together with substrate dependent properties; contact angle of secretion θ, volume deposited by a single attachment pad V, and tangential sliding velocity of the whole insect v.

A_c (μm^2)	η ($mPas$)	R (μm)		θ (°)	V (μm^3)	ν (mms^{-1})
7840 ± 440	28 ± 8	50 ± 5	Hydrophilic Hydrophobic	22±3 28±2	488±204 68±44	3.8±1 4.8±1

Chapter 5

Physical Mechanisms of Insect Adhesion - Measurement of Attachment Forces & Comparison with Theoretical Models

5.1 Introduction

In the previous chapter we characterised the adhesive pad systems and adhesive secretion of the ant *Polyrhachis dives* and the ladybird *Harmonia axyridis*. In this chapter we will feed the characteristic parameters of each insects' attachment system into the theoretical models outlined in Section 4.3 and compare the resulting force predictions with adhesive and frictional forces measured *in vivo* using a centrifuge technique, similar to that described in Section 2.6.

The predictions of the different models are discussed in the context of the magnitudes of different surface forces that may be acting during adhesive and frictional detachment processes, as well as the influence of the substrate surface energy. The differences between the hairy and smooth attachment devices are discussed and conclusions regarding the underlying physical mechanism of insect adhesion are drawn.

5.2 Materials & Methods

Force measurements

To determine attachment forces of insects, a centrifuge technique similar to that employed in several previous studies is used [12, 13, 66, 201]. Using a custom built centrifuge device (housed within a perspex chamber) with either a cylindrical glass surface (radius r=25 mm) to measure normal adhesion forces or a flat circular glass turntable (radius r=50 mm) to measure tangential friction forces, Figure 5.2.1. To test attachment forces on hydrophilic and hydrophobic glass surfaces, substrates were used in an untreated condition (hydrophilic) and after chemical silanisation (hydrophobic) with dichlorodimethylsilane ($(Si(CH_3)_2Cl_2)$; 99%, Sigma Aldrich, UK) using a method based on procedures found in

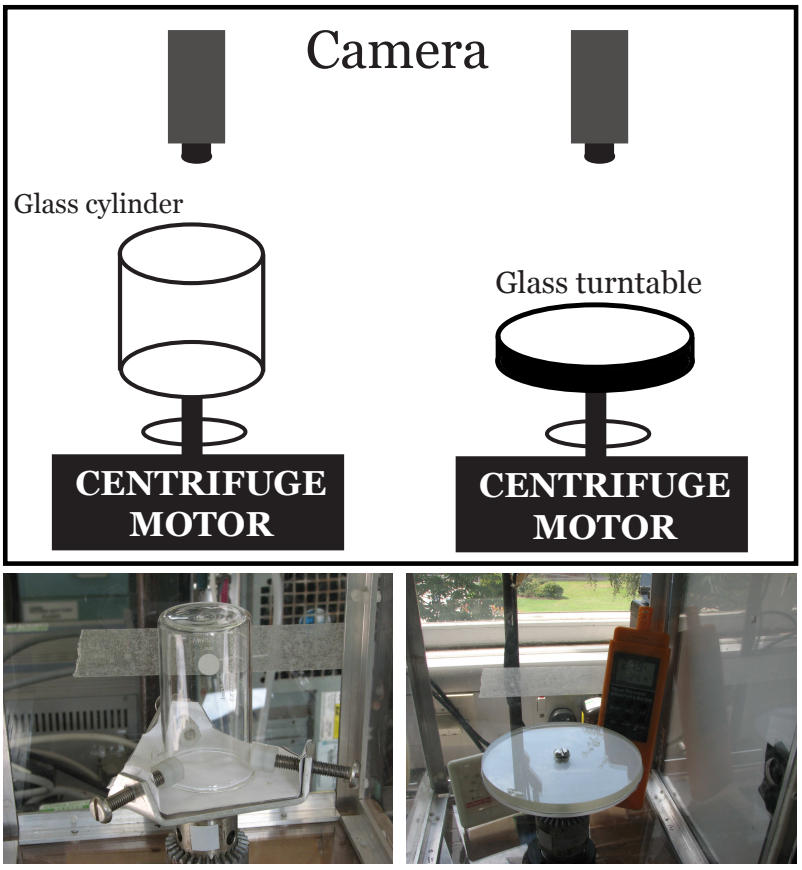

Figure 5.2.1: Schematic and photographs of centrifuge apparatus. The glass substrates (cylinder or turntable) were connected to a motor held inside a custom-made perspex box and monitored from above with a camera. Humidity and temperature sensors were placed within the box to monitor conditions during the experiments.

the literature [186]. Individual insects were weighed using an analytical balance (Ohaus Adventurer Pro AV264C, Oakleyweigh, Aylesbury, UK) and placed within the centrifuge experiment with hydrophilic or hydrophobic glass which could be manually accelerated from 200 to 2500 revs·min^{-1}.

Centrifuge experiments were filmed from above using a webcam (Quickcam Pro for Notebooks, Logitech UK Ltd., Slough, Berkshire) controlled by HandyAVI 4.3 software (Azcendant, AZ, USA) to determine the radius at which the onset of sliding occurred (friction) and the point of detachment (adhesion and friction). Angular velocity ω was recorded using an optical tachometer (Standard AT-6, Premier Farnell Ltd, Bristol, UK). The mass and position of the insect were used together with its angular velocity to calculate *i*) adhesion force, *ii*) friction force at the onset of sliding, and *iii*) the safety factors (friction or adhesion force normalised to insect body mass) for each trial.

Previous investigations have demonstrated that attachment forces in insects are largely humidity independent between approximately RH = 30–80 % [68], thus experiments were carried out at RH=35–50 % and temperature $T = 20\pm5$ °C. To avoid any moisture induced improvement of adhesion between trials (as found by Voigt *et al.* [202]) all insects were held within a closed PET plastic container (Microbiological Supply Company, Toddington, Bedfordshire, UK) at the same RH for at least 30 minutes prior to use. Individuals of both insects were given at least 12 hours to recover between trials to avoid replication biases.

Data Analysis

Statistical analyses were performed using Mathematica 8.0.0 software (Wolfram Research Europe Ltd., Long Hanborough, Oxfordshire, UK). When comparing between groups, parametric data sets were analysed with a one-way ANOVA followed by a *post-hoc* Tukey test, non-parametric data sets were tested for normal distribution and equal variance before appropriate analysis with either a Mann-Whitney U-test or an unpaired t-test.

5.3 Results & Discussion

In this section will be presented the results for direct experimental measurements of friction and adhesion forces in ants and ladybirds *via* centrifuge techniques.

5.3.1 Normal Forces

The maximum *adhesion* force is defined to be equal to the centrifugal force normal to the substrate acting on the insect at the point of detachment. When placed in contact with the cylinder insects were observed to walk without difficulty on the vertical surface, even after rotation had begun. However, above a certain threshold of angular velocity insects were observed to cease movement. This behaviour is similar to the *freezing response* described for the Weaver ant *Oecophylla smaragdina* [12], and is consistent with that found for other ant species [13]. Note that in this state, the insect brings all 6 legs into contact with the substrate. Although there is no documented evidence in the literature of ladybirds eliciting the same freezing response as ants, at high angular velocities ladybirds were also observed to cease movement.

In Figure 5.3.1A is presented the absolute adhesion forces for both insects. As would be expected due to their significantly greater body mass (t-test, t=243.335, P<0.001), ladybirds generated significantly larger forces than ants on both hydrophilic (t-test, t=64.8397, P<0.001) and hydrophobic (t-test, t=51.2613, P<0.001) substrates. The ladybird *H. axyridis* was found to generate significantly greater forces on the hydrophilic compared to hydrophobic glass (t-test,t=21.0555, P<0.001), generating forces of 3.5±1.6 mN on hydrophilic glass, and 1.7±0.6 mN on hydrophobic glass (mean±s.d.), indicating a significant substrate dependence between substrates. However, no statistically significant difference was found for *P. dives* (t-test, t=0.2791, P=0.6004), generating forces of 0.5±0.2 mN on hydrophilic and 0.6±0.4 mN on hydrophobic glass. The fact that, for *P. dives* ants, no statistically significant dependence of normal forces was found between hydrophilic

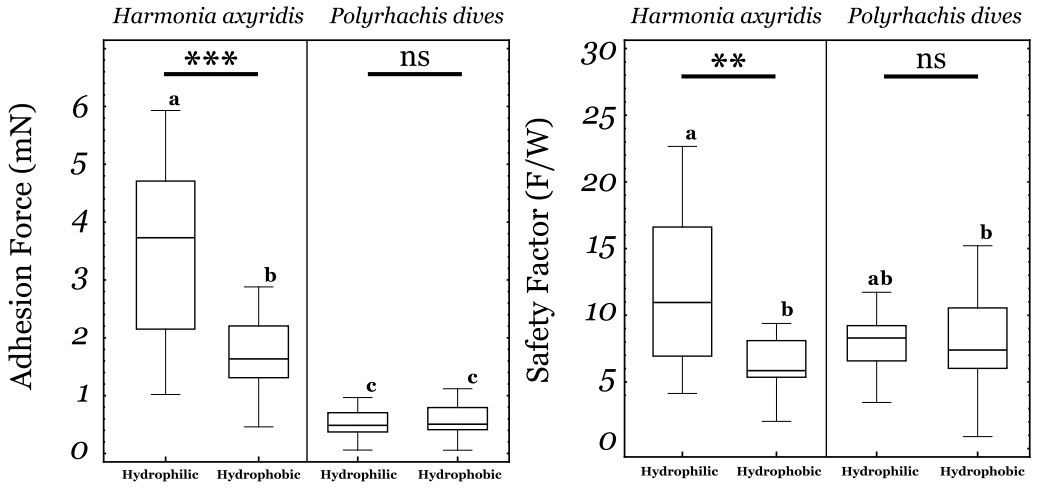

Figure 5.3.1: Measured adhesion forces and safety factors of *Harmonia axyridis* and *Polyrhachis dives* on hydrophilic and hydrophobic glass substrates. Boxes show upper and lower quartiles with a median line between them. Whiskers represent 10th and 90th percentiles. Lower case letters denote significant differences between forces or safety factors. ***, $P < 0.001$, **, $P < 0.01$, ns = not significant.

and hydrophobic surfaces is consistent with findings for other insects with smooth pads [33, 65, 66, 203]. Mean adhesion detachment forces of both insects are given in Table 5.3.1. In order to factor out the effect of body mass, the safety factors for each species were analysed, Figure 5.3.1B. The ladybird *H. axyridis* showed a significant difference for adhesion safety factors (t-test, t=17.074, P< 0.001) between hydrophilic and hydrophobic glass surfaces, generating safety factors of 12.0±6 (N=19) on hydrophilic and 6.3±2 (N=20) on hydrophobic glass (mean±s.d). No significant difference was found for safety factors of ants (Mann-Whitney U-test, Z=227, P=0.473), which achieved values of 8.8±5 (N=20) on hydrophilic and 7.7±4 (N=20) on hydrophobic glass.

The safety factor values for *H. axyridis* reported here on hydrophilic glass are comparable to previous measurements with ladybirds using strain-gauge techniques, including *Epilachna vigintioctomaculata* [35], as well as a number of aphids [65, 66]. However adhesion safety factors reported here for the weaver ant *P. dives* are approximately 5–10 times smaller than those measured by Federle *et al.* [13] with smaller ant species on Perspex surfaces (eg: *Crematogaster cf. artifex* safety factor=53.9), and the larger weaver ant *O. smaragdina* (safety factor=118.4) using a similar centrifuge method. This may be due to morphological differences in the adhesive pads between the ant species used in this study

and those used by Federle *et al.*.

5.3.2 Tangential Forces

On the smooth turntable, strong shear forces cause both *P. dives* ants and *H. axyridis* ladybirds to slide outwards before detachment occurs, Figure 5.3.3. The *friction* force is defined to be equal to the centrifugal force tangential to the substrate acting on the insect at the onset of sliding. The ladybird *H. axyridis* generated significantly greater friction forces at the onset of sliding on hydrophilic glass compared to hydrophobic glass (Mann-Whitney U-test, Z=164, P<0.01), but no statistically significant difference between friction forces was found for the ant *P. dives* (Mann-Whitney U-test, Z=515, P=0.984). In Figure 5.3.2 is presented absolute friction forces and corresponding safety factors for ladybirds and ants on hydrophilic and hydrophobic glass substrates at the point sliding begins. Friction forces were generally several times larger than the adhesion detachment force, consistent with results for the beetle *Chrysolina polita* [34], blowflys [37] and ants [12]. Friction forces at the point of detachment were even greater. Tangential forces at the onset of sliding for both insects are given in Table 5.3.1.

Ants achieved friction safety factors at the onset of sliding of 31.4±17 (N=38, mean±s.d.) on hydrophilic and 27.7±17 (N=27) on hydrophobic glass (Mann-Whitney U-test, Z=548, P=0.645), and ladybirds achieved 43.2±19 (N=13) on hydrophilic and 16.7±11 (N=15) on hydrophobic glass, indicating a statistically significant substrate dependence of friction safety factors (t-test, t=21.1029, P<0.001), as well as absolute forces. Detachment forces measured during the friction turntable experiments were much greater than those at the onset of sliding, and were sometimes substantial. For example, several ladybirds were measured to detach at forces exceeding safety factors of 100, and two individuals were measured to detach at the edge of the turntable at a safety factor > 200 on hydrophilic glass. Similarly, maximum detachment safety factors for ants were between 120–150, also on hydrophilic glass. The substrate dependence of detachment forces also showed similar

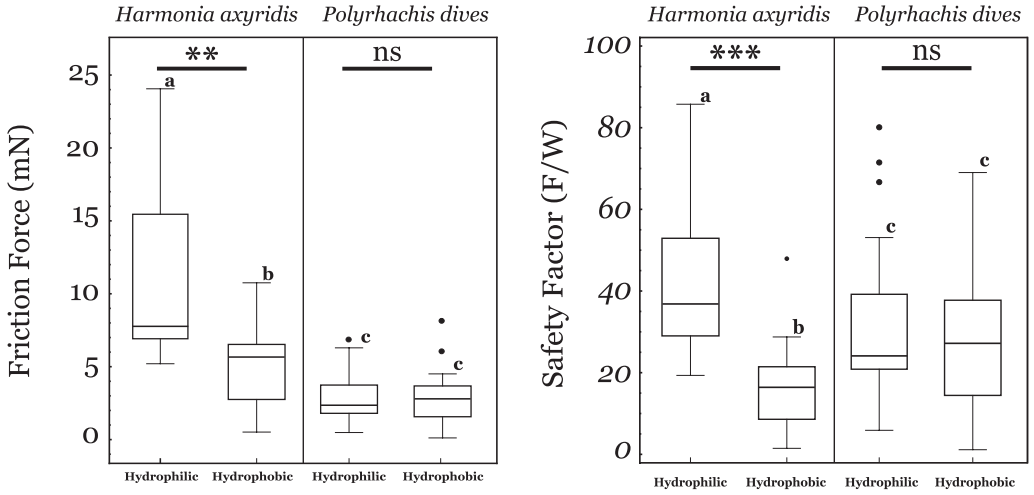

Figure 5.3.2: Measured friction forces and safety factors of *Harmonia axyridis* and *Polyrhachis dives* at the onset of sliding on hydrophilic and hydrophobic glass substrates. Ladybirds exhibit significantly larger forces, and safety factors, on hydrophilic glass than the hydrophobic glass surfaces. Lower case letters denote significant differences between forces or safety factors. Boxes show upper and lower quartiles with a median line between them, boxes represent 10th and 90th percentiles, and black dots represent outliers. *** P < 0.001, ** P < 0.01, ns = not significant.

trends to those seen in Figure 5.3.2 for forces at the onset of sliding. From radius *vs.* time plots it is possible to estimate an average radial sliding velocity v of each insect on the different substrates between the onset of sliding and the point of detachment (see Figure 5.3.3 and Tables 4.4.4,4.4.5).

Observations of insects during the experiments showed that insects faced inwards during rotation of the centrifuge. Considering the previous finding that attachment forces are direction-dependent, with stronger forces generated when the adhesive pads are pulled in the proximal direction [120], this may suggest that the insects are aware of this direction

Table 5.3.1: Attachment forces of the ladybird *H. axyridis* and ant *P. dives* as measured with the centrifuge device on hydrophilic and hydrophobic glass substrates. The normal load due to the insect weight L is used with the adhesion force F^N, friction force F^T, and coefficient of friction μ calculated using Equation 4.3.10. Values given correspond to the mean ± standard deviation.

		Hydrophilic			**Hydrophobic**		
Species	**L** (mN)	F^N (mN)	F^T (mN)	μ	F^N (mN)	F^T (mN)	μ
H. axyridis	0.292	3.5±1.6	10.7±5.2	2.8	1.7±0.6	5.2±2.8	2.6
P. dives	0.0687	0.5±0.2	2.88±1.5	5.1	0.6±0.4	2.89±1.8	4.3

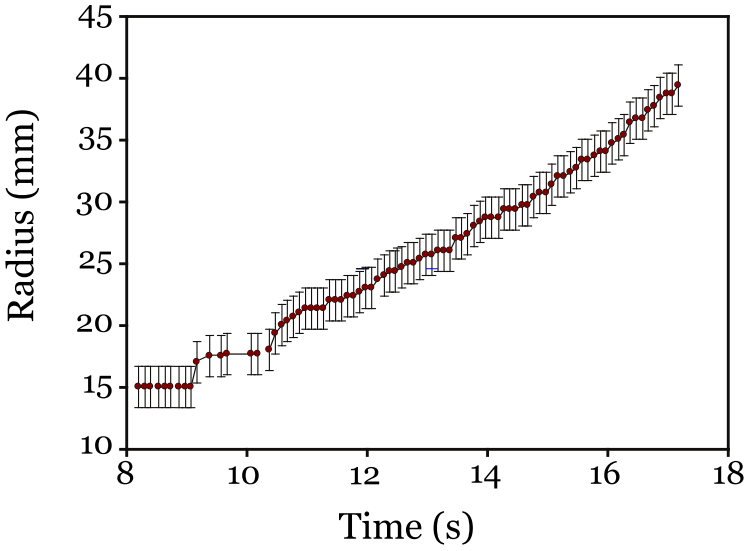

Figure 5.3.3: Representative graph of the radial position of the insect *vs.* time for friction centrifuge experiments. For friction tests, insects remain at a fixed radial position until the centrifugal force overcomes the static friction and the insect begins to slowly slide outwards.

dependence and alter their body posture accordingly under strong perturbations such as those experienced within the centrifuge experiment. Insects may also take advantage of this during defensive situations [3, 138], or whilst building their nests [4] in order to maximise their generated frictional force.

5.3.3 Comparison of Adhesion Models with Measurements

In this section we compare the different theoretical models in Table 4.3.1 with the experimentally measured adhesive and friction forces in the previous section in order to assess whether any of these models are able to reproduce the measured forces, both in terms of magnitude and substrate dependence of these forces. Note that in Tables 4.4.4 & 4.4.5, the measurements of θ and V using IRM were performed on bare and hydrophobised silicon, while the centrifuge force measurements were performed on bare and hydrophobised glass. We perform the IRM measurements on silicon wafers rather than directly on glass because the reflectivity from glass substrates using the IRM microscope (Section 4.2) was rather weak and the resolution of the interference fringes was very poor. However, using squalane again as a reference liquid-hydrocarbon with CAs of 20±2° and 39±1° on hydrophilic and

hydrophobic silicon respectively, Figure 4.4.13, compared to 24±4° and 43±2° measured on hydrophilic and hydrophobic glass respectively, it is not expected that θ and V will change significantly between silicon and glass (both hydrophilic and hydrophobic versions), and the θ and V values for silicon are used in the theoretical models when comparing theory to the centrifuge experiments.

Adhesion Forces

Comparison of adhesion forces with calculations is given in Figure 5.3.4 & 5.3.5 for *P. dives* and *H. axyridis* respectively for both hydrophilic and hydrophobic substrates.

For *P. dives*, the parallel-plate model over predicts adhesion force by factors of 95 and 1020 on hydrophilic and hydrophobic substrates respectively. The sphere on flat model under predicts the adhesion force by factors of 2.5 on hydrophilic and 5 on hydrophobic surfaces. In this context, it is important to recall that the rigid parallel plate model provides *upper bound* predictions to the adhesive force since the secretion volumes quoted in Tables 4.4.4 & 4.4.5 are *lower bounds* for the actual volume. However, even accounting for this fact, it is concluded that the sphere on flat model most closely captures the actual contact mechanics for the smooth pad adhesive system of ants. In particular, the reasonable agreement between the sphere on flat model and experiment is a significant improvement over the parallel-plate-model. This suggests that the thickness of the secretion film is not uniform (consistent with findings of Dirks *et al.* [92] for smooth pads of cockroaches) and there may be dry contact between the adhesive pad and the substrate.

As already mentioned, the adhesion forces calculated from the sphere-on-flat model are $\sim$ 2–3 times lower than the experimentally measured forces, but we recall that the capillary force in Equation 4.3.3 within the sphere-on-flat model neglects the additional contribution to the capillary force due to the elasticity of the smooth attachment pad (Equation 2.4.18). For soft materials this contribution can be significant [108], and could account for the discrepancy between this model and experiment. Unfortunately, it is difficult to estimate

the magnitude of this contribution because of the difficulty in accurately estimating the meniscus radius of curvature that is used within Equation 2.4.18.

For *H. axyridis*, the parallel-plate model over predicts adhesion force by 475 and 669 times for hydrophilic and hydrophobic substrates respectively, the sphere-on-flat model over predicts the adhesion force by factors of 4.4 and 4.7 on hydrophilic and hydrophobic substrates respectively, while the peeling model under predicts the experimental results by 5.4 and 3.2 times on hydrophilic and hydrophobic substrates.

Note that the additional contribution to the capillary force due to the elasticity of the setae cannot explain the discrepancy between the sphere-on-flat model and experiment, firstly

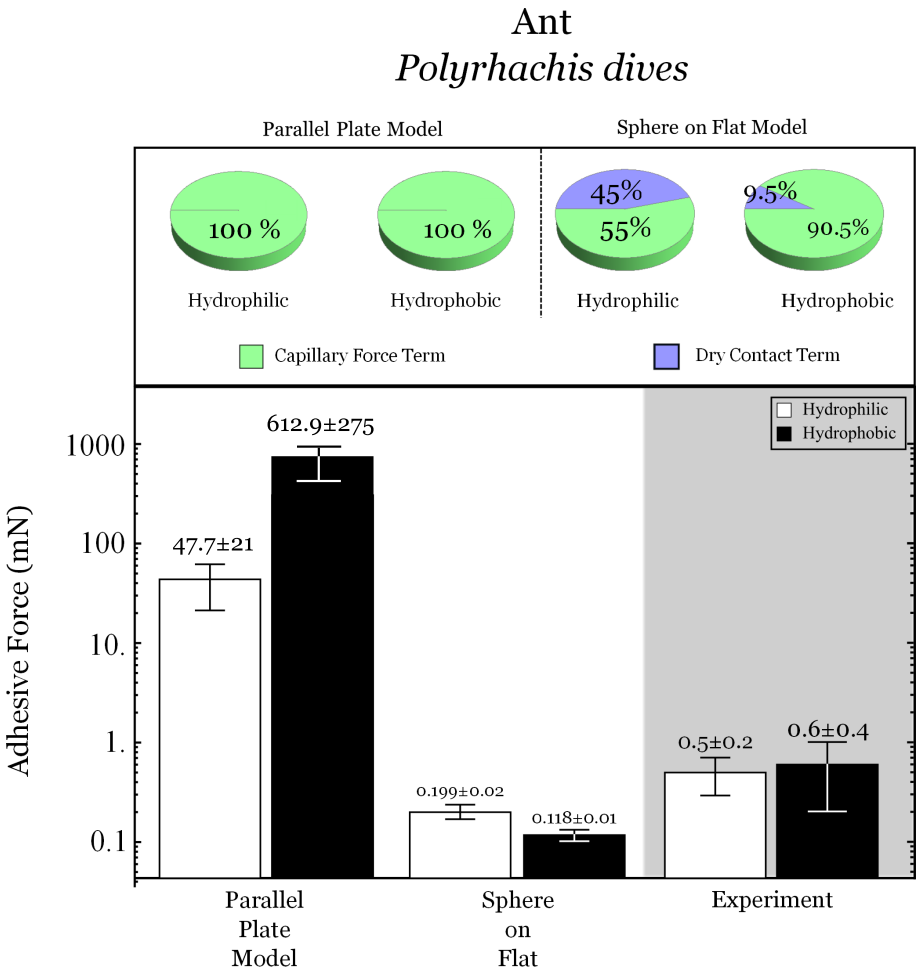

Figure 5.3.4: Measured attachment forces compared with whole-insect theoretical calculations of the different models for *P. dives*. Numbers above each bar give the total friction force in mN. Pie charts depict the relative contributions from the dry contact contribution and the capillary force contribution for each model on either hydrophilic or hydrophobic substrates. Note the Log scale on the Force axis.

because the setae are fairly rigid, and secondly because this term would lead to a greater discrepancy between the model and experiment. Instead, we believe the discrepancy may be due to the assumption of equal load sharing between all the setae within this model.

In fact, this assumption is unlikely to be the case in reality. For example, previous work on geckos suggests that not all setae may be in contact with the surface [204], and the real area of contact of the beetle *G. viridula* was estimated by Bullock *et al.* [194] who found that the overall projected area was greater than the real area of contact formed during attachment to a glass substrate by approximately a factor of 2. Implementing this difference into the theoretical models would bring calculated forces to closer agreement with experiment. It is noted that the measured forces lie between the model which assumes equal load sharing and

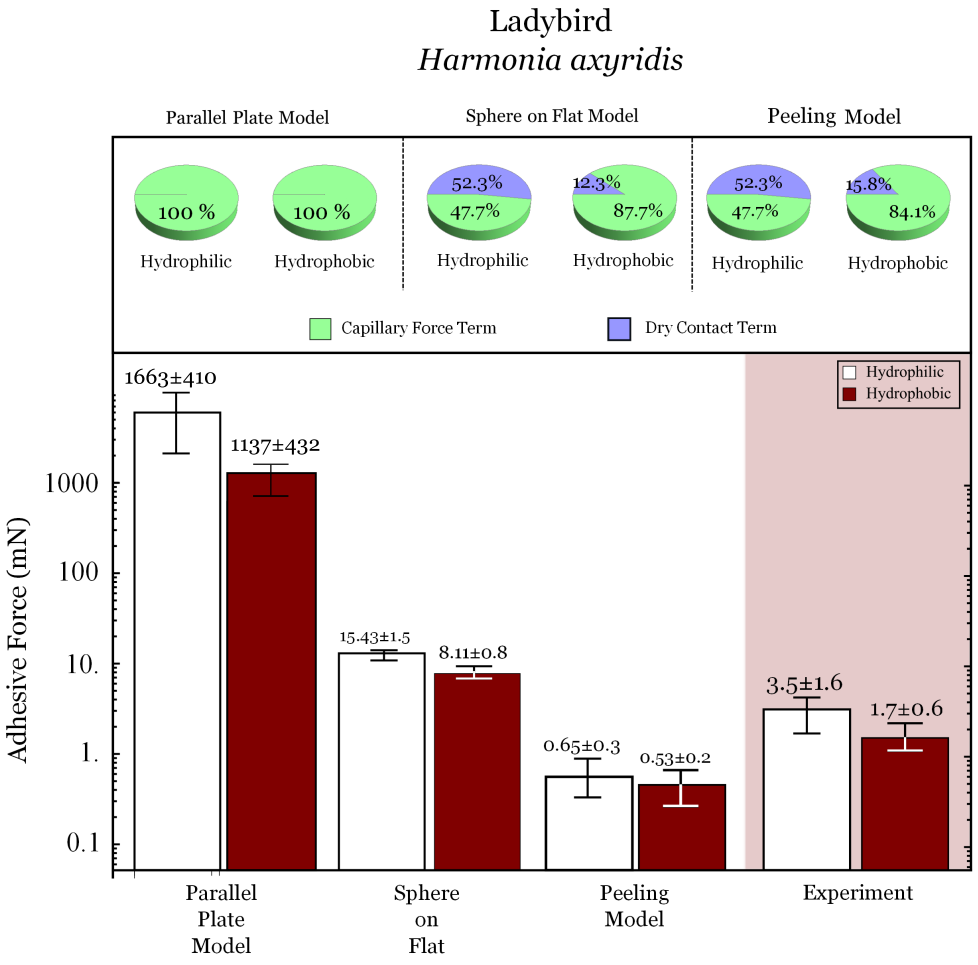

Figure 5.3.5: Measured attachment forces compared with whole-insect theoretical calculations of the different models for *H. axyridis*. Numbers above each bar give the total friction force in mN. Pie charts depict the relative contributions from the dry contact contribution and the capillary force contribution for each model on either hydrophilic or hydrophobic substrates. Note the Log scale on the Force axis.

that which assumes the extreme of stress concentration along one row of setae, Figure 5.3.5. This may suggest that there was some degree of stress concentration during detachment, but that it was concentrated along more than one row of setae. Given the morphology of the hairy pads of the Harlequin ladybird it is possible that each pad (T1 and T2, Figure 4.4.3) may have detached separately. This is somewhat in contrast to the recent results of Bullock & Federle [194] who, using a strain gauge force transducer to measure detachment forces of individual setae and whole pads, found evidence to suggest that adhesive pads of the beetle *G. viridula* are able to achieve equal load sharing, preventing peeling during detachment. Differences between the results of Bullock & Federle and the results presented here may be due to the different force measurement techniques deployed to measure the adhesion forces.

Next we consider whether it is possible to understand the substrate dependence of the adhesive forces (or lack thereof) in both ants and ladybirds using the sphere-on-flat models. It is first noted that for ladybirds, the measured contact angle of the secretion is significantly smaller on hydrophilic substrates compared to hydrophobic substrates (Table 4.4.4); this would lead to a smaller capillary force on hydrophobic substrates (Equation 4.3.4). It is therefore tempting to attribute reduced adhesive force of ladybirds on hydrophobic substrates to the increased contact angle. However a change in θ of $\sim 10^{\circ}$, Figure 4.4.13 leads to a decrease in capillary force of only 4% compared to a drop of approximately 50% observed experimentally for *H. axyridis*. It is therefore not possible to explain ladybirds substrate dependence of normal adhesive forces in terms of contact angles alone.

On the other hand, there is a stronger substrate dependence of the dry contact forces (see calculations of W_{AB} in Section 4.4.3). Noting that on hydrophilic substrates, the relative contribution of the dry adhesive force is larger in ladybirds compared to ants. Specifically 52% dry, 48% wet for *H. axyridis c.f.* 45% dry and 55% wet for *P. dives*. As discussed earlier, the larger contribution of dry contact forces in this case in ladybirds is due to dry contact forces in ladybirds being modelled using the DMT model (where detachment occurs via cohesive failure of the dry contact), while the dry contact forces in ants is modelled

using the JKR model (where detachment occurs via peeling from the edge of the dry contact zone). The larger contribution of dry forces in ladybirds means that when going from hydrophilic to hydrophobic substrates, our sphere-on-flat models predict a larger drop in the *total* adhesive force for ladybirds compared to ants (49% compared to 41% , Figures 5.3.5 & 5.3.4) which is qualitatively consistent with what is found experimentally, but still not large enough to explain the significant substrate dependence seen in ladybirds, Figure 5.3.1 & Figure 5.3.2. In addition, for ants, we note that the sphere-on-flat model predicts a significant dependence of the adhesive force on the substrate surface energy, which is in fact not observed experimentally. An adequate explanation for the substrate dependence (or lack thereof) in both ladybirds and ants is therefore currently lacking.

Notwithstanding the stronger substrate dependence observed experimentally in ladybirds compared to ants, in absolute terms, the substrate dependence of the adhesive force for both insects is relatively weak. From a biological point of view, the ability of insects, especially crawling insects such as ants, to successfully adhere to substrates with a range of surface energies with comparable force is vital for the insect's survival. This is because surface chemistry can be quite variable in nature and it is important that insects be able to resist unpredictable pulling forces due to sudden winds, gravity *etc.* on a variety of surfaces. Our study suggests that the underlying reason for the substrate insensitivity may be due to the fact that, for both insects, the capillary force contribution is comparable to or greater than the dry contact contribution, so that any drop in the dry contact force due to changes in the surface energy of the substrate does not lead to a drastic drop in the overall adhesive force. Even a drop of $\sim 50\%$ still allows the insects to generate forces equivalent to $\sim$5–10 times their body weight.

The reason why capillary force is weakly substrate dependent is in turn due to the fact that CAs of the secretion is only weakly dependent on the surface energy of the substrate, Figure 4.4.13. The fact that the secretion wets both hydrophilic and hydrophobic substrates has been cited as possible evidence that the secretion is a bi-phasic emulsion consisting of both hydrophilic and hydrophobic components [21]. In fact this assumption

may be unnecessary since, as it has been shown in Section 4.4, the CA of moderately long-chain hydrocarbons such as squalane ($C_{30}H_{62}$) are also relatively insensitive to the surface energy of the substrate, and able to wet the surface with a CA that is significantly smaller than 90°. The results in Figure 4.4.13 are therefore consistent with previous chemical analyses of the adhesive secretion which show that they consist of hydrocarbons with chain-lengths in the range $C_{16} - C_{28}$ [21, 74].

The chemical composition of insect adhesive secretions are highly complex [21], and still poorly understood, meaning that any conclusions about the rheology of these liquids from force measurement experiments should be treated with care. Evidence does seem to imply that hydrophilic components are present, but it is still debatable what benefits they may provide during attachment and detachment processes. The emulsion composition may have additional functionality which has not yet been eluded to, as briefly discussed in Section 4.4.2.

Finally, it is noted that the sphere-on-flat models predict that adhesive forces in both smooth and hairy pads are proportional to R (see Equations 4.3.3 & 4.3.4). This is in contrast with experimental results obtained from the wet adhesive system of tree-frogs where it is found that adhesive force is proportional to R^2 [109]. Thus although the sphere-on-flat model represents a big improvement on the parallel-plate-model in terms of accuracy of its predictions, it is clearly still an oversimplification of actual wet adhesive systems. To accurately account for both the magnitude and R scaling of the adhesive force, one would presumably need to employ a much more sophisticated finite element model that accurately captures the contact mechanics of wet adhesive systems. Such models unfortunately lie beyond the scope of this thesis, but it is noted that they have been studied for dry adhesive systems of Geckos [27].

Friction Forces

Figure 5.3.6 compares the tangential friction force calculated from the parallel-plate-model (Equations 4.3.8 & 4.3.9) with experimental measurements for *P. dives* and *H. axyridis* on both substrates. For *P. dives* ants, it is found that the parallel-plate-model predicts frictional forces that are much *lower* than experiment for hydrophilic glass, but which are comparable to experiment for hydrophobic glass. The main reason for the large difference of calculated forces between hydrophilic and hydrophobic glass in this case is due to the difference in secretion volume measured for this species on both substrates, Figure 4.4.14. The under-estimation of forces by this model on hydrophilic substrates has also been found previously in the literature, for example; Federle *et al.* [12] performed a similar calculation of friction forces for the Weaver ant *O. smaragdina* on Plexiglass and found that calculated shear stress was an order of magnitude too low in comparison to experimentally measured forces, and the authors concluded that their results indicated the adhesive secretion alone cannot explain the large frictional forces. For *H. axyridis* the predictions of the parallel-plate-model are comparable to measured friction forces in ladybirds, for both hydrophilic and hydrophobic substrates, Figure 5.3.6B. It is tempting to attribute the frictional force in this insect, and in ants for hydrophobic substrates, to viscous forces. However, as discussed in the previous sections, the parallel-plate-model is unlikely to be a correct representation of the contact geometry because it fails to correctly predict adhesion forces.

Moreover, it should be remembered that the experimental forces reported in Figures 5.3.2A and 5.3.6B are friction forces at the onset of sliding, and forces at the point of detachment were often much larger than this. For example; extreme detachment forces for *H. axyridis* reached in excess of 80 mN on hydrophilic glass. For the parallel-plate-model to match these substantial friction forces (in ladybirds) the liquid layer would need to have a sub-nanometre thickness. This would lead to dry contact on most surfaces, due to the presence of surface roughness, and would invalidate the notion of a viscous layer of fluid between

the two surfaces. A similar discrepancy in the frictional force between the parallel-plate-model and experiment has also been found by Federle and coworkers in the Weaver ant *O. smaragdina* and tree frogs [12, 109].

Finally, and most importantly, the parallel-plate-model cannot explain the magnitude of the static frictional force just *prior* to sliding. Equation 4.3.8 predicts zero friction forces when the sliding velocity is zero, *i.e.*, during static conditions, however static friction forces were substantial, Figure 5.3.2. Indeed Federle *et al.* [12] found that the Weaver ant *Oecophylla smaragdina* and stick insect *Carausius morosus* can sustain considerable static friction forces in the absence of any tangential sliding, which is clearly inconsistent with the parallel plate model [68, 183].

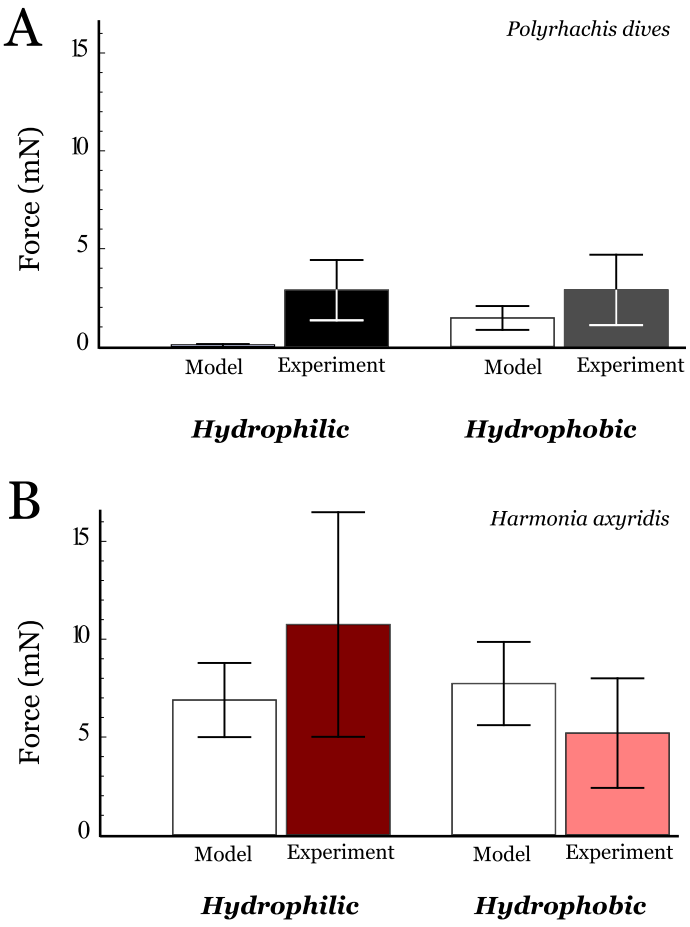

Figure 5.3.6: Experimentally measured friction forces at the onset of sliding compared with whole-insect theoretical calculations for A) the ant *P. dives* and B) the ladybird *H. axyridis* on hydrophilic and hydrophobic glass substrates. Errors for experimental results represent the standard deviation of the mean.

Two suggestions have been put forward to explain the static frictional force observed in insects. The first is the 'rubber friction model', proposed by Federle and coworkers [12, 183] where the friction force is due to dry adhesive friction between the soft, deformable adhesive pad and the substrate. More recently Drechsler [68] put forward an alternative 'emulsion hypothesis' where it is suggested that the adhesive secretion is a biphasic emulsion and the large static frictional forces come from the yield stress and effective viscosity of this emulsion [68, 90]. However, while the emulsion model is conceptually appealing, emulsions only possess a yield stress when the volume fraction of the dispersed phase exceeds the close-packed volume fraction, *i.e.*, where drops begin to contact each other and deform into polyhedra with rounded edges and corners [205, 206]. From the currently available data on the secretion morphology in the literature [12, 90], the volume fraction of the dispersed phase appears to be well below this threshold value and the dispersed drops remain well separated from each other, see Section 2.3.2. For such low volume fractions of the dispersed phase, emulsions do not possess a yield stress.

Instead, we argue that the most likely explanation for the large static and dynamic friction observed in insects is the 'rubber' friction model [183]. Firstly, this model is consistent with our analysis of the normal adhesive force which suggests that there is dry contact between adhesive pad and the substrate. Secondly, noting that the measured frictional force (Figure 5.3.2) is around 2 to 5 times larger than the measured adhesive force, which has also been observed in many previous studies for both hairy [34, 37] and smooth [12, 183] pads. Thus, the effective friction coefficient μ between the adhesive pad and the substrate is greater than unity, Table 5.3.1. Typical values for μ for friction between rigid solids are in the range $\mu \sim 0.1 - 0.4$ [114], but values of μ greater than unity are possible for dry friction involving soft, viscoelastic materials such as rubber where friction is dominated by adhesion [115–117]. Previous workers have shown that smooth and hairy adhesive pads [22, 48] have very low *effective* elastic moduli. In this case, unlike rigid solids where real contact only occurs where surface asperities touch each other, soft rubbery materials can conform to surface topography much more closely and achieve larger real contact-areas.

The large values of μ observed for both ants and ladybirds, together with the possible 'stick-slip' evidence within the secretion deposits of ants (Section 4.4.2) provides support for the theory that static friction is due to rubber friction between the soft adhesive pads and the substrate. The rubber-like viscoelasticity of soft adhesive pads would give rise to rate-dependent frictional forces, as found in insects such as ants [183], as will be discussed in Chapter 6.

5.4 Conclusions & Further Work

In summary, we have measured adhesion and friction forces in ants and ladybirds using a centrifuge technique on hydrophilic and hydrophobic glass surfaces. Ladybirds were found to generate significantly greater forces, and safety factors, on hydrophilic substrates than on hydrophobic glass, indicating a significant substrate dependence in this species. Ants generated comparable forces across both substrates, and were not significantly affected by substrate surface energy for either adhesion or friction. This may be an adaptation required of walking/crawling insects which encounter variable and unpredictable surface energies within their natural environments, as unexpected detachment from elevated surfaces could be potentially fatal for these insects.

By comparing experimental data to a number of simple theoretical models which encompass a range of possible contact geometries, and contact mechanics relevant to real insect adhesive pads, we have confirmed that the parallel-plate-model both qualitatively and quantitatively fails to account for both adhesive *and* frictional forces in insects. The sphere-on-flat models predict forces which are in much better agreement with experiment for both insects and is a large improvement over the parallel-plate-model. Quantitative differences between measurement and theoretical models are most likely due to deviations in contact-area and insect orientation during the detachment process, which were not considered within the models.

Therefore, results from the adhesion models suggest that, within the contact zone of both the smooth and hairy pad insects, the thickness of the secretion film is not uniform, and there may be a significant degree of dry contact between adhesive pad and substrate, meaning that both capillary forces and dry contact forces contribute significantly to the total adhesive force. Within this model, the relatively weak substrate dependence of adhesive forces in both insects can be explained due to capillary force contribution being at-least comparable to, or greater than, the dry contact contribution so that any drop in dry contact forces due to changes in surface energy does not lead to a drastic drop in the *overall* adhesive force, and the insect remains attached to the surface. In contrast to adhesion forces, friction forces calculated from the parallel-plate-model were found to be lower than measured forces, particularly for where variations in secretion volume between the two substrates was responsible for large differences between surfaces. Finally, considering the morphology of adhesive secretion and the high effective friction coefficients, we argue that large static and dynamic friction forces - particularly at the point of detachment - observed in both insects are due to dry 'rubber-friction' between the soft adhesive pad and the substrate, rather than because the adhesive secretion is an emulsion, as previously suggested within the literature.

The weakest parts of the analysis employed here is the measurement of the secretion volume within the contact zone, because this volume can have a large impact on the calculated forces within the parallel-plate-model (adhesion and friction), and may also affect the magnitude of the forces generated by the insects. To achieve more accurate and reliable measurements of this parameter, the use of more advanced interference reflection microscopy techniques, capable of measuring the thickness of a fluid layer between the substrate and contacting attachment pad *in vivo*, could be used. For example, the use of shorter wavelengths of light, together with the imaging of droplets with more than one wavelength of light (eg., blue and green), would also improve the accuracy of the measurement of interference fringe positions. This would reduce any uncertainty due to the evaporation of liquid from the droplet, and would allow for a more accurate estimation

of the volume per unit area deposited by each pad. It would also allow us to determine the contact geometry within the contact zone more accurately, thus allowing us to refine the theoretical models used for wet adhesion.

Chapter 6

Adhesion & Friction Forces - Other Techniques

6.1 Introduction

In Chapters 4 and 5 we studied the characteristic morphology and properties of the adhesive secretion of the tarsal pads of insects, and studied the adhesion and friction forces under slow, quasi-static, conditions measured with a centrifuge force measurement technique. Insects, however, will often encounter fast, 'dynamic' detachment forces in nature, such as those from sudden movement of leaves due to gusts of wind, rain drops or attacking predators.

In this chapter, we investigate the adhesive and frictional forces of the Asian Weaver ant *Polyrhachis dives* and the Seven-spot ladybird *Coccinella septempunctata* under impulsive forces. To our knowledge, no such force measurement technique has been deployed previously. We also measure the 'natural' pulling forces generated by these insects when allowed to walk freely and pull on a force meter. The results of the different measurement techniques are discussed, and a comparison is drawn between the measured detachment forces of ants and ladybirds under the different experimental conditions.

6.2 Materials & Methods

Insects

The seven-spot ladybird *Coccinella septempunctata* [Linnaeus, 1758] (Coleoptera; Coccinellidae) and the Weaver ant *Polyrhachis dives* (see Section 4.2) were used as study insects. The seven-spot ladybird is a monomorphic aphidophageous beetle native to central and western Europe, Figure 6.2.1. Its elytra (wing casings) are a red colour, but punctuated with seven black spots, from which the species derives its scientific and colloquial name. Adults are approximately 6–10 mm in length. Ladybirds were collected from the University of Hull campus and surrounding areas between the months of April and October. Insects were maintained as described in the Materials & Methods section of Chapter 4.

Average body mass was 37.2±5 *mg* (mean±s.d.) for *C. septempunctata* and 7.0±1 mg for *P. dives*. Within this chapter, both male and female ladybirds were used for force measurements.

Figure 6.2.1: Top view of a 7-spot ladybird *Coccinella septempunctata*. Scalebar = 5 mm.

Impact-Rig Experiment

To measure impulsive adhesion and friction forces a custom built impact-force apparatus was used which contained a glass box (internal dimensions: 40 x 40 x 40 mm, UQG Optics), which held the study insect, on a moveable carriage placed onto a short metal track (RS Components, UK), Figure 6.2.2. The carriage was attached to springs which propelled it towards a metal block housing a dynamic load cell containing a piezoelectric crystal that generates an analog voltage in response to an applied dynamic force (DLC101-50, dynamic load cell, OMEGA Engineering, Manchester, UK), Figure 6.2.2. The dynamic load cell (sensor) was connected to an external power supply (ACC-PSI Current Source, OMEGA Engineering, Manchester, UK) which connected the sensor to a PC based oscilloscope (Picoscope 6, Pico Technology Ltd., St Neots, Cambridgeshire, UK). Voltage was converted to impact force (F_{cell}) by the relation $1\ V = 10.7\ lb/F$ as defined by the supplier, and converted to SI units. The sensor had a saturation voltage of $5\ V$ which limited the maximum impact force that could be measured. The impact zone of the apparatus shown in Figure 6.2.2 was imaged with high-speed photography. The camera (Pixci Silicon Video 642M, Epix Inc, IL, USA) was fixed in place focused on the impact zone, connected to a

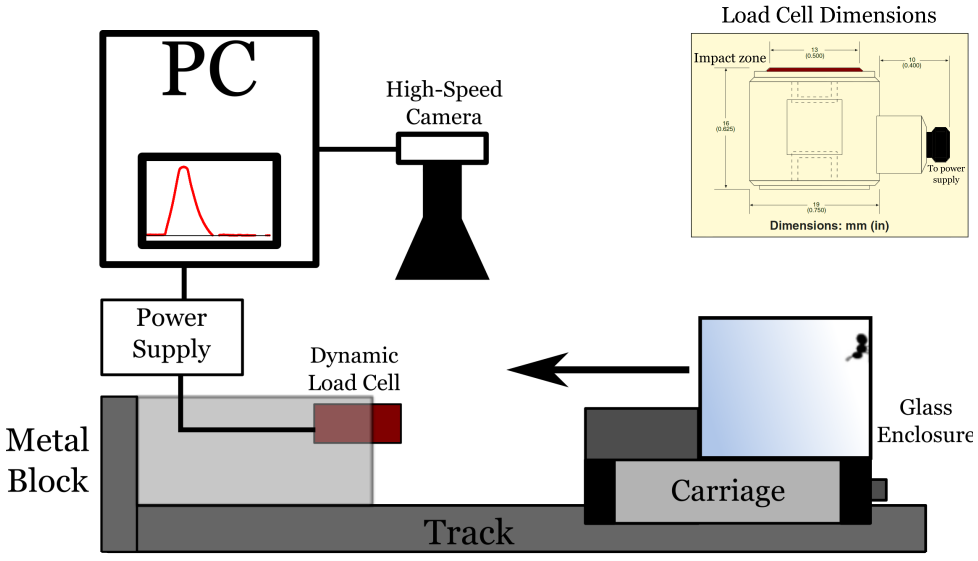

Figure 6.2.2: Impact-Rig design schematic. A glass enclosure, being either hydrophilic or hydrophobic, placed on top of a carriage is run along a train towards a metal block with a dynamic load cell which registers the force of impact when connected to a PC-based oscilloscope. The impact zone was recorded using a high-speed video camera.

PC and controlled by Xcap software (EPIX, Inc., IL, USA). The default field of view was 4×4 cm. In order to compare the detachment forces on hydrophilic and hydrophobic surfaces, a single glass box was treated with DCDMS ($(Si(CH_3)_2Cl_2)$; 99%, Sigma Aldrich, UK) to make the internal surfaces hydrophobic using a method based on procedures found in the literature [186], and the same method as described in Chapter 5.

Insects were individually weighed (mass m_{in}) and placed within the glass box which was then closed, and the insect was free to explore the box. Total mass of both the cart, and the glass enclosure was $M_{cart} = 238$ g. The carriage was then drawn back to a set extension by hand and released when the insect was observed to be in full contact with the desired internal surface. The inertial force acting on the insect as a result of the impact is calculated from:

$$F_i = \frac{m_{in}}{M_{cart}} \cdot F_{cell} \tag{6.2.1}$$

After the impact the insect either remained attached to the surface, or had detached. Extension lengths were increased by 1 cm intervals up to the maximum allowable length of the track. Six insects were tested at each extension length, each insect was subjected to 3 impacts separated by at least 30 s, and each insect was used in this way only once in any 24 hour period to avoid any replications biases. Experiments were conducted under laboratory conditions, within the temperature range T=18°–27°C, relative humidity RH=30–50% monitored with a thermo-hygrometer (RH83, Omega Engineering, Manchester, UK).

Natural Pulling Force Experiment

To measure the natural pulling, or frictional 'drag', forces generated by the insects, a custom-built direct-force measurement technique was used. An electronic balance (Ohaus Adventurer Pro AV264C, Oakleyweigh, Aylesbury, UK) was placed on-top of a metal stage with a cut out hole. The weigh-plate of the balance could be accessed from the underside to allow for measurement of pulling forces from underneath, and a cotton thread was attached to it. The thread was then attached to the insect under study, Figure 6.2.3.

The thread was attached to the ants by carefully manually tying a knot around the ants' petiole, mid-section. Threads were attached to the elytra of ladybirds by immersing the thread into a small drop of molten beeswax (Sigma Aldrich, UK), applied to the back of the ladybird using a plastic pipette straddling the gap between the elytra casings ensuring the ladybirds could not take flight, see Figure 6.2.3.

Substrates were held with a motorised micro-manipulator in a vertical orientation and the insect was brought into contact with the surface in an inverted condition (head-down). The insect was encouraged by gentle taps with a pair of entomological tweezers to walk vertically downwards, pulling on the thread attached to its body. The force was registered by the electronic balance, which sent it to an Excel spreadsheet *via* an RS232-USB interface connected to a WinWedge (TALtech Instrumental Software Solutions, Philadelphia, USA) software macro. Measurements were taken over the course of 1 minute and the maximum force over the course of the experiment was extracted. Each insect was only used once in any 24 hour period to avoid any replication bias.

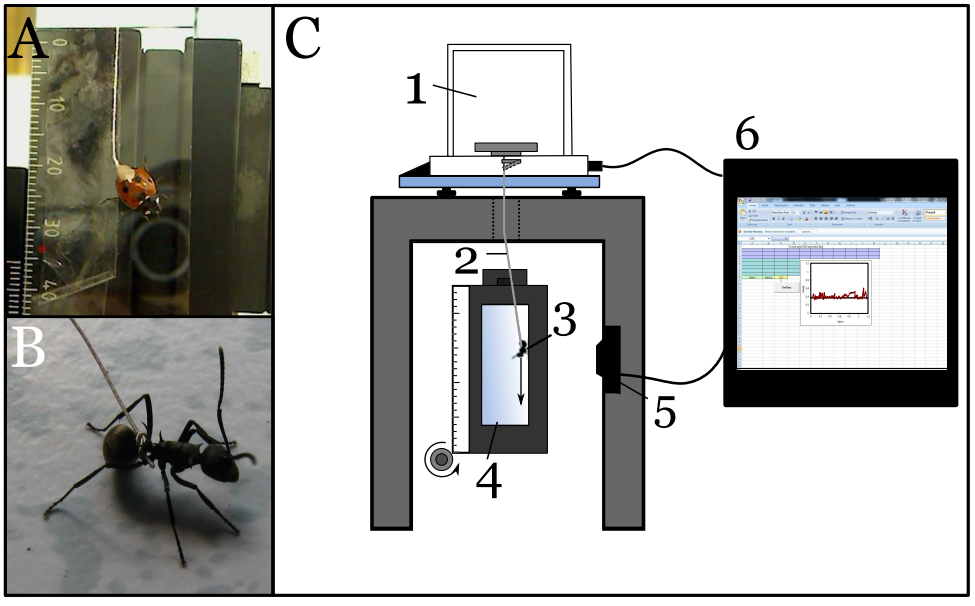

Figure 6.2.3: A) 7-spot ladbyird *C. septempunctata* attached to a thread immersed in a small drop of bees-wax. B) The Weaver ant *P. dives* with a thread tied around its petiole mid-section. C) Schematic of direct-force measurement apparatus. 1) Electronic Balance, 2) thread, 3) insect, 4) substrate, 5) webcam, 6) PC & data logging software.

Data Analysis for Impact Rig and Natural Pulling Force Experiments

Impact Rig

The results of each individual impact test were binary, being either *detach*, or *non-detach*. Impact forces were separated into distinct bin-ranges, and the proportion of insects which detached within that force-range was calculated as a percentage. If F_i is defined as the force the insect is subjected to upon impact, the fraction of insects which detach at each force-range, $Q(F_i)$, (where F_i is the arithmetic mean of the bin boundaries) represents the proportion of insects which will detach at a force $F \leq F_i$. Let $P(F)$ be the cumulative distribution function which gives the fraction of insects with a detachment force F, then it immediately follows that the mathematical relationship between $Q(F_i)$ and $P(F)$ is

$$Q(F_i) = \int_0^{F_i} P(F)\, dF \tag{6.2.2}$$

and

$$P(F) = \frac{dQ(F)}{dF} \tag{6.2.3}$$

Thus we can extract $P(F)$ from $Q(F)$ measured from the impact rig experimental data. In principle the relationship outlined in Equation 6.2.3 could be used for this purpose, however using this relationship involves taking a numerical derivative which is notoriously very noisy. We will therefore use Equation 6.2.2 instead to extract $P(F)$ from $Q(F)$. Specifically, first we need to find a convenient parametrisation for $P(F)$. Since F lies between 0 and ∞, we will use the *log-normal* distribution for $P(F)$ [207], where

$$P(F_i) = \frac{1}{\sigma\sqrt{2\pi}} \frac{1}{F_i} \exp\left[-\frac{(\ln F_i - \mu)^2}{2\sigma^2}\right] \tag{6.2.4}$$

where the mean μ and variance σ^2 parameters control the shape of $P(F)$. Integrating Equation 6.2.4 gives the cumulative distribution function $Q(F_i)$ which can be fitted to the

experimental data to find μ and σ:

$$Q(F) = \int_0^{F_i} \frac{1}{\sigma\sqrt{2\pi}} \frac{1}{F} \exp\left[-\frac{(\ln F - \mu)^2}{2\sigma^2}\right] \tag{6.2.5}$$

The mean force, $\bar{F}$, and standard deviation, ΔF, are then related to μ and σ according to [207]:

$$\bar{F} = \exp\left(\mu + \frac{1}{2}\sigma^2\right) \tag{6.2.6}$$

and

$$\Delta F = \sqrt{\exp\left(2\mu + \sigma^2\right)\left[\exp(\sigma^2) - 1\right]} \tag{6.2.7}$$

Natural Pulling Forces

Statistical analysis of difference in means of direct-force measurements were performed using Mathematica 8.0.0 software (Wolfram Research Europe Ltd., Long Hanborough, Oxfordshire, UK). Data sets were tested for normal distribution and equal variance before appropriately analysing the difference between groups with either a Mann-Whitney U-test (median comparison) or an unpaired t-test (mean comparison).

6.3 Results

When placed within the glass enclosure, insects were observed to traverse all sides of the hydrophilic glass box with ease, but walking velocity was slower on the hydrophobic enclosure, the front feet were observed to slip and slide proximally during locomotion, and the frequency of foot repositioning motions whilst the insect remained stationary increased, suggesting that the hydrophobic surface was 'slippery' for the insects. It was observed that, when placed within the hydrophobic box, a small number of ladybirds were unable to climb the vertical wall to reach the inverted surface. It was decided to remove these insects from the test group on the basis that they clearly could not generate a safety factor of 1 under their own strength, and would skew the results. Due to the fact that insects were free to walk around inside the enclosure before impact, it could not be guaranteed that all 6 feet were in contact with the glass surface upon impact, but most insects walked with a gait whereby atleast 3 feet were in contact with the surface at any time. Upon impact, insects were subjected to impulsive detachment forces of varying magnitude for a duration of several milliseconds, Figure 6.3.1.

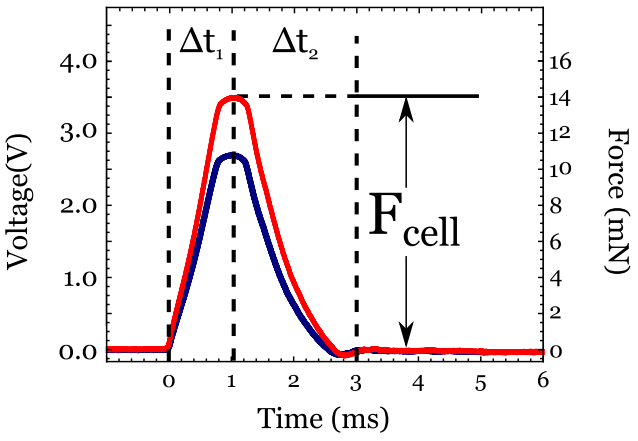

Figure 6.3.1: Example waveforms of dynamic load cell following impact by the cart. The load cell reports the voltage measured by the piezoelectric crystal, which is converted to the force felt by the insect due to the deceleration. The change in force F_{cell} due to the impact is reached in time Δt_1, and the total impact time is given by Δt_2.

6.3.1 Normal Forces

Normal impulsive detachment forces were measured by launching the cart towards the sensor when the insect under study was seen to be wholly attached to the vertical surface of the enclosure.

Detachment Process

The detachment process after impact was to some extent determined by the orientation of the insect prior to the collision. Figure 6.3.2 schematically outlines two of the detachment modes identified under normal detachment conditions. Although insects would be oriented differently prior to impact (eg., head-up or head-down orientation), the detachment dynamics did not change substantially due to the insects' pre-impact orientation.

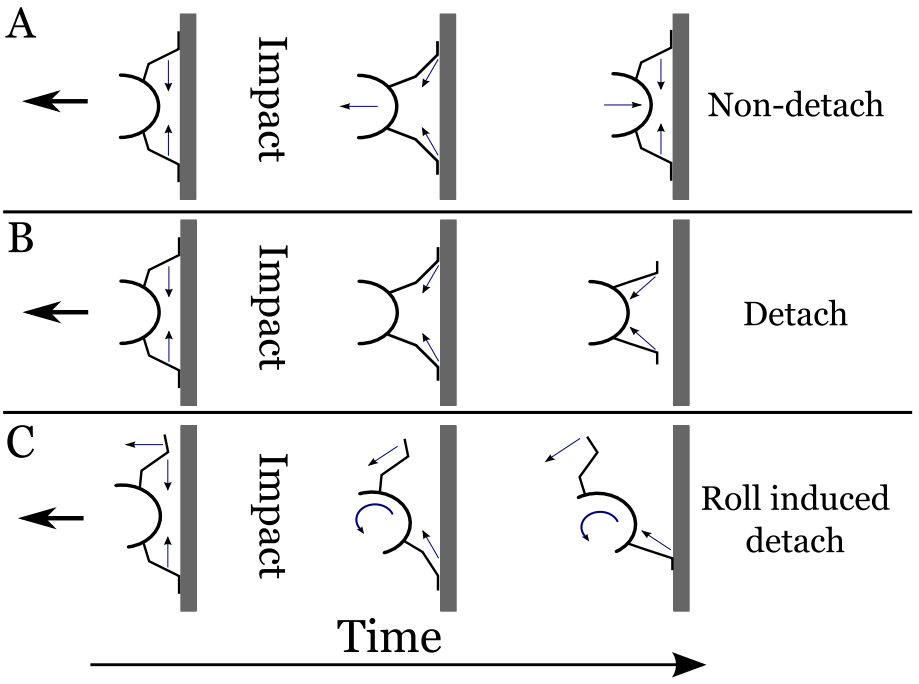

Figure 6.3.2: Different behaviours of insect tarsi after an impulsive impact force is applied in the normal direction to the substrate. Images show insects attached to a substrate, viewed along the anteroposterior axis from head to tail, and the legs shown correspond to left and right sides if the insect. A) Insects absorbed lower impact forces without detaching, B) At higher forces the insects feet were observed to move proximally after detachment. C) If insect feet did not detach simultaneously, the moment of forces causes the insect to spin or roll during detachment.

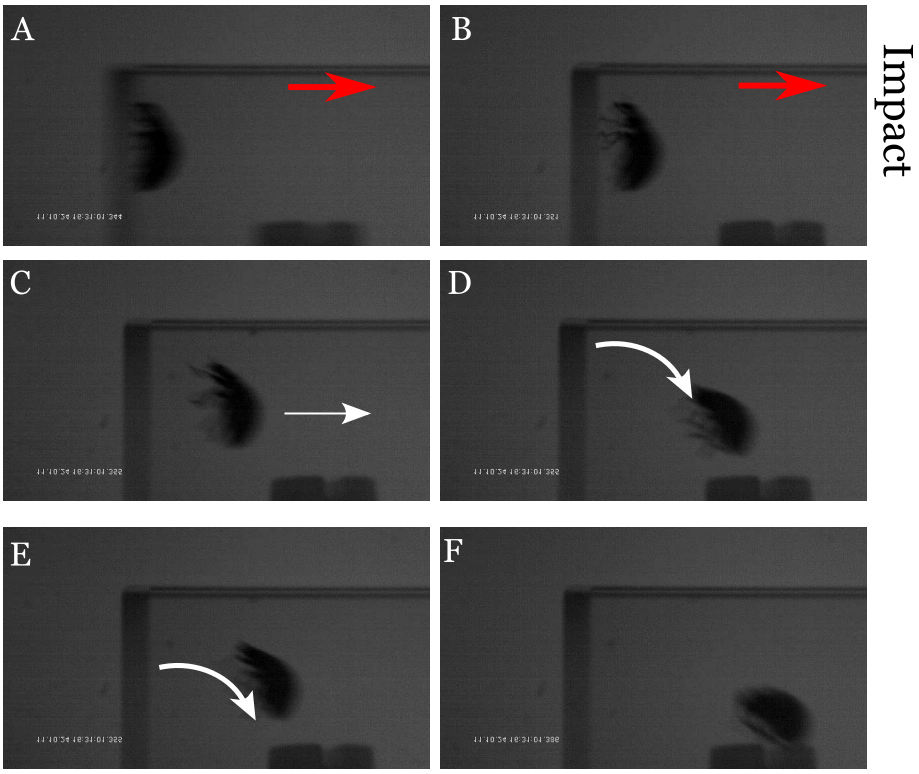

Figure 6.3.3: High-speed snapshots of *C. septempunctata* detaching during Impact-rig experiment from a hydrophilic glass surface, normal to the substrate. A)–B) the ladybird travels at the same velocity as the cart, C)–D) after impact the insect continues on a curved trajectory as it falls due to gravity, E)–F) during the fall, the head of the insect begins to rotate about the centre of mass. This detachment behaviour is depicted in Figure 6.3.2A. Red arrow indicates the movement of the cart, white arrows indicate movement of the insect.

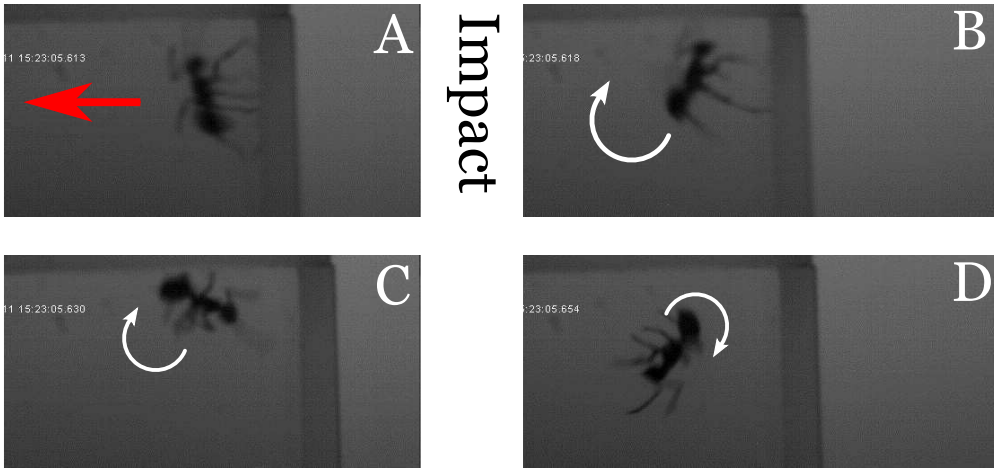

Figure 6.3.4: Irregular tarsus detachment caused some insects to spin in mid-air after impact. After impact, a *P. dives* ant's hind legs detach first, causing the insect to rotate about the centre of mass after impact. Red arrow indicates the movement of the cart, white arrows indicate movement of the insect. This is depicted schematically in Figure 6.3.2B.

At low impact forces, a high proportion of insects were able to absorb much of the impulse and reduce their post-impact velocity, or remain attached to the surface. Insects which were not fully detached from the glass surface often had a number of legs detach from the surface due to the impact, and the insect remaining adhered to the glass due only to one or two tarsi remaining in place. At higher impact forces the insect can be seen to simply continue on its original path, clearly detaching with little resistance, *eg.*, Figure 6.3.3. For situations where all tarsi are attached at impact, differences in posture and gait of the insect caused the insects to detach in unpredictable, and chaotic manners. During the detachment process it was seen that if all the feet were in contact with the surface, the feet of the insects are drawn inwards, proximally, Figure 6.3.2A. On the other hand, sudden detachment of a number of the tarsi from the substrate initiated by the impulsive force leads to forces tangential to the substrate to act on the insect, which causes the insect to spin, or roll over, Figure 6.3.2B & Figure 6.3.4. These spinning, and torsional motions add further stress to the contact zone, and act to detach the insect from the substrate. Due to the limitation of the high-speed camera's resolution, it was not possible to visualise fine details of the detachment process on the level of the arolia or setae from the glass surfaces.

Adhesion Forces from Impact-Rig Experiments

The fraction of insects which detached at different impact forces, F_i, together with the cumulative probability distribution fits for *C. septempunctata* and *P. dives* in the direction normal to the surface are shown in Figure 6.3.5. Using Equations 6.2.6 & 6.2.7, the mean detachment forces of *C. septempunctata* and *P. dives* on hydrophilic and hydrophobic glass were determined, Table 6.3.1, and the mean detachment force from the centrifuge experiments F_c performed on the same, species and substrate pair, are shown in Figure 6.3.5 for comparison. Although the safety factors of individual insects during the impulsive tests cannot be determined because the exact detachment force for the individual insects is unknown, using the mean detachment force determined from Equations 6.2.6 & 6.2.7

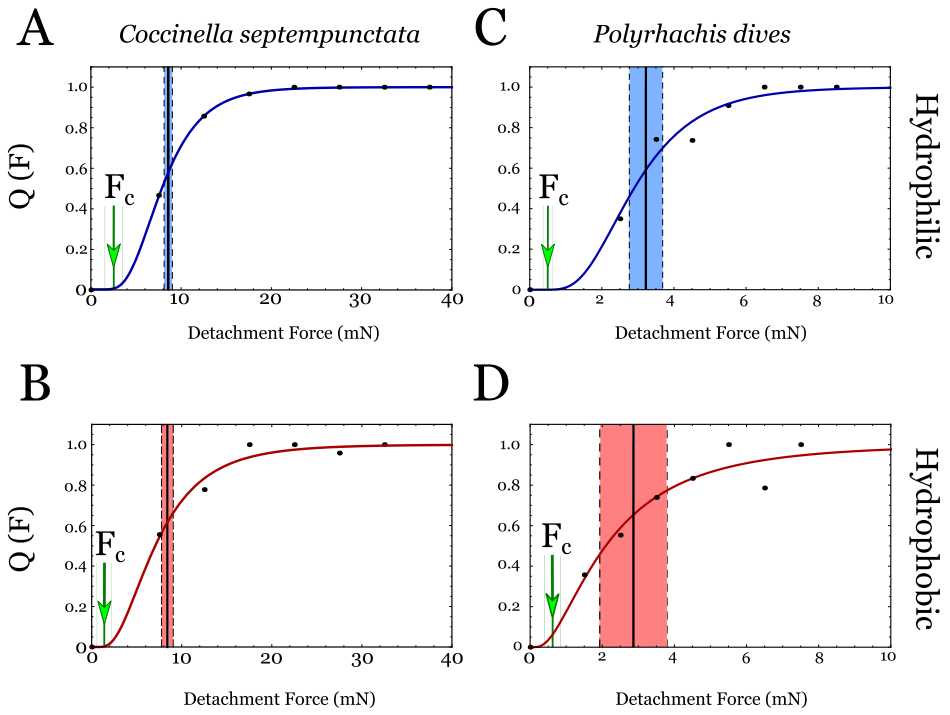

Figure 6.3.5: Probability distribution function fits to Impact-rig adhesion force data for *Coccinella septempunctata* and *Polyrhachis dives*. Vertical black line shows the mean force calculated from the PDF fit, the coloured area either side of the solid line represents the standard deviation of the mean. The green arrow F_c indicates the mean detachment force found in the centrifuge experiments on the same type of substrate, and the standard deviation either side of the mean, as determined in Chapter 5.

Table 6.3.1: Measured adhesion forces and safety factors for ants and ladybirds on hydrophilic and hydrophobic surfaces using different force measurement techniques.

Insect	**Mass** (mg)	**Method**	**Substrate**	**Mean** (mN)	**SD** (mN)	**Safety Factor**
C. septempunctata	37.2	Centrifuge	Hydrophilic	2.3	1.8	5.4±4
C. septempunctata			Hydrophobic	1.8	0.9	4.9±2
H. axyridis	29.8		Hydrophilic	3.5	1.6	12±6
H. axyridis			Hydrophobic	1.7	0.6	6±2
P. dives	7.0		Hydrophilic	0.5	0.2	8.8±5
P. dives			Hydrophobic	0.6	0.4	7.7±4
C. septempunctata		Impact-Rig	Hydrophilic	8.6	0.5	24
C. septempunctata			Hydrophobic	8.4	0.7	23
P. dives			Hydrophilic	3.2	0.5	47
P. dives			Hydrophobic	2.9	0.9	42

and the mean body weights of the insects mentioned in section 6.2, the safety factor on the hydrophilic and hydrophobic substrates can be estimated. The ladybird *C. septempunctata* generated adhesion safety factors of 24 on hydrophilic and 23 on hydrophobic glass, and for *P. dives* these values were 47 on hydrophilic and 42 on hydrophobic glass.

Normal Detachment Velocity

From the high-speed video images, eg., Figure 6.3.3, the detachment velocity of the insect can be estimated in an effort to determine to what extent viscous forces plays a role during the detachment process, Figure 6.3.6. Mean detachment velocities were not significantly different between hydrophilic and hydrophobic glass substrates for ants (t-test, t=1.46037, P=0.254671) or ladybirds (Mann-Whitney U-test, U=12, P=0.297107). Thus, mean detachment velocities for *C. septempunctata* were 797 ± 52 (mean±s.e.m.) mm/s (N=12) and for *P. dives* was 455 ± 35 mm/s (N=12).

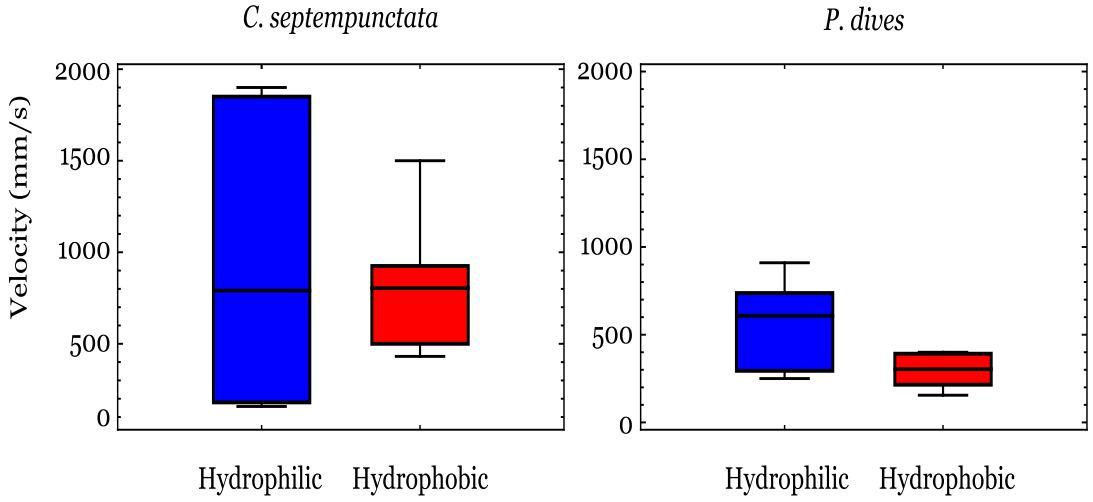

Figure 6.3.6: Detachment velocity of ants and ladybirds from glass surfaces. Normal detachment velocities were not statistically different between hydrophilic and hydrophobic glass for both ants (t-test, t=1.46037, P=0.254671) and ladybirds (Mann-Whitney U-test, Z=12, P=0.297107).

6.3.2 Tangential Forces - Impulsive Detachments

Tangential impulsive detachment forces were measured by launching the cart towards the sensor when the insect under study was seen to be wholly attached to the top surface of the enclosure, being fully inverted at the point of impact.

Detachment Process

Insects were noticeably more difficult to detach from the substrates during the tangential tests compared to the adhesion experiments described above, requiring a larger force to be applied during tangential impulses, than during the adhesion tests described above. We were unable to fully detach 100 % of ants, even using the maximum impact force allowed by the impact sensor. Several different modes of detachment were observed, the most frequently observed modes of detachment are depicted schematically in Figure 6.3.7. While Figure 6.3.7 depicts modes of detachment with the insect oriented to face the observer (out of the page where the legs of the insects represent the left and right sides of the insect), similar modes were observed if the front or the back of the insect faced the impact wall.

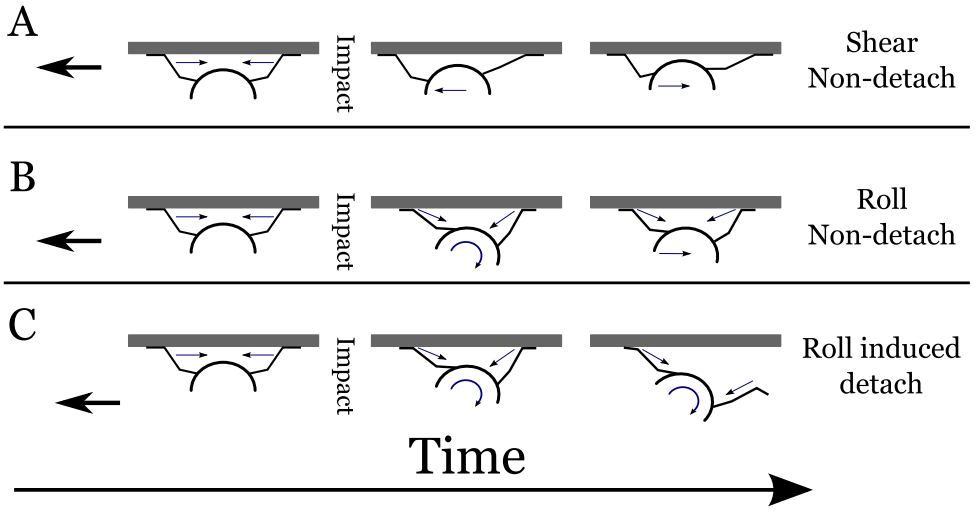

Figure 6.3.7: Behaviour of insect tarsi after an impulsive impact force is applied in the direction tangential to the substrate. The legs of the insects in the figures represent the left and right sides of the insect. A) At low forces the feet remain in place and the body moves tangentially before returning to the original position. B) At higher impact forces the feet remain in place but the legs are straightened and the body rocks tangentially, pivoting about the insects' centre of mass before returning to the original position. C) On detachment the foot located furthest from the impact zone slides forwards as the body rotates about the centre of mass, increasing the angle between foot and the substrate, causing detachment.

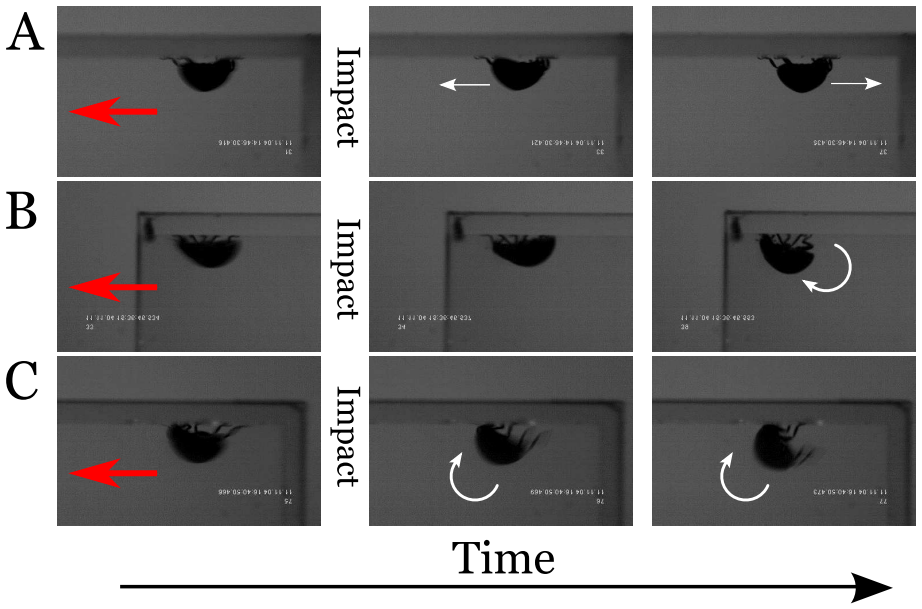

Figure 6.3.8: Image array showing different modes of reaction after a tangential impulse was applied to a *C. septempunctata* ladybird as depicted in Figure 6.3.7. A) Slow impact forces cause the insect to rock back and forth, and tarsi remain in place. B) At higher impact forces, depending on the orientation of the insect, the insect rotates about the centre of mass to a greater degree before returning to the original position. C) If the insect detaches the foot located furthest from the impact zone detaches as the body rotates about the centre of mass, increasing the angle between foot and the substrate, causing detachment.

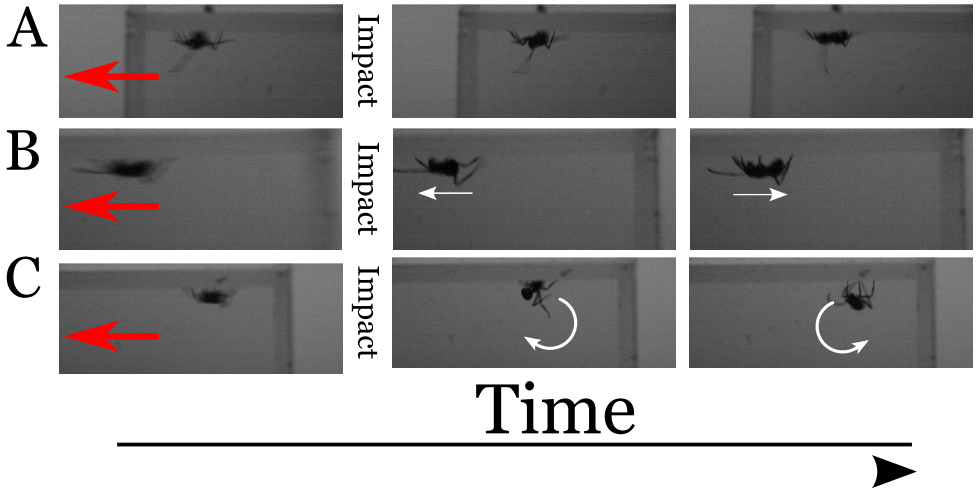

Figure 6.3.9: Image array showing different modes of reaction after a tangential impulse was applied to a *P. dives* ant. A) Slow impact forces cause the insect to rock back and forth, the body is drawn closer to the substrate and tarsi remain in place. B) At higher impact forces the insect's body rotates about the centre of mass and is forced forwards, before returning to the original position. C) At even higher forces the feet furthest from the impact zone detach and the insect rotates about the centre of mass. In this case the ant was able to resist the detachment force and returns to its original orientation.

Frictional Detachment Forces

For tangential detachments, the fraction of insects which detached at different impact forces, F_i, together with adhesion forces for *C. septempunctata* and *P. dives* as determined by the PDF are shown in Figure 6.3.10. For comparison, the mean detachment force from the centrifuge experiments are also shown in Figure 6.3.10. Unfortunately time restraints prevented us being able to measure the centrifuge forces of *C. septempunctata*, but instead we used the centrifuge forces measured with the closely related species *H. axyridis* for comparison, as measured in Chapter 5. It is noted that the pulling forces of these two ladybirds are comparable, Section 6.3.3, and we should expect that comparable forces will be generated by the 7-spot ladybird under impulsive conditions. Ladybirds generated friction safety factors of 82 and 74 on hydrophilic and hydrophobic substrates respectively. The PDF fitting was unable to determine mean and standard deviation values for *P. dives*

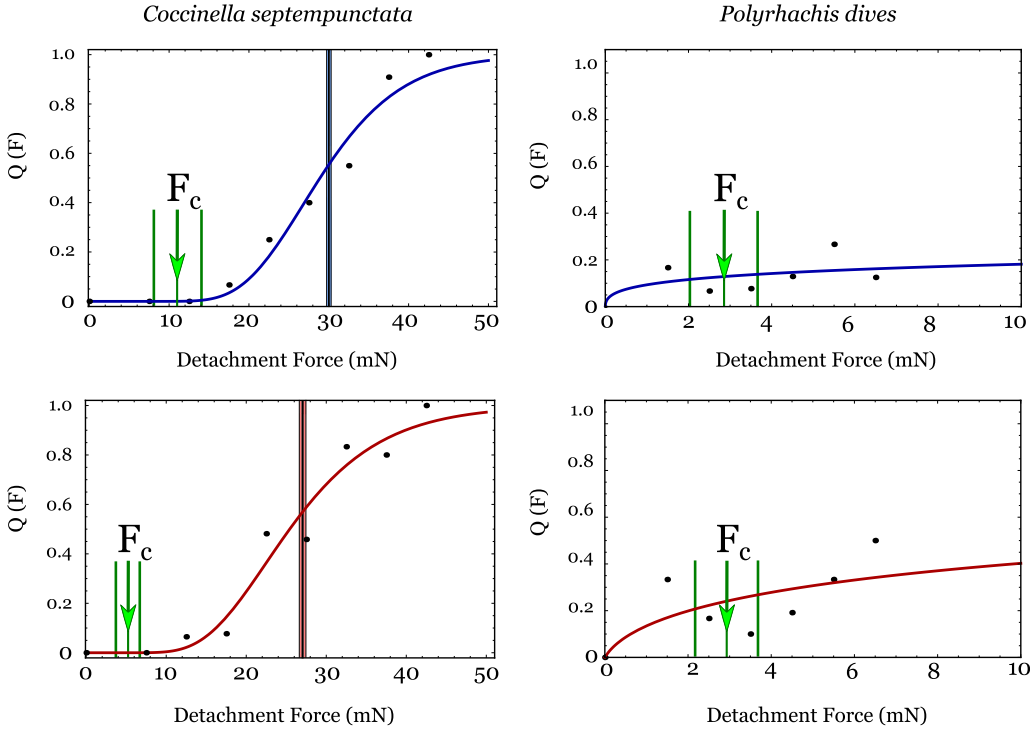

Figure 6.3.10: Probability distribution function fits to Impact-rig friction force data for *Coccinella septempunctata* and *Polyrhachis dives*. Vertical black line shows the mean force calculated from the PDF fit, the coloured area either side of the solid line represents the standard deviation of the mean. The PDF was unable to determine mean values for *P. dives* tangential data. The green arrow F_c indicates the mean detachment force found in the centrifuge experiments on the same type of substrate, and the standard deviation either side of the mean, as determined in Chapter 5.

tangential data because the dynamic load cell was not capable of measuring the forces high enough to detach 100% of the ants from either the hydrophilic or hydrophobic surfaces, and the distribution data is incomplete. However, from the Figures 6.3.5 and 6.3.10 it can be seen that the extracted values of $\bar{F}$ approximate to the force between $Q(F)$=0.5–0.6. From this it can be crudely estimated that the ants had a mean friction detachment force under impulsive conditions $> 7\ mN$ and approximately $7\ mN$ on hydrophilic and hydrophobic glass respectively, corresponding to safety factor values in excess of 100, Table 6.3.2.

Table 6.3.2: Measured friction forces and safety factors for ants and ladybirds using different force measurement techniques.

Insect	**Mass** (mg)	**Method**	**Substrate**	**Mean** (mN)	**SD** (mN)	**Safety Factor**
H. axyridis	29.8	Centrifuge	Hydrophilic	10.75	5.7	43.2±19
H. axyridis			Hydrophobic	5.16	2.8	16.7±11
P. dives	7.0		Hydrophilic	2.90	1.8	31.4±17
P. dives			Hydrophobic	2.89	1.5	27.7±17
C. septempunctata	37.2	Pulling Forces	Hydrophilic	12.2	3	34±8
C. septempunctata			Hydrophobic	10.2	4	28±11
H. axyridis	29.8		Hydrophilic	9.28	3.8	32±13
H. axyridis			Hydrophobic	6.86	2.8	23±10
P. dives	7.0		Hydrophilic	2.9	2	42±7
P. dives			Hydrophobic	1.5	1	22±3
C. septempunctata	37.2	Impact-Rig	Hydrophilic	30.0	0.3	82.2± 1
C. septempunctata			Hydrophobic	27.0	0.4	74.0± 1
P. dives	7.0		Hydrophilic	> 7	–	> 101
P. dives			Hydrophobic	> 7	–	> 101

6.3.3 Tangential Forces - Natural Pulling Forces

Insects were allowed to pull in the downwards direction for up to 1 minute and the force measured for the duration, Figure 6.3.11. Taking the maximum force measured from each insect, the mean force measured for *C. septempunctata* and *P. dives* on hydrophilic and hydrophobic glass substrates were determined, Figure 6.3.12. Pulling forces were found to be slightly greater on hydrophilic surfaces for both insects, but statistical analysis showed no significant difference between the forces on different substrates for either insect. Mean pulling forces for *C. septempunctata* were 12.2±3 mN (mean±s.d.) on hydrophilic and 10.2±4 mN on hydrophobic glass (t-test, t=1.597, P=0.222); for *P. dives* mean forces were 2.9±2 mN on hydrophilic and 1.5± 0.9 mN on hydrophobic glass (t-test, t=1.1009, P=0.31317). Using the insect masses mentioned in Section 6.2, these values correspond to safety factors of 34 on hydrophilic and 28 on hydrophobic glass for *C. septempunctata*, and 42 on hydrophilic and 22 on hydrophobic glass for *P. dives*.

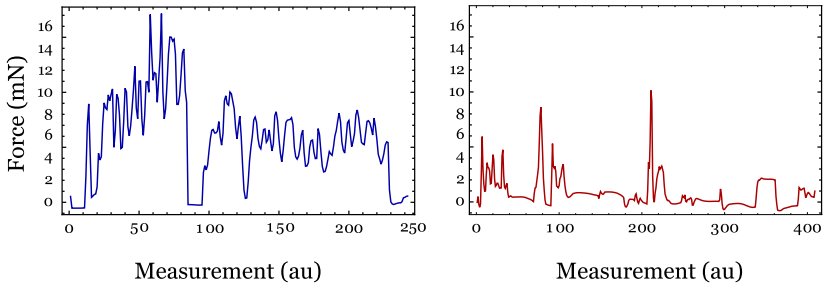

Figure 6.3.11: Representative force curves for the direct force measurements of *C. septempunctata* on hydrophilic (blue) and hydrophobic (red) glass surfaces over the course of approximately 1 minute.

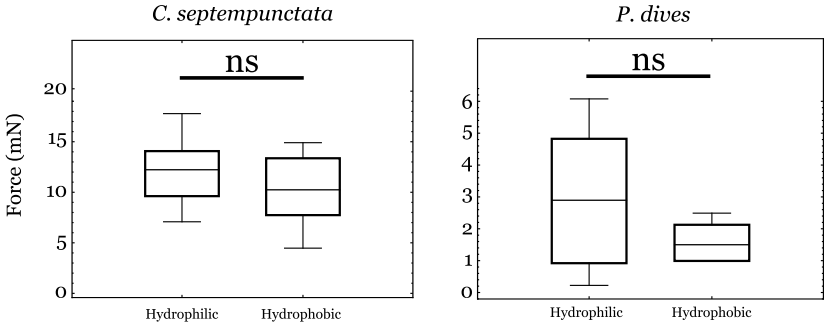

Figure 6.3.12: Measured pulling forces of *C. septempunctata* and *P. dives* on hydrophilic and hydrophobic glass surfaces. Boxes represent upper and lower quartiles with a black mean line between them, whiskers represent 10th and 90th percentiles. ns = not significantly different. Note the different scales on the force-axes.

6.4 Discussion

Comparing the adhesive and frictional force data in Tables 6.3.1 and 6.3.2 for the different insects, substrate surface energy, and force measurement techniques, several interesting trends emerge.

6.4.1 Normal Adhesion Forces

Measurement of impulsive detachment forces indicates significantly greater forces can be generated by insects during short, impulsive perturbations, than during slow, or static conditions. For example, the Weaver ant *P. dives* generated normal detachment forces under impulsive conditions approximately 6 times greater than under quasi-static conditions of the centrifuge experiment, Table 6.3.1. The ladybird *C. septempunctata* showed a similar increase in force when comparing forces between impulsive detachments and the centrifuge experiment, generating adhesion forces approximately 3.5× and 4.5× greater on hydrophilic and hydrophobic glass respectively, corresponding to an increase in safety factors of almost a factor of 5.

Results also suggest that ants, possessing the smooth adhesive pad, perform better than the ladybirds, with hairy pads, under impulsive detachment conditions. Comparison of the safety factors of the two insects indicates that during impulsive perturbations the ants are capable of withstanding greater *relative* forces compared to the ladybird by nearly a factor of 2, although the ladybirds are still able to generate forces equivalent to more than 20 times their own body weight, Table 6.3.1. This is contrary to the results of the centrifuge experiments, Chapter 5, where it was found that the Weaver ants generated adhesion safety factors comparable to those of the Harlequin ladybird, and were not statistically different between these insects (*hydrophilic:* Mann-Whitney U-test, U=2561, P=0.089; *hydrophobic:* *t*-test, t=2.019, P=0.1634).

Several possible mechanisms might explain the larger normal forces during impulsive detachments compared to quasi-static detachments. Firstly, there could be an additional contribution to adhesion due to the viscosity of the adhesive secretion, i.e. the so called Stefan force described in section 2.4.2.2. The contribution of viscous forces to adhesion in insects and frogs has been considered previously [12, 208], which concluding that the contribution is small or negligible during conditions of normal locomotion, but these estimates are based on force measurements taken at much lower detachment velocities. However, when movements are fast, the presence of a liquid secretion will lead to a significant contribution to adhesion from viscosity [12]. As discussed in Chapter 5, the pad–substrate geometry which most closely captures the contact mechanics of both smooth and hairy pads is that of a sphere-on-flat arrangement. The Stefan force for this geometry, explained in Chapter 2 section 2.4.2.2, is [111, 112] given by:

$$F_{visc} = \frac{3\pi}{2} R^2 \eta \frac{v_d}{h} \tag{6.4.1}$$

The contact radius R and the secretion viscosity η were determined in the previous chapter, and have the values R=50 μm and R=2.22 μm for ants and ladybirds respectively, and needs to be doubled for a sphere-on-flat calculation, see Section 6.3.1. Viscosity of the adhesive secretions were taken as 107±27 $mPas$ for ladybirds and 28±8 $mPas$ for ants, and the detachment velocity v_d measured in Section 6.3.1, has values of 797±52 mms^{-1} and 455±35 mms^{-1} for ladybirds and ants respectively. The difficulty in using Equation 6.4.1 lies in estimating the closest separation distance h of the two surfaces. Using interference microscopy Federle et al. [12] estimated the thickness of the adhesive secretion in *C. morosus* and *O. smaragdina* to range between 90 and 160 nm near the edge of the contact zone, and secretion films of roughly 50 nm thickness were deposited by sliding pads. Dirks & Federle [92] showed that for smooth adhesive pads in contact with a substrate there is a wedge of fluid which increases in thickness towards the outer meniscus, suggesting the film thickness towards the centre of the contact zone is even less than this. As a first estimate, it is assumed that a minimum film thickness corresponds to the roughness scale

of the substrate, and a value of h=10 nm was used.

Using these values with Equation 6.4.1 for *P. dives* ants yields a Stefan force of approximately 360±118 mN per insect. A similar calculation for ladybirds, assuming all setae were deployed, the detachment was wholly perpendicular, and using the parameters determined in Chapter 4 for the Harlequin ladybird *H. axyridis* together with the detachment velocity measured for *C. septempunctata* quoted above (Figure 6.3.6), yields a Stefan force >7.1 N which is an order of magnitude greater than that measured experimentally. Comparing these results with experimentally measured forces, eg., Table 6.3.1, for these species it is found that the calculated Stefan adhesion forces are substantially greater than the difference between static and dynamic adhesion forces measured *in vivo*. Specifically the difference between the centrifuge and impulsive detachment forces (on hydrophilic glass) for the ants is $\sim$ 2.8 mN, and 6.3 mN for ladybirds - significantly less than the Stefan force calculated here with Equation 6.4.1.

There are several possible reasons why the calculated Stefan force is much greater than the dynamic forces measured *in vivo*. 1) The film thickness chosen, h, is an absolute minimum value under these conditions, and the actual effective thickness may be significantly greater than this, and 2) Equation 6.4.1 used to estimate this viscous force also assumes the foot of the insect detaches entirely perpendicularly from the surface, but it was experimentally observed that the tarsi are pulled proximally during detachment. This would increase the angle between the leg and substrate, aiding detachment of the arolium, or hairy pad, *via* peeling, reducing the detachment force. It is unlikely that the entire contact area of the attachment pads detach in a single detachment event, but will likely peel from contact. 3) The calculation assumes the entirety of the available contact area of the pads (arolia, or setal pads) makes sufficient contact with the substrate, enabling the full strength of resistance of the interfacing contact zone. It is clear from previous findings that this is not representative of reality, for example in geckos it has previously been reported that during attachment, since contacting surfaces never match perfectly, it is likely that the attachment of fewer spatulae or a smaller contact fraction per spatula than is maximally

available occurs, leading to a reduction in contact area [104, 204]. Moreover, the dynamics and orientation of beetle pads during adhesive stress are complex [194]. Regardless of the reason why the calculated Stefan force is so much greater than the measured dynamic forces, it is clear that viscous forces could certainly be a contributing factor to adhesion under impulsive detachment conditions and need to be considered here.

A further reason why adhesive forces are larger under dynamic conditions compared to quasi-static conditions is, there could be an additional contribution to normal adhesive force due to the viscoelasticity of the adhesive pad. Drechsler [209] studied the adhesion forces of single pads of the stick insect *Carausius morosus* (smooth pads) finding that for a given preload, detachment forces in smooth pads increased with increasing detachment velocity [39], and concluded that the large detachment velocities led to a stiffening of the pad material, increasing detachment forces. Viscoelastic solids are often modelled as a combination of linear springs and viscous dashpots in parallel (*i.e.*, Kelvin-Voigt model, Figure 6.4.1). These systems behave elastically at low velocities due to the material response being dominated by the elastic springs. Conversely, at high velocities the viscous elements will dominate, generating a higher adhesive force. The higher adhesive forces measured in the impulsive detachment experiments are consistent with both the viscous contribution of the secretion and the viscoelastic contribution of the adhesive pad, and could quite possibly be a combination of both effects, particularly for smooth pads which

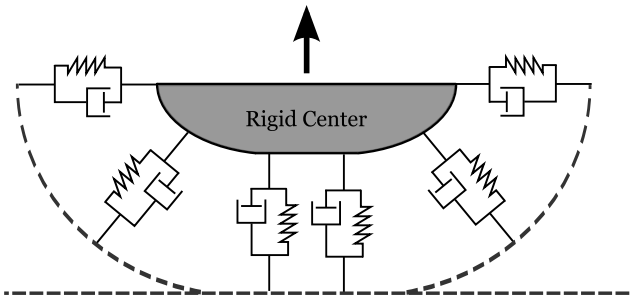

Figure 6.4.1: Viscoelastic model of attachment pads based on viscous dashpots and linear springs. Adhesive pads are composed of viscous and elastic filaments depicted as Kelvin-Voigt models. During rapid detachment the dashpots will lengthen slowly and the pad material behaves as a stiff material. Once the dashpot elements have reached their maximum elongation, the springs will determine the behaviour of the system by detaching ('peeling') from the edge of the contact zone. Slower detachments will allow the linear springs to relax in sufficient time to return elastic energy, reducing detachment force, and the pad will peel from the substrate from the peripheral edge inwards.

have been shown to have viscoelastic behaviour in a number of insects, and have effective elastic moduli orders of magnitude lower than hairy setal pads. Further experimental results are required in order to determine the magnitude of each contribution, and to disentangle these possibilities.

6.4.2 Tangential Friction Forces

Friction forces generated by the ant *P. dives* during natural pulling experiments were found to be comparable to the forces generated during the centrifuge experiments, Table 6.3.2, and the ladybird *C. septempunctata* generated mean pulling forces on hydrophobic glass which were significantly greater than those generated by *H. axyridis* within the friction centrifuge experiments (t-test, t=14.6924, P<0.001). Due to time restraints we were unable to collect and test the 7-spot ladybird on the centrifuge turntable (friction), but it is noted that the safety factors generated by the two ladybirds *C. septempunctata* and *H. axyridis* during the dragging experiment are comparable, thus we do not expect centrifuge safety factors and forces to be too dissimilar between these two species.

Impulsive friction forces were substantially greater than other force measurement techniques, similar to the results for adhesion forces. The insects which remained attached to the substrates after impact were not observed to slide forward noticeably, indicating a substantial static friction component, although due to limits of resolution of the high-speed camera it is not possible to conclude that no sliding occurred on the level of the adhesive pads. In this situation viscous forces would be negligible and the increase in detachment force most likely due to the viscoelasticity of the adhesive pad, as for the normal adhesive forces.

Consistent with other force measurement techniques, friction forces were found to be several times greater than adhesion for both insects studied, on both hydrophilic and hydrophobic surfaces [120, 183]. For example, comparing results in Figures 6.3.5 and 6.3.10, and using the values of the normal force F^N given in Table 6.3.1 with Equation 2.5.2, it is

possible to estimate a friction coefficient for these ladybirds under tangential detachment conditions. The values of μ in this case are 3.5 and 3.2 for hydrophilic and hydrophobic glass respectively. Similarly high values of μ can be inferred for *P. dives* ants, but it was not possible with the available apparatus to generate impulsive forces sufficiently high to detach 100% of test insects on either hydrophilic or hydrophobic glass surfaces. Indeed, it was only possible to detach 50% of the tested ants from hydrophobic glass surfaces at impact forces of approximately 6.5 mN, twice the mean detachment force determined from the impulsive adhesion measurements, Figure 6.3.5 and Table 6.3.1, and several times greater than the mean detachment force as measured with the centrifuge apparatus in Chapter 5 (see Figure 5.3.2). This suggests that the mean impulsive detachment friction force for ants would be substantial. Such high values of μ suggest a significant contribution from dry contact between adhesive pad and the substrate, as discussed in Chapter 5, and are consistent with the other force measurement techniques deployed in the literature [12, 13].

A proximal pull of the legs has been shown to increase contact area in insects [40], and the scaling of friction with contact area has been found where friction is dominated by adhesion, such as the sliding friction of rubber on glass [46, 94, 116]. Adhesive systems in insects are invariably characterised by the presence of micro- and nanostructured surfaces [50, 53] (see Chapter 2), which will increase friction forces and the presence of channels on the smooth pad surface promote fluid drainage, reducing the thickness of any lubricating liquid layer. Bullock *et al.* [120] studied friction forces in the beetle *G. viridula* and concluded that friction forces are fully determined by the contact area generated by the attachment pads. Given the known viscoelastic behaviour of insect attachment pad cuticle in smooth pads [23], and the close conformation of setal tips of hairy pads to the surface profile of a substrate [53, 120] it is likely that adhesion will play a significant role in the generation of friction forces, and friction is not due to simple Amonton friction.

6.4.3 Static *vs.* Dynamic Forces

Extreme detachment forces, and high detachment velocities, will be present in many insects' natural habitats in the form of the actions of predators, rain-drops or gusts of wind which can cause trembling of leaves [210]. The observation that ants are able to produce significantly greater forces under impulsive conditions is probably an adaptation to prevent unexpected detachment from elevated surfaces such as tree-tops, which would invariably lead to the death of the insect. Flying insects, however, could simply take flight and, in comparison, the detrimental effects of detachment in this case are much less. Rapid detachment accelerations will increase adhesion forces due to either the viscous resistance of the adhesive secretion, or the viscoelastic response of the pad material (spring-dashpot model, Figure 6.4.1) or a combination of these effects. However, this is contradictory to the facilitation of fast locomotion - thus insects require further control over the detachment process. A large Stefan adhesion force, for example, would be detrimental to fast movement under conditions of normal locomotion, but during impulsive perturbations, such as those experienced in the Impact-rig experiment, viscous adhesion forces would be advantageous as a passive mechanism against detachment when the insect cannot actively deploy its attachment pads. This extra control will be facilitated by peeling actions during detachment [40], rolling of feet [120], or possibly by variations in posture and gait which could change the detachment angle between the leg and substrate [209]. Because the amount of secretion delivered to the contact zone cannot be controlled (by the experimenter), differences in secretion volume within the contact zone during detachment may also have an influence on detachment forces. This functionality would be a useful reason for insects to have active control over the secretion volume. However, to date, only passive control *via* capillary action has been eluded to [92]. The attachment pad systems of insects have clearly evolved to enable different functional mechanisms to dominate under different detachment scenarios, which allows the insect to traverse diverse substrates under their own power, as well as passively enable strong resistance during instantaneous, unpredictable impulsive detachments.

6.5 Conclusions

Results of the impulsive force measurement technique have given new insights to the detachment dynamics and forces insects with smooth and hairy pads are capable of generating, but further experiments must be performed to determine to what extent viscosity plays a significant role during detachment, and to investigate the difference between capabilities of hairy and smooth pads during impulsive perturbations. Significantly greater adhesion forces are generated by ants and ladybirds under impulsive conditions than during other force measurement techniques, and ants generated larger adhesion safety factors than ladybirds in this case. Two possible mechanisms might explain the generation of such large detachment forces, namely contributions from the adhesive secretion viscosity, or an increase in detachment force due to the viscoelastic nature of the attachment pads in insects, but from available data it is not possible to determine to what extent each of these may have contributed to the measured forces.

The impulsive force measurement technique provides new and interesting results, but the experimental apparatus fell short of being able to detach all representatives of the ant *P. dives* from the surface. Further modification and alteration of the current experimental design - including the use of larger force sensors, higher resolution video imagery, and extension of the impulsive force measurement technique to other insect species, will greatly help confirm the origin of the detachment forces, and possibly provide new insights into the nature of insect attachment. Understanding insect attachment abilities under these conditions will aid understanding of insect ecology, as well as provide new possibilities for the creation of novel adhesives for use in scenarios which encounter short impulsive detachment forces.

Chapter 7

Effect of Particulate Contamination on Adhesive Ability in Ants

7.1 Introduction

[1]Tarsal adhesive pads are crucial for the ability of insects to traverse their natural environment. In the previous chapters we studied the morphological characteristics of smooth and hairy attachment pads, and the physical mechanisms of insect attachment to smooth surfaces. In this, and the next, chapter we study artificial surfaces and materials used to *prevent* insect attachment. Previous studies have demonstrated that for both hairy and smooth pads, significant reduction in adhesion occurs due to contamination by wax crystals present on plant surfaces, or synthetic micro-spheres.

Focusing on the smooth pads of ants we study systematically how particulate contamination and the subsequent loss of adhesion depends on particle size, particle surface energy, humidity and species size. To this end, workers of *Polyrhachis dives* and *Myrmica scabrinodis* (Hymenoptera; Formicidae) were presented with loose synthetic powder barriers with a range of powder diameters and surface energies, which they would have to cross in order to escape the experimental arena, and their behaviour and adhesive ability after crossing the barrier was observed. During all experiments the effects of the powder particles on attachment ability were investigated systematically by changing the particle material, size, and the relative humidity at which the experiments were performed, to elucidate the factors affecting insect adhesion and repellance. A literature review pertaining to barriers against insect adhesion and the effects of particulate contamination is given in Chapter 3. This is the first time such a systematic study of the influences of synthetic powder barriers has been performed.

[1]As part of the interdisciplinary collaboration of this research project, the experimental procedures, results and analysis detailed in this chapter were performed and shared equally between the author and M.J. Orchard from the Department of Biological Sciences.

7.2 Materials and Methods

Insects

Worker ants were extracted from colonies of *Polyrhachis dives* [Smith 1857] and *Myrmica scabrinodis* [Nylander 1846] (Hymenoptera, Formicidae), Figure 7.2.1, and see Chapter 4 for details of how insects were maintained. The length of the insects claws, and claw basal distance - defined here as the distance between the claws at the point at which they emerge from the tarsal cuticle - were measured by imaging the tarsi with a digital camera (Canon Powershot S31S, Canon (UK) Ltd, Surrey, UK) connected to a stereo-optical microscope (SMZ2800 Nikon) *via* an adaptor mount (MM99 S/N 3506, Martin Microscope Co., Easley, SC, USA). Visualisation of clean and contaminated insect tarsi and antennae was achieved using scanning electron microscopy (SEM). Insect samples were air-dried, coated with 2 nm of gold-palladium and imaged using a Zeiss EVO60 electron microscope in high-vacuum mode at 2 kV beam voltage and 100 pA probe current.

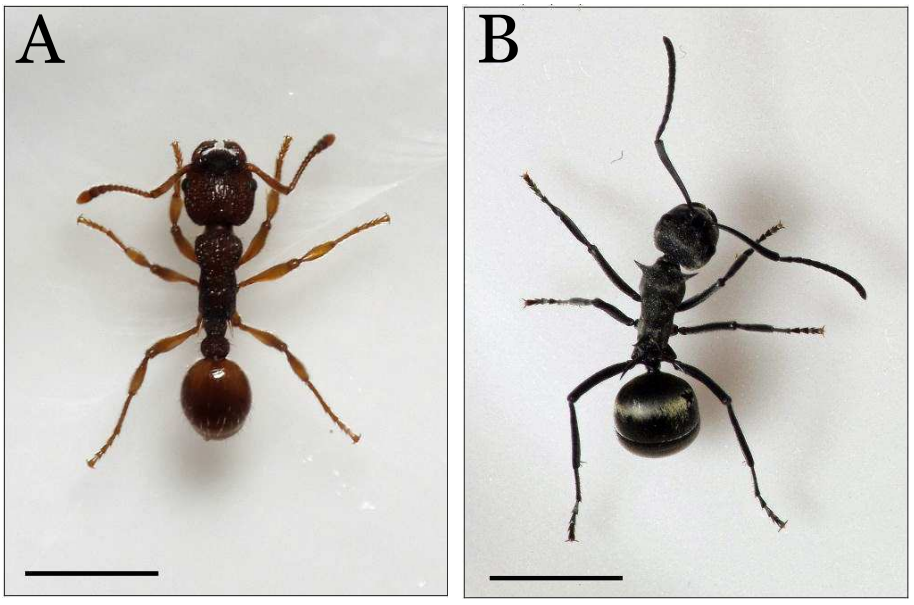

Figure 7.2.1: Top view of A) the red elbowed Spanish ant *Myrmica scabrinodis*, and B) Asian weaver ant *Polyrhachis dives*. Scalebars = 2 mm.

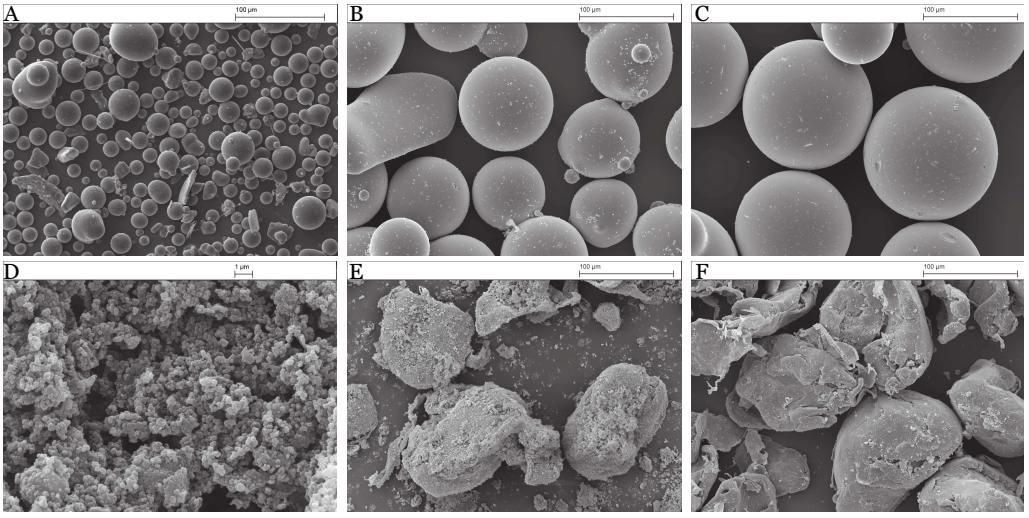

Figure 7.2.2: SEM images of some representative powder fractions of glass (**A** - **C**) and PTFE (**D** - **F**) particles used to construct the loose powder barriers. Glass particles are shaped as regular spheres, in contrast to the PTFE particles which are irregularly shaped. The mean size of the particles are reported in Table 7.2.1. Scale bars: 100 μm in all images except **D**) 1 μm.

Powder Particles

Polytetrafluoroethylene, PTFE (Sigma-Aldrich Company Ltd, Dorset, UK) and soda lime Ballotini glass (VWR-Jencons, Leicestershire, UK) particles of various diameters, along with 1 μm diameter silica-glass (Angström Spheres, Fibre Optic Centre inc., MA, USA) were used in this study. The PTFE and glass particles are representative of particles with low and high surface energy respectively. Particles were separated into well defined size fractions by manual agitation through a series of Endecott powder sieves (UKGE Ltd, Southwold, Suffolk, UK) of decreasing grating diameter between 500 and 10 μm. The geometry and morphology of the two materials differed, with glass particles shaped as regular spheres, in contrast to the PTFE particles which were irregularly shaped and rough, Figure 7.2.2. Using light microscopy and SEM images the physical size distributions of the particles within each fraction were determined using an in-built macro in ImageJ which counts and determines the size of objects within the image, Table 7.2.1. Diameters of the PTFE particles were determined from the mean value of the major and minor length axes, which led to a small variation in the mean values of each fraction between materials, as reported in Table 7.2.1.

Table 7.2.1: Measured particle sizes ± standard deviation of the particles after sieving. Particle sizes were determined using optical and scanning electron micrograph images, typical sample size ∼ 150 particles. 1 μm diameter glass particles had a standard deviation of < 10 % as defined by the supplier. * indicates particles which were used as supplied and were not sieved

Material	**Mean Diameter** (μm)
PTFE	476 ± 72
PTFE	123 ± 60
PTFE	105 ± 76
PTFE	21 ± 23*
Glass	141 ± 25
Glass	111 ± 24
Glass	19 ± 8
Glass	1 ± 0.1*

Barrier Experiments

Circular powder barriers of width ∼ 1 cm were constructed inside open glass petri dishes of radius r=6.4 cm and r=3.3 cm for *P. dives* and *M. scabrinodis* respectively ($h_{dish} \gg h_{ant}$). Particles from each of the size fractions were gently poured manually along the inside wall of the dish using a small Teflon funnel. Prior to construction Petri dishes were rinsed with HPLC grade iso-propanol (Fisher Scientific UK, Ltd, Loughborough, UK), wiped with a clean-room Spec-Wipe (VWR-Jencons, Leicestershire, UK) and dried with a filtered air supply. A fresh barrier was constructed for each replicate to reduce any effects of chemical signalling between workers from one experiment to the next. To neutralize any static charges an ion gun (Zerostat 3, Milty, Bishops Stortford, UK) was used on each barrier before the experiments were begun. Petri dishes containing the barriers were placed upon an Ecotherm heat/cold stage (Torrey Pines Scientific Inc., Carlsbad, CA, USA) within a custom built Perspex chamber to allow for temperature control within the experimental arena, Figure 7.2.3. An air supply was passed through a series of moisture (R&D Separations MT200-4, Krackeler Scientific, Inc., Albany, NY, USA) and hydrocarbon traps (Agilent HT200-4, Agilent Technologies, Edinburgh, UK) which allowed control of the relative humidity (RH) of the air-flow linked to the chamber. RH was monitored using a HIH-4000-001 Integrated Circuitry Humidity Sensor (Honeywell Sensing and Control,

MN, Golden Valley, USA) and logged with a Picoscope 3224 PC based oscilloscope (Pico Technology Ltd, St Neots, UK).

In order to study the effect of humidity, if any, on the number of ants to escape from a given fraction the initial barrier experiments were carried out at 10, 50 and 70 % RH (± 5 %) at a fixed temperature of 25 ± 2 °C. This range was chosen as it represented a natural range of RH each ant species was likely to encounter in their natural habitats when traversing dry surfaces [4]. Finally to avoid any moisture induced improvement of adhesion between insect species and powder fractions during the experiments, all insects were held within closed dishes at the same RH for at least 30 minutes prior to use [202]. Control experiments were performed at each humidity using clean dishes with no powders.

Workers were carefully extracted from their colonies and placed into the centre of the

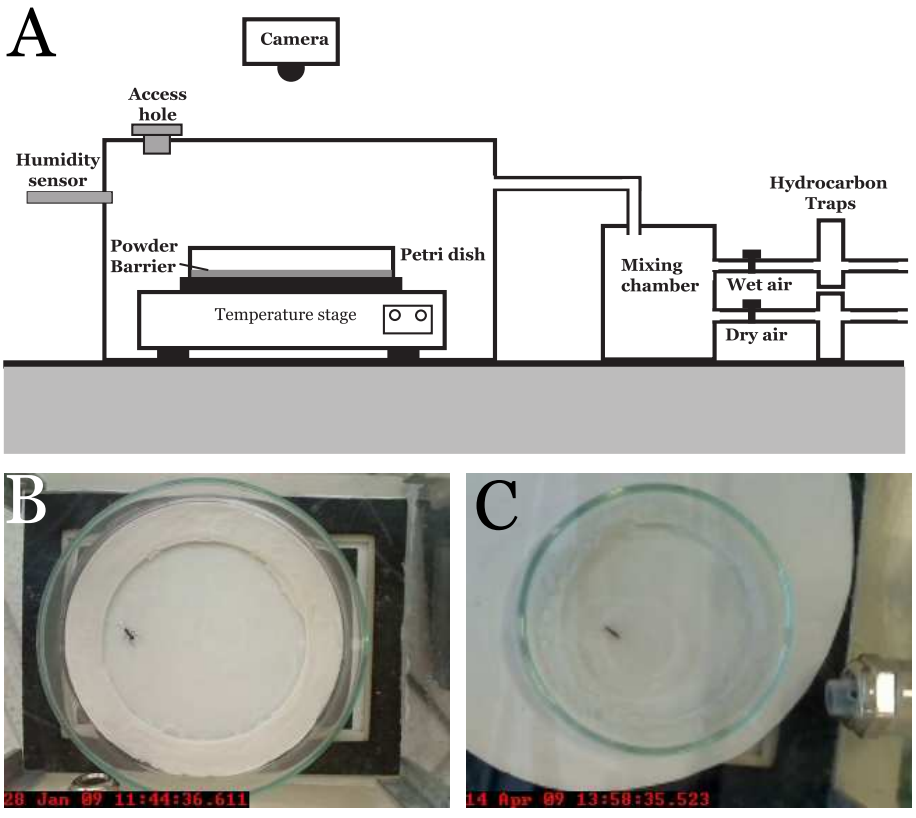

Figure 7.2.3: Schematic of the apparatus for the barrier experiments. A) The glass Petri-dish sits on a heat/cold stage which maintains the temperature within the arena for the duration of the experiment. The insects are carefully introduced to the centre of the Petri-dish via an access hole at the top using soft tweezers and filmed from above for 5 minutes. B)–C) Top views of arena showing an individual A) *P. dives* worker in the larger Petri-dish, and B) *M. scabrinodis* worker in the smaller Petri-dish.

Petri-dish using soft metal tweezers *via* a small access hole on the top surface of the chamber, Figure 7.2.3. Ants were observed for a maximum of 5 minutes, or until the ant had escaped, with each ant used only once and between 30–40 replicates performed for each parameter combination (*M. scabrinodis* $N_{total} = 264$, *P. dives* $N_{total} = 277$). Experiments were filmed from above using a digital camera (QuickCam Pro for Notebooks, Logitech UK Ltd, Slough UK) controlled by HandyAVI 4.3 (Azcendant, Tempe, AZ, USA) using the time-lapse capture mode, in a similar way to that detailed by Loeffler [211]. Two parameters were measured.

i) Firstly, the number of ants that were trapped inside the arena by the powders. Specifically the results of each barrier experiment had three classifications; *escape* - the ant successfully escaped from the arena within 5 minutes, *trapped* - the insect attempted to, but failed to escape within 5 minutes, and *no attempt* - the insect made no attempt to cross the barrier and escape from the arena within 5 minutes. Denoting the number of ants that escaped, were trapped or made no attempt to cross the barriers as N_e, N_t and N_n respectively, the percentage of ants trapped for each parameter combination was defined as

$$\%Trapped = \frac{N_t}{N_t + N_e} \times 100 \tag{7.2.1}$$

Although N_n needed to be taken into account, it was excluded from our analyses since these outcomes could not be attributed to any effects of contamination by the barriers.

ii) To determine to what extent the powders repelled the ants, the activity of each worker was recorded throughout the experiments and the length of time between the start of the experiment and the ant's first attempt to cross powder barrier threshold, T_r, was measured.

Rigid *vs.* Fragile Barriers

To investigate the effect barrier fragility has on the measured parameters, 19 μm diameter glass particles were also used to construct a series of solid, or 'caked', barriers for comparison. The caked barriers were prepared by constructing loose barriers, in the same manner as described above, which were then covered with a non-airtight plastic lid to protect them from any dust particles, and left exposed to the atmosphere for at least 24 hours (RH 30–40 %). Glass particles, such as those used in this study, form weak siloxane bonds at humidities greater than 30 % at the contact points of the particles due to the amount of water vapour present in the atmosphere, which leads to a slow solidification of the barrier [212–214]. These barriers were sturdy enough to remain intact when the dish was inverted, but could be easily broken apart by manual pressure. This effect does not occur for PTFE particles so this experiment could only be performed using high surface energy particles. All caked barrier replicates were performed under laboratory atmosphere (T = 25 ± 5 °C, RH = 35 ± 5 %) with the same procedure as above and were filmed for a maximum of 10 mins, and the time to fully escape from the dish T_e was used to compare escape times between caked and fragile barriers.

Statistical Analyses

Statistical analyses were performed using **R** *v.*2.8.1 [215]. Escape data was analysed using a general linear model (GLM) with binomial distribution, while time repelled (T_r) and time escape (T_e) was analysed with either an ANOVA test for parametric data, or a linear model for non-parametric data.

7.3 Results

7.3.1 Insects

Individual workers were weighed and their claw length and basal distance were measured from optical and SEM images to allow for comparison of the two species, Table 7.3.1, Figure 7.3.1.

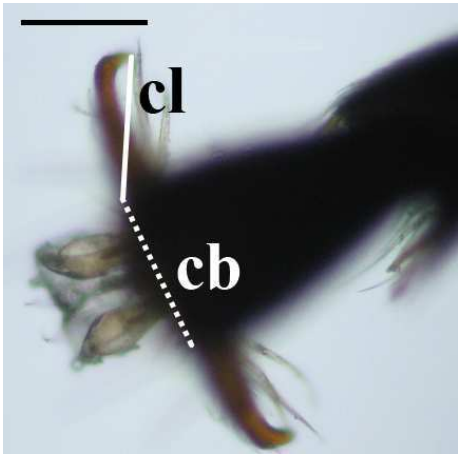

Figure 7.3.1: Optical image of a dorsal view of the distal tarsal segment of *P. dives* showing a deployed arolium in between the claws in contact with a glass surface. White lines depict the claw length (cl) and claw-base distance (cb), the mean values of which for each species are tabulated in Table 7.3.1. Scale bar = $100\mu m$.

Table 7.3.1: Summary of characteristic measurements made of the two ant species used in this study. Measurements were taken of multiple individuals of each species (N=10).

Species	**Mass** mg (± s.e.m.)	**cl** μm (± s.d.)	**cb** μm (± s.d.)
Myrmica scabrinodis	4.83 ± 0.2	64 ± 7	34.7 ± 6
Polyrhachis dives	5.97 ± 0.2	110 ± 10	123.0 ± 26

7.3.2 Loose Powder Barriers

Trapping of Ants

Control experiments with clean dishes trapped no ants of either species for all humidities investigated. Within the measured range of humidities, when subject to Kaplan-Meir survival analysis the effect of relative humidity (RH) was found to be non-significant on the percentage of ants trapped by any loose barriers for either species ($\chi^2 = 3.52$, df = 2, P>0.05), thus replicates from experiments across different RH were subsequently pooled for further analyses. The percentage of ants trapped, as defined by Equation 7.2.1 was determined for each particle fraction, Figure 7.3.2.

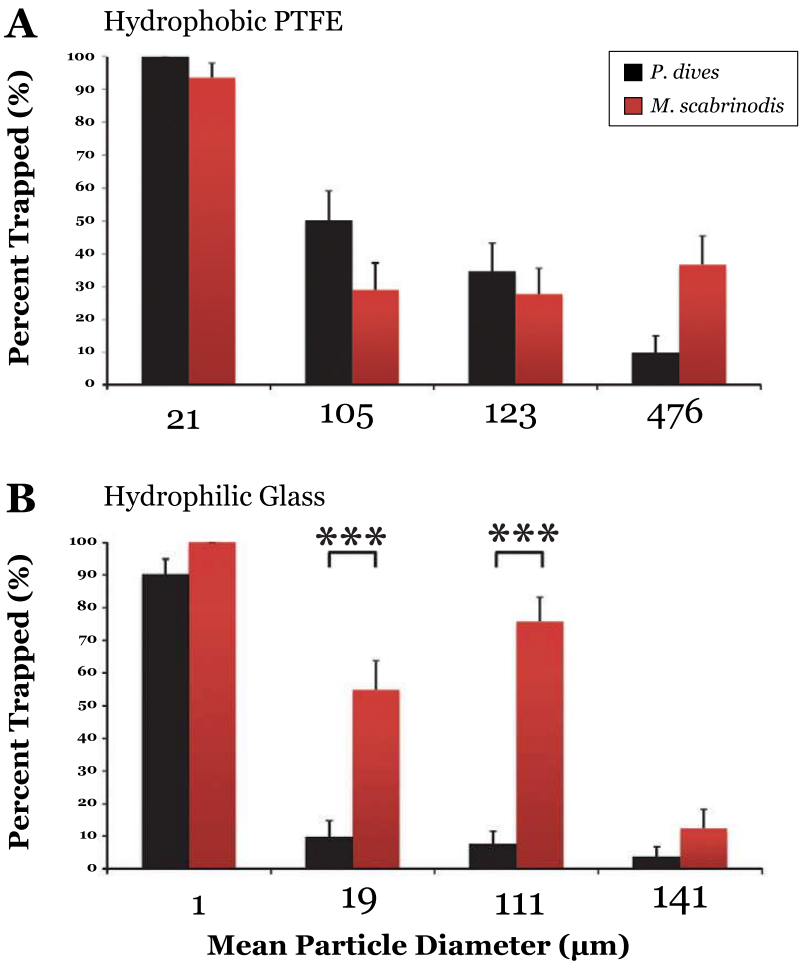

Figure 7.3.2: Percentage of ants trapped as a function of particle size for both A) hydrophobic PTFE and B) hydrophilic glass powder barriers. The percentage of P. dives (black bars) and *M. scabrinodis* (white bars) workers trapped is inversely correlated to particle-size for both species (ANOVA, F_7=43.982, P<0.001). *** P<0.001, all others not significantly different between species. Error bars show s.e.

For both *P. dives* and *M. scabrinodis* the percentage of ants trapped was found to be inversely related to the particle diameter for both materials (*P. dives*: Glass,$F_{3,134}$=92.96,P<0.001; PTFE,$F_{3,135}$=50.75,P<0.001; *M. scabrinodis*: Glass, $F_{3,135}$=41.037, P<0.001; PTFE, $F_{3,121}$ =15.04, P<0.001). Specifically, within each species of ant, smaller particles of both materials trapped a larger percentage of ants compared with larger particles (GLM: *P. dives*: $F_{7,223}$=48.70, P<0.001; *M. scabrinodis*: $F_{7,270}$=20.12, P<0.001). Several *P. dives* workers that had traversed the different barriers, but manually prevented from attempting to climb the vertical glass wall, were killed immediately after they had crossed the barrier and their tarsi imaged *via* SEM, Figure 7.3.3B-H; as a control, we also show the uncontaminated tarsi of *P. dives*, Figure 7.3.3A. Contamination of the arolia by particles was observed for both PTFE and glass barriers made from small particles. Specifically the arolia along with the tarsal claws and portions of the most distal tarsal segment were heavily contaminated by small particles (Figure 7.3.3B–D) and the amount of particles observed to remain adhered to the tarsus and arolium increased with decreasing particle diameter, for both materials. Indeed the 1 μm glass particles almost completely coated the distal segment of the tarsi. When pooling the results for both ants *P.dives* and *M. scabrinodis*, the percentage of ants trapped by glass or PTFE powders did not differ significantly between the two materials (GLM; $F_{1,513}$=0.8802, P>0.05), however, after closer examination it was found that when compared *within* each species there was a significant effect of particle type on percentage of ants trapped (*P. dives*: $F_{1,277}$=8.88, P<0.05; *M. scabrinodis*: $F_{1,278}$=4.56, P<0.05). Specifically, we note that a significantly greater number of *P. dives* workers escaped from within the 19 μm glass barriers compared to the 21 μm PTFE, even though the tarsi of the ants are clearly contaminated in both cases (Figure 7.3.3). This difference was found to be present and significant for both species (*P. dives*: F_1=48.702, P<0.001; *M. scabrinodis*: F_1=20.122, P<0.01); see Figure 7.3.2.

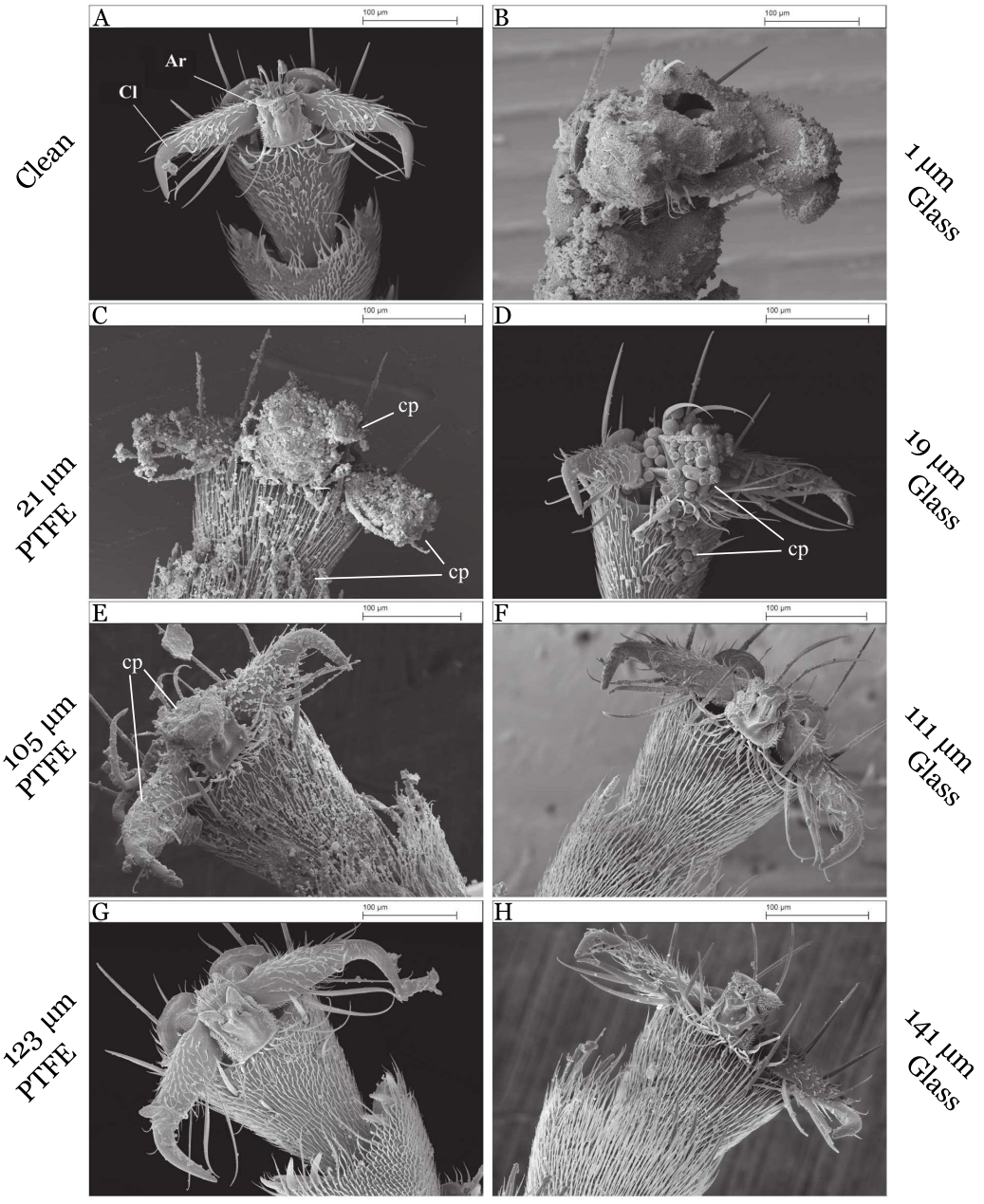

Figure 7.3.3: SEM micrographs of *P. dives* tarsi **A**) uncontaminated, and after traversing powder barriers constructed of glass (**B,D,F,H**) and PTFE (**C,E,G**); (**B**) 1 μm glass, (**C**) 21 μm PTFE, (**D**) 19 μm glass, (**E**) 105 μm PTFE, (**F**) 111 μm glass, (**G**) 123 μm PTFE, (**H**) 141 μm glass. The level of contamination decreases with increasing particle size, and is not strongly affected by material type. Larger particles of glass and PTFE were not found to adhere to the arolium, as evidenced by the lack of particles in **F**), **G**) & **H**). *Tc*, tarsal claw; *Ar*, arolium; *cp*, contaminating particles; Scale bars: 100 μm

Repellent Effects of Barriers

Ants were observed to investigate several sections of the barriers with their antennae before crossing. Having touched the barriers ants were often observed to spend time grooming their antennae and tarsi. In order to quantify the degree to which the ants were repelled by a powder barrier, the time taken before attempting to cross, T_r, was measured for each species–material combination, Figure 7.3.4. It should be noted that whilst this measurement was used as an indication of the repellence of the barriers, it is only a qualitative estimate due to the fact that, as mentioned above, a number of ants spent some of their

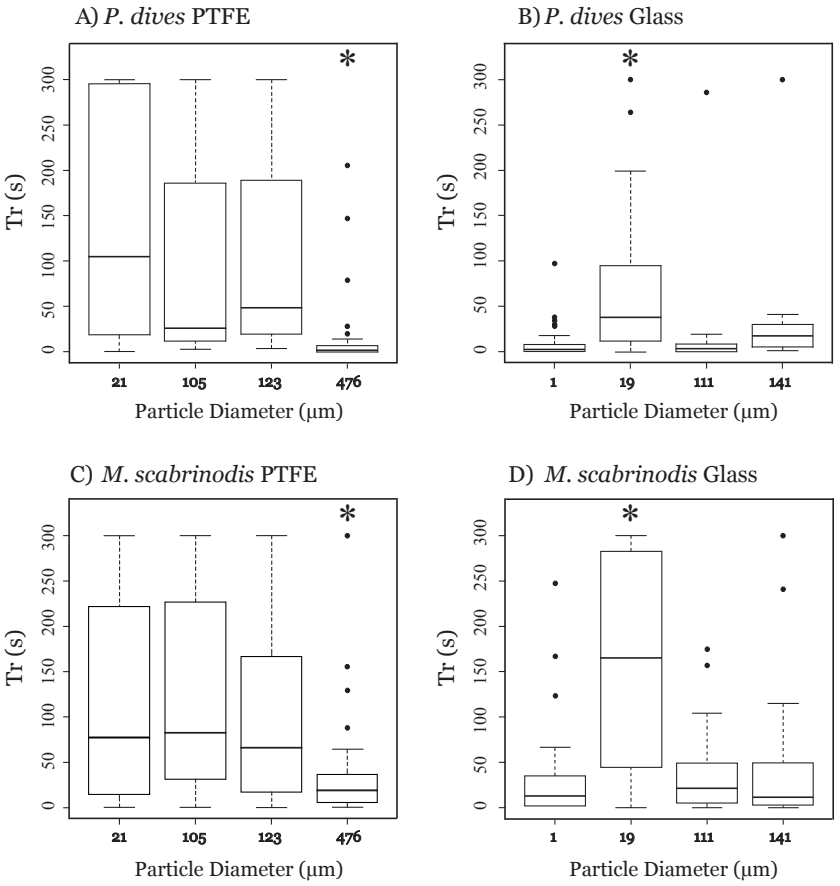

Figure 7.3.4: Time taken to attempt to cross the threshold of the loose barriers, T_r, for different mean particle diameters for *P. dives* and *M. scabrinodis*. Experiments were capped at 300 s (5 mins). Plot shows medians (centre line), inter-quartile range (boxes) and the largest and smallest values (whiskers) that are not outliers dots. * indicates median values which were significantly different from all other particle types. **A**) ANOVA df = 3, F = 7.47; 476 μm - 21 μm P < 0.001, 476 μm - 105 μm P < 0.05, 476 μm - 123 μm P < 0.01 **B**) ANOVA df = 3, F = 9.09; 19 μm - 1 μm P < 0.001, 19 μm - 111 μm P < 0.001, 19 μm - 141 μm P < 0.05, **C**) ANOVA df = 3, F = 5.94; 476 μm - 21 μm P < 0.001, 476 μm - 105 μm P < 0.001, 476 μm - 123 μm P < 0.001, **D**) ANOVA df = 3, F = 22.00; 19 μm - 1 μm P < 0.01, 19 μm - 111 μm P < 0.001, 19 μm - 141 μm P < 0.05, all others were not significant.

time within the experimental arena grooming themselves. To attain a more accurate measure of actual time spent antennating before crossing the barriers, any time spent cleaning could be measured and subtracted from T_r; this could be the subject for future study. A statistical difference was found when analysing T_r as a function of particle diameter for both species (ANOVA: *P. dives*:$F_{7,225}$=14.41, P<0.001; *M. scabrinodis*:$F_{7,272}$=20.21, P<0.001). Time repelled data shown in Figure 7.3.4 indicates that for PTFE, T_r is inversely related to particle size for both species of ant, with ants presented with larger particles taking a significantly shorter time to cross the barriers, Figure 7.3.4A,C. For glass particles, values of T_r for 19 μm diameter particles were significantly greater than all other particle diameters, Figure 7.3.4B,D. There was no significant difference between time measured for the different particle types for *M. scabrinodis* (ANOVA;$F_{1,262}$=2.12, P> 0.05), however a significant difference was found for *P. dives* (ANOVA;$F_{1,275}$=15.92, P=0.03), indicating that, for this ant species, time taken to cross the barriers differed between glass and PTFE.

To ascertain the reason for observed lack of antennating behaviour by ants presented with the 1 μm powder barriers, SEM images of the antennae of both ants were taken after workers had crossed barriers constructed of these particles, Figure 7.3.5. SEM micrographs of *P. dives* and *M. scabrinodis* antennae show hairs facing in the distal direction, the shafts of which are separated by approximately 5–10 μm. After crossing the 1 μm glass powders the antennae of both species of ants show a coating of particles in between the hairs,

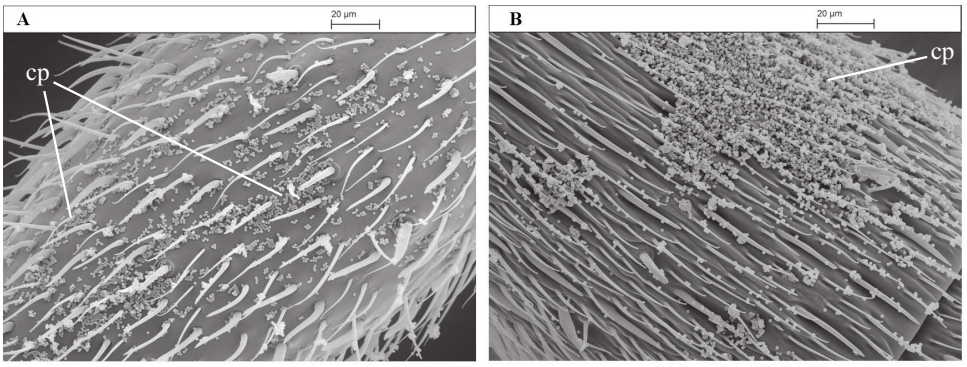

Figure 7.3.5: Scanning electron micrograph images of the terminal antenna segments (flagellomeres) of **A**) *M. scabrinodis* and **B**) *P. dives* contaminated with 1 μm glass particles. Scale bars: 20 μm.

Figure 7.3.5. To determine the role antennae have on the time repelled, T_r, a series of barrier experiments using 19 μm glass powders was carried out using ants with and without their antennae, Figure 7.3.6. A significant difference was found for both species when comparing T_r between individuals with and without antennae: ants without their antennae spent a significantly shorter length of time investigating the barriers before crossing compared to ants with their antennae intact (ANOVA: *P. dives*: $F_{1,62}$=17.93, P<0.001; *M. scabrinodis*:$F_{1,61}$=31.538, P<0.001).

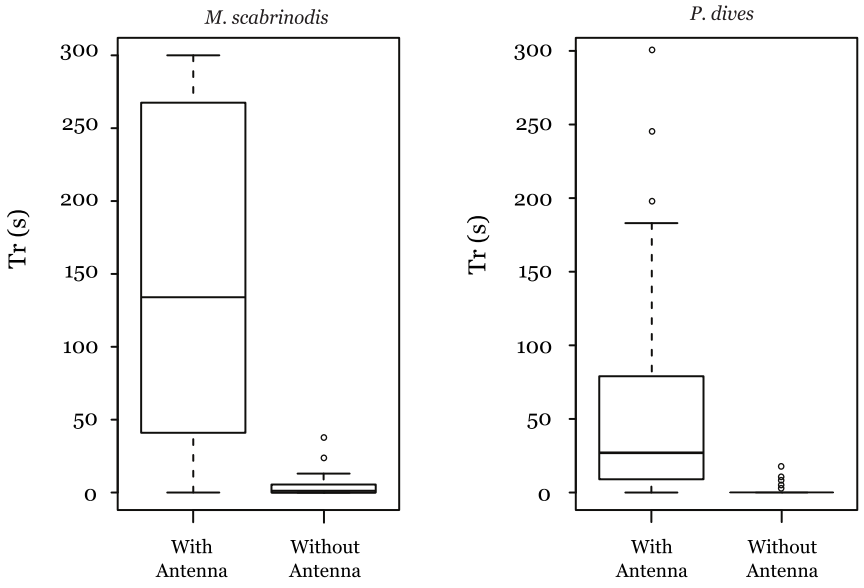

Figure 7.3.6: Time repelled, T_r, by 19 μm glass particles for both *M. scabrinodis* and *P. dives* with and without their antennae. There was a significant drop in time repelled for ants without antennae (*P. dives*; $F_{1,62}$=17.93, P<0.001, *M. scabrinodis*; $F_{1,61}$=31.538, P<0.001).

7.3.3 Rigid Powder Barriers

To determine if the anti-adhesive effect and the observed repellence of the powder barriers is caused by their particulate nature and mechanical fragility, a series of caked powder barriers were constructed with 19 μm glass particles and escape experiments with both caked and fragile barriers were repeated. When comparing between caked and fragile barriers, the percentage of ants trapped as a function of barrier fragility for *M. scabrinodis* was found to be statistically significant, Figure 7.3.7 ($F_{1,78}$=102.6, P<0.001). Specifically,

Figure 7.3.7 shows only 7.5% of *M. scabrinodis* remained inside the arena at the end of the experiment with caked barriers compared with 82.5% for the loose barriers whereas for *P. dives* there was no significant effect of barrier fragility on percentage of individuals trapped ($F_{1,64}$=1.0,P=0.3), with all individuals escaping within the time-limit, hence they are not shown in Figure 7.3.7. When considering the time to escape, Figure 7.3.8, there was a significant difference found between the different barriers for both species of ant (ANOVA: *M. scabrinodis*;$F_{1,78}$=162.92, P<0.001: *P. dives*;$F_{1,64}$=13.076, P<0.001).

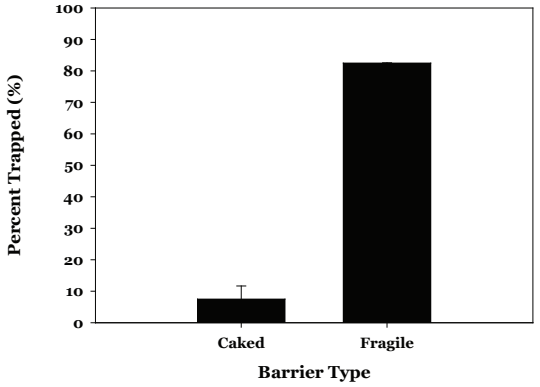

Figure 7.3.7: Percentage of *M. scabrinodis* workers trapped by the loose (N = 40) and caked (N = 40) barriers constructed of the 19 μm glass particles. There was a significant decrease in the number of ants trapped by the caked barriers for *M. scabrinodis* (df = 1, F = 102.6, P < 0.001). Error bars show s.e.

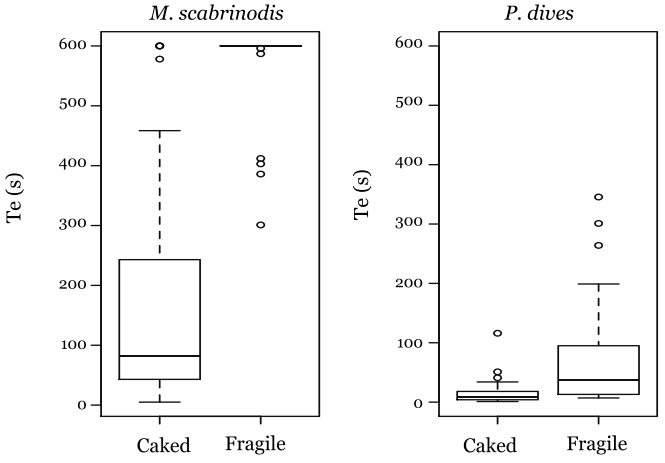

Figure 7.3.8: Time to cross the powder barrier and escape, T_e, as a function of barrier type for *M. scabrinodis* and *P. dives*. T_e was found to be significantly different between caked and loose barriers (*P. dives*; $F_{1,64}$=13.076, P<0.001. *M. scabrinodis*: $F_{1,78}$=162.92, P<0.001).

7.4 Discussion

7.4.1 Trapping of Ants by Loose Powders

For loose powder experiments, after placing the ants within the centre of the dish, workers were observed to pause and briefly investigate the barriers with their antennae before moving to another section or attempting to cross. Barriers constructed of the largest particles did not present a problem for the ants to either cross or escape from the dish after crossing. However, after crossing the powder barriers constructed of smaller particles, a loss of adhesion on the vertical smooth walls of the Petri-dish was observed for both species of ant, with these adhesion failure events becoming more frequent with decreasing particle diameter. Several ants were observed to fall from the vertical glass wall back into the powder barrier after temporarily achieving adhesion to the glass. Smaller particles were found to trap a significantly greater percentage of ants for both species, suggesting that contamination becomes a greater problem for locomotion the smaller the particles insects encounter. For example, powder barriers constructed of the 1 μm diameter silica-glass particles and the 21 μm diameter PTFE particles each trapped over 90% of test insects for both species, Figure 7.3.2. The particle sizes found to heavily contaminate the arolium and tarsus of the ants corresponded well to those which also trapped greater than 50% of individual ants, with the exception of the 19 μm glass particles for *P. dives* (Figure 7.3.2). This is reasonable since heavy contamination reduces the available contact area between arolium and substrate which dramatically reduces adhesion and friction forces [55, 56]. Our results therefore give further confirmation that the 'contamination hypothesis proposed by Gorb & Gorb [55] for hairy pad systems, also applies to insects with smooth adhesive pads. Ants with contaminated arolia, however, displayed no obvious change in behaviour whilst walking on a horizontal surface, suggesting that arolia are not deployed to a significant extent in this case. From Figure 7.3.3 it can be seen that for both particle types when imaging with SEM, the arolia of ants which had traversed barriers made from the particles with diameters greater than approximately 100 μm were

free from, or only lightly contaminated. One possible explanation for this observation is that when an ant crosses a powder barrier (consisting of multiple layers of particles) the relative magnitude of the competing forces between the pad and particles compared to inter-particle forces or particle weight may decrease with increasing particle size so that only particles below a certain threshold size will spontaneously adhere to the arolium. In Appendix A we explore this possibility in detail through theoretical estimates of the different relevant forces. These estimates predict that only particles with diameter greater than 4 mm will not adhere to the arolia. This is more than one order of magnitude larger than the threshold size observed in Figure 7.3.3 and we therefore conclude that this is not the explanation for the observed threshold particle size. We observe substantial contamination by large quantities of particles when particle diameters are smaller than the claw dimensions for both materials. For PTFE particles, heavy contamination was observed for particles with mean diameter 21 μm, light contamination by 105 μm, and no contamination by 123 μm particles. The light contamination by 105 μm mean-diameter PTFE particles (Figure 7.3.3E) appears to only consist of particulates of smaller size than the mean particle diameter. For glass we observe heavy contamination by particles of mean diameter 1 μm and 19 μm (Figure 7.3.3B,D), and no contamination by 111 μm and 141 μm (Figure 7.3.3F,H). From Table 7.2.1 it can be seen that the standard deviation of the particle diameters for PTFE are relatively larger than those for glass, which may suggest only the smaller particles within a particular particle range adhere spontaneously - this may warrant further investigation. We note that the transition from heavily contaminated arolia to non-contaminated for *P. dives* (Figure 7.3.3) occurs at a particle size comparable to the claw dimensions, Table 7.3.1. We propose that the size dependence for contamination may be explained by the fact that individual particles with diameter comparable to, or greater than, the claw dimensions are prevented from adhering to the arolium by the presence of the claws themselves during locomotion, whereas particles much smaller than the claw dimensions are able to make contact with, and contaminate, the most distal tarsal segment of the ant, including the arolium, in large

numbers, Figure 7.4.1. This leads to a reduction in real contact area with the substrate and a loss of adhesive force on subsequent steps, preventing the insect from scaling the vertical glass surface within the time limit. Thus we propose that, in ants, the claws may provide some protection from large contaminants relative to the claw dimensions becoming affixed to the adhesive pad, or interfering with efficient arolium deployment. Presumably this would also work towards reducing the amount of active grooming the insect may need to perform to keep the arolium functioning efficiently [56].

It was found that a significantly lower percentage of ants were trapped by the 19 μm glass particle barriers than the 21 μm PTFE particles for both species of ant, even though the arolium and parts of the surrounding areas were contaminated in each case, Figure 7.3.3. In order to understand this difference, we consider the behaviour of the ants after they had crossed the barrier threshold. After crossing the powder, and approaching the vertical glass wall, the fore-legs of the ants were observed to slide in a downwards direction on the walls of the Petri-dish in a scrambling, or shearing, motion as the ant attempted to gain adhesion to the surface. This behaviour was observed for both species, but *P.*

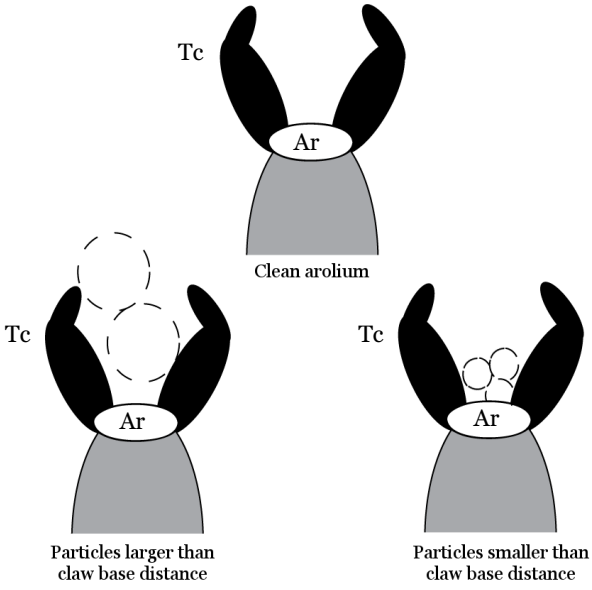

Figure 7.4.1: Schematic of a ventral view of the distal tarsomere of an ant tarsus showing the arolium Ar, and tarsal claws Tc. A possible mechanism by which the tarsal claws may prevent large particles from attaching to the partially exposed arolium is shown. Particles with diameters greater than the claw dimensions are prevented from making contact with the soft adhesive pad.

dives were, in general, noticeably more active and would often spend a greater amount of time scrambling at the inner wall of the Petri-dish attempting to escape. This behaviour occurred more frequently for smaller particles and often continued for some time with the result that sufficient adhesion sometimes returned, and escape was achieved within the time-limit for a number of ants. Additionally, after scrambling at the wall for some time, a number of ants would stop to groom their antennae and tarsi before continuing to attempt escape. This sequence of behaviours is similar to that found recently for the leaf beetle *Gastrophysa viridula* [56] but included grooming of the antennae as well as the tarsus. We suspect that contaminated tarsi of the ants could remove some adherent particles *via* the observed scrambling or shearing motion of the feet against the glass wall of the arena, in a behaviour akin to self-cleaning in insects [149], and geckos [151]. However this action will only be effective if *i*) the downward pulling force exerted by the ant is large enough, and *ii*) the frictional force between the particle and the substrate is large enough to cause the particles attached to the pad to be dislodged during this shearing motion. We note that *P. dives* workers are on average stronger than *M. scabrinodis* owing to their larger size (Table 7.3.1). We also note that the friction coefficient of glass on glass is higher than for PTFE on glass [114]. Thus, it is reasonable to assume that the observed scrambling motion should be most effective in removing the contaminating particles for *P. dives* contaminated by glass particles. This may explain why most of the *P. dives* workers (90.6%) were able to escape from the 19 μm glass powder barriers (Figure 7.3.2) even though the arolium was clearly contaminated by these particles, Figure 7.3.3, and would support the mechanism of self-cleaning in geckos proposed by Hansen & Autumn [151]. It was found by Clemente *et al.* [149] that with a shearing motion, smooth adhesive pads are able to remove adherent particles after several steps. Individuals of *P. dives* in the present study took longer than this to regain sufficient adhesion in order to escape. This could be due to several factors: (1) the deposition of particles, and subsequent re-contamination of the arolium, from the glass surface as the ant attempted to escape from the same location of the dish; (2) a number of particles becoming embedded in the soft cuticle of

the arolia within the contact zone; or (3) simply the sheer numbers of particles present in our case. As contamination and recovery time are strongly dependent upon contact area with the substrate, this continued presence of particles would slow the recovery process [12]. This scrambling motion may work in a similar manner to that seen for hairy pads of insects [149], and gecko lizards [151]; however a detailed analysis of the mechanisms of the observed self-cleaning action in ants is beyond the scope of the current investigation, and was studied separately in the related research of Orchard *et al.* [150].

7.4.2 Repellent Effects of Barriers

As reported above, ants were observed to investigate the barriers with their antennae before attempting to cross. Ants would probe several sections of the barrier with their antennae in a similar manner to that reported for stick insects assessing gap sizes [216], and for cockroaches performing orientation behaviours [157, 217], before either crossing or moving to another section. This behaviour was observed for barriers constructed of all particle diameters and materials. Ant workers of both species were observed to be repelled by the powders to some extent, but particularly so with the smaller particles. Since the ants studied here are not repelled by smooth, flat surfaces of either PTFE or glass, this suggests that it is the particulate nature of the materials which causes the ants to be repelled. However the 1 μm glass particles were an exception to this observation, with the majority of ants spending less time investigating these barriers compared with the others, Figure 7.3.4. Considering the low values of T_r observed for ants crossing the 1 μm glass barriers (shown in Figure 7.3.4), this may also be explained to some extent by the ants' behaviour. In many cases, ants presented with $1\mu m$ glass barriers did not stop to investigate the powder and simply ran across the threshold, moving up to the glass wall without hesitation. In the remaining cases, the ants only investigated for a relatively short time, as evidenced by the low values of T_r in Figure 7.3.4. These observations suggest that the ants were either unable to detect the barriers, or did not consider the barriers as something to be avoided. Often it was observed that after having touched the barriers with their antennae ants would spend

time cleaning, or grooming, their antennae in a way similar to that described by Wheeler [218] and others (eg: Farish [219]). It has been found previously that hairs present on the antennae are involved in detection of various aspects of an ants environment including air-flow, chemical signalling, as well as tactile sensing [4, 155, 220]. In the present case, these hairs may also be used to gain some degree of direct tactile feedback on physical properties of their environment, such as mechanical fragility, which subsequently influences the ant's behaviour. Contamination of the antenna's flagellomeres (sections) (shown in Figure 7.3.5) may inhibit the insect's ability to accurately detect tactile cues such as mechanical fragility and make the 1 μm diameter powder barriers essentially 'invisible' to the ants used in this study. A combination of dense contamination of the adhesive pads, tarsi, and antennae, along with the apparent inability to detect the individual particles makes the barrier of 1 μm particles particularly effective at preventing insect locomotion on smooth surfaces. To investigate this hypothesis we performed a series of barrier experiments with 19 μm glass particles using ants with and without antennae, Figure 7.3.6. We found that ants without antennae spent significantly less time investigating the barriers *before* crossing. The values for T_r found in this case were similar to those found for ants crossing the 1 μm glass particles, Figure 7.3.4, providing evidence to support this hypothesis.

7.4.3 Rigid Powder Barriers

We note that for each species-material combination, the dependence of T_r on particle diameter, Figure 7.3.4, demonstrates a similar trend to the relationship between particle diameter and the percentage trapped, Figure 7.3.2. This relation suggests that repellance becomes more pronounced for particles which lead to a greater amount of contamination, which produces a significant reduction in adhesion *via* the reduction of the available contact area. The value T_r measures the time taken by an insect to investigate the barriers with their antennae before crossing, and as such is not determined by arolia contamination. Instead the correlation of T_r with the percentage of ants trapped suggests that the ants are able to gather information about the barriers *via* the observed antennating action. To

determine if the observed repellance was principally due to the barriers' particulate nature, escape experiments with both caked and fragile barriers were repeated. After placing the ants inside the circular barriers it was obvious that the caked barriers were significantly easier to traverse and caused very little difficulty for the ants to subsequently climb the smooth glass wall of the dish and escape. A significantly lower percentage of *M. scabrinodis* were trapped by the caked barriers, and a significant drop in T_e suggests that individuals of this species were not repelled by these rigid and rough surfaces. For *P. dives* there was no significant difference found between the barrier types because all individuals of this species were able to escape. However, those *P. dives* workers that did escape took a significantly longer time to do so, as shown in Figure 7.3.8. Because the barriers differ only in their fragility, these results provide evidence to support the suggestion (see the previous section) that the fragile nature of the powder barriers is crucial to their effectiveness at trapping ants *via* contamination of the adhesive pads, in much the same way that plant epicuticular wax blooms function [25, 136, 221], and that ants may assess the contamination risk of the powders by using their antennae to probe the mechanical fragility of the barriers

7.5 Conclusions

We have studied the escape of the ant species *Polyrhachis dives* and *Myrmica scabrinodis* from circular powder barriers to determine the effect of barrier properties such as particle size, surface energy, mechanical fragility and environmental factors such as humidity on insect adhesion and repellance. Results demonstrate that the anti-adhesive effect of barriers, constructed from loose synthetic powders, is due to contamination of the insects attachment devices causing a reduced contact area between the adhesive pad and the adherent surface, and was independent of RH within the range tested. Adhesive loss is due principally to this loss of contact area between the substrate and the adhesive pad, preventing adhesion to smooth surfaces for some time after contamination. Our results

therefore show that the contamination hypothesis, proposed by Gorb & Gorb [55] for hairy pad systems, also applies to insects with smooth adhesive pads.

We found that contamination of the adhesive arolia, and proportion of ants trapped by loose powder barriers is strongly dependent on the size of the individual particles, only weakly dependent on free surface energy, and not affected by relative humidity. Results suggest that the claws may offer the arolium some protection from being contaminated by particles which are large relative to the claw dimensions. Workers of *P. dives* contaminated with high-energy particles regain adhesion after time spent scrambling at a high-energy smooth substrate in a shearing motion, similar to that seen in geckos and other insects in previous studies, and may be a further example of self-cleaning in smooth pads [150]. We also find evidence that ants are repelled by loose powders, particularly those made from smaller particles which lead to a greater amount of arolia contamination and loss of adhesion, with the exception of 1 μm, and repellance by a given powder barrier is significantly reduced when the mechanical rigidity of the barrier is increased, suggesting ants may be able to use their antennae to probe the mechanical fragility of the barriers, and furthermore use this information to alter their behaviour in order to minimise the risk of contamination.

Results show that similar effects of contamination of adhesive pads in ants can occur for both natural (plant waxes) and synthetic particles, and show some agreement with data published for particulate control of insect pests [142, 144–148, 222] and suggest that the results presented in these studies are likely to be due to the small particle sizes used. Mimicking the effect of natural barriers could lead to the production of more efficient synthetic and non-toxic means of controlling pest species in agriculture, as well as for domestic purposes.

Further detailed investigations of an ants' ability to probe vital physical properties of its environment using its antennae can be found in the companion thesis of M.J. Orchard from the Department of Biological Sciences.

Chapter 8

Superhydrophobic Surfaces as Barriers to Insect Adhesion

8.1 Introduction

[1] In the previous chapter we studied the effect of loose particulate barriers on the attachment ability of ants. The use of particulate barriers can have an adverse effect on insect attachment ability, but the use of these types of barriers in large scale industrial or agricultural settings is problematic. Particle layers need to be constantly re-applied and maintained, and very small particles can be washed off and accumulate in the environment, causing un-wanted problems for non-target organisms. The production of rigid, but easily applied, barriers to insect adhesion would no doubt save a lot of time, effort and money, and the use of biologically and environmentally friendly methods of advanced pest-control would benefit humans in domestic, industrial, commercial and agricultural settings. In this chapter we study the effect of rigid barriers constructed from colloidal solutions of glass nano-particles, and compare these coatings' efficacy in comparison to an already commercially available 'anti-insect-adhesion' product.

The aim of this chapter was to develop rigid barriers capable of reducing insect attachment forces based on the formulation of colloidal nano-particle solutions, develop a formulation that is easy to deliver and apply to substrates, and compare the resulting solution to commercially available barriers sold to achieve this purpose.

[1] As part of the interdisciplinary collaboration of this research project, some of the experimental results in this chapter were gathered jointly by the author and M.J. Orchard from the Department of Biological Sciences. Specifically, the tests performed to determine the attachment ability of *C. septempunctata* to 'non-stick' surfaces were gathered by M.J. Orchard and Ms. N. Grayson. Preparation, development and characterisation of the different surface coatings described in this chapter, along with the weathering tests, were conducted and analysed by the author.

8.2 Materials and Methods

Study Insects

The 7-spot ladybird *Coccinella septempunctata* [Linnaeus, 1758] (Coleoptera; Coccinellidae) was used as representative of insects with the hairy attachment pad, Figure 6.2.1. See Section 4.4.1 for further details on hairy pad morphology.

Colloidal Solution

A solution of nano-particles within a solvent medium was prepared. A 5% w/w particle suspension of hydrophobic functionalised silica particles was prepared by using 500 *mg* of hydrophobic silica particles (Aerosil R202, Evonik Industries AG, Hanau, Germany. Nominal diameter 14 *nm* as defined by the supplier) in 10 *ml* of ethanol (Fisher Scientific UK, Ltd, Loughborough, UK), Figure 8.2.1. This suspension was sonically vibrated using an ultrasonic processor (Vibracell VCX130, Jencons PLS, UK) at 60 W for 10 minutes. The vial was kept in an ice-water bath during sonication. After mixing the solution, the result is an opaque white liquid which can then be stored at room temperature, Figure 8.2.2. The colloidal suspensions remain stable for several days before sedimentation of the solute

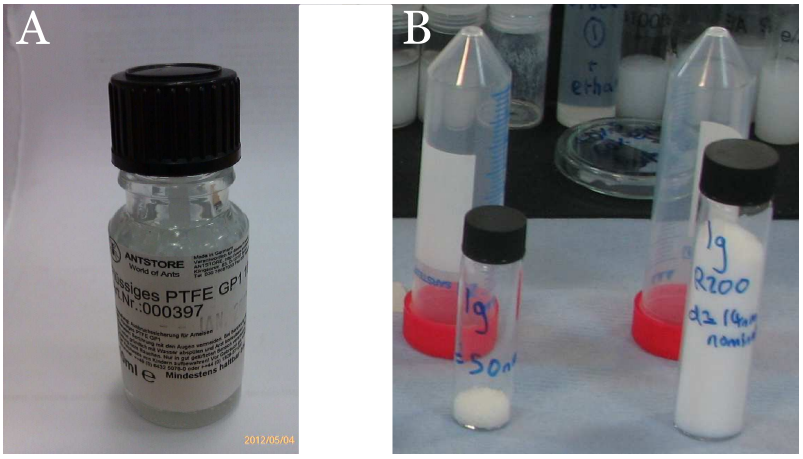

Figure 8.2.1: Sample preparation of the hydrophobic surface coatings. A) Commercially available liquid PTFE, or *fluon*, used for comparison to the nanorough surface coatings. B) Preparation of the nanometre diameter silica particle solution. 500 *mg* of particles are mixed in a vial with 10 *mL* of ethanol.

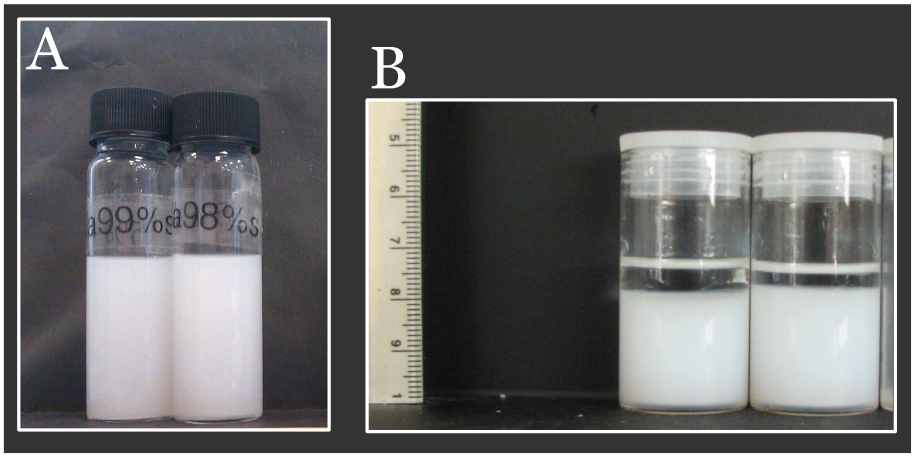

Figure 8.2.2: Colloidal solutions after A) fresh preparation, and B) after 2 weeks left undisturbed. Sedimentation of the solid particles has occurred after several weeks and the solid particles have begun to settle to the bottom of the vials. Solutions can be returned to full suspension after hand agitation.

component begins. After approximately 1 week sedimentation of the solution occurs, Figure 8.2.2. The solution can be returned to its previous suspended condition by rigorously shaking the container by hand for $\sim$ 30 - 60 s.

Preparation of Hydrophobic Surface Coatings

The solution was applied to substrates *via* two mechanisms - *i*) *spin-coating*: to allow for characterisation of the properties of this surface coating, the solution was spin-coated onto glass substrates. Microscope slides were immersed in isopropanol (HPLC grade, Fischer Scientific Ltd, Loughborough, UK) and ultrasonically cleaned for 5 mins, rinsed with isopropanol and air dried. 400 μL of solution was deposited onto a clean microscope slide using a micro-pipette and spun for 40 s at 2000 RPM in a spin-coating machine (P6700 SpinCoating Machine, Coockson Electronics Equipment, Providence, Rhode Island, USA).

ii) *aerosol spraying*: to facilitate testing of large surface areas, and to allow for the measurement of attachment ability on cylindrical surfaces, the solution was also deposited on to glass and plastic substrates by means of pump-activated spray bottles. Spray bottles (100 mL) were held 20 cm from the target substrate and sprayed 4 times in quick succession to assure a total covering.

To compare the colloidal solution surface-coating with a commercially available product sold as having the same anti-insect effect, beakers were coated with two layers of Fluon dispersion, Figure 8.2.1 (Liquid PTFE GP1- Fluoropolymer dispersion - Batch No. 000397, Antstore, Berlin, Germany), using a paintbrush. The beakers were allowed to dry under laboratory conditions before a second coating was added.

UV-Light Treatment

After spray coating glass substrates with the colloidal solution a number of microscope slides were treated with ultraviolet light at 3 positions for 5 minutes at each position, using an ultraviolet bulb. The bulb could be slowly moved along the length of the glass slide, ensuring the whole slide is irradiated. Treating the superhydrophobic slides with UV light removes the surface layer of functional hydrocarbons and in turn makes the surface hydrophilic, while other surface properties, such as roughness and porosity, are unaffected.

Surface Characterisation

Scanning electron microscopy (SEM) was used to visualise the surface coatings deposited on microscope slides, images were captured with a Zeiss EVO60 electron microscope (Carl Zeiss AG, Germany) or a Cambridge Stereoscan 360 SEM (Cambridge Instruments, UK) in high-vacuum mode after sputter-coating with gold-palladium.

The wettability of the freshly coated substrates was determined by measuring the three-phase contact angle of a $\sim 10\ \mu L$ water droplet, using a contact-angle goniometer (Krüss, DSA-10, Krüss GmbH, Hamburg, Germany). Measurements were taken at random intervals over the course of the first 5 minutes after applying the droplet. Surface roughness of the substrates was measured using a white-light optical profiling system (Wyko NT1100, Veeco, Tucson, AZ, USA), at 10× magnification. Optical transmittance of the coated surfaces was measured using a spectrophotometer (Unicam5625 UV/VIS, Unicam Ltd., Cambridge, UK) in the range 400 – 710 nm at $T \simeq 20°\mathrm{C}$.

Measurement of Insect Attachment Ability

To quantify the attachment abilities of the ladybirds on the various surface coatings, 600 *ml* pyrex glass (diameter: 86.1 *mm*) and polypropylene plastic beakers (diameter: 97.0 *mm*) were used to determine the maximum angle of inclination achieved by the test insects after the inner surface had been coated with appropriate coatings. Uncoated beakers were also used as controls. Coated beakers were placed on their side in front of a webcam (QuickCam Pro for Notebooks, Logitech UK Ltd, Slough, UK) controlled by HandyAVI 4.3 software (Azcendant, Tempe, AZ, USA), and the movement of the insects within the beaker was recorded at 4-fps. The experiment was carried out 20 times on each type of beaker, and no individual insect was used twice in 24 hours.

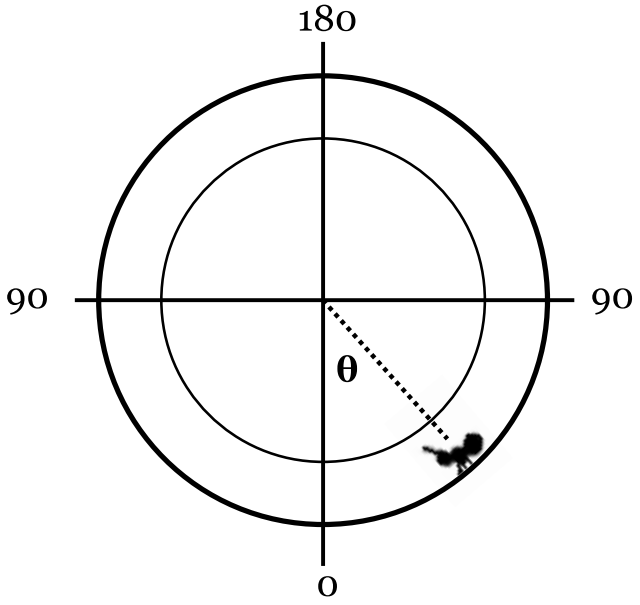

Figure 8.2.3: Schematic showing the beaker and the determination of the angle of inclination θ.

Statistical Analysis

Statistical analyses were performed using data analysis packages within Mathematica v.8.0.0 (Wolfram Research Inc., Champaign, IL, USA). To compare between groups, data were tested for normality using a Shapiro-Wilk test. Non-parametric data were analysed using a Mann-Whitney U-test.

Weathering tests

To test the durability of the surface coatings under natural conditions the beakers were left outside and inspected at regular intervals. Beakers coated with the sprayed colloidal solution were weathered over the course of 5 weeks by placing them outside at the University of Hull Botanical gardens (Cottingham, East Yorkshire, England) and were inspected and photographed after 2 and 5 weeks to determine the effects of weathering on the surface coatings.

8.3 Results & Discussion

8.3.1 Surface Roughness of Coatings

Depositing the colloidal solution onto flat substrates *via* spin-coating produces even surface coatings of nano-metre sized colloidal particles. Typical scanning electron micrographs of these coatings, Figure 8.3.1, show a multi-particle layer approximately 1–2 μm thick loosely attached to the substrate - the coating can be scratched from the substrate with a finger-nail or sharp object. The thickness of the particle coating can be altered by varying the speed and rotation time of the spin-coating machine [223]. Cracks can be seen running throughout the spray-coated surface at both the micro-, Figure 8.3.2, and macroscale (not shown), and the sprayed surfaces often had large asperities randomly distributed across the surface, suggestive of an overall increase in roughness, and variations in film thickness.

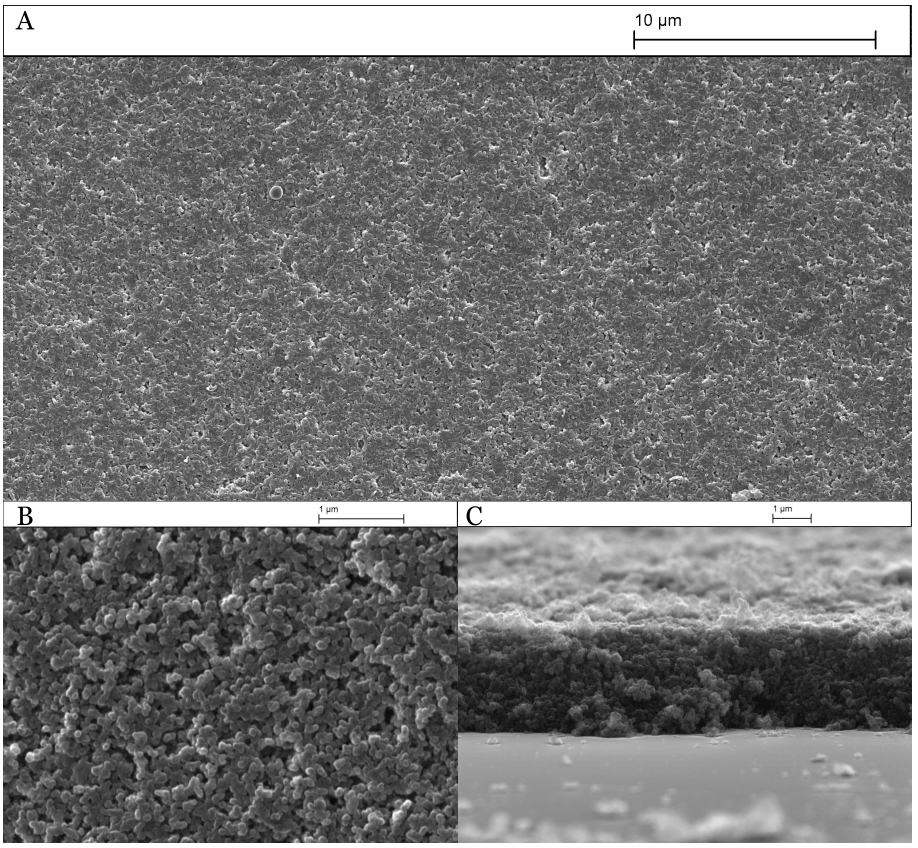

Figure 8.3.1: A) SEM top-view image of the anti-stick solution spin-coated onto a glass surface at 2000 RPM for 40 seconds. B) Lower magnification image of the same coating, and C) an edge view of the coating showing the multiple layers of silica particles. Scale bars, A) 10 μm, B & C) 1 μm.

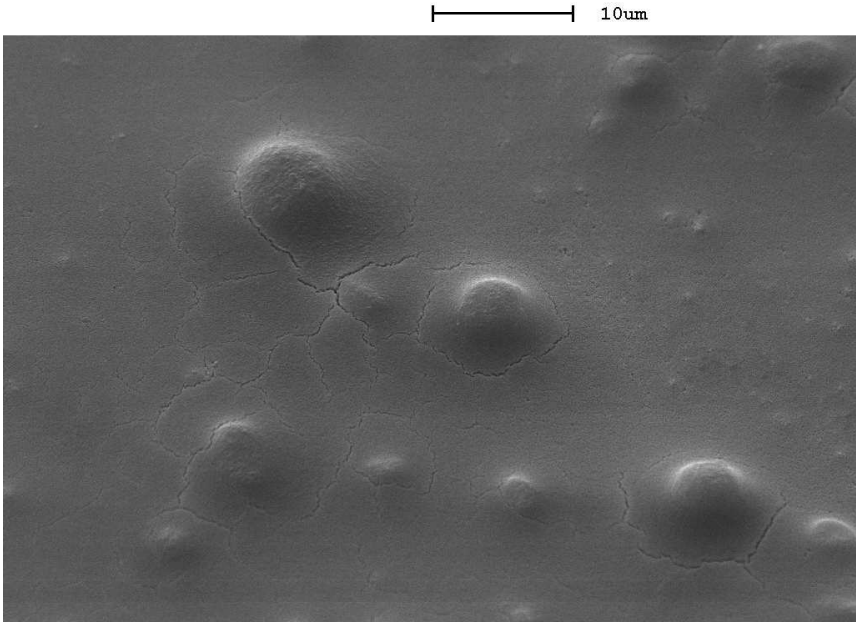

Figure 8.3.2: SEM top-view image of the anti-stick solution sprayed onto a glass surface. Scale bar 10 μm

The surface roughness of the different coatings was measured using interferometry, Table 8.3.1. 3D surface plots for the different colloidal solution coated surfaces, the fluon paint and a glass control slide are shown in Figures 8.3.3 and 8.3.4. Spin-coated colloidal solution coatings were found to be very uniform and consistently generated surfaces with a roughness of approximately 20 nm, whereas the spray-coated surfaces had a greater RMS roughness value and maximum asperity height, Table 8.3.1. In contrast, the fluon coating was visually uneven and broken, and found to contain relatively deep cracks and large surface asperities, with a maximum asperity height of 4 μm.

Using the interferometer the depth of a number of the cracks on the substrates coated with fluon dispersion was determined. Crack depths ranged from 2 μm to approximately 55 μm,

Table 8.3.1: Surface roughness of the colloidal solution coated surface measured using white light interferometry. RMS – root-mean-square, R_t – maximum asperity height.

Substrate	**Scan Size** (μm)	**RMS** (nm)	$\mathbf{R_t}$ (μm)	**N**
Glass control	458.4×602.5	1.3	0.1	3
Fluon paint	458.4×602.5	203.6	3.9	6
Spin deposited	458.4×602.5	19.8	1.4	5
Spray deposited	458.4×602.5	221.8	19.6	7

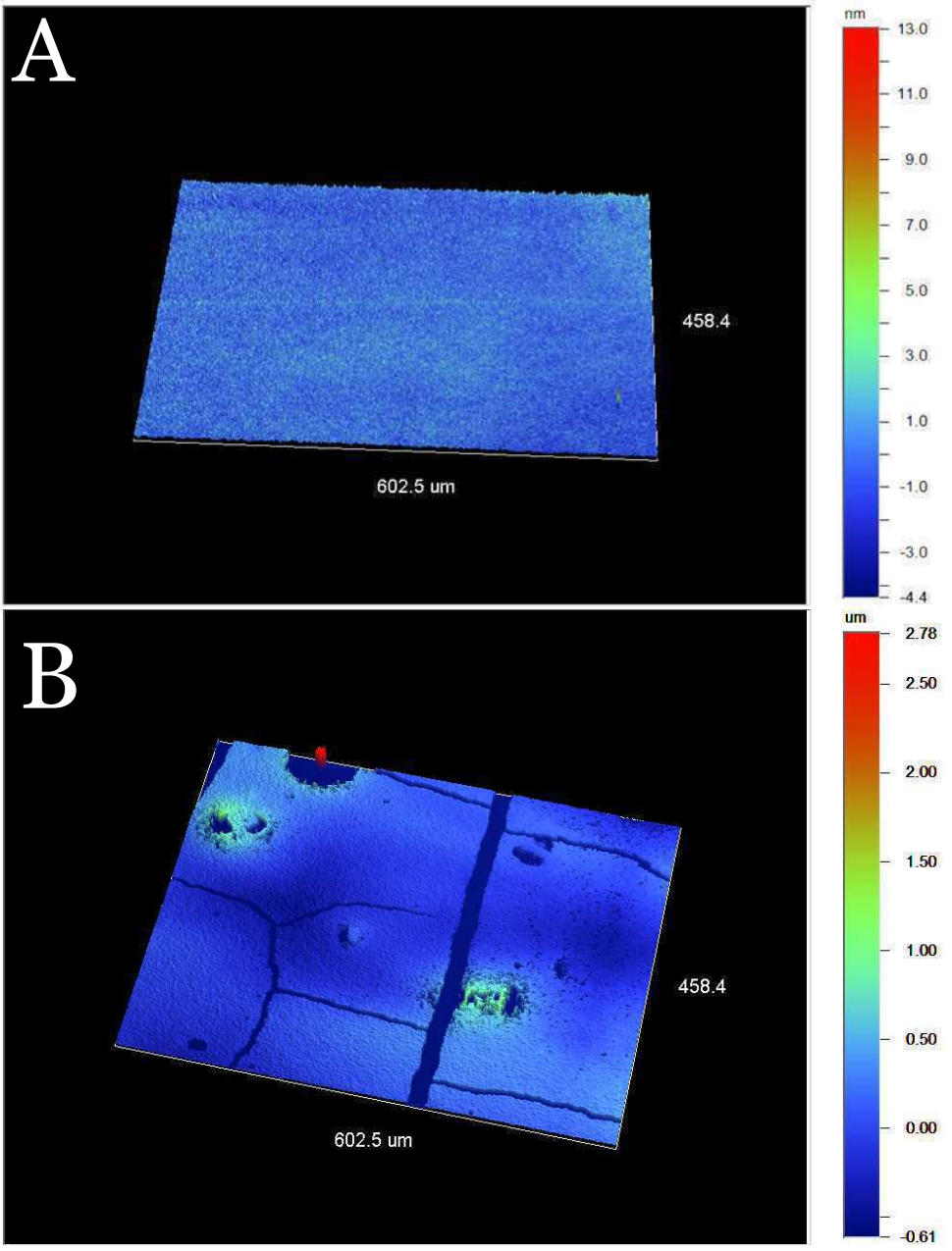

Figure 8.3.3: 3D white-light interferometry surface plots of A) a glass microscope slide as a control, B) the fluon dispersion painted on a glass slide with a paintbrush. Magnification 10×. Scan size 458.4 × 602.5 μm for all images. Please note the difference in scale on the right hand side of each image.

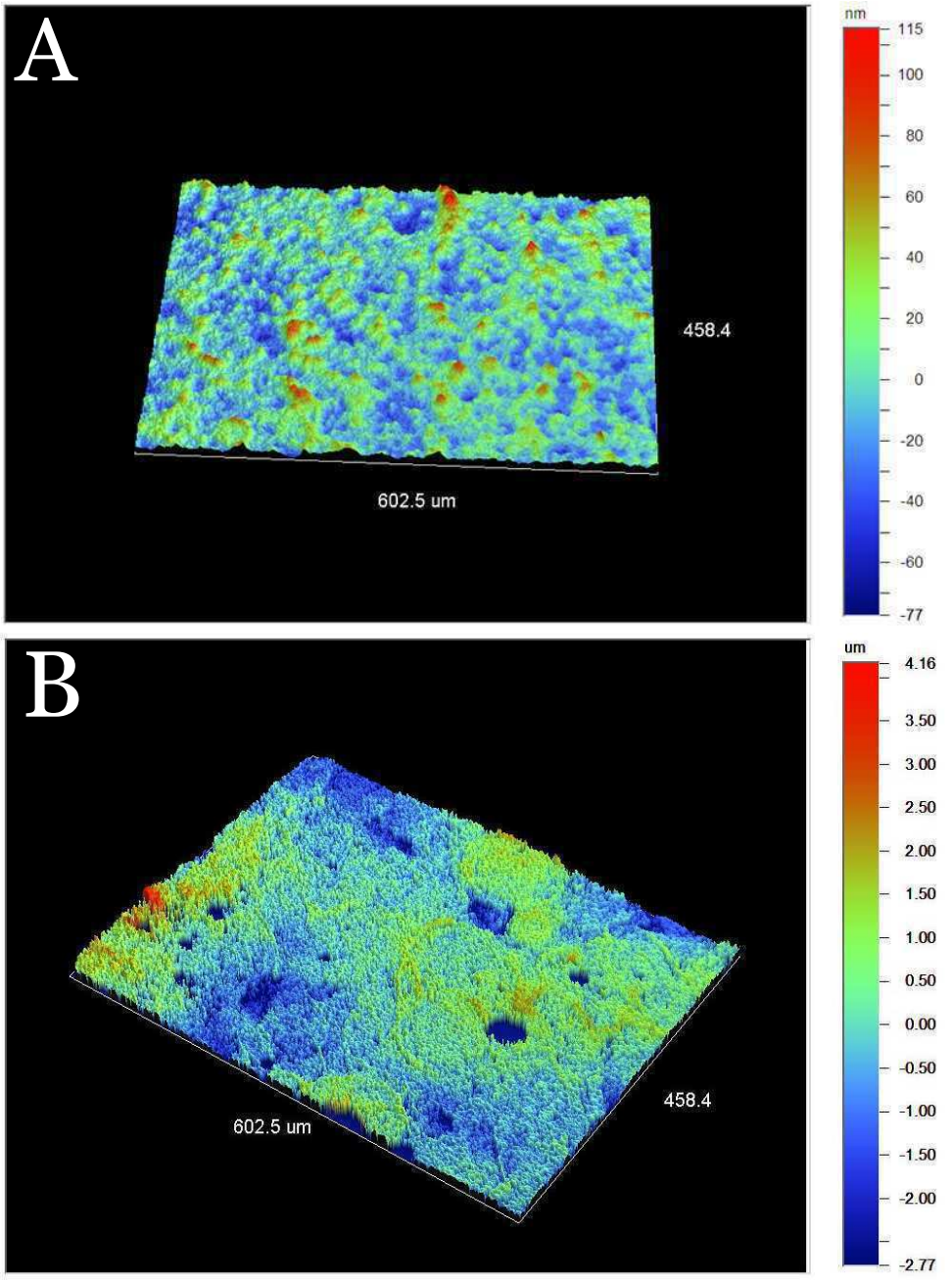

Figure 8.3.4: White-light interferometry surface plots of A) the colloidal solution spin-coated onto a glass slide at 2000 RPM for 40 s, and B) a glass surface coated with the colloidal solution spray. Magnification 10×. Scan size 458.4 × 602.5 μm for all images. Please note the difference in scale on the right hand side of each image.

indicating these fluon coatings were much thicker than the other coatings, Figure 8.3.1. Areas between the deep cracks were measured to be relatively smooth in comparison to the surface as a whole, but the cracks contributed significantly to an overall RMS roughness value which was much greater. By measuring the roughness of these fluon coatings over smaller areas than those shown in Figure 8.3.3 it was found that the surface roughness between the cracks was comparable to the colloidal solution coatings (RMS: 59 nm, N=3). Large spherical asperities found across the surfaces coated with the sprayed colloidal solution are believed to be macro-particle aggregates composed of many smaller individual particles present due to them having not been sufficiently separated by the ultrasonic probe during sample preparation. Longer sonication times and increased ultrasonic power would reduce the occurrence of these artefacts, further reducing overall surface roughness. The increased roughness of the sprayed coatings is most likely due to the method of deposition: due to sprayed droplets falling onto the substrate randomly, particles will settle in a less ordered manner, unlikely to pack closely with their neighbours.

Wettability of Surfaces

Measurement of the contact angles of water droplets on the different coatings indicate that the colloidal solutions produce superhydrophobic coatings with significantly greater contact angles than the other surfaces. Measured values for the colloidal coatings were slightly lower than 150°, regardless of the method of deposition, *i.e.* sprayed or spin-coated, Figure 8.3.5. The water contact angle on fluon was $\sim$ 102°, significantly lower than the colloidal coatings (Mann-Whitney U-test, U = 0, P<0.001), but still hydrophobic (*i.e.* > 90°). After treatment of the hydrophobic colloidal surfaces with the UV light, the contact angles were measured again. The resultant burnt surfaces had contact angles of 7.8 $\pm$ 1° for those which were spin-coated, and less than 5° for the spray-deposited surfaces. Measurement of contact angles becomes significantly less accurate below values of $\sim$10° due to limits of resolution of the camera imaging the droplets, hence the results for the UV burnt surfaces which were spray deposited are not included in Figure 8.3.5, but are

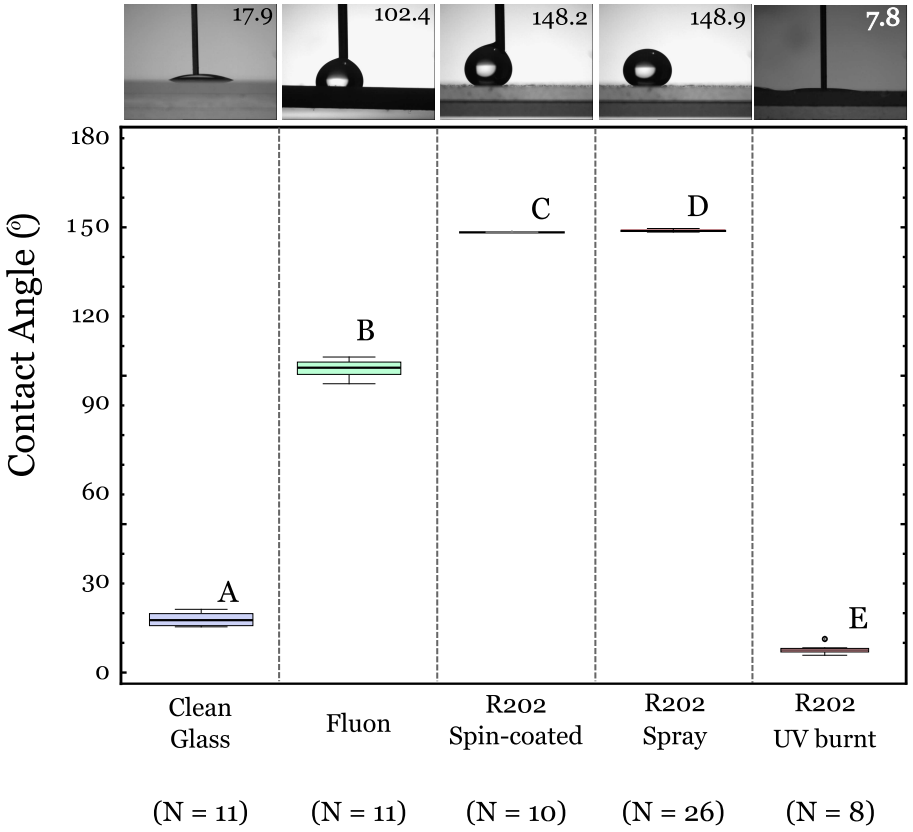

Figure 8.3.5: Contact angles of sprayed and spin-coated colloidal solution coated substrates compared with fluon and hydrophilic glass. While fluon is considered non-stick, the colloidal solution produces a superhydrophobic surface coating. Numbers in the insets denote the mean value measured. Boxes represent upper and lower quartiles, whiskers represent 10th and 90th percentiles, dots represent outliers. Upper case letters indicate significant differences between substrates, Mann-Whitney U-test $P<0.001$

given in Table 8.3.2. Due to the behaviour of water droplets on the coatings, the colloidal solution surface coatings can be classified as superhydrophobic, having a contact angle $>$ 140° and a low hysteresis. These surfaces also had very low tilt angles - the angle needed to induce rolling of the droplet - which is another requisite for superhydrophobicty, as discussed in Chapter 3, and the ability to self-clean [174]. In contrast, water droplets do not easily roll off the surfaces coated with fluon, with a contact angle in the region of 100°, Figure 8.3.5. Fluon coated slides could be completely inverted without water droplets detaching, suggesting that the water droplets were in the Wenzel state of wetting.

The self-cleaning property of the colloidal solution coating provides an important advantage which the fluon and hydrophilic surfaces lack. The fluon coatings can become contaminated and fouled by dust particles, dirt and other material detritus, especially when

Table 8.3.2: Contact angle θ of water measured on glass microscope slides with different surface coatings. * accuracy of values below 10° is reduced due to very small angles and the limits of resolution of the camera used to image the droplets.

Substrate	**Contact Angle** (° ± s.d)	**N**
Untreated Glass	17.9 ± 2	11
Fluon	102.4 ± 3	11
Spin deposited (hydrophobic)	148.2 ± 1	10
Spray deposited (hydrophobic)	149.3 ± 1	26
UV burnt - spin deposited (hydrophilic)	7.8 ± 1	8
UV burnt - spray deposited (hydrophilic)	$\leqslant 5$ ° *	6

stored or used outdoors, which reduces the effectiveness of the coating, and the same is true of hydrophilic surfaces. Other 'non-stick' products currently commercially available require regular re-application to the target substrate for them to remain at their optimal efficiency [142, 224].

Optical Transmittance

When deposited onto glass substrates the colloidal solution spray allows visible light to transmit through the coating, but images observed through it appear blurry, likely due to light scattering through the multiple interfaces of the glass substrate and the multiple layers of glass particles. Coatings appear translucent, and have a slight blue tint to the surface where the coating is quite thick. The transmittance of visible light through microscope slides coated with the colloidal solution was measured using spectrophotometry, Figure 8.3.6. A desirable property of synthetic superhydrophobic, 'anti-stick' coatings is to have an even surface with no micro-cracks or scratches, since these can lead to contact-line pinning of water droplets, reducing the self-cleaning and superhydrophobic properties, and may provide areas of grip or traction for insect claws attempting to climb the surface, if for example their dimensions are greater than the claw tip diameter of the insect [15]. In reality, surface roughness, optical transparency and the minimisation of coating thickness are competing factors which make the generation of anti-stick, self-cleaning, see-through surfaces a significant challenge, particularly if these surfaces are desired to be applied

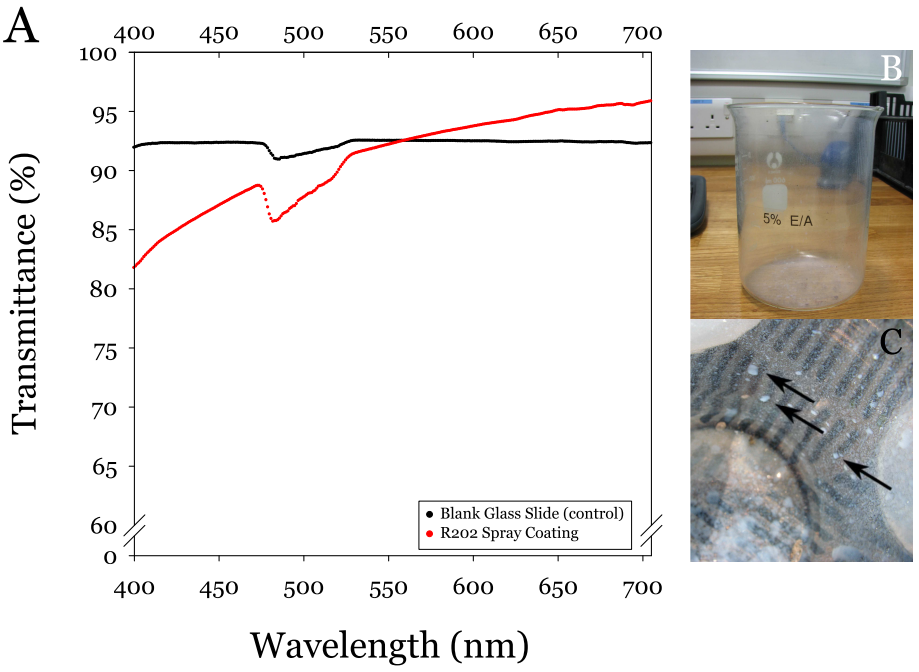

Figure 8.3.6: A) Transmittance of optical light through the coated surfaces as measured using spectrophotometry. Black line represents transmittance of a glass microscope slide relative to air. Red line represents transmittance of coated slide relative to the control glass slide. B) Coated glass surface appear translucent, and C) have blue-tinted areas scattered across their surface due to thicker portions of coating (*arrows*).

on-demand, on irregular surfaces *via* methods such as spray-deposition. From the consideration of surface roughness, hydrophobicity and transparency are competitive properties. When roughness increases, hydrophobicity increases but transparency decreases. Given that visible light is *ca.* 400–750 *nm*, the surface roughness scale for a transparent film should be less than 100 *nm*. The spray deposited colloidal solution surfaces have a mean RMS roughness of approximately double this value, Table 8.3.2, and a thickness of several micrometres, if not greater. The spin-coated surfaces coated with the colloidal solution had an RMS roughness value of approximately 20 *nm*, suggesting that these coatings should scatter less light, and produce a clearer image. However observing objects through these slides also produced blurred images, suggesting that the multiple interfaces induced scattering. Figure 8.3.1 shows that the spin-coated surfaces were constructed of many particle layers. By altering the spin time and rotation speed, the thickness of the coating can be altered, as demonstrated by Tang [223] who was able to produce thinner layers of particles in this manner, but the transparency of light through these surfaces was not considered in the study of Tang [223]. However, both the spin-coated and spray-deposited

colloidal coatings are drastically more transparent than the fluon dispersion which, once dried appears as a white coating layer, and is completely opaque.

8.3.2 Attachment Ability of *C. septempunctata*

When introduced to the beakers coated with the colloidal solution, qualitative observations of ladybirds attempting to traverse the beakers indicated that the surfaces proved difficult to adhere to for angles above approximately 45°. Ladybirds were able to successfully attach to, and walk over, both control beakers without difficulty, and were able to reach the inverted position of 180° on both beakers, Figure 8.3.7, but when placed within the coated beakers it was observed that ladybirds struggled to adhere to the beakers' surface, indicating that the insects were unable to generate sufficient adhesive forces to facilitate vertical or inverted climbing.

The frequency of visitations to angles above 60° became extremely rare on either fluon coated beakers, or those coated with the colloidal solution, Figure 8.3.8, and the maximum

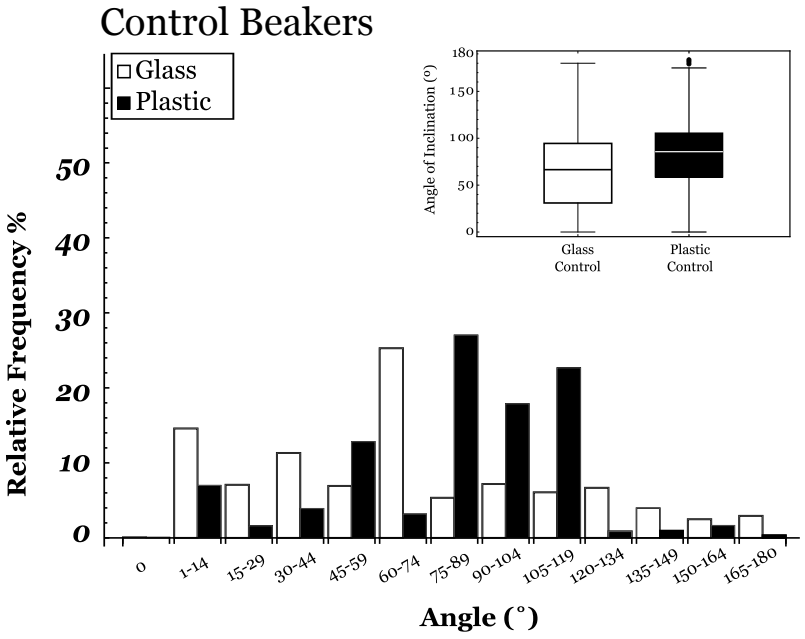

Figure 8.3.7: Relative frequency of visitations as a function of angle of inclination for the control beakers. Ladybirds were able to traverse the beakers under all angles of inclination. White bars, glass, Black bars, plastic. Inset shows a box-whisker plot of the same data. Boxes represent upper and lower quartiles, whiskers represent 10th and 90th percentile, dots represent outliers.

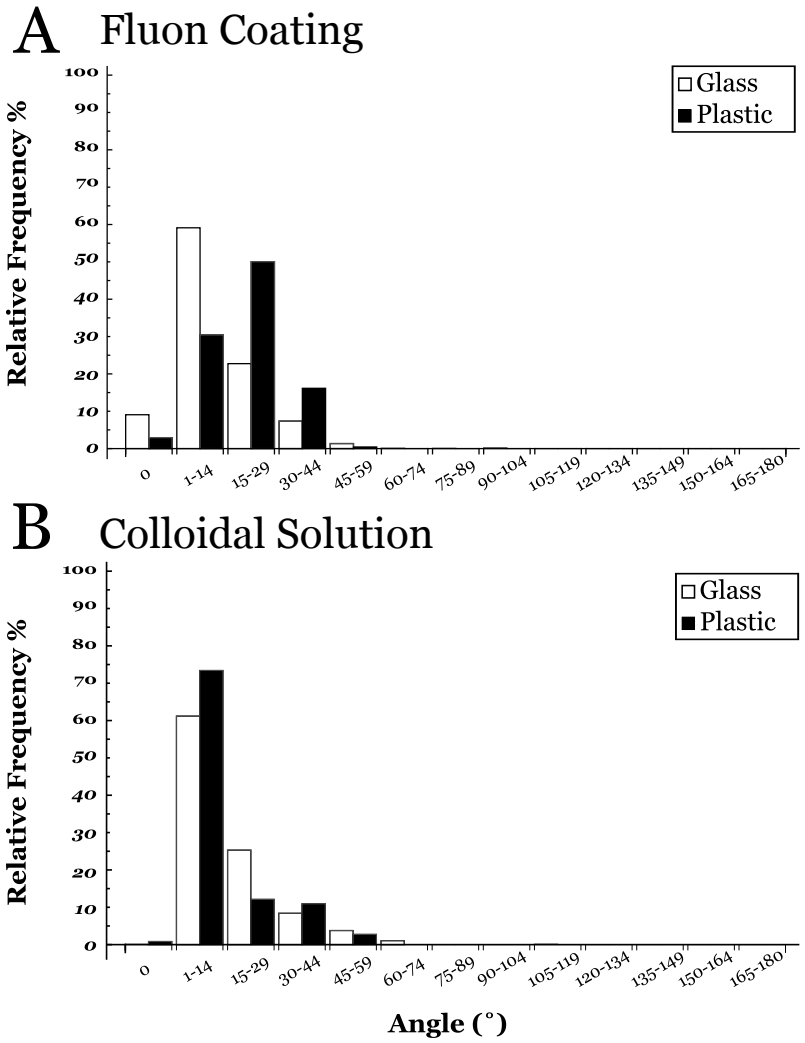

Figure 8.3.8: Bar charts of the relative frequency of visitations as a function of angle of inclination for the coated beakers. A) Fluon coated beakers, B) colloidal solution covered beakers. Angles are separated into distinct ranges. White bars, glass beakers, Black bars, plastic beakers.

angles achieved on each surface is given in Table 8.3.3. The loss of adhesive ability observed in these tests was similar to the loss of adhesive ability seen for ants after crossing particle barriers in Chapter 7. One possibility to explain this, is that the reduction in adhesion was caused by contamination of the tarsal attachment pads of the ladybirds. Tarsal adhesive pads of *C. septempunctata* which had traversed the coated beakers were imaged with SEM, Figure 8.3.9, which shows that the hairy attachment pads were not strongly contaminated by particles of either fluon or the colloidal solution. A small number of contaminating particles were observed, usually attached to the tips of the tarsal claws, and it is noted that the claw tips were contaminated by material after traversing the

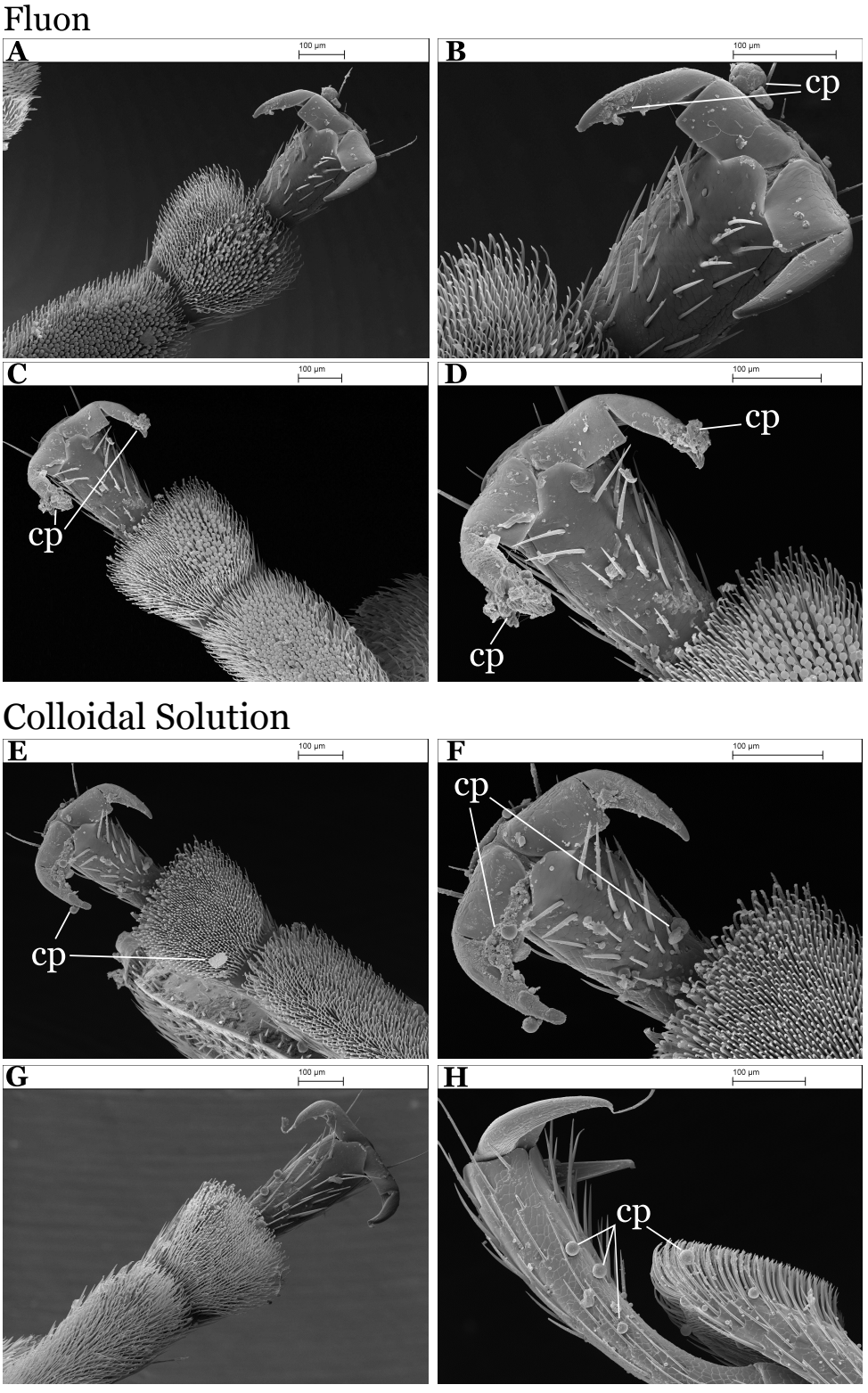

Figure 8.3.9: SEM image of tarsi of *C. septempunctata* after traversing the beakers coated by the A - D) fluon dispersion and E - H) colloidal solution. *cp* - contaminating particles. Scale bars = 100μm.

fluon beaker, eg., Figure 8.3.9C,D, hinting that the ladybirds may have attempted to use their claws to either grip surface asperities, or penetrate into the surface, possibly trying to use the deep cracks as leverage during ascent. The majority of setal hairs of the ladybirds remained almost entirely free of contamination by colloidal particles from the surface coating. Contamination by particles, or flakes, of fluon were comprised of uneven clumps surrounded by long, thin, thread-like fibres. Therefore it was concluded that significant contamination of the adhesive pads of the ladybirds was not occurring, and was not responsible for the loss of adhesive ability on these surface coatings.

A second possible reason for the loss of adhesion is the hydrophobic glass particles could be reducing the capillary forces provided by the adhesive secretion (discussed in Chapter 2) to such an extent that insects become unable to traverse vertical surfaces. Reduction of surface energy will increase the contact angle of liquid with the substrate, and the addition of surface roughness to a hydrophobic surface will increase the contact angle further, causing a transition from the Wenzel state, to the Cassie & Baxter state of wetting, as described in Chapter 3. As the contact angle of an insects' adhesive secretion increases the capillary force is also reduced, possibly to the extent whereby successful attachment is prevented, and if the contact angle becomes $> 90^\circ$ the capillary force will be repulsive. However, as mentioned in previous chapters, it is well known that the adhesive secretion in insects is primarily composed of hydrophobic compounds, so it is not immediately obvious how a low FSE of the substrate may affect the attachment ability of the ladybirds.

To test this second hypothesis, several ladybirds were allowed to walk upon glass slides on

Table 8.3.3: Maximum and mean angle of inclination achieved by the ladybird *C. septempunctata* on the curved beaker surfaces.

Surface and coating	**Max angle** (°)	**Mean angle** (°)
Glass control	180	67
Plastic control	180	81
Colloidal solution - Glass	107	14
Colloidal solution - Plastic	56	14
Fluon - Glass	101	13
Fluon - Plastic	52	19

a tilt-stage (to measure the angle of inclination) coated with the colloidal solution which had been treated with UV light to make them hydrophilic, see Figure 8.3.5. Qualitative observations of the behaviour of *C. septempunctata* walking on these UV-treated surfaces indicated that these surface coatings were equally as effective at reducing the attachment strength of these insects as the original hydrophobic colloidal solution coatings. Preliminary tests found that ladybirds fell from the surface under the force of gravity at angles approaching 45°, similar to the results seen in Figure 8.3.8, demonstrating that the difference in hydrophobicity between these surfaces gave little to no effect with respect to the adhesive force produced by the ladybird. We were unable to perform the same treatment on the coated beakers with the UV light bulb in the same manner, and so a quantitative comparison between hydrophilic and hydrophobic coatings in the way described in Section 8.2 & Figure 8.2.3 could not be made.

However, the tilt angle tests clearly suggest that the determining factor which causes the substantial loss of adhesive ability in the ladybird *C. septempunctata* is the surface roughness of the substrate. The effect of surface roughness on the adhesive ability of insects has been studied a number of times before on both natural [55, 123] and synthetic substrates [8, 54], as discussed in Chapter 3.

For example, Dai *et al.* [15] studied the friction force of the beetle *Pachnoda marginata* and found that when the average asperity diameter is less than the claw tip diameter the insect is unable to deploy the claws and must rely on the adhesive pad system. The claw tips of *C. septempunctata* were measured to be between 8–10 μm (N=5), see Figure 8.3.9, which is substantially greater than the roughness profiles of the surface coatings used in this study, meaning the ladybirds had to rely on the adhesive ability of their hairy pads. However, a critical roughness regime of surface roughness has been found previously within which the generation of adhesion forces is reduced to a minimum. Voigt *et al.* [6] found a minimum of friction force in the beetle *L. decemlineata* on surfaces with a nominal asperity size of between 0.3–1.0 μm, corresponding to a root-mean-squared roughness between 90 and 238 nm, and a similar effect has been observed in *G. viridula* [225] and gecko lizards [226].

The effect is explained by the reduction of contact area between small surface irregularities and the characteristic size and shape of setal tips in hairy pads. Other rough substrates, with larger asperity sizes, provide sufficient amounts of smooth sites for the terminal plate to establish an intimate contact. The colloidal solution coatings, as well as the fluon coating, had RMS roughness values which are very similar to the rough surfaces reported in the literature which elicit this minimisation of adhesion forces. It is therefore concluded that the colloidal solution coatings have a roughness profile which is within the critical roughness regime for the seven-spot ladybird *C. septempunctata*, and as such these insects were unable to climb these coatings due to a drastic reduction in the real area of contact between attachment pad and the substrate. Interestingly, substrates with the 0.3–1.0 μm nominal roughness (asperity diameter) corresponds to the dimension of epicuticular wax crystals, which have been previously reported to prevent insect attachment [131, 133, 134] by the reduction of contact area between terminal plates and the plant surface.

The combined effects of critical roughness profile, and a hydrophobic, or low surface energy, surface coating will work to reduce the attachment forces of insects attempting to traverse the vertical surfaces, making these surfaces particularly effective, such as that observed for the beetle *Gastrophysa viridula*, which possess the hairy attachment pad, where it was found that attachment forces were significantly affected by a combination of the physico-chemical properties and surface roughness [225].

8.3.3 Weathering Tests

To test the durability of the surface coatings the hydrophobic colloidal solution was sprayed on to glass and plastic beakers, also a beaker was coated with the fluon dispersion, and they were placed outside for several weeks, and observed at regular intervals. After 2 weeks outside the colloidal solution coatings had not been adversely affected by the weathering, and was still easily visible due to its slight blue tint. Small areas of flaking and a small

number of cracks in the coating were identified. In contrast, Fluon coated beakers deteriorated much more rapidly, and had much of the coating removed after the 2 week stage. Large flakes and cracks were visible, and many large portions of the coating had been removed by the weather. After a period of 5 weeks the beakers were brought back inside and inspected. It was found that the fluon coated beakers were almost completely free of the coating, but those treated with the colloidal solution had both dead and live insects remaining inside the beakers, together with many different types of plant matter. Both glass and plastic beakers coated with colloidal solution remained hydrophobic, evidenced by rain water found at the bottom of the plastic beakers which had a convex meniscus. The colloidal solution coating remained attached to the beakers over the majority of the beakers' interior surface, again identified by the blue tint given to both beakers' surfaces. After 5 weeks, small areas of cracks and flaking across the coating were still visible but had not spread from the position identified at the 2 week inspection.

Although the surfaces appeared to have been damaged, and portions of the coating had fallen off, the discovery of insects inside the beakers after several weeks is a good indication that the surfaces remained anti-stick for the duration of the weathering tests, and that the colloidal solution coatings remained effective at creating a hydrophobic surface and preventing insect attachment for up to several weeks after application. This suggests that the top few layers of particles may have been removed from the coating, leaving behind single-figure layers of hydrophobic particles attached to the beakers, in contrast to the fluon, whereby removal of the thick coating removed any hydrophobic effects from the beakers. Over long periods of outdoor weather exposure, the superhydrophobic property of artificially created anti-wetting surfaces will gradually decrease due to accumulation of stains and debris adhering to the surface, and due to extended periods of mechanical wear from rainfall or wind. But natural hydrophobic surfaces, such as the Lotus leaf, avoid this problem of degradation by continuously metabolising and regenerating new surface-wax layers [227]. Since synthetic coatings cannot be given this self-replicating property, improvement of the coatings' durability is an important consideration.

The addition of different solvents within the solution may improve the drying process and could improve the durability of the surface coatings. The use of solvents with relatively low-boiling points such as acetone (C_3H_6O, boiling point 56°), hexane (C_6H_{14}, boiling point 60°), or ethyl acetate ($C_4H_8O_2$, boiling point 77°) may have desirable effects due to rapid evaporation of the aerosol drops. For example, Steele *et al.* added small amounts of acetone to a solution of water, polymer, and zinc-oxide nanoparticles to counteract the coffee-stain effect during drying and produced hierarchical surface morphologies which were superhydro- and superoleophobic [228]. Some qualitative success was achieved with this approach with the colloidal solution but a detailed and systematic investigation and comparison was not possible within the time available.

8.4 Conclusions & Further Work

The colloidal solution investigated is able to generate superhydrophobic surfaces due to the nano-metre sized particles it contains. The superhydrophobicity occurs due to the combined effects of low surface energy and nano-scale roughness, which makes water droplets sit on the surface in equilibrium in the Cassie & Baxter wetting state, resting on the tips of the surface asperities. These factors combine to create surfaces which also prove extremely difficult for insects to traverse when orientated vertically or inverted.

The surface coatings have a roughness small enough to prevent the use of tarsal claws during climbing, and the surface roughness is also comparable to the critical roughness regime found to adversely affect other insects on rough surfaces. It is concluded that the reduction in real contact area is the main factor contributing to the loss of adhesive ability, and that generation of a large area of real contact between the adhesive pads and the substrate is fundamental to successful adhesion, but the low surface energy of the coating will also work to reduce any capillary forces. In comparison to the currently available fluon-paint alternative the colloidal solution coatings had a number of benefits; the spraying method made application much easier and the coating dried significantly quicker, colloidal solution

coatings had significantly greater contact-angles with water and were superhydrophobic, and were optically translucent. Fluon coatings and the colloidal solution were approximately equal in their effectiveness at reducing insect adhesion when fresh, and clean, but the colloidal coatings developed were able to maintain their effectiveness for a greater length of time, and did not suffer from the effects of wear for several weeks.

Recent reviews of synthetic self-cleaning surfaces have described several different methodologies for producing different solid surfaces with superhydrophilicity, or superhydrophobicity induced self-cleaning abilities, but the availability of easy-to-apply products with these properties is still limited, and may prove to be very useful [229, 230]. The use of spray deposited surface coatings in domestic situations would require repeated application onto the target substrate, so the production of durable coatings would reduce the overall cost of maintenance of coated surfaces.

A number of issues, however, remain outstanding that require further development before these coatings could be successfully deployed on a large scale. The most prominent issues remaining are namely: *i*) the currently limited durability of the coatings in the form of their attachment strength to the underlying substrate, *ii*) the translucent appearance of the coatings on glass, and *iii*) the variable reproducibility of the surface properties due to the spray-deposition method.

These issues could be solved, or addressed in a number of ways; further development of the solution to increase particle attachment strength to the underlying substrate would improve the durability of the coatings, extending useful lifetime in the field by increasing the length of time that the self-cleaning properties would remain effective. For example; as mentioned in the previous section, the systematic study of how the addition of different solvents within the solution may improve the drying process could improve the durability of the surface coatings, as shown by studies such as that by Steele *et al.* [228].

The tailoring of desirable surface properties such as transparency, contact-angle, surface-roughness and coating durability for production of effective and durable anti-stick surfaces

can be achieved by altering the parameters of the solution and colloidal particle, such as particle size and shape and surface chemistry functionality, which will enable further development and use of these types of surface coatings within domestic and commercial environments for the purpose of preventing insect adhesion. The construction of silica particles to required size dimensions can be achieved by such processes as a modified *Stöber process*, which has been used extensively to produce micro-metre and sub-micrometre sized particles [231], and the production of different sized particles, with different size distributions, is a straight forward process that can be altered as required. Surface chemistry modification can then be performed *via* a number of different techniques with a range of fluoroalkyl silanes (*eg.*, Hikita *et al.* [232]), but, as demonstrated in this chapter and Chapter 7, the most important factor for the reduction of insect attachment by either loose or rigid synthetic particle barriers is not the surface chemistry, but is principally determined by the particle size - with smaller particles, or sub-micrometre scale surface roughness, causing the most detrimental loss of adhesion for insects. This is not unlike the trend seen in epicuticular wax layers, or crystals, deployed by plants in an effort to reduce insect locomotion across their surfaces.

Development of easily deployed, bio-compatible and environmentally friendly means for reducing or entirely preventing insect adhesive abilities will compliment currently available data on integrated pest-management (*eg.*, Vincent [224]) and extend the applications of superhydrophobic surfaces to various industrial and commercial environments. The use of particle film technology on man-made solid surfaces for the prevention of insect invasion in domestic situations is currently limited to a small number of products based on fluoropolymer resins (*eg.*, PTFE) similar to the fluon paint used in the present study. The alternative colloidal solution approach described here appears to have comparable, if not better, anti-adhesive properties, is easier to apply, possibly cheaper to produce and is durable for several weeks outdoors, without the need for re-application. Further development of these solutions and application methods could dramatically improve these functional surfaces and could have many important applications.

Chapter 9

Concluding Remarks

In this thesis we have used a multi-disciplinary approach to study the adhesive ability of ladybirds and ants under several different detachment conditions, as well as investigate how carefully controlled substrate conditions can adversely affect the attachment capabilities of these insects. By utilising both established and novel experimental methods of measuring attachment strength, we have gathered much information on the forces generated by these insects, as well as discover some of the limiting factors of these advanced natural structures by investigating a range of substrates which reduce attachment ability.

Using simple physical models to describe and explain the results of force measurements conducted on insects *invivo* has allowed researchers, and ourselves, to develop an adequate working theory of how insects use their attachment devices and adhesive secretions to achieve successful attachment to a wide variety of surfaces, consistent with known physical laws. However several unexplained results remain to be sufficiently explained, and the attachment-detachment process has only been studied under a relatively small number of well controlled experimental conditions, and for a limited range of insects.

The study of insect attachment forces under a greater variety of detachment scenarios will aid in further understanding the physical nature of insects' attachment devices, and the physical factors at play during the attachment-detachment cycle. For example, as exemplified by the novel 'Impact-Rig' experiment described in this thesis, the force required to detach an insect from a particular surface is not simply dependent upon the direction in which the detachment force is applied, but can also depend upon, and be influenced by, other factors such as perturbation time. This effect has only briefly been eluded to in the past, and clearly should be investigated further.

Further investigation of this effect, beyond the preliminary results gathered and reported within this thesis, will lead us to a greater understanding of the physical nature of these

attachment organs, the forces at play, and hopefully allow us to replicate such abilities synthetically. Thus, progress in this field requires that more integrated and detailed investigations be carried out to understand the exact mechanisms at work for given insects under the many different detachment scenarios which insects encounter in their natural environments.

Due to recent technological advances, the ability to study small insects and the physical mechanisms underlying their ability to successfully traverse diverse surfaces has become, and will continue to be, relatively easier. Nonetheless, given the morphological and biological complexities of insect attachment devices, an integrative and multi-disciplinary approach will need to be taken, involving the disciplines of physics, physical-chemistry, biology, ecology and engineering.

The limited diversity in attachment pad morphology within the insect world strongly suggests that these structures are highly optimised for surface attachment. Therefore understanding the functional biomechanics which underpin this ability will be useful in further advancing knowledge of adhesion and friction phenomena, as well as providing new insights into the evolutionary and ecological relationships involved in insect-plant interactions. From an ecological point of view, observations of the interactions between insects and plants provide a spectacular demonstration of the effect of substrate properties on the foraging behaviour of insects.

Further detailed studies of the physical nature of insect adhesive pads may yield rich returns leading to the development of new technologies in the areas of surface adhesion and friction. The adhesive liquid secreted by insects during surface attachment has also presumably been optimised by evolution to promote adhesion between a wide variety of surfaces, and could therefore provide the basis for a new generation of adhesion promoters., and understanding the ability of insects to attach and detach at will could also hold the key to the development of a new class of releasable adhesives.

In contrast, attaining a deeper understanding of the adhesive ability of insects could potentially lead to the development and deployment of environmentally friendly strategies for the control of insect pests in agriculture, public health, and domestic situations. For example, a surface to which no insects can adhere would serve as an effective physical barrier against crawling insects, as well as preventing flying insects from successfully landing, and would be of great benefit to many people, in a variety of environments.

Studying the natural engineering of insects, and many other living creatures in recent decades has led to the development of various products and processes that have benefited mankind vastly, and will hopefully continue to do so.

Appendix A

Competing Forces in Particle Barriers

Competing Forces in Particle Barriers

In this Appendix we estimate the pad-particle force compared to inter-particle forces, or particle weight, for an ant crossing a powder barrier (which consists of multiple particle layers) to estimate how the relative magnitude of these competing forces varies with particle diameter. We make the plausible assumption that contamination of the arolium will only occur when the particlearolium force exceeds both the particleparticle force and the force due to the particle weight. This then allows us to make a theoretical estimate of the threshold diameter below which particle contamination of the arolium should occur, in a similar approach to Hansen & Autumn [151].

Particle–Arolium Force

In order to estimate the particle-arolium force, we assume that the particle is rigid while the arolia is a soft elastic material with Youngs modulus E and Poisson ratio ν which is covered by a uniform thin film of adhesive secretion of thickness h. Assuming that the particle-arolium force arises from capillary forces due to the adhesive secretion and that the secretion perfectly wets the arolia and both the particle types, the attractive force between the particle and arolia is given by Butt *et al.* [108]:

$$F = 4\pi\gamma R + \left(\frac{\pi\gamma}{2r}\right)^3 \frac{2R^2}{3E^{*2}} \tag{A.0.1}$$

with

$$E^* = \frac{E}{1-\nu^2} \tag{A.0.2}$$

Here γ is the surface tension of the secretion, R is the radius of the particle asperity in contact with the arolium and r is the radius of curvature of the meniscus formed by the thin film of adhesive secretion wicking up around the particle asperity. For spherical particles, such as the glass particles used in this study, R is equal to the radius of the particle while for irregularly shaped particles, such as the PTFE particles used in this study, R is less than the mean radius of the particle. On the other hand, the radius of curvature of the meniscus r arises from a balance of the capillary pressure of the meniscus and disjoining pressure of the thin liquid film [94]. The first term on the r.h.s. of Equation A.0.1 represents the capillary force between a rigid particle and a rigid flat substrate [94] while the second term is the additional contribution to the capillary force arising from the deformation of the soft elastic substrate, eg., Butt *et al.* [108]. For soft

substrates and small meniscus radii r, the second term can be significant. However its exact magnitude is difficult to estimate due to the fact that it contains a number of parameters such as E, ν and r which are difficult to measure and are therefore not accurately known for the system at hand. Fortunately, for the purposes of estimating a threshold diameter, it is sufficient to approximate the particle-arolia force using the first term only, *i.e.*,

$$F_{pa} \approx 4\pi\gamma R \tag{A.0.3}$$

This represents a lower bound for the adhesive force. Having predicted a threshold diameter, we will then include the second term to see what qualitative effect it has on the predicted value.

Particle-Particle Force

Capillary forces between particles within the barrier were assumed to be negligible below relative humidities of 95 % due to the small value of the Kelvin radius below this point. For example Kohonen & Christenson [233] showed that the mean radius of curvature of capillary condensates between rinsed mica surfaces is $<$ 10 nm for relative humidities below 96 %. Particleparticle forces are thus primarily due to van der Waals (VdW) attractive forces [234] which are given by Israelachvili [95] and Mate [94]:

$$F_{pp} = \frac{AR}{12D^2} \tag{A.0.4}$$

where R is the radius of the two asperities in contact with each other (assumed to be equal), A is the particle-air-particle Hamaker constant, D is the distance of closest approach between the two asperities.

Particle Weight

The weight of a particle is given by

$$F_w = \frac{4\pi}{3} R_p^3 g\rho \tag{A.0.5}$$

where ρ is the density of the particle material, g is the acceleration due to gravity and R_p is here defined as the (mean) radius of the particle rather than the asperity radius.

Relative Magnitude of Forces

We first compare the relative magnitude of particle-arolium and particle-particle forces. From Equation A.0.3 and A.0.4, this is given by

$$\frac{F_{pp}}{F_{pa}} = \frac{A}{48\pi\gamma D^2} \tag{A.0.6}$$

We note that the ratio above is independent of asperity radius R. For γ, we use the literature estimate of $\gamma \approx$ 30 mN/m [12]. The Hamaker constant for glass particle-air-glass particle is given by $A_{glass-air-glass} \approx 6\times 10^{-20}$ J while the Hamaker for PTFE particle-air-PTFE particle is $A_{PTFE-air-PTFE} \approx 4\times10^{-20}$ J [95]. Finally we estimate the minimum separation distance D to be $D \approx 10$ nm based on the nano-roughness of the asperities making contact. Using these parameters, we find $F_{pp}/F_{pa} = 1.3\times10^{-4}$ in the case of glass particles and for PTFE particles on glass, and $F_{pp} = F_{pa} = 8.8\times10^{-5}$ in the case of PTFE particles. This shows that that the capillary forces acting between the arolium and the particles is always about four orders of magnitude greater than the VdW attractive forces between the particles within the barrier, independent of R. If we include the substrate deformation contribution to the particle-arolium force (i.e., Equation A.0.1, this will lead to an even greater discrepancy between the particle-arolium force and the particle-particle forces. We next compare the relative magnitude of the particle-arolium force to the weight of the particle. From Equation A.0.3 and A.0.5, this is given by

$$\frac{F_{pw}}{F_{pa}} = \frac{3\gamma}{R_p^2\rho g} \tag{A.0.7}$$

For the irregular PTFE particles, making this assumption leads to an overestimate of the particle-arolium force. However we believe that this approximation is adequate since we are only interested in making order of magnitude estimates of the different forces here. When the above ratio is equal to unity, the weight of the particle is comparable to the adhesive force generated by the capillary force between the arolium and the particle. This occurs for the threshold radius:

$$R_c = \sqrt{\frac{3\gamma}{\rho g}} \tag{A.0.8}$$

i.e., the particle-arolium force exceeds the particle weight only for $R_p < R_c$. Using $\rho = 2000\ kg/m^3$ for PTFE and $\rho = 2350\ kg/m^3$ for the glass particles, we find $R_c \approx 2\ mm$ for both PTFE and glass particles, *i.e.*, a threshold diameter of around 4 mm. This value is over one order of magnitude larger than the threshold size of 100 μm observed experimentally for both PTFE and glass particles (Figure 7.3.3). Including the substrate deformation contribution to the particle-arolium force will lead to an even higher value for the threshold diameter. We therefore conclude that the threshold particle size for contamination is not determined by a competition between the particle-arolium forces and either particle-particle or gravitational forces.

Appendix B

Scanning Electron Micrographs

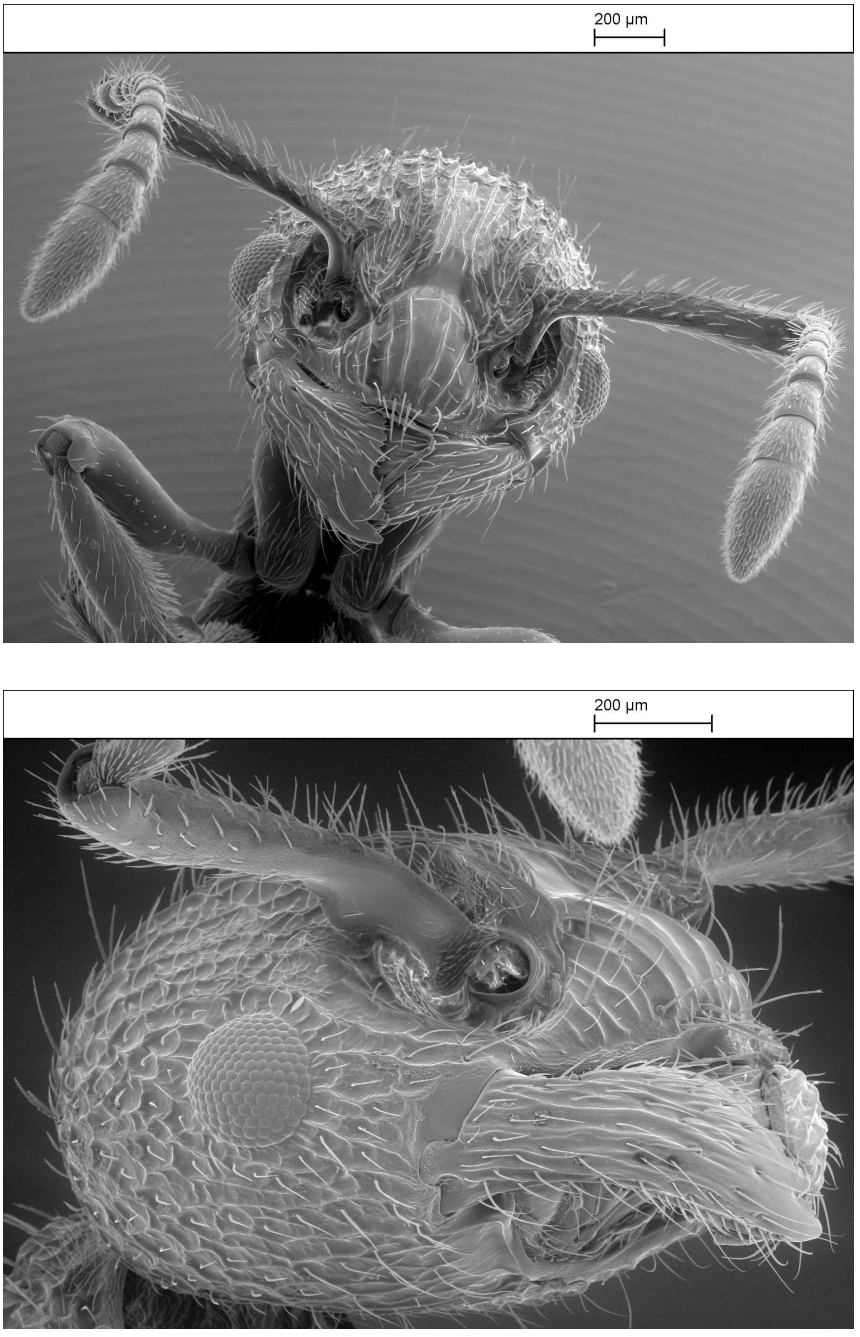

Figure B.0.1: The Red Elbowed ant *Myrmica scabrinodis* (Hymenoptera: Formicidae)

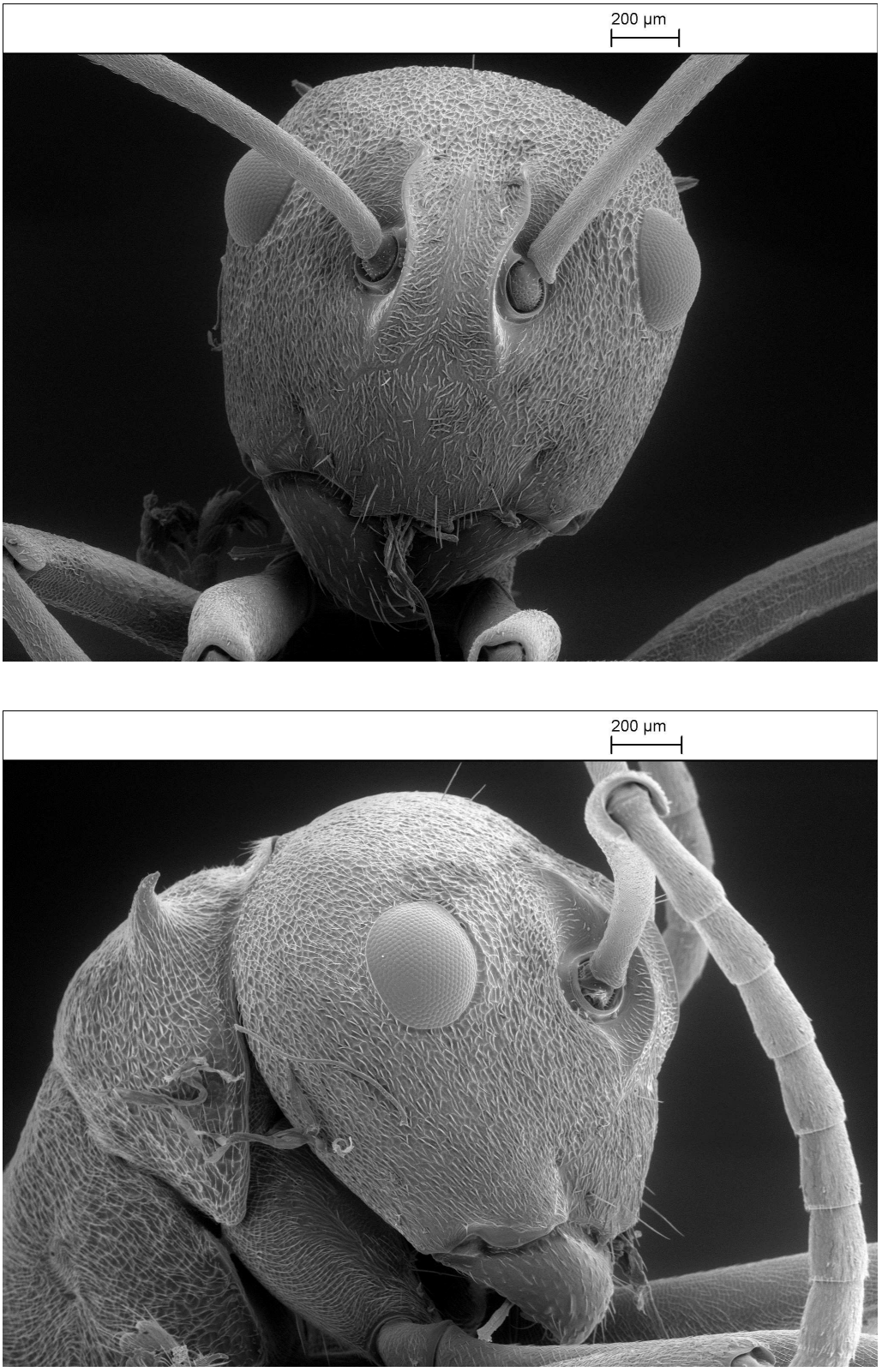

Figure B.0.2: The Weaver ant *Polyrhachis dives* (Hymenoptera: Formicidae)

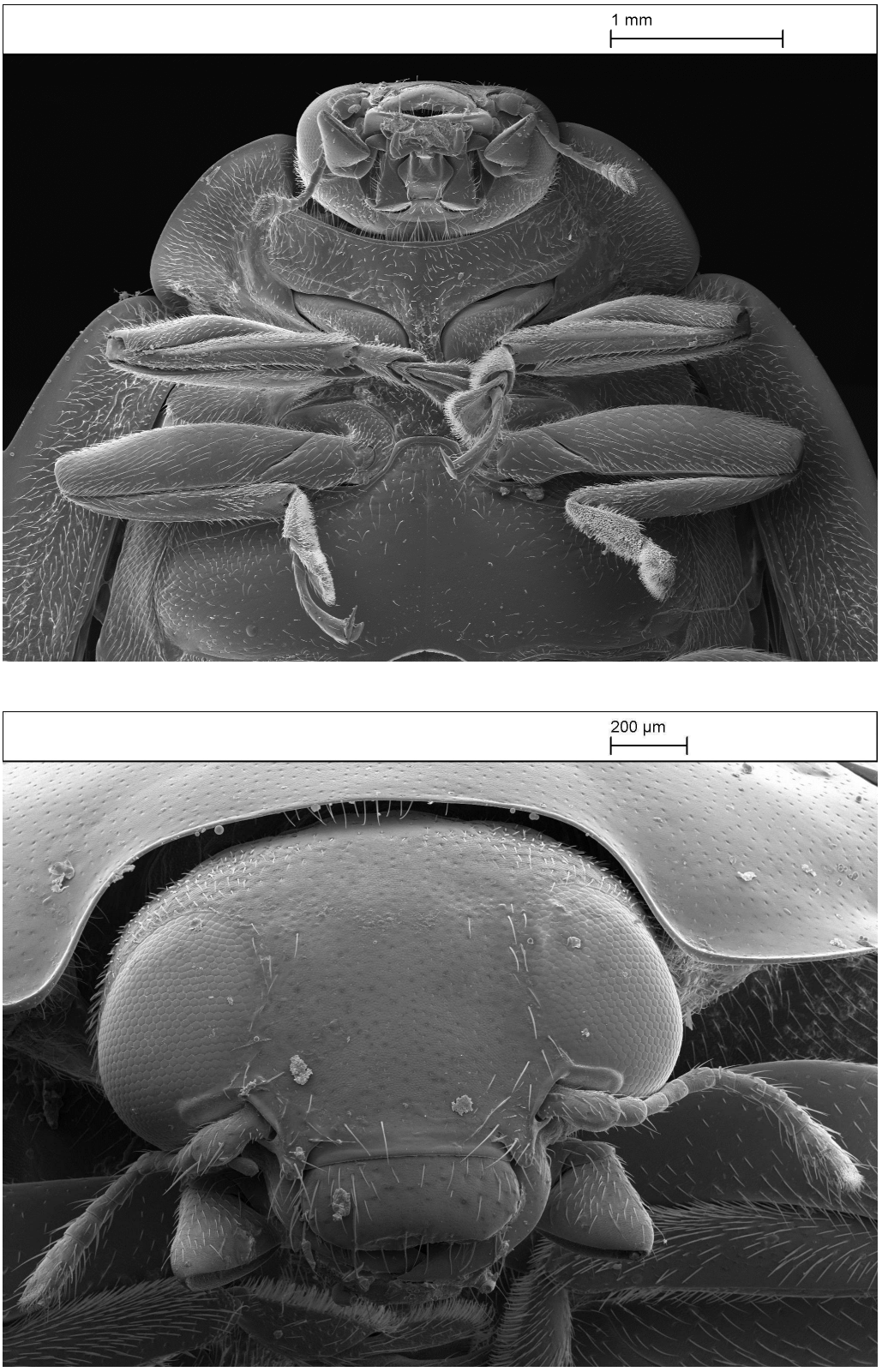

Figure B.0.3: The Harlequin ladybird *Harmonia axyridis* (Coleoptera: Coccinellidae)

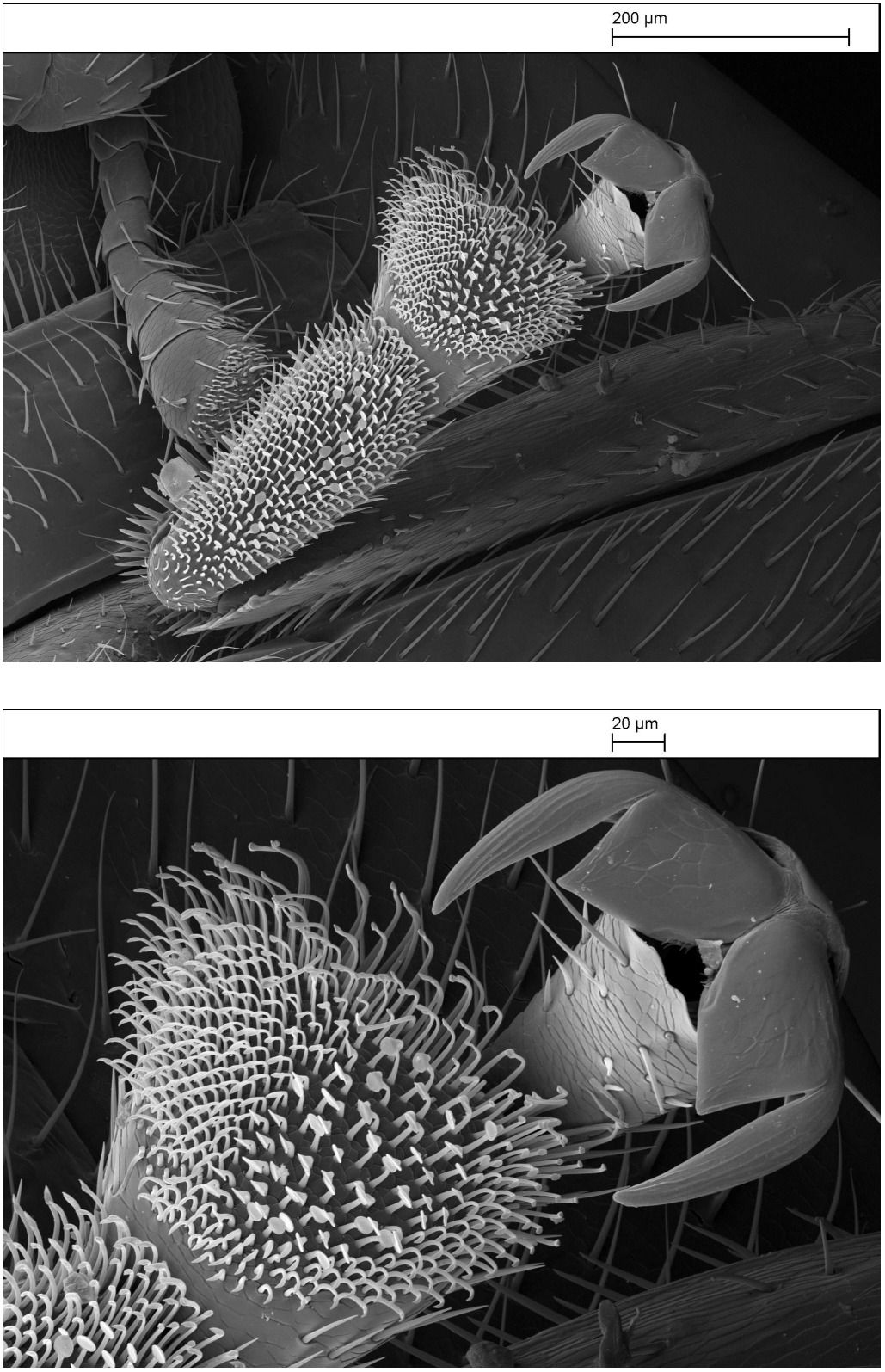

Figure B.0.4: The 2-spot ladybird *Adalia bipunctata* (Coleoptera: Coccinellidae)

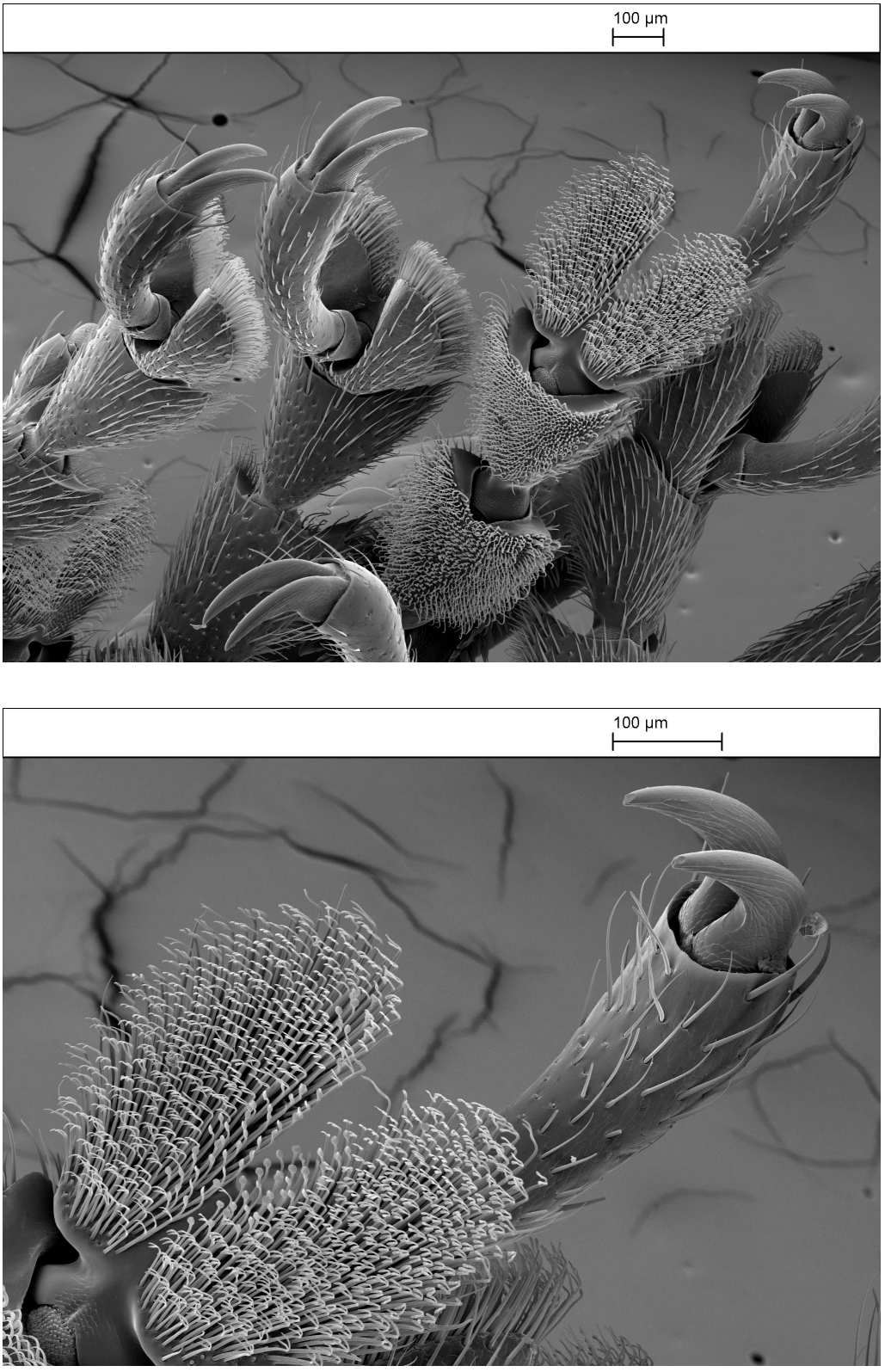

Figure B.0.5: The Cardinal beetle *Pyrochroa serraticornis* (Coleoptera: Pyrochroidae)

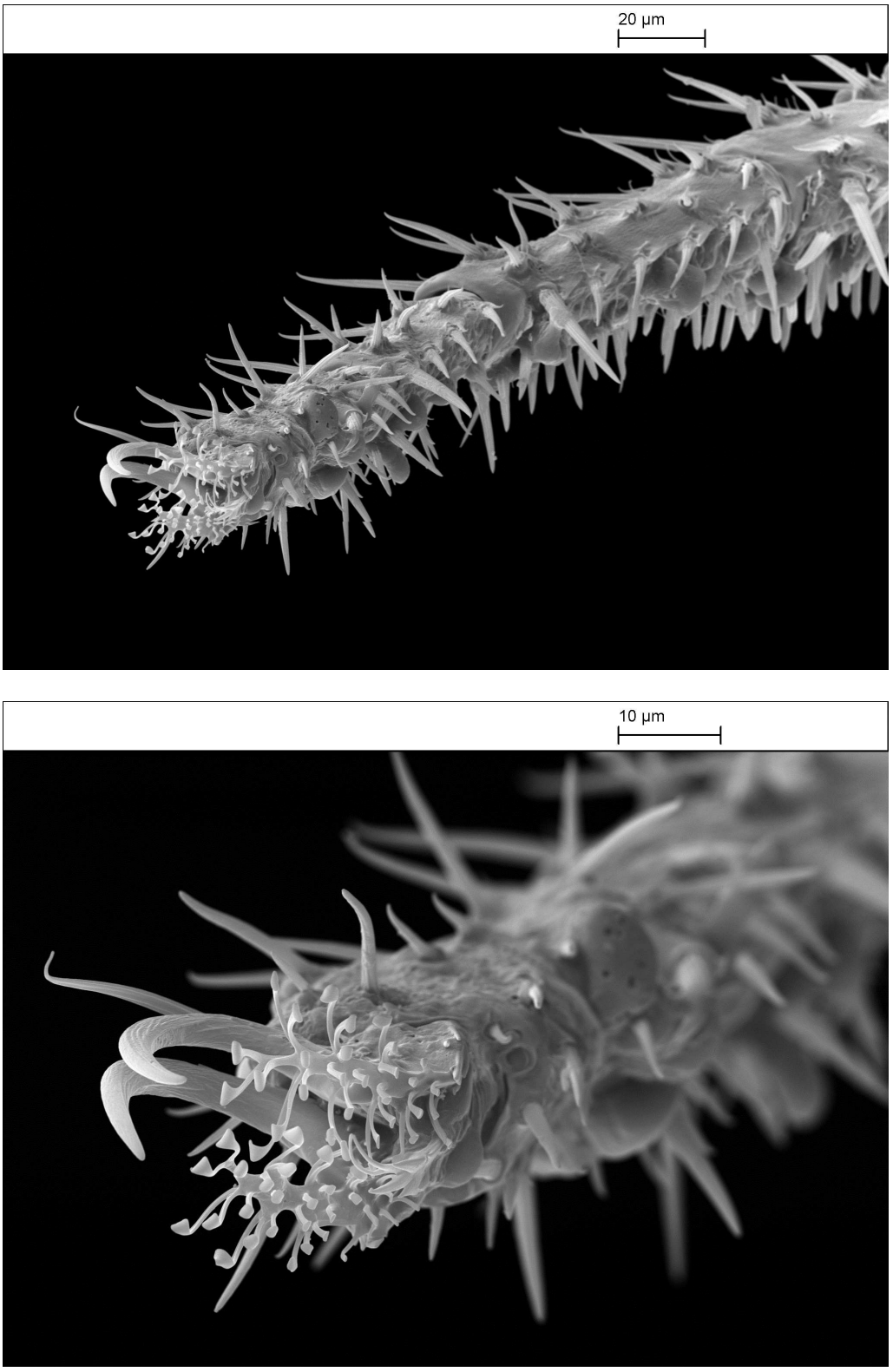

Figure B.0.6: The fruit fly *Drosophila melanogaster* (Diptera: Drosophilidae)

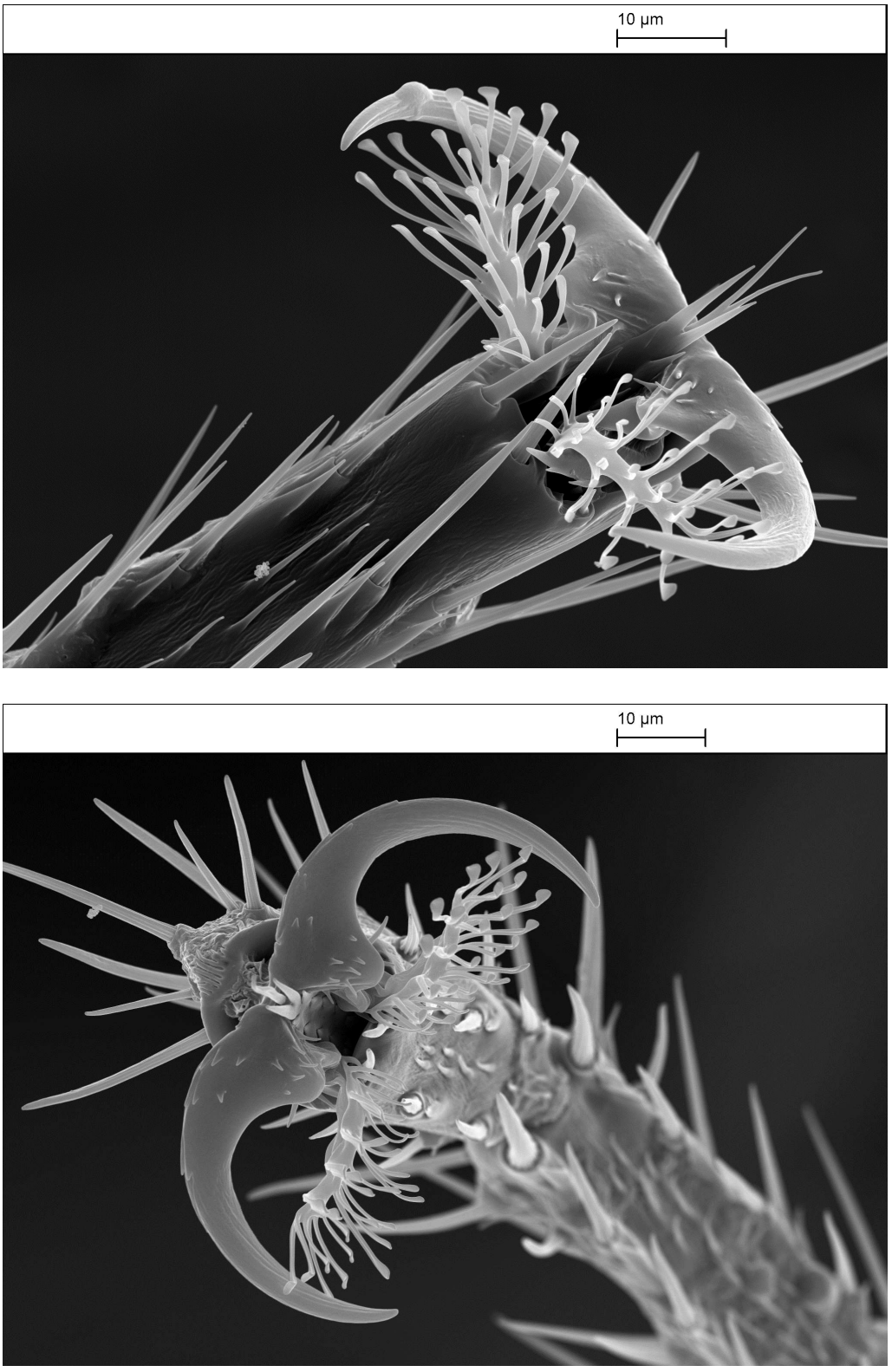

Figure B.0.7: The fruit fly *Drosophila melanogaster* (Diptera: Drosophilidae)

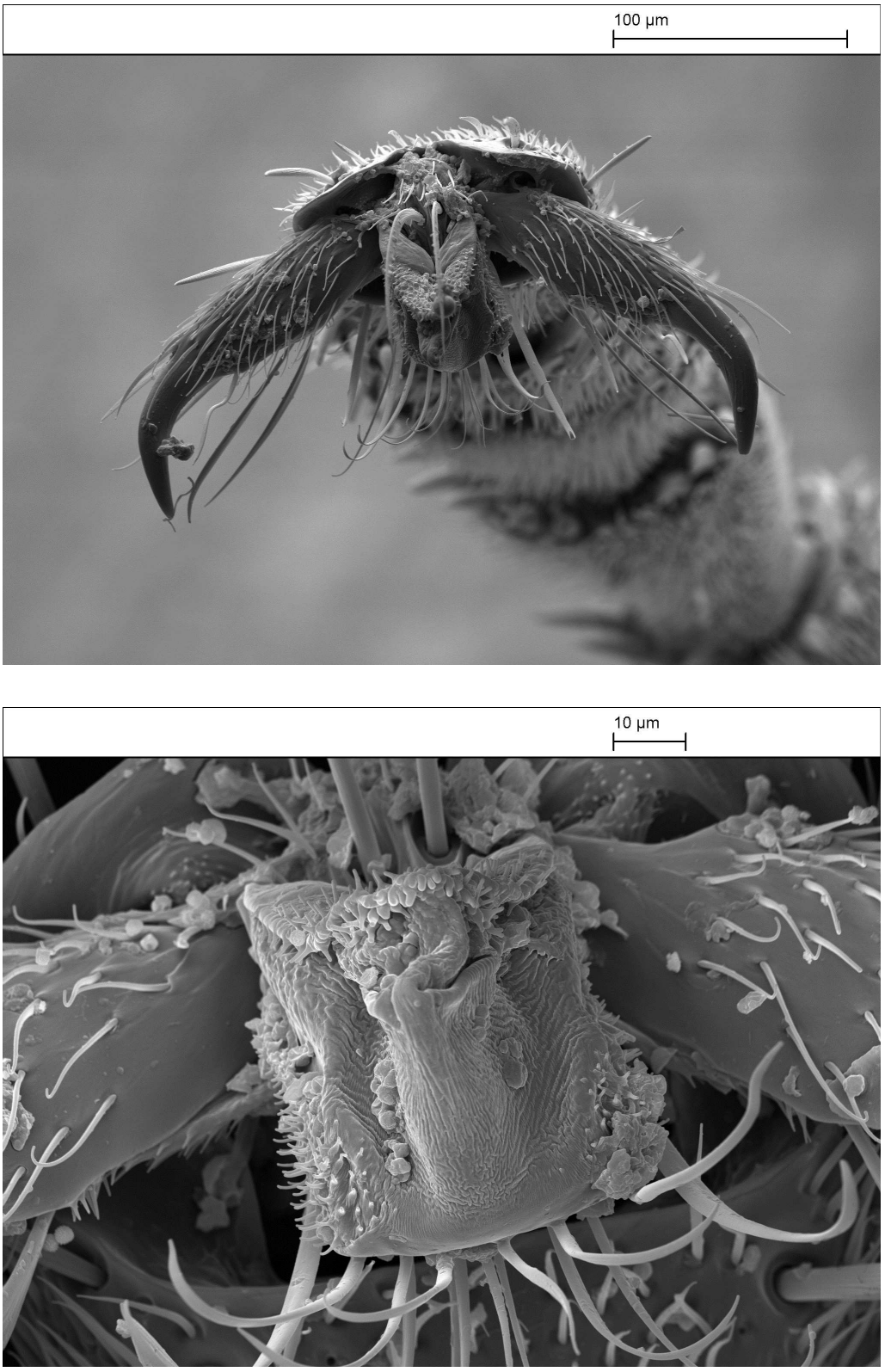

Figure B.0.8: The Weaver ant *Polyrhachis dives* (Hymenoptera: Formicidae)

References

[1] R. Hooke. *Micrographia or, Some Physiological Descriptions of Minute Bodies Made by Magnifying Glasses, With Observations and Inquiries Thereupon.* New York: Dover Publications, 1665.

[2] J. Blackwall. Remarks on the pulvilli of insects. *Transactions of the Linnean Society London*, 16:487–492, 1830.

[3] O. Betz and G. Kolsch. The role of adhesion in prey capture and predator defence in arthropods. *Arthropod Structure & Development*, 33:3–30, 2004. doi: 10.1016/j.asd.2003.10.002.

[4] B. Hölldobler and E.O. Wilson. *The Ants.* Belknap Press of Harvard University Press, 1990.

[5] U. Bauer, H. F. Bohn, and W. Federle. Harmless nectar source or deadly trap: Nepenthes pitchers are activated by rain, condensation and nectar. *Proceedings of the Royal Society B*, 275:259–265, 2008. doi: 10.1098/rspb.2007.1402.

[6] D. Voigt, J. M. Schuppert, S. Dattinger, and S. N. Gorb. Sexual dimorphism in the attachment ability of the Colorado beetle *Leptinotarsa decemlineata* (Coleoptera: Chrysomelidae) to rough substrates. *Journal of Insect Physiology*, 54:765–776, 2008. doi: 10.1016/j.jinsphys.2008.02.006.

[7] L. A. Al Bitar, D. Voigt, C. P. W. Zebitz, and S. N. Gorb. Tarsal morphology and attachment ability of the codling moth *Cydia pomonella* l. (*Lepidoptera*, *Tortricidae*) to smooth surfaces. *Journal of Insect Physiology*, 55:1029–1038, 2009. doi: 10.1016/j.jinsphys.2009.07.008.

[8] L. A. Al Bitar, D. Voigt, C. P. W. Zebitz, and S. N. Gorb. Attachment ability of the codling moth *Cydia pomonella* L. to rough substrates. *Journal of Insect Physiology*, 56:1966–1972, 2010. doi: 10.1016/j.jinsphys.2010.08.021.

[9] D. Li, M.G. Huson, and L.D. Graham. Proteinaceous adhesive secretions from insects, and in particular the egg attachment glue of *Opodiphthera* sp. moths. *Archives of Insect Biochemistry and Physiology*, 69:85–105, 2008.

[10] D. Voigt and S. Gorb. Egg attachment of the asparagus beetle *Crioceris asparagi* to the crystalline waxy surface of *Asparagus officinalis*. *Proceedings of the Royal Society B*, 277: 895–903, 2010.

[11] W. Federle, U. Maschwitz, B. Fiala, M. Riederer, and B. Hölldobler. Slippery ant-plants and skilful climbers: selection and protection of specific ant partners by epicuticular wax blooms in macaranga (Euphorbiaceae). *Oecologia*, 112:217–224, 1997.

[12] W. Federle, M. Riehle, A. S. G. Curtis, and R. J. Full. An integrative study of insect adhesion: mechanics and wet adhesion of pretarsal pads in ants. *Integrative Comparative Biology*, 42: 1100–1106, 2002.

[13] W. Federle, K. Rohrseitz, and B. Hölldobler. Attachment forces of ants measured with a centrifuge : Better 'wax-runners' have a poorer attachment to a smooth surface. *Journal of Experimental Biology*, 203:505–512, 2000.

[14] W. Nachtigall. *Biological Mechanisms of Attachment: The Comparative Morphology and Bioengineering of Organs for Linkage, Suction, and Adhesion.* Springer-Verlag, Berlin, Heidelberg & New York, 1974.

[15] Z. Dai, S. N. Gorb, and U. Schwarz. Roughness-dependent friction force of the tarsal claw system in the beetle *Pachnoda marginata* (Coleoptera: Scarabaeidae). *Journal of Experimental Biology*, 205:2479–2488, 2002. doi: 10.1073/pnas.111139298.

[16] S. Vogel. *Comparative Biomechanics.* Princeton University Press, Princeton, 2003.

[17] M. Scherge and S. N. Gorb. *Biological Micro- and Nano- Tribology, Nature's Solutions*. Springer, Berlin, 2001.

[18] R.M. Alexander. *Principles of Animal Locomotion*. Princeton University Press, Princeton, 2003.

[19] J. von Byern and I. Grunwald, editors. *Biological Adhesive Systems: From Nature to Technical and Medical Application*. Springer Wien, New York, 2010.

[20] W. Federle. Biomechanics of the moveable pretarsal adhesive organ in ants and bees. *Proceedings of National Academy of Science USA*, 98:6215–6220, 2001. doi: 10.1073/pnas.111139298.

[21] W. Vötsch, G. Nicholson, R. Muller, Y.-D. Stierhof, S. Gorb, and U. Schwarz. Chemical composition of the attachment pad secretion of the locust (*Locusta migratoria*). *Insect Biochemistry and Molecular Biology*, 32:1605–1613, 2002.

[22] I. Scholz, W. Baumgartner, and W. Federle. Micromechanics of smooth adhesive organs in stick insects: pads are mechanically anisotropic and softer towards the adhesive surface. *Journal of Comparative Physiology A*, 194:373–384, 2008. doi: 10.1007/s00359-008-0314-6.

[23] P. Perez Goodwyn, A. Peressadko, H. Schwarz, V. Kastner, and S.N. Gorb. Material structure, stiffness, and adhesion: why attachment pads of the grasshopper (*Tettigonia viridissima*) adhere more strongly than those of the locust (*Locusta migratoria*) (Insecta: Orthoptera). *Journal of Comparative Physiology A*, 192: 1233–1243, 2006.

[24] M. G. Langer, J. P. Ruppersberg, and S. N. Gorb. Adhesion forces measured at the level of a terminal plate of the fly's seta. *Proceedings of the Royal Society B*, 271:2209–2215, 2004. doi: 10.1098/rspb.2004.2850.

[25] E. Gorb, D. Voigt, S. D. Eigenbrode, and S. N. Gorb. Attachment force of the beetle *Cryptolaemus montrouzieri* (Coleoptera: Coccinellidae) on leaflet surfaces of mutants of the pea *Pisum sativum* (Fabaceae) with regular and reduced wax coverage. *Arthropod-Plant Interactions*, 2:247–259, 2008. doi: 10.1007/s11829-008-9049-0.

[26] A. B. Kesel, A. Martin, and T. Seidel. Adhesion measurements on the attachment devices of the jumping spider *Evarcha arcuata*. *Journal of Experimental Biology*, 206:2733–2738, 2003.

[27] H. Gao, X. Wang, H. Yao, S. Gorb, and E. Arzt. Mechanics of hierarchical adhesion structures of geckos. *Mechanics of Materials*, 37:275–285, 2005. doi: 10.1016/j.mechmat.2004.03.008.

[28] A.M. Peattie. Functional demands of dynamic biological adhesion: an integrative approach. *Journal of Comparative Physiology B*, 179:231–239, 2009. doi: 10.1007/s00360-008-0310-8.

[29] C. A. Dahlquist. *Treatise on Adhesion and Adhesives, Vol. 2*, chapter Pressure-sensitive adhesives, pages 219–260. Marcel Dekker, 1969.

[30] S. N. Gorb and R. G. Beutel. Evolution of locomotory attachment pads of hexapods. *Naturwissenschaften*, 88:530–534, 2001. doi: 10.1007/s00114-001-0274-y.

[31] F. Haas and S. Gorb. Evolution of locomotory attachment pads in the Dermaptera (Insecta). *Arthropod Structure & Development*, 33:45–66, 2004. doi: 10.1016/j.asd.2003.11.003.

[32] R.G. Beutel and S.N. Gorb. Ultrastructure of attachment specialisations of hexapods (Arthropoda): evolutionary patterns inderred from a revised ordinal phylogeny. *Journal of Zoological Systematics and Evolutionary Research*, 39:177–207, 2001.

[33] L. M. Roth and E. R. Willis. Tarsal structure and climbing ability of cockroaches. *Journal of Experimental Zoology*, 119:483–517, 1952.

[34] N. E. Stork. Experimental analysis of adhesion of *Chrysolina polita* (Chrysomelidae: Coleoptera) on a variety of surfaces. *Journal of Experimental Biology*, 88:91–107, 1980.

[35] S. Ishii. Adhesion of a leaf feeding ladybird *Epilachna vigintioctomaculta* (Coleoptera: Coccinellidae) on a vertically smooth surface. *Appl. Ent. Zool.*, 22:222–228, 1987.

[36] O. Betz. Structure of the tarsi in some stenus species (Coleoptera, Staphylinidae): External morphology, ultrastructure, and tarsal secretion. *Journal of Morphology*, 255:24–43, 2003. doi: 10.1002/jmor.10044.

[37] G. Walker, A. B. Yulf, and J. Ratcliffe. The adhesive organ of the blowfly, *Calliphora vomitoria*: a functional approach (Diptera: Calliphoridae). *Journal of Zoology*, 205:297–307, 1985.

[38] S. Niederegger, S.N. Gorb, and Y. Jiao. Contact behaviour of tenent setae in attachment pads of the blowfly *Calliphora vicinia* (Diptera, Calliphoridae). *Journal of Comparative Physiology A*, 187:961–970, 2002. doi: 10.1007/s00359-001-0265-7.

[39] Y. Jiao, S. Gorb, and M. Scherge. Adhesion measured on the attachment pads of *Tettigonia viridissima* (Orthoptera, Insecta). *Journal of Experimental Biology*, 203:1887–1895, 2000.

[40] W. Federle and T. Endlein. Locomotion and adhesion: dynamic control of adhesive surface contact in ants. *Arthropod Structure & Development*, 33:67–75, 2004. doi: 10.1016/j.asd.2003.11.001.

[41] T. Endlein and W. Federle. Walking in smooth or rough ground: passive control of pretarsal attachment in ants. *Journal of Comparative Physiology A*, 194:49–60, 2008. doi: 10.1007/s00359-007-0287-x.

[42] L.I. Frantsevich and S.N. Gorb. Structure and mechanics of the tarsal chain in the hornet *Vespa crabro* (Hymenoptera: Vespidae): implications on the attacment mechanism. *Arthropod Structure & Development*, 33:77–89, 2004. doi: 10.1016/j.asd.2003.10.003.

[43] R.G. Beutel and S.N. Gorb. Evolutionary scenarios for unusual attachment devices of Phasmatodea and Mantophasmatodea (Insecta). *Systematic Entomology*, 33:501–510, 2008.

[44] S. N. Gorb, R. G. Beutel, E. V. Gorb, Y. Jiao, V. Kastner, S. Niederegger, V. L. Popov, M. Scherge, U. Schwarz, and W. Votsch. Structural design and biomechanics of friction-based releasable attachment devices in insects. *Integrative Comparative Biology*, 42:1127–1139, 2002.

[45] S. Gorb. *Attachment devices of insect cuticle.* Kluwer Academic Publishers, Dordrecht, Boston, 2002.

[46] F. P. Bowden and D. Tabor. *The Friction and Lubrication of Solids.* Oxford Clarendon Press, 1950.

[47] L. Frantsevich and S. Gorb. Arcus as a tensegrity sturcture in the arolium of wasps (Hymenoptera: Vespidae). *Zoology*, 105:225–237, 2002.

[48] S. Gorb and M. Scherge. Biological microtribology: anisotropy in frictional forces of orthopteran attachment pads reflects the ultrastructure of a highly deformable material. *Proceedings of the Royal Society B*, 267:1239–1244, 2000. doi: 10.1098/rspb.2000.1133.

[49] S. N. Gorb. Smooth attachment devices in insects: Functional morphology and biomechanics. *Advanced Insect Physiology*, 34:81–115, 2008. doi: 10.1016/s0065-2806(07)34002-2.

[50] C. J. Clemente, H-H. Dirks, D. R. Barbero, U. Steiner, and W. Federle. Friction ridges in cockroach climbing pads: anisotropy of shear stress measured on transparent, microstructured substrates. *Journal of Comparative Physiology A*, 195:805–814, 2009. doi: 10.1007/s00359-009-0457-0.

[51] S. Gorb, Y. Jiao, and M. Scherge. Ultrastructural architecture and mechanical properties of attachment pads in *Tettigonia viridissima* (Orthoptera Tettigoniidae). *Journal of Comparative Physiology A*, 186:821–831, 2000.

[52] C.J. Clemente and W. Federle. Pushing versus pulling: division of labour between tarsal attachment pads in cockroaches. *Proceedings of the Royal Society B*, 275:1329–1336, 2008. doi: 10.1098/rspb.2007.1660.

[53] T. Eimüller, P. Guttmann, and S.N. Gorb. Terminal contact elements of insect attachment devices studied by transmission x-ray microscopy. *Journal of Experimental Biology*, 211: 1958–1963, 2008. doi: 10.1242/jeb.014308.

[54] S. Gorb. *Attachment Devices of Insect Cuticle*. Kluwer Academic Publishers, Dordrecht, 2001.

[55] E.V. Gorb and S.N. Gorb. Attachment ability of the beetle *Chrysolina fastuosa* on various plant surfaces. *Entomologia Experimentalis et Applicata*, 105:13–28, 2002.

[56] N. Hosoda and S. Gorb. Friction force reduction triggers foot grooming behaviour in beetles. *Proceedings of the Royal Society B*, 278:1748–1752, 2011. doi: 10.1098/rspb.2010.1772.

[57] K. Autumn, C. Majidi, R. E. Groff, A. Dittmore, and R. Fearing. Effective elastic modulus of isolated gecko setal arrays. *Journal of Experimental Biology*, 209:3558–3568, 2006. doi: 10.1242/jeb.02469.

[58] A.M. Peattie, C. Majidi, A. Corder, and R.J. Full. Ancestrally high elastic modulus of gecko setal beta-keratin. *Journal of the Royal Society Interface*, 4:1071–1076, 2007. doi: 10.1098/rsif.2007.0226.

[59] W. Federle. Why are so many adhesive pads hairy? *Journal of Experimental Biology*, 209: 2611–2621, 2006. doi: 10.1242/jeb.02323.

[60] G. Huber, H. Mantz, R. Spolenak, K. Mecke, K. Jacobs, S.N. Gorb, and E. Arzt. Evidence for capillarity contributions to gecko adhesion from single spatula nanomechanical measurements. *Proceedings of National Academy of Science USA*, 102:16293–16296, 2005. doi: 10.1073/pnas.0506328102.

[61] T.W. Kim and B. Bhushan. The adhesion model considering capillarity for gecko attachment system. *Journal of the Royal Society Interface*, 5:319–327, 2008. doi: 10.1098/rsif.2007.1078.

[62] P.Y. Hsu, L. Ge, X. Li, A.Y. Stark, C. Wesdemiotis, P.H. Niewiarowski, and D. Dhinojwala. Direct evidence of phospholipids in gecko footprints and spatula-substrate contact interface detected using surface-sensitive spectroscopy. *Journal of the Royal Society Interface*, Published online, 2011. doi: 10.1098/rsif.2011.0370.

[63] V. B. Wigglesworth. *The Principles of Insect Physiology*. Chapman and Hall, London, 1972.

[64] V. B. Wigglesworth. How does a fly cling to the under surface of a glass sheet? *Journal of Experimental Biology*, 129:373–376, 1987.

[65] A. D. Lees and J. Hardie. The organs of adhesion in the aphid *Megoura viciae*. *Journal of Experimental Biology*, 136:209–228, 1988.

[66] A.F.G. Dixon, P.C. Grogan, and R.P. Gowing. The mechanism by which aphids adhere to smooth surfaces. *Journal of Experimental Biology*, 152:243–253, 1990.

[67] J.S. Edwards and M. Tarkanian. The adhesive pads of heteroptera: a re-examination. *Proceedings of the Royal Entomological Society London*, A45(1-3):1–5, 1970.

[68] P. Drechsler and W. Federle. Biomechanics of smooth adhesive pads in insects: influence of tarsal secretion on attachment performance. *Journal of Comparative Physiology A*, 192: 1213–1222, 2006. doi: 10.1007/s00359-006-0150-5.

[69] G. Walker. Adhesion to smooth surfaces by insects - a review. *Int. J. Adh & Adh*, 13:3–7, 1993.

[70] S. N. Gorb. The design of the fly adhesive pad: distal tenent setae are adapted to the delivery of an adhesive secretion. *Proceedings of the Royal Society B*, 265:747–752, 1998.

[71] W. J. P. Barnes, J. Smith, C. Oines, and R. Mundl. Bionics and wet grip. *Tire Technol. Int.*, pages 56–60, 2002.

[72] S. F. Geiselhardt, W. Federle, B. Prum, S. Geiselhardt, S. Lamm, and K. Peschke. Impact of chemical manipulation of tarsal liquids on attachment in the colorado potato beetle, *Leptinotarsa decemlineata*. *Journal of Insect Physiology*, 56:398–404, 2010.

[73] S. Martin and F. Drijfhout. A review of ant hydrocarbons. *Journal of Chemical Ecology*, 35: 1151–1161, 2009. doi: 10.1007/s10886-009-9695-4.

[74] A. Kosaki and R. Yamaoka. Chemical composition of footprints and cuticular lipids of three species of lady beetles. *Japanese Journal of Applied Entomology & Zoology*, 40:47–53, 1996.

[75] A.B. Attygale, D.J. Aneshansley, J. Meinwald, and T. Eisner. Defense by foot adhesion in a chrysomelid beetle *Hemisphaerota cyanea*: Characterization of the adhesive oil. *Zoology*, 103:1–6, 2000.

[76] F.C. Adballa, G.R. Jones, E.D. Morgan, and C. da Cruz-Landim. Comparative study of the cuticular hydrocarbon composition of *Melipona bicolor* Lepeletier, 1836 (Hymenoptera, Meliponini) workers and queens. *Genetics and Molecular Research*, 2:191–199, 2003.

[77] S. F. Geiselhardt, S. Geiselhardt, and K. Peschke. Congruence of epicuticular hydrocarbons and tarsal secretions as a principle in beetles. *Chemoecology*, 21:181–186, 2011. doi: 10.1007/s00049-011-0077-3.

[78] J.W.L. Beament. The cuticular lipoids of insects. *Journal of Experimental Biology*, 21: 115–131, 1945.

[79] M.W. Holdgate. Transpiration through the cuticles of some aquatic insects. *Journal of Experimental Biology*, 33:107–118, 1956.

[80] A.G. Gibbs. Water-proofing properties of cuticular lipids. *American Zoology*, 38:471–482, 1998.

[81] B.D. Jackson and E.D. Morgan. Insect chemical communication: phereomones and exocrine glands of ants. *Chemoecology*, 4:125–144, 1993.

[82] E. Provost, O. Blight, A. Tirard, and M. Renucci. *Insect Physiology: New Research*, chapter 1 - Hydrocarbons and insects' social physiology, pages 19–72. Nova Science Publishers Inc., 2008.

[83] B. Hölldobler and E.O. Wilson. *The Superorganism: The Beauty, Elegance, and Strangeness of Insect Societies*. W. W. Norton and Company, New York, 2009.

[84] S. F. Geiselhardt, S. Geiselhardt, and K. Peschke. Comparison of tarsal and cuticular chemistry in the leaf beetle *Gastrophysa viridula* (Coleoptera: Chrysomelidae) and an evaluation of solid-phase microextraction and solvent extraction techniques. *Chemoecology*, 19:185–193, 2009. doi: 10.1007/s00049-009-0021-y.

[85] I. Hasenfuss. The adhesive devices in larvae of Lepitoptera (Insecta, Pterygota). *Zoomorphology*, 119:143–162, 1999.

[86] S. N. Gorb, D. Voigt, and E. V. Gorb. Visualisation of small fluid droplets on biological and artificial surfaces using the cryo-sem approach. In A. Mendez-Vilas and J. Diaz, editors, *Modern Research and Educational Topics in Microscopy*, pages 812–819. Formatex, 2007.

[87] M. Sundberg, A. Månsson, and S. Tågerud. Contact angle measurements by confocal microscopy for non-destructive microscale surface characterization. *Journal of Colloid Interface Science*, 313:454–460, 2007.

[88] E. Bauchhenß. Die pulvillen von *Calliphora erythrocephala* (Diptera, Brachycera) als adhäsionsorgane. *Zoomorphologie*, 93:99–123, 1979.

[89] H. Peisker and S.N. Gorb. Evaporation dynamics of tarsal liquid footprints in flies (*Calliphora vicina*) and beetles (*Coccinella septempunctata*). *Journal of Experimental Biology*, 215:1266–1271, 2012.

[90] J-H. Dirks, C.J. Clemente, and W. Federle. Insect tricks: two phasic foot pad secretion prevents slipping. *Journal of the Royal Society Interface*, 7:587–593, 2010. doi: 10.1098/rsif.2009.0308.

[91] O. Betz. *Biological Adhesive Systems: From Nature to Technical and Medical Application*, chapter 8 - Adhesive exocrine glands in insects: Morphology, ultrastructure, and adhesive secretion, pages 111–152. Springer Wien, New York, 2010.

[92] J-H. Dirks and W. Federle. Mechanisms of fluid production in smooth adhesive pads of insects. *Journal of the Royal Society Interface*, 8:952–960, 2011. doi: 10.1098/rsif.2010.0575.

[93] K. Autumn and A.M. Peattie. Mechanisms of adhesion in geckos. *Integrative Comparative Biology*, 42:1081–1090, 2002.

[94] C. Mathew Mate. *Tribology on the Small Scale - A Bottom Up Approach to Friction, Lubrication and Wear*. Oxford University Press Inc, New York, 2008.

[95] J. Israelachvili. *Intermolecular & Surface Forces 2nd Edition*. Academic Press, London, 1991.

[96] L.A. Girifalco and R.J. Good. A theory for the estimation of surface and interfacial energies. i. derivation and application to interfacial tension. *Journal of Physical Chemistry*, 61:904–909, 1957.

[97] R. J. Good and L. A. Girifalco. A theory for the estimation of surface and interfacial energies. iii. estimation of surface energies of solids from contact angle data. *Journal of Physical Chemistry*, 64:561–565, 1960. doi: 10.1021/j100834a012.

[98] M. Müller, L.G. MacDowell, P. Müller-Buschbaum, O. Wunnike, and M. Stamm. Nanodewetting: Interplay between van der waals- and short-ranged interactions. *Journal of Chemical Physics*, 115:9960–9969, 2001.

[99] Q. Li, V. Rudolph, B. Weigl, and A. Earl. Interparticle van der waals force in powder flowability and compactibility. *International Journal of Pharmaceutics*, 280:77–93, 2004. doi: 10.1016/j.ijpharm.2004.05.001.

[100] A.A. Griffith. The phenomena of rupture and flow in solids. *Philosophical Transactions of the Royal Society A*, 221:163–198, 1921.

[101] H. Gao, B. Ji, I.J. Jäger, E. Arzt, and P. Fratzl. Materials becomes insensitive to flaws at nanoscale: Lessons from nature. *Proceedings of National Academy of Science USA*, 100: 5597–5600, 2003.

[102] M.J. Buehler, H. Yao, H. Gao, , and B. Ji. Cracking and adhesion at small scales: atomistic and continuum studies of flaw tolerant nanostructures. *Modelling and Simulation in Materials Science and Engineering*, 14:799–816, 2006. doi: 10.1088/0965-0393/14/5/001.

[103] H. Gao, B. Ji, M.J. Buehler, and H. Yao. Flaw tolerant nanostructures of biological materials - proceedings of the 21st ictam. In W. Gutowski and T.A. Kowalewski, editors, *Mechanics of the 21st Century*, pages 131–138. Springer, 2005. doi: 10.1007/1-4020-3559-4_7. URL `http://www.springerlink.com/content/978-1-4020-3456-5/`.

[104] E. Arzt. Biological and artificial attachment devices: Lessons for materials scientists from flies and geckos. *Materials Science and Engineering C*, 26:1245–1250, 2006. doi: 10.1016/j.msec.2005.08.033.

[105] B. V. Derjaguin, V. M. Muller, and Y. P. Toporov. Effect of contact deformations on the adhesion of particles. *Journal of Colloid Interface Science*, 53:314–326, 1975.

[106] K. L. Johnson, K. Kendall, and A. D. Roberts. Surface energy and the contact of elastic solids. *Proceedings of the Royal Society A*, 324:301–313, 1971.

[107] D. J. Maugis. Adhesion of spheres: The JKR-DMT transition using a Dugdale model. *Journal of Colloid Interface Science*, 150:243–269, 1992.

[108] H.J. Butt, W.J.P. Barnes, A. del Campo, M. Kappl, and Schönfeld. Capillary forces between soft, elastic spheres. *Soft Matter*, 6:5930–5963, 2010. doi: 10.1039/c0sm00455c.

[109] W. J. P. Barnes. Functional morphology and design constraints of smooth adhesive pads. *MRS Bulletin*, 32:479–485, 2007. doi: 10.1557/mrs2007.81.

[110] J. Stefan. Versuche ber die scheinbare adhäsion. *Annalen der Physik und Chemie*, 230: 316–318, 1875.

[111] B.J. Ennis, G. Tardos, and R. Pfeffer. A microlevel-based characterization of granulation phenomena. *Powder Technology*, 65:257–272, 1991.

[112] A. Fingerle and S. Herminghaus. Mechanisms of dissipation in wet granular matter. *arXiv*, arXiv:0708.2597v1 [cond-mat.soft], 2007. URL `http://arxiv.org/abs/0708.2597`.

[113] C.-Y. Hui, N. J. Glassmaker, T. Tang, and A. Jagota. Design of biomimetic fibrillar interfaces: 2. Mechanics of enhanced adhesion. *Journal of the Royal Society Interface*, 1:35–48, 2004. doi: 10.1098/rsif.2004.0005.

[114] David R. Lide. *CRC Handbook of Chemistry and Physics, 88th Edition (CD-ROM Version 2008)*. CRC Press/Taylor and Francis, Boca Raton, FL., 2008.

[115] K. A. Grosch. The relation between the friction and visco-elastic properties of rubber. *Proceedings of the Royal Society A*, 274:21–39, 1963.

[116] M. Barquins and A. D. Roberts. Rubber friction variation with rate and temperature: some new observations. *Journal of Physics D: Applied Physics*, 19:547–563, 1986. URL `http://iopscience.iop.org/0022-3727/19/4/010`.

[117] B. N. J. Persson. On the theory of rubber friction. *Surface Science*, 401:445–454, 1998.

[118] J.O. Wolff and S.N. Gorb. The influence of humidity on the attachment ability of the spider *Philodromus dispar* (Araneae, Philodromidae). *Proceedings of the Royal Society B*, 279: 139–143, 2011. doi: 10.1098/rspb.2011.0505.

[119] A. van Casteren and J.R. Codd. Foot morphology and substrate adhesion in the madagascan hissing cockroach, *Gromphadorhina portentosa*. *Journal of Insect Science*, 10:1–12, 2010. doi: 10.1673/031.010.4001. URL `http://www.bioone.org/doi/full/10.1673/031.010.4001`.

[120] J. M. R. Bullock, P. Drechsler, and W. Federle. Comparison of smooth and hairy attachment pads in insects: friction, adhesion and mechanisms for direction-dependence. *Journal of Experimental Biology*, 211:3333–3343, 2008. doi: 10.1242/jeb.020941.

[121] A.B. Kesel, A. Martin, and T. Seidel. Getting a grip on spider attachment: an AFM approach to microstrucure adhesion in arthropods. *Smart Materials and Structures*, 13:512–518, 2004. doi: 10.1088/0964-1726/13/3/009.

[122] E.L. Brainerd. Adhesion force of ants on smooth surfaces. *Amer. Zool.*, 34:128A, 1994.

[123] I. Scholz, M. Bückins, L. Dolge, T. Erlinghagen, A. Weth, F. Hischen, J. Mayer, S. Hoffman, M. Reiederer, M. Riedel, and W. Baumgartner. Slippery surfaces of pitcher plants: *Nepenthes* wax crystals minimize insect attachment *via* microscopic surface roughness. *Journal of Experimental Biology*, 213:1115–1125, 2010.

[124] E. Gorb, K. Haas, A. Henrich, S. Enders, N. Barbakadze, and S. Gorb. Composite structure of the crystalline epicuticular wax layer of the slippery zone in the pitchers of the carnivorous plant *Nepenthes alata* and its effect on insect attachment. *Journal of Experimental Biology*, 208:4651–4662, 2005. doi: 10.1242/jeb.01939.

[125] E. Gorb and S. Gorb. Effects of surface topography and chemistry of *Rumex obstudifolius* leaves on the attachment of the beetle *Gastrophysa viridula*. *Entomologia Experimentalis et Applicata*, 130:222–228, 2009. doi: 10.1111/j.1570-7458.2008.00806.x.

[126] W. Barthlott, C. Neinhuis, D. Cutler, F. Ditsch, I. Meusel, I. Theisen, and H Wilhelmi. Classification and terminology of plant epicuticular waxes. *Botanical Journal of the Linnean Society*, 126:237–260, 1998.

[127] R. Spolenak, S. Gorb, and E. Arzt. Adhesion design maps for bio-inspired attachment systems. *Acta Biomaterialia*, 1:5–13, 2005.

[128] A. del Campo, Greiner. C., and E. Arzt. Contact shape controls adhesion of bioinspired fribrillar surfaces. *Langmuir*, 23:10235–10243, 2007. doi: 10.1021/la7010502.

[129] S. N. Gorb and M. Varenberg. Mushroom-shaped geometry of contact elements in biological adhesive systems. *J. Adh. Sci. Technol.*, 21:1175–1183, 2007.

[130] J. M. R. Bullock and W. Federle. Division of labour and sex differences between fibrillar, tarsal adhesive pads in beetles: effective elastic modulus and attachment performance. *Journal of Experimental Biology*, 212:1876–1888, 2009. doi: 10.1242/jeb.030551.

[131] K. Koch and H-J. Ensikat. The hydrophobic coatings of plant surfaces: Epicuticular wax crystals and their morphologies, crystallinity and molecular self-assembly. *Micron*, 39:759–772, 2008. doi: 10.1016/j.micron.2007.11.010.

[132] F. Haas and I. Rentschler. Discrimination between epicuticular and intracuticular wax in blackberry leaves: Ultrastructural and chemical evidence. *Plant Science Letters*, 36:143–147, 1984.

[133] O. Guhling, C. Kinzler, M. Dreyer, G. Bringmann, and R. Jetter. Surface composition of myrmecophilic plants: cuticular wax and glandular trichomes on leaves of *Macaranga*. *Journal of Chemical Ecology*, 31:2323–2341, 2005. doi: 10.1007/s10886-005-7104-1.

[134] S. Eigenbrode. The effects of plant epicuticular waxy blooms on attachment and effectiveness of predatory insects. *Arthropod Structure & Development*, 33:91–102, 2004.

[135] L. Gaume, P. Perret, E. Gorb, S. Gorb, J.-J. Labat, and N. Rowe. How do plant waxes cause flies to slide? Experimental tests of wax-based trapping mechanisms in three pitfall carnivorous plants. *Arthropod Structure & Development*, 33:103–111, 2004.

[136] F. Borodich, E. Gorb, and S. Gorb. Fracture behaviour of plant epicuticular wax crystals and its role in preventing insect attachment: a theoretical approach. *Applied Physics A*, 100: 63–71, 2010. doi: 10.1007/s00339-010-5794-x.

[137] C. Markstädter, W. Federle, R. Jetter, M. Riederer, and B. Hölldobler. Chemical composition of the slippery epicuticular wax blooms on Macaranga (Euphorbiaceae) ant-plants. *Chemoecology*, 10:33–40, 2000.

[138] T. Eisner and D. J. Aneshansley. Defense by foot adhesion in a beetle (*Hemisphaerota cyanea*). *Proceedings of National Academy of Science USA*, 97:6568–6573, 2000.

[139] E. V. Gorb and S. N. Gorb. *Ecology and Biomechanics - A Mechanical Appoach to the Ecology of Animals and Plants*, chapter 7 - Do plant waxes make insect attachment structures dirty? Experimental evidence for the contamination hypothesis. CRC Taylor & Francis, 2006.

[140] E.V. Gorb, N. Hosoda, C. Miksch, and S.N. Gorb. Slippery pores: anti-adhesive effect of nanoporous substrates on the beetle attachment system. *Journal of the Royal Society Interface*, 7:1571–1579, 2010. doi: 10.1098/rsif.2010.0081.

[141] L. Gaume, S. Gorb, and N. Rowe. Function of epidermal surfaces in the trapping efficiency of *Nepenthes alata* pitchers. *New Phytologist*, 156:479–489, 2002.

[142] D. M. Glenn, G. J. Puterka, T. Vanderzwet, R. E. Byers, and C. Feldhake. Hydrophobic particle films: A new paradigm for suppression of arthropod pests and plant diseases. *Journal of Economic Entomology*, 92:759–771, 1999.

[143] B. Fiala, U. Maschwitz, and K. E. Linsenmair. *Macaranga caladiifolia*, a new type of ant-plant among southeast asian myrmecophytic *Macaranga* species. *Biotropica*, 28:408–412, 1996.

[144] T. Merton. On a barrier against insects. *Proceedings of the Royal Society A*, 234:218–220, 1956.

[145] H. V. A. Briscoe. Some new properties of inorganic dusts. *J. R. Soc. Arts.*, 91:593–607, 1943.

[146] P. Alexander, J. A. Kitchener, and H. V. A. Briscoe. Inert dust insecticides. *Ann Appl Biol.*, 31:143–159, 1944.

[147] G. Boiteau, Y Pelletier, G. C. Misener, and G. Bernard. Development and evaluation of a plastic trench barrier for protection of potato from walking adult Colorado potato beetles (Coleoptera: Chrysomelidae). *Journal of Economic Entomology*, 87:1325–1331, 1994.

[148] D. Hunt and R. Vernon. Portable trench barrier for protecting edges of tomato fields from Colorado potato beetles (Coleoptera: Chrysomelidae). *Journal of Economic Entomology*, 94: 204–207, 2001.

[149] C.J. Clemente, J.M.R. Bullock, A. Beale, and W. Federle. Evidence for self-cleaning in fluid based smooth and hairy adhesive systems of insects. *Journal of Experimental Biology*, 213: 635–642, 2010. doi: 10.1242/jeb.038232.

[150] M. J. Orchard, M.M. Kohonen, and S. Humphries. The influence of surface energy on the self-cleaning of insect adhesive devices. *Journal of Experimental Biology*, 215:279–286, 2012.

[151] W.R. Hansen and K. Autumn. Evidence for self-cleaning in gecko setae. *Proceedings of National Academy of Science USA*, 102:358–389, 2005. doi: 10.1073/pnas.0408304102.

[152] J. Lee and R. S. Fearing. Contact self-cleaning of synthetic gecko adhesive from polymer microfibres. *Langmuir*, 24:10587–10591, 2008. doi: 10.1021/la8021485.

[153] P. Kevan and M. Lane. Flower petal microtexture is a tactile cue for bees. *Proceedings of National Academy of Science USA*, 82:4750–4752, 1985.

[154] D. J. Crook, L. M. Kerr, and V. C. Mastro. Sensilla on the antennal flagellum of *Sirex noctilio* (hymenoptera: Siricidae). *Ent. Soc. Am.*, 101:1094–1102, 2008.

[155] A. Bernadou and V. Fourcassie. Does substrate coarseness matter for foraging ants? an experiment with *Lasius niger* (Hymenoptera; Formicidae). *Journal of Insect Physiology*, 54:534–542, 2008. doi: 10.1016/j.jinsphys.2007.12.001.

[156] A. Bernadou, F. Démares, T. Couret-Fauvel, J.C. Sandoz, and M. Gauthier. Effect of fipronil on side-specific antennal tactile learning in the honeybee. *J. Ins. Physiol.*, 55:1099–1106, 2009.

[157] J. M. Camhi and E. N. Johnson. High-frequency steering maneuvers mediated by tactile cues: antennal wall-following in the cockroach. *Journal of Experimental Biology*, 202:631–643, 1999.

[158] H.J. Ensikat, P. Ditsche-Kuru, C. Neinhuis, and W. Barthlott. Superhydrophobicity in perfection: the outstanding properties of the lotus leaf. *Beilstein J. Nanotechnol.*, 2:152–161, 2011. doi: 10.3762/bjnano.2.19.

[159] A. Solga, Z. Cerman, B.F. Striffler, M. Spaeth, and W. Barthlott. The dream of staying clean: Lotus and biomimetic surfaces. *Bioinsp. Biomim.*, 2:S126–S134, 2007. doi: 10.1088/1748-3182/2/4/S02.

[160] W.E. Ward. The lotus symbol: Its meaning in buddhist art and philosophy. *Journal of Aesthetics and Art Criticism*, 11:135–146, 1952. URL `http://www.jstor.org/stable/426039`.

[161] T.G. Rochow and E.G. Rochow. *An Introduction to Microscopy by Means of Light, Electrons, X-rays, or Ultrasound*. Plenum Press, New York, 1978.

[162] W. Barthlott and C. Neinhuis. Purity of the sacred lotus, or escape from contamination in biological surfaces. *Planta*, 202:1–8, 1997.

[163] L. Feng, Y. Zhang, J. Xi, Y. Zhu, N. Wang, F. Xia, and L. Jiang. Petal effect: A superhydrophobic state with high adhesive force. *Langmuir*, 24:4114–4119, 2008. doi: 10.1021/la703821h.

[164] K. Koch, B. Bhushan, and W. Barthlott. Multifunctional surface structures of plants : An inspiration for biomimetics. *Prog. Mater. Sci.*, 54:137–178, 2009. doi: 10.1016/j.pmatsci.2008.07.003.

[165] H.J. Lee, C.R. Willis, and C.A. Stone. Modeling and preparation of a super-oleophobic non-woven fabric. *Journal of Material Science*, 46:3907–3913, 2011. doi: 10.1007/s10853-011-5314-1.

[166] G.D. Bixler and B. Bhushan. Biofouling: lessons from nature. *Philosophical Transactions of the Royal Society A*, 370:2381–2417, 2012.

[167] X. Feng and L. Jiang. Design and creation of superwetting/antiwetting surfaces. *Advanced Materials*, 18:3063–3078, 2006. doi: 10.1002/adma.200501961.

[168] B. Bhushan and Y.C. Jung. Wetting, adhesion and friction of superhydrophobic and hydrophilic leaves and fabricated micro/nanopatterned surfaces. *J. Phys. Condens. Matter*, 20:225010, 2008. doi: 10.1088/0953-8984/20/22/225010.

[169] K. Koch and W. Barthlott. Superhydrophobic and superhydrophilic plant surfaces: an inspiration for biomimetic materials. *Philosophical Transactions of the Royal Society A*, 367:1487–1509, 2009. doi: 10.1098/rsta.2009.0022.

[170] W. Chen, A.Y. Fadeev, M.C. Hsieh, D. Öner, J. Youngblood, and T.J. McCarthy. Ultrahydrophobic and ultralyophobic surfaces: Some comments and examples. *Langmuir*, 15:3395–3399, 1999. doi: 10.1021/la990074s.

[171] K. Autumn and W. Hansen. Ultrahydrophobicity indicates a non-adhesive default state in gecko setae. *J. Comp. Physiol. A*, 192:1205–1212, 2006. doi: 10.1007/s00359-006-0149-y.

[172] H.Y. Erbil. *Surface Chemistry of Solid and Liquid Interfaces.* Blackwell Publishing Ltd, 2006.

[173] A.B.D. Cassie and S. Baxter. Wettability of porous surfaces. *Transactions of the Faraday Society*, 40:546–551, 1944.

[174] R. Blossey. Self-cleaning surfaces - virtual realities. *Nature Materials*, 2:301–306, 2003.

[175] L. Gao and T.J. McCarthy. The "lotus effect" explained: Two reasons why two length scales of topography are important. *Langmuir*, 22:2966–2967, 2006. doi: 10.1021/la0532149.

[176] Z. Burton and B. Bhushan. Surface characterization and adhesion and friction properties of hydrophobic leaf surfaces. *Ultramicroscopy*, 106:709–719, 2006.

[177] E.V. Gorb and S.N. Gorb. *Functional Surfaces in Biology - Adhesion Related Phenomena Vol.2*, chapter 8 - Functional surfaces in the pitcher of the carnivorous plant *Nepenthes alata*: A cryo-SEM approach, pages 205–238. Springer, 2009.

[178] L. Wang, Q. Zhou, Y. Zheng, and S. Xu. Composite structure and properties of the pitcher surface of the carnivorous plant *Nepenthes* and its influence on the insect attachment system. *Prog. Nat. Sci*, 19:1657–1664, 2009. doi: 10.1016/j.pnsc.2009.09.005.

[179] U. Bauer, C.J. Clemente, T. Renner, and W. Federle. Form follows function: morphological diversification and alternative trapping strategies in carnivorous *Nepenthes* pitcher plants. *Journal of Evolutionary Biology*, 25:90–102, 2012. doi: 10.1111/j.1420-9101.2011.02406.x.

[180] E.V. Gorb and S.N. Gorb. Physicochemical properties of functional surfaces in pitchers of the carnivorous plant *Nepenthes alata* Blanco (Nepenthaceae). *Plant Biology*, 8:841–848, 2006. doi: 10.1055/s-2006-923929.

[181] H. B. Bohn and W. Federle. Insect aquaplaning: *Nepenthes* pitcher plants capture prey with the peristome, a fully wettable water-lubricated anisotropic surface. *Proceedings of National Academy of Science USA*, 101:14138–14143, 2004. doi: 10.1073/pnas.0405885101.

[182] B. Bhushan. Adhesion and stiction: Mechanics, measurement techniques, and methods for reduction. *J. Vac. Sci. Technol. B.*, 21:2262–2296, 2003.

[183] W. Federle, W. Baumgartner, and B. Hölldobler. Biomechanics of ant adhesive pads: frictional forces are rate- and temperature- dependent. *Journal of Experimental Biology*, 206: 67–74, 2004. doi: 10.1242/jeb.00716.

[184] M. Majerus and P. Kearns. *Ladybirds (Naturalists' Handbooks 10)*. Richmond Publishing, Slough, UK, 1989.

[185] W.S Rasband. ImageJ 1.40, 1997–2009. URL `http://rsb.info.nih.gov/ij/`. Accessed 20/9/2008.

[186] A. Y. Fadeev and Y. V. Kazakevich. Covalently attached monolayers of oligo(dimethylsiloxane)s on silica: A siloxane chemistry approach for surface modification. *Langmuir*, 18:2665–2672, 2002.

[187] K. W. Stöckelhuber, B. Radoev, and H. J. Schulze. Some new observations on line tension of microscopic droplets. *Colloids Surface A.*, 156:323–333, 1999.

[188] M. Dandon and H. Y. Erbil. Evaporation rate of graphite liquid marbles: Comparison with water droplets. *Langmuir*, 25:8362–8367, 2009.

[189] P. G. de Gennes, F. Brochard-Wyart, and D. Quere. *Capillarity and Wetting Phenomena; Drops, Bubbles, Pearls, Waves*. Springer, 2004.

[190] C. Redon, F. Brochard-Wyart, and F. Rondalez. Dynamics of dewetting. *Physical Review Letters*, 66:715–718, 1991.

[191] T. Stifter, O. Marti, and B. Bhushan. Theoretical investigation of the distance dependence of capillary and van der waals forces in scanning force microscopy. *Physical Review B*, 62: 13667–13673, 2000. doi: 10.1103/PhysRevB.62.13667.

[192] E. Arzt, S. N. Gorb, and R. Spolenak. From micro to nano contacts in biological attachment devices. *Proc. Natl. Acad. Sci. USA*, 100:10603–10606, 2003.

[193] D. Gladun, S. N. Gorb, and L. Frantsevich. *Functional Surfaces in Biology - Adhesion related phenomena Vol. 2*, chapter 3 - Alternative tasks of the insect arolium with special reference to Hymenoptera, pages 67–103. Springer, 2009.

[194] J. M. R. Bullock and W. Federle. Beetle adhesive hairs differ in stiffness and stickiness: in vivo adhesion measurements on individual setae. *Naturwissenschaften*, 98:381–387, 2011. doi: 10.1007/s00114-011-0781-4.

[195] A. Gibbs and J.G. Pomonis. Physical properties of insect cuticular hydrocarbons: The effects of chain length, methyl-branching and unsaturation. *Comparative Biochemistry & Physiology*, 112B:243–249, 1995.

[196] G. J. Blomquist and A-G. Bagneres, editors. *Insect Hydrocarbons: Biology, Biochemistry, and Chemical Ecology*. Cambridge University Press, 2010.

[197] B. Brei, J. D. Edman, B. Gerade, and J. M. Clark. Relative abundance of two cuticular hydrocarbons indicates whether a mosquito is old enough to transmit malaria parasites. *Journal of Medical Entomology*, 41:807–809, 2004. doi: 10.1603/0022-2585-41.4.807.

[198] S.F. Geiselhardt, S. Lamm, C. Gack, and K. Peschke. Interaction of liquid epicuticular hydrocarbons and tarsal adhesive secretion in *Leptinotarsa decemlineata* say (coleoptera: Chrysomelidae). *Journal of Comparative Physiology A*, 196:369–378, 2010. doi: 10.1007/s00359-010-0522-8.

[199] B. Abou, C. Gay, B. Laurent, O. Cardoso, D. Voigt, H. Peisker, and S. N. Gorb. Extensive collection of femtoliter pad secretion droplets in beetle *Leptinotarsa decemlineata* allows nanoliter microrheology. *Journal of the Royal Society Interface*, 7:1745–1752, 2010. doi: 10.1098/rsif.2010.0075.

[200] A. G. Cunha, S. C. M. Fernandes, C. S. R. Freire, A. J. D. Silvestre, C. P. Neto, and A. Gandini. What is the real value of chitosans's surface energy? *Biomacromolecules*, 9: 610–614, 2008. doi: 10.1021/bm701199g.

[201] S. N. Gorb and E. V. Gorb. Ontogenesis of the attachment ability in the bug *Coreus margiatus* (Heteroptera, Insecta). *Journal of Experimental Biology*, 207:2917–2924, 2004. doi: 10.1242/jeb.01127.

[202] D. Voigt, J. M. Schuppert, S. Dattinger, and S. N. Gorb. Temporary stay at various environmental humidities affects attachment ability of Colorado potato beetles *Leptinotarsa decemlineata* (Coleoptera, Chrysomelidae). *Zoology*, 281:227–231, 2010. doi: 10.1111/j.1469-7998.2010.00704.x.

[203] D. Voigt and S. N. Gorb. Attachment ability of sawfly larvae to smooth surfaces. *Arthropod Structure & Development*, 41:145–153, 2012.

[204] K. Autumn and N. Gravish. Gecko adhesion: evolutionary nanotechnology. *Philosophical Transactions of the Royal Society A*, 366:1575–1590, 2008. doi: 10.1098/rsta.2007.2173.

[205] H. M. Princen and A. D. Kiss. Rheology of foams and highly concentrated emulsions: IV. An experimental study of the shear viscosity and yield stress of concentrated emulsions. *Journal of Colloid Interface Science*, 128:176–187, 1989.

[206] D. M. A. Buzza and M. E. Cates. Uniaxial elastic modulus of concentrated emulsions. *Langmuir*, 10:4503–4508, 1994.

[207] K. F. Riley, M. P. Hobson, and S. J. Bence. *Mathematical Methods for Physics and Engineering - Second Edition*. Cambridge Univeristy Press, Cambridge, UK, 2002.

[208] G. Hanna and W. J. P. Barnes. Adhesion and detachment of the toe pads of tree frogs. *Journal of Experimental Biology*, 155:103–125, 1991.

[209] P. H. Drechsler. *Mechanics of adhesion and friction in stick insects and tree frogs*. PhD thesis, Bayerischen Julius-Maximilians-Universität Würzburg, 2008. URL `http://opus.bibliothek.uni-wuerzburg.de/volltexte/2008/2683/pdf/pd_thesis_rev1113_final.pdf`.

[210] K. Yamazaki. Gone with the wind: trembling leaves may deter herbivory. *Biological Journal of the Linnean Society*, 104:738–747, 2011.

[211] H. Loeffler. Ant adhesion and its implications for ant behaviour. Master's thesis, University of Hull, UK, 2009.

[212] L. Bocquet, E. Charlaix, S. Cilberto, and J. Crassous. Moisture-induced ageing in granular media and the kinetics of capillary condensation. *Nature*, 396:735–737, 1998.

[213] N. Fraysse, H. Thomé, and L Petit. Humidity effects on the stability of a sandpile. *The European Physical Journal B*, 11:615–619, 1999.

[214] L. Bocquet, È. Charlaix, and F Restagno. Physics of humid granular media. *Comptes Rendus Physique*, 3:207–215, 2002.

[215] R Development Core Team. *R: A Language and Environment for Statistical Computing*. R Foundation for Statistical Computing, Vienna, Austria, 2010. ISBN 3-900051-07-0, http://www.R-project.org.

[216] B. Blaseing and H. Cruhe. Stick insect locomotion in a complex environment: Climbing over large gaps. *Journal of Experimental Biology*, 207:1273–1286, 2004.

[217] J. Okada and Y. Toh. Active tactile sensing for localization of objects by the cockroach antenna. *Journal of Comparative Physiology A*, 192:715–726, 2006. doi: 10.1007/s00359-006-0106-9.

[218] W. M. Wheeler. On certain modified hairs peculiar to the ants of arid regions. *Biological Bulletin*, 13:185–202, 1907.

[219] D.J. Farish. The evolutionary implications of qualitative variation in the grooming behaviour of the Hymenoptera (Insecta). *Animal Behaviour*, 20:662–676, 1972.

[220] R. Benton. Chemical signalling in Drosophila. *Current Opinion in Neurobiology*, 18:357–363, 2008.

[221] N.E. Stork. Role of waxblooms in preventing attachment to Brassicas by the mustard beetle, *Phaedon coclechiae*. *Entomologia Experimentalis et Applicata*, 28:100–107, 1980.

[222] G. Puterka, D. M. Glenn, D. G. Sekutowski, T. R. Unruh, and S. K. Jones. Progress towards liquid formulations of particle films for insect and sisease control in pear. *Environmental Entomology*, 29:329–339, 2000.

[223] B. Tang. Fabrication of superhydrophilic patterns on superhydrophobic substrates: Towards open microfluidic applications. Master's thesis, Department of Chemistry, University of Hull, 2009.

[224] C. Vincent, G Hallman, B. Panneton, and F. Fleurat-Lessard. Management of agricultural insects with physical control methods. *Annual Review of Entomology*, 48:261–281, 2003. doi: 10.1146/annurev.ento.48.091801.112639.

[225] J. M. R. Bullock and W. Federle. The effect of surface roughness on claw and adhesive hair performance in the dock beetle *gastrophysa viridula*. *Insect Science*, 18:298–304, 2011. doi: 10.1111/j.1744-7917.2010.01369.x.

[226] G. Huber, S.N. Gorb, N. Hosoda, R. Spolenak, and E. Arzt. Influence of surface roughness on gecko adhesion. *Acta Biomaterialia*, 3:607–610, 2007.

[227] C. Neinhuis and W. Barthlott. Characterization and distribution of water-repellent, self-cleaning plant surfaces. *Annals of Botany*, 79:667–677, 1997.

[228] A. Steele, I. Bayer, and E. Loth. Inherently superoleophobic nanocomposite coatings by spray atomization. *Nano Letters*, 9:501–505, 2009. doi: 10.1021/nl8037272.

[229] I. P. Parkin and R. G. Palgrave. Self-cleaning coatings. *J. Mater. Chem.*, 15:1689–1695, 2005.

[230] V. A. Ganesh, H. K. Raut, and S. Nair, A. S. Ramakrishna. A review on self-cleaning coatings. *J. Mater. Chem.*, 21:16304–16322, 2011. doi: 10.1039/c1jm12523k.

[231] Y. Kobayashi, H. Katakami, E. Mine, D. Nagao, M. Konna, and L.M. Liz-Marzàn. Silica coating of silver nanoparticles using a modified stöber process. *Journal of Colloid Interface Science*, 283:392–396, 2005.

[232] M. Hikita, K. Tanaka, T. Nakamura, T. Kajiyama, and A. Takahara. Super-liquid-repellent surfaces prepared by colloidal silica nanoparticles covered with fluoroalkyl groups. *Langmuir*, 21:7299–7302, 2005. doi: 10.1021/la050901r.

[233] M. M. Kohonen and H. K. Christenson. Capillary condensation of water between rinsed mica surfaces. *Langmuir*, 16:7285–7288, 2000.

[234] R.P. Duncan, K. Autumn, and G. J. Binford. Convergent setal morphology in sand-covering spiders suggests a design principle for particle capture. *Proceedings of the Royal Society B*, 274:3049–3056, 2007. doi: 10.1098/rspb.2007.1039.